ION FLUXES IN PLANTS

RELATED TO ACID GROWTH

by

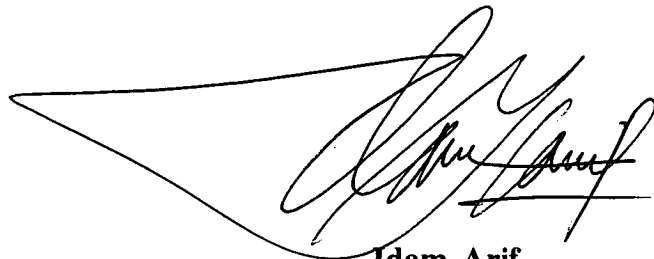**Idam Arif, S-1 (Indonesia)**

Submitted in fulfilment of the requirements

for the degree of

Doctor of Philosophy

UNIVERSITY OF TASMANIA

Hobart, Tasmania

March, 1993

DECLARATION

This thesis contains no material which has been accepted for the award of any other degree or diploma in any tertiary institution and that, to the best of my knowledge and belief, this thesis contains no material previously published or written by another person, except when due reference is made in the text of the thesis.

Idam Arif

ABSTRACT

The walls of plant cells are considered as a system containing weak acid polymers where the interaction of ions on the polymers obeys Manning condensation theory and Donnan theory (the Weak Acid Donnan Manning, or WADM, model). When protons are extruded to the walls during the growth of plant cells, the pH of the walls and therefore the ionic conditions of the walls change with time. The Microelectrode Ion Flux Estimation (MIFE) technique was used to measure simultaneously proton and calcium fluxes during the fusicoccin- or IAA-induced growth of 4-day-old split coleoptile segments of *Avena sativa* L. and 6- to 7-day-old peeled epicotyl segments of *Pisum sativum* L. line 107.

The WADM model for fluxes is now extended to analyse the change of the ionic condition in the walls, as well as the ion fluxes outside the walls, during proton extrusion from the cells to the cell walls. The analysis shows that when there is calcium condensation in the walls, proton extrusion from the cells to the cell walls causes effluxes of both protons and calcium outside the walls. However when the walls are considered as a classical Donnan system only, which is a special case of the WADM model for fluxes, proton extrusion from the cells to the cell walls would not cause any calcium release from the walls.

Fusicoccin induces immediate and transient proton and calcium effluxes from oat segments preincubated 4.5 hours. The fusicoccin-induced proton efflux saturates at 115 nmol. m^{-2} s^{-1} for 10^{-3} mole m^{-3} fusicoccin. The fusicoccin-induced calcium efflux saturates at about 120 nmol. m^{-2} s^{-1}. On peas, the fusicoccin-induced proton and calcium effluxes are smaller than on oats. When the WADM model for fluxes is applied to the observed data of both oats and peas, the calculated proton and calcium effluxes match well with the observed effluxes. This indicates that proton-calcium exchange happens in the walls during fusicoccin-induced proton extrusion across the plasmalemma and that the observed calcium efflux is the evidence for the validity of the model.

IAA at 10^{-2} mole m^{-3} induces proton efflux with a lag of about 13 minutes on oats. The proton efflux is smaller when the preincubation time is shorter (15 or 5 nmol. m^{-2} s^{-1} for 4.5 or 1 hour preincubation). IAA also induces biphasic calcium efflux but without a noticeable lag. The increase of the calcium efflux induced by IAA is about 30 nmol. m^{-2} s^{-1}. On pea segments preincubated for 4.5 hours, IAA at 10^{-2} mole m^{-3} causes, without a noticeable lag, transient proton and calcium effluxes, lasting about 15 minutes. The IAA-induced proton and calcium effluxes are about 5 and 25 nmol. m^{-2} s^{-1} respectively. The responses to IAA of oats and peas are also consistent with the proton-calcium exchange in the walls during IAA-induced proton extrusion.

The WADM model does not specify the function of condensed calcium in the walls that is released during proton extrusion from the cells to the cell walls. In this present work, it is discussed that condensed calcium may serve a role of stiffening the walls and therefore the proton-calcium exchange during proton extrusion has some role, as well as other processes, in causing wall loosening.

Proton flux determination by measuring the electrochemical potential gradient of protons can be in error when the measurements are carried out in buffered solutions and the error depends on the pH of the solutions. Analysis is done to quantify this error and take it into account.

Besides proton and calcium fluxes, potassium flux and membrane potential were also measured. Fusicoccin induces immediate potassium efflux and membrane hyperpolarization on both oats and peas where their magnitudes depend on the fusicoccin concentration. On both plants, IAA does not cause any significant effects on potassium flux. IAA induces transient membrane hyperpolarization with a lag of about 7 minutes on oats. On peas, IAA causes transient membrane hyperpolarization without a noticeable lag and it is followed by membrane depolarization. Solid-state chloride microelectrodes were specially developed to measure the flux of chloride during IAA action on oats. IAA does not cause any significant change on chloride flux. The effects of some treatments, such as cutting, preincubation time and solution change are also discussed.

ACKNOWLEDGMENTS

CONTENTS

Chapter 1

INTRODUCTION

1.1 The Growth of Plants

Many reviews on various aspects of plant growth have been written. The topics include the kinematics of plant growth (Silk 1984), the properties of cell walls (Taiz 1984; Cleland 1983; Bates and Ray 1981; Kutschera and Briggs 1987a; Kutschera and Briggs 1987b; Yamaoka and Chiba 1983; Masuda et al. 1972), the role of calcium on plant development (Hepler and Wayne 1985; Bennet-Clark 1956; Brummell and Hall 1987; Tepfer and Taylor 1981; Cohen and Nadler 1976; Brummer and Parish 1983; Cleland and Rayle 1977), the biophysics of plant growth (Cosgrove 1986), membrane potential of plant growth (Cleland et al. 1977; Senn and Goldsmith 1988; Bates and Goldsmith 1983), gene expression (Key 1969), water stress and water transport (Morgan 1984, Boyer 1985), and the effects of auxin and other plant growth substances (Kutschera and Schopfer 1985a; Kutschera and Schopfer 1985b; Vanderhoef 1980; Cleland 1976; Cleland 1980). In this chapter I discuss some general aspects of plant growth and later bring the discussion in more detail to the early process of growth that I am interested in. The discussion is then followed by the development of the hypothesis to be tested in this thesis.

1.1.1 Growth Process

Growth means increase in size. Therefore when the size of plants increases, we can say that the plants are growing. It looks simple. However the processes involved in the growth of plants are quite complex. The processes include cell division, cell enlargement, differentiation and development (Raven

1986, Salisbury 1986), even though differentiation and development give little contribution to size change.

Growth of plants originates in parts of the plants called meristems. The meristems contain physiologically young cells capable of enlarging and dividing repeatedly. Meristems that are located in the tips of plants are responsible for the extension of plant body (primary growth), while lateral meristems are responsible for the thickening of the plant body (secondary growth).

In order to grow, plants need materials such as water, minerals, carbon dioxide and light from their environment and synthesize them into their own substances necessary for the growth of the plants.

1.1.2 Growth Factors

The processes of growth and development in plants depend on both internal and external factors (Raven 1986). The external factors such as light, gravity and temperature come from the environment of the plants. These factors influence the plants by giving some physical stimuli to them so that they can adapt to changes in their environment. The internal factors are specific organic substances, effective in low concentration, produced in specific tissues in plants. From the tissues, they are transported to other tissues in the plants to give physiological effects by regulating important metabolic reactions (Salisbury 1985). This is the reason of why the term "plant growth hormone" is often used.

The first experiments on plant growth hormones were done by Dutch plant physiologist F.W. Went in 1926. He did the experiments to show that the tips of oat *Avena sativa* coleoptiles contain substances that induce elongation of the coleoptiles. These experiments answered questions which arose from many observations reported previously that the tips of oat coleoptiles have an important role on the elongation of the coleoptiles. Went called the substances *auxin*, from the Greek word *auxein* which means "to increase". Although these experiments were done using oat coleoptiles, experiments on other grass seedlings have also shown similar results.

Since Went reported these results, many experiments have been performed to find out how auxin is formed, how it is transported and how it is

able to induce cells to elongate. Auxin that has been extracted from the tips of oat coleoptiles is Indole-3-acetic acid (IAA) and the concentration of IAA present in a coleoptile tip is very small. In plants, IAA is formed from an amino acid named tryptophan. Tryptophan is inactive ie. tryptophan itself does not induce cells to elongate. Although tryptophan is inactive, when it is injected into a plant, elongation occurs. This indicates that tryptophan in plants is converted to form IAA.

IAA is generally produced in the tips of plants, and then transported to the whole parts of the plants. In principle, therefore, IAA can be found every where in the plant body. The transport is through cells. It moves slowly with the speed of about 1 cm/hour. The movement is polar ie. it enters a cell at one end and moves out at the opposite end. The movement also requires metabolic energy.

IAA is lipophilic so that IAA can easily diffuse into a cell as undissociated acids (IAAH), ie. the membrane permeability to IAA anions is smaller than the membrane permeability to the acids. IAA is also a weak acid. Therefore, the ratio between the concentration of IAA anions and the acids depends on the pH according to the Henderson-Hasselbalch equation:

$$pH = pK + \log \frac{[IAA^-]}{[IAAH]}$$ 1.1

In this case, the total concentration of IAA is $[IAAH] + [IAA^-]$. Because the pH inside the cell is smaller than the pH of the external medium, there will be an accumulation of IAA in the cell since the pK of IAA is constant (pK=4.7). To allow movement of IAA out of the cell at the opposite end (polar transport), the membrane permeability ratio of IAA anions and undissociated acids in this position should be bigger than their permeability ratio at the position where IAA enters the cell (Goldsmith 1977).

After IAA moves out from a cell, the IAA then enters the adjacent cell with similar processes. Hence, in the whole picture, this mechanism is expected to explain the polar transport of IAA from one cell to another in plants.

The fact that there is very little IAA in plants which can be extracted and that IAA is very important as a plant growth hormone, has led to efforts to produce IAA chemically. Compounds similar to IAA have also been

synthesized. Now, there are many kinds of synthetic auxins such as indole-3-propionic acid, indole-3-butyric acid, naphthaleneacetic acid, 2,4-dichlorophenoxyacetic acid, 2,4,5-trichlorophenoxyacetic acid, 2-methyl,4-chlorophenoxyacetic acid, and S-carboxymethyl-N,N-dimethyl dithio carbamate. A common characteristic of auxins is the presence of a carboxyl group attached to an aromatic ring. However some others such as S-carboxymethyl-N,N-dimethyl dithio carbamate do not show this characteristic. Since they include synthetic auxins, now the term "plant growth substances" is also used instead of plant growth hormones.

Beside endogenous auxin, there are other natural growth substances which have been identified in plants such as gibberellins, cytokinins, ethylene, and abscisic acid. These natural growth substances have different roles and physiological effects on plants. Some of them even work together to cause particular effects on plants.

There is also a substance that plant physiologists often use as a tool in plant physiology because it influences many important physiological processes in plants. The substance is fusicoccin (FC), the major toxin produced by fungus *Fusicoccum amygdali* Del. The structure of fusicoccin has been worked out by Ballio (1977). Some of the effects, including induction of cell elongation, mimic the effects of auxin, gibberellin and cytokinin, and some others antagonize the effect of abscisic acid (Marrè 1979). This is the reason why fusicoccin is also used as a tool to understand hormone action.

In this study, concern is only focused on the growth induced by exogenous IAA and the growth induced by fusicoccin for comparison.

1.2 IAA and Fusicoccin Responses

IAA causes many different physiological effects in plants and the effects are tissue-specific (Raven 1986, Salisbury 1985). It causes cell enlargement in the tips of coleoptiles and stems so that they elongate. It influences vascular differentiation in cut tissues and calluses. It also stimulates the development of fruit without fertilization. Its combination with other growth substances promotes cell division and the growth of vascular cambium, and controls the process of leaf abscission. IAA also involves in phototropism and geotropism. Beside promoting growth, IAA also has inhibitory effects on the growth of

some tissues such as lateral buds. Generally, when the concentration of IAA is high, it also inhibits growth. For example, at very low concentration, IAA causes cell enlargement in roots thereby promoting elongation of the roots. However, a large amount of IAA inhibits the growth of already growing roots.

IAA-induced cell enlargement observed by the increase of growth rate is not immediate. The increase starts several minutes after IAA is applied.

During cell enlargement induced by IAA, it has been observed widely that the surrounding medium becomes more acid after several minutes. However, the range of the reported IAA-induced medium acidification is very wide. Results showed that the pH of the medium can fall below 5 but others failed to obtain pH as low as 5. Beside a wide range of IAA-induced medium acidification, the time lags when medium acidification induced by IAA begins are also diverse. As discussed in the Acid-Growth Hypothesis section in this chapter, some evidence shows that the medium acidification begins at the same time as the increased growth rate induced by IAA. However under certain circumstances, the medium acidification is delayed longer than the increase in growth rate.

During IAA action in monocots, the membrane potential, the potential difference between the inside and the outside of the cells, also hyperpolarizes with a lag similar to the lag of the increase of the growth rate induced by IAA (Senn and Goldsmith 1988, Bates and Goldsmith 1983, Cleland et al. 1977, Brummer et al. 1985). This indicates that a net positive charge is transported out from the cells.

Cell enlargement is also promoted by fusicoccin. However it is not tissue specific. Fusicoccin-induced cell enlargement happens not only in tissues giving this response to IAA but also in other tissues such as root and leaf segments and seed embryos (Marrè 1979). Fusicoccin-induced cell enlargement is also immediate and more substantial.

Fusicoccin also causes immediate and substantial medium acidification and membrane hyperpolarization. It promotes uptake of potassium and other solutes, seed germination and stomatal opening (Marrè 1979, Kutschera and Schopfer 1985b, Senn and Goldsmith 1988, Lüthen et al. 1990).

1.3 Wall Loosening and Wall Structure

1.3.1 Growth Initiated by Wall loosening

It has generally been believed that the early process of the growth of plant cells is in the loosening of cell walls. The wall loosening is then followed by processes that allow the cells to increase their sizes.

Under normal conditions, the water potential inside and outside the cells is in equilibrium. At this time, there is no water movement. Because the osmotic pressure inside the cell is greater than outside, there must be a hydrostatic pressure inside the cell since the pressure outside the cell is the atmospheric pressure. The existence of the internal hydrostatic pressure within the cell produces stresses on its walls and compression on the cell contents. However, the cell walls are semi rigid and strong enough to resist the stresses. Therefore the volume of the cell cannot extend.

When IAA or fusicoccin is applied to the cell, the stress-bearing parts of the walls become loosened and the wall extensibility increases. As a result, the stresses in these parts decrease. Because the stresses in the stress-bearing parts of the walls are represented by the internal hydrostatic pressure, the decrease in the stresses means the decrease of the internal hydrostatic pressure. The water potential inside the cell that depends linearly on the hydrostatic pressure also decreases. As a result, the water potential is no longer in equilibrium because the water potential inside the cell is less than the water potential outside. The difference between the water potential inside and outside the cell will then act as the driving force of the water movement into the cell where the water potential is smaller. When water moves into the cell, the walls are simultaneously yielding and the volume of the cell increases. In this time, the internal hydrostatic pressure is slightly bigger than the minimum pressure that can cause the loosened walls to yield, and, the rate of the wall yielding is the same as the rate of the volume increase. The increase of the volume of the cell indicates that the cell is growing. The growth of the cell does not continue if this process is not followed by other complex processes that include production of materials necessary for further extension (see also Lockhart 1965a, Taiz 1984, Cosgrove 1986).

1.3.2 The Structure of Plant Cell Walls

In general, plant cell walls that limit the growth of plant cells are composed of two major organic materials, cellulose and non-cellulosic materials (see Nobel 1974 pages 32-41 and Raven *et al.* 1986 pages 32-35). Cellulose is the major component of plant cell walls. It constitutes almost 25-50% of the wall organic materials. Cellulose is a linear molecule consisting of glucose molecules attached end to end so that it has a chainlike form. Several cellulose molecules in a lattice arrangement form a micelle. Micelles form a microfibril and microfibrils form a macrofibril (Figure 1.1).

In plant cell walls, celluloses are interconnected by a matrix of non-cellulosic materials: hemicelluloses, pectins, and glycoproteins. They contain weak acids. Therefore cell walls can be considered as a system of weak acid polymers. In Chapter 4, this consideration is used to analyse the ionic condition in the walls during proton extrusion. Cell walls may also contain lignins that add rigidity to the walls. In outer, protective tissues, walls may also contain fatty substances such as cutin, suberin and waxes. The wall matrix also contains free and bound water, calcium, and other cations. Under normal conditions, calcium is the major cation present in the walls (Nobel 1974). Part of the bound calcium appears to link acidic pectins in the walls. It has been reported that external calcium inhibits growth of plant cells. This leads to the suggestion that calcium binding present between wall pectins is the load-bearing bond in the walls.

The thickness of cell walls varies as the cells are growing. In growing cells, cell walls can be divided in two regions, the primary wall and the middle lamella. However, when the cells undergo differentiation and stop growing, the cell walls become thicker because the cells form other layers between the inner surfaces of the primary walls and their plasmalemma. The new wall layers are called the secondary walls. In this case, the middle lamella which is composed mainly of pectins occurs between the primary wall of its own and the primary walls of adjacent cells. The primary walls are composed of cellulose, hemicelluloses, pectins, and glycoproteins (Figure 1.2). The presence of pectins makes it possible for the primary walls to stretch under certain circumstances during the growth of the cells (Raven *et al.* 1986). In the secondary walls, however, the presence of pectins is less than in the primary walls. Furthermore the presence of celluloses is bigger and glycoproteins are absent. This composition causes the secondary walls to be rigid so that they are difficult to stretch.
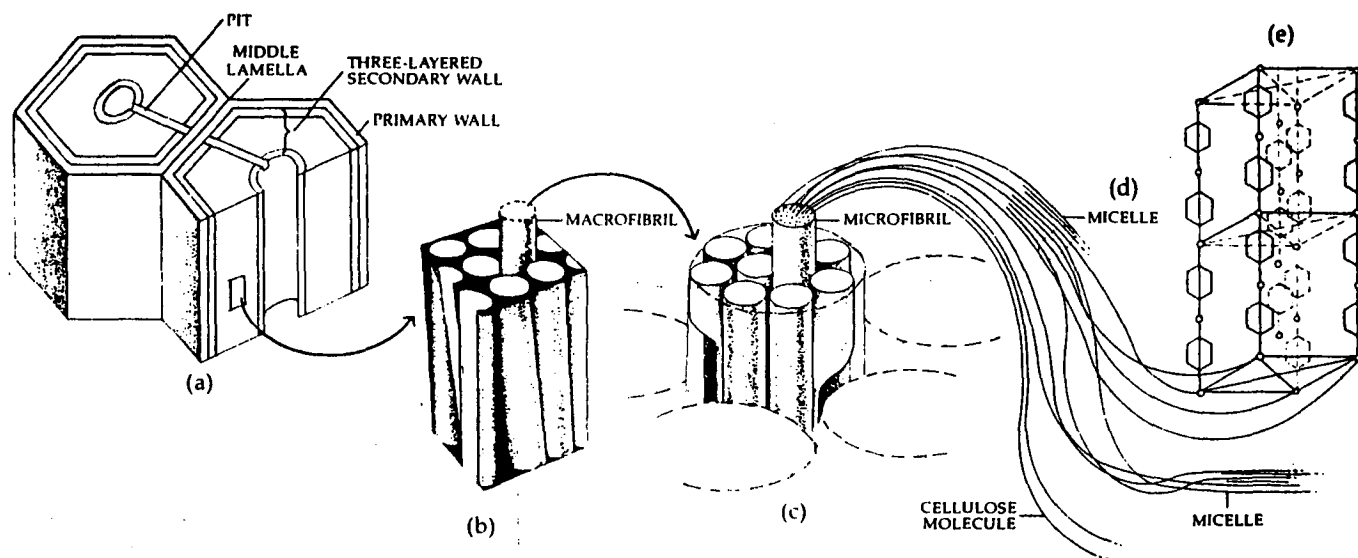
Figure 1.1

The detailed structure of a cell wall. (From Raven et al. 1986 p.33)
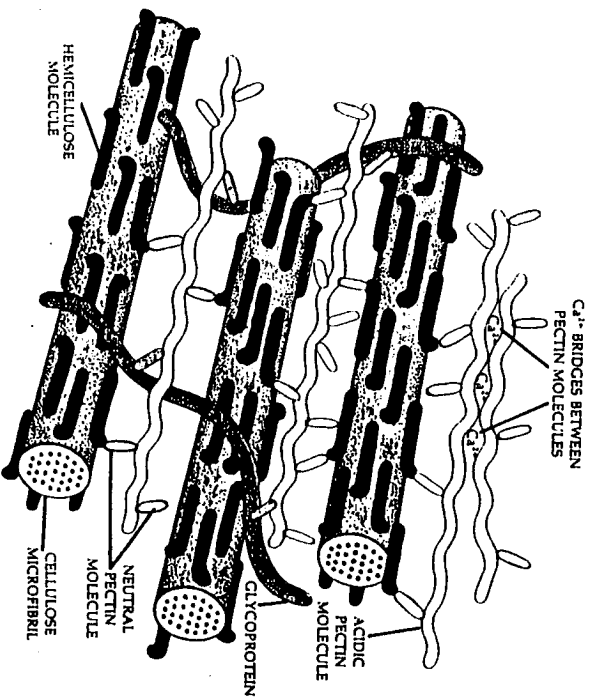
Figure 1.2
Schematic diagram of the cellulose microfibrils and matrix components in a cell wall. (From Raven et al. 1986 p.33)

The direction of the growth depends on both the shape of the cells and the structure of the cell walls (Taiz 1984). The contribution of the cell shape in determining the direction of the cell growth is based on the distribution of stresses on the surface of the walls in response to the internal hydrostatic pressure. The contribution of the cell wall structure in determining the direction of cell growth is based on the orientation of the cellulose macrofibrils in the walls, especially in the inner walls which directly bear the stress arising from the turgor pressure (Richmond et al. 1980). In this case, when the orientation of the cellulose macrofibril is parallel to the stress, the stress causes minimum strain. However, when the orientation is perpendicular to the stress, the strain is maximum.

1.4 Mechanism of Wall Loosening

Several mechanisms have been proposed for the process of wall loosening that initiates the growth of plant cells. The earlier mechanism is the calcium bridge hypothesis. In this hypothesis, the wall loosening process is explained in terms of binding sites of calcium in the walls. However, the validity of this hypothesis has been put into question since some evidence against it has been reported. Another proposed mechanism is the acid-growth hypothesis. The hypothesis that explains the wall loosening process in terms of wall acidification becomes an attractive mechanism because of its simplicity. However, like the calcium bridge hypothesis, there are people who still feel that the acid-growth hypothesis is also not adequate to explain the process.

1.4.1 The Calcium Bridge Hypothesis

The calcium bridge hypothesis was formulated independently by Bennet-Clark (1956) and Carlier and Buffel (1955). This hypothesis states that auxin interferes with the binding sites of calcium in the cell walls so that the calcium is removed from the walls. The function of calcium in the walls is to stiffen the walls by making cross-links between pectic chains of the walls (pectic gelatinization). The cross linking formed by calcium and other ions in the walls is recognized later as the egg-box model (Grant et al. 1973, Rees 1977). Bennet-Clark explained that in the cell walls, calcium links pectins by making covalent bindings between their carboxyl groups. In this condition, the wall extensibility is minimal. When calcium is removed by auxin, the carboxyl

groups bind with hydrogen and this condition gives more extensibility to the walls. The wall extensibility is maximal when the carboxyl groups are converted to methyl esters. Bennet-Clark also showed that the calcium chelator ethylenediamine tetraacetic acid (EDTA) stimulates the growth of plants. Based on this evidence, he also suggested that auxin interferes with the calcium binding sites in wall pectins by chelation. This hypothesis is also supported by the evidence that the addition of calcium to the external medium inhibits the growth of plant cells (Bennet-Clark 1956, Tagawa and Borner 1957, Reddy et al. 1988).

In relation to this hypothesis, Cleland (1960) commented that if this hypothesis is suitable for auxin-induced cell elongation, there must be calcium coming out from the cell walls during auxin action. However, when he examined this, no significant loss of calcium from the cell walls was observed during the auxin action. In this experiment, measurements of the loss of calcium were carried out by comparing the amount of calcium in walls with intact cuticles before and after auxin treatment. With this condition, if the calcium is released by auxin from the walls, the calcium can not come out from the walls because it can not go through the cuticles (Taiz 1984). Besides, the amount of calcium in the walls is much bigger compared to the amount of calcium removed from the walls by auxin. Therefore the difference between the amount of calcium in the walls extracted before and after auxin treatment may not be clear enough. In this case, it is still desirable to employ a more sensitive method to observe the amount of calcium removed during auxin action. In this present work, the measurements of calcium flux using the Microelectrode Ion Flux Estimation (MIFE) technique show that auxin clearly causes calcium efflux (see Chapter 6).

Cleland (1960) also argued that although calcium addition to the external medium causes growth inhibition, it does not mean that the added calcium inhibits the growth by forming cross-linkages between wall pectins to increase the rigidity of the walls. It is still possible that the growth inhibition occurs by another mechanism. Several years later, Cleland and Rayle(1977) strongly questioned the claim that the addition of calcium to the external solution inhibits growth by forming wall-stiffening calcium bridges. This was based on the fact that they did not find a decrease in wall extensibility when isolated walls were treated with an amount of calcium that can cause inhibition of plant growth. In living sections, however, the wall extensibility decreased when the section was treated with the same amount of calcium. Therefore, this strongly supports the

theory that calcium causes a decrease in wall extensibility by another mechanism. Cleland and Rayle (1977) proposed that calcium inhibits the growth by inhibiting proton extrusion that causes wall loosening. This is discussed later in the Acid-Growth Hypothesis section.

Tepfer and Taylor (1981) also provided the evidence that inhibition of growth by divalent cations, including calcium, is not related to the ability of the cations to induce pectic gelatinization. They used five different divalent cations, Mg^{2+}, Mn^{2+}, Ca^{2+}, Co^{2+}, and Zn^{2+}. They found that although Mg^{2+} and Mn^{2+} can not form pectic gelatinization, these cations do inhibit growth with the effectiveness similar to Ca^{2+}. In the case of the three other cations, the cations inhibit growth and form pectic gelatinization. This refutes the claim that the pectic gelatinization is necessary to inhibit growth (Bennet-Clark 1956, Tagawa and Borner 1957). This is supported also with the evidence that the abilities of the divalent cations to form pectic gelatinization have no correspondence with their binding affinities to the pectins (Tepfer and Taylor 1981). In this case, the binding affinities were determined by the abilities of the cations to replace protons from the pectins. Their binding affinities in the pectins also did not relate to the abilities of the cations to inhibit growth. However, when the binding affinities of the cations in the whole walls are compared to their abilities to inhibit growth, they show a good correlation. These results indicate that the state of cation binding site in the whole walls plays an important role during the growth of plants. Based on this fact, the inhibition of plant growth by added calcium to the external medium may relate to the occupation of the cation binding sites in the whole walls by the added calcium.

The mechanism of how occupation of binding sites in the walls by divalent cations inhibits the growth of plant cells is still in investigation. The cations may interact directly with the enzymes for the wall loosening process (Cleland and Rayle 1977, Tepfer and Taylor 1981). However, Tepfer and Taylor (1981) also mentioned that it still does not close the possibility that the wall loosening process is not enzymatic, ie. the inhibitory effect of the cations on growth is caused by their interaction with the wall matrix to give some structural changes in the walls.

The growth of the plant requires some calcium from the external medium. This suggests that the presence of calcium in the external medium does not always inhibit growth. Whether the presence of calcium in the external medium inhibits growth or not depends on the amount of calcium in the medium

(Cohen and Nadler 1976). Cohen and Nadler (1976) also provided the evidence that the amount of calcium in the external medium influences the magnitude of proton extrusion during auxin action. In this case, the addition of calcium increases the auxin-induced proton extrusion. This leads them to propose that the Ca^{2+}-H^+ exchange between cells and the external medium is involved in the mechanism of the auxin-induced medium acidification.

Since the binding affinity of calcium in the walls can be represented by the ability of the calcium to displace protons from the walls (Tepfer and Taylor 1981), the evidence provided by Cohen and Nadler (1976) can be interpreted in another way. During auxin-induced proton extrusion, some of the extruded protons occupy the cation binding sites in the walls and the rest diffuses to the external medium. When calcium is added to the external medium, the added calcium goes to the walls and occupies the cation binding sites in the walls. At this time, it is difficult for the auxin-induced extruded protons to occupy the binding sites in the walls by displacing the calcium. Therefore, more extruded protons diffuse to the external medium. This appears as an exchange between extruded protons and added calcium. However, the exchange does not happen between the cells and the external medium as suggested by Cohen and Nadler (1976), but between the walls of the cells and the external medium.

Richter and Dainty (1989a, 1989b, 1990a, 1990b) have proposed the weak acid Donnan Manning (WADM) model for ion behaviour in the walls of plant cells. Beside the Donnan interaction, this model also considers the Manning condensation theory (Manning 1969) for the interaction of ions in the plant cell walls that contain weak acid polymers. This model is diferent to the model proposed by Sentenac and Grignon (1981) that uses the Donnan interaction and the mass action law to predict the equilibrium concentration of ions in the walls. In the WADM model, bound calcium in the walls of plant cells is separated into calcium condensed to wall's weak acids and calcium in the Donnan free space (DFS). Following this work, Ryan, Newman & Arif (1992) have calculated the concentrations of the main ions in *Chara* cell walls when the composition of the ions in the external solution was altered. The results show that the decrease of the external pH decreases the total concentration of calcium in the walls. This supports the Ca^{2+}-H^+ exchange between the cell walls and the external medium.

Virk and Cleland (1988) reported that calcium chelator EGTA and low pH increase the wall extensibility of frozen-thawed soybean hypocotyl sections.

Therefore they suggested that calcium cross links in the walls is part of the load-bearing bonds and that breakage of these cross links by apoplastic acid participates in wall loosening. However later, it was reported that these load-bearing bonds are not the same as the load-bearing bonds that are broken during acid-mediated cell elongation (Virk and Cleland 1990, Cleland et al. 1990). This was based on their evidence that calcium chelator EGTA in strong buffer or another calcium chelator Quin 2 causes removal calcium without an increase in wall extensibility. This response also happens in *Avena* coleoptiles (Rayle 1989). The pH of the walls during the addition of EGTA in strong buffer or Quin 2 does not change. According to the WADM model (Richter and Dainty 1990, Ryan, Newman and Arif 1992), if the pH does not change, the removed calcium may have come not from the calcium condensed to weak acids of the wall matrix but from the Donnan free space (DFS). Calcium loss from the DFS need not cause any increase of wall extensibility. This argumentation is discussed in more detail in Chapter 5 by providing the concentration of calcium condensed to wall's weak acids and the concentration of calcium in the DFS obtained from the WADM model.

1.4.2 The Acid-Growth Hypothesis

This hypothesis was formulated by Cleland (1971) and Hager et al. (1971). It becomes the most attractive hypothesis for auxin action because of its simplicity. It states that auxins induce cells to excrete protons to their surrounding wall medium. The pH of the walls drops and the walls become acid. The low pH then activates some wall enzymes to break bonds between growth-restrictive polysaccharides within the walls. The walls become loosened and the turgor pressure of the cells drives the cells to grow. To justify whether the hypothesis is appropriate or not for the mechanism of the auxin-induced growth, Cleland (1980) gives four predictions that are consequences of the hypothesis: 1. Auxins must cause cells to excrete protons; 2. Exogenous protons must be able to substitute for auxins in causing cell wall loosening in the process of growth; 3. Neutral buffers infiltrated into the walls must inhibit auxin-induced growth; and 4. Other agents which induce H^+-extrusion, such as the phytotoxin fusicoccin (FC), must cause a parallel promotion of growth. If these four predictions can be satisfied, the acid-growth hypothesis is applicable for the mechanism of the auxin-induced growth.

Many experiments with different plants using different techniques have been carried out in order to provide evidence related to these four predictions. In general, people are still arguing that auxin-induced cell elongation is the result of medium acidification. People agree that to induce cell elongation proportional to the elongation of the cells induced by auxin, the pH of the medium should be about 5 to 4. However, the lowered medium pH caused by auxin action varies from above 5 to below 5 depending on the techniques and conditions used (Cleland 1975, Cleland 1976, Lüthen and Böttger 1989, Lüthen et al. 1990, Kutschera and Schopfer 1985a, Senn and Goldsmith 1988, Schopfer 1989, Cleland et al. 1991). Beside that, the time lag when medium acidification induced by auxin begins is not always the same as the time lag when the auxin-induced increase in growth rate begins. Under certain circumstances, the time lag of the medium acidification is delayed longer.

The suggestion arising from the absence of sufficiently low pH induced by auxin and from the variable time lag was that the cuticle prevented the protons diffusing out (Cleland 1980, Rayle and Cleland 1992). A cuticle has low permeability to protons. Therefore, when the cuticle is left intact in the tissue segments during the measurements of auxin-induced medium acidification, the cuticle traps some of the protons extruded from the cells and it reduces or delays the detection of the extruded protons outside the segments. Auxin-induced extruded protons are more readily detected when the cuticle is removed from the segments. However, the removal of the cuticle must not itself significantly affect the growth of the segments.

Since protons are extruded out to the external medium during auxin action, the volume ratio between the solution and the tissues is also important in affecting the results of the external pH measurements. Therefore, to obtain better sensitivity in the measurements of the auxin-induced medium acidification, it is also necessary to keep the solution/tissue volume ratio as small as possible.

Various techniques for peeling or scrubbing (abrading) to remove cuticle are available. Kutschera and Schopfer (1985a) suggested scrubbing with emery cloth because this gives uniform scratches and little damage occurs on the epidermal layers. They also showed that auxin-induced elongation of the scrubbed segments is similar to that of the unscrubbed segments. Cleland (1980) provided a list of plants in which auxin-induced proton excretion has

been observed. In this list, different ways of scrubbing were used to remove cuticles.

In relation to the method of removing cuticles by peeling, Kutschera and Schopfer (1985a) and Kutschera et al. (1987) argued that some of the epidermal layers necessary for growth may also be removed. However, recent papers of Cleland (1991) and Rayle et al. (1991) claimed that epidermis is not a unique target tissue for auxin-induced growth. Therefore the evidence obtained from peeled sections supporting the acid-growth hypothesis is still valid (Rayle and Cleland 1992).

Splitting the segments is another way of allowing detection of proton extrusion from tissues during auxin action. This method is carried out in order to avoid removing epidermal layers that may be important for the growth of tissues (see Durran and Rayle 1973). The elongation of the split segments of oats has also been shown to be equivalent to the elongation of peeled segments in response to auxin (Senn and Goldsmith 1988). In coleoptile segments, since the splitting can be done between their vascular bundles, it does not give much stimulus to the segments so that the split segments still behave like the unsplit segments. The method can also be standardized more easily than peeling so that variability in results is diminished.

Based on the available evidence at present, auxin decreases the pH of the external medium to about pH 5. The question related to the second prediction of the acid-growth hypothesis is whether external buffered solutions at this pH can stimulate growth with the same magnitude as auxin does. Kutschera and Schopfer (1985a) provided evidence that to induce growth with similar magnitude as auxin does, the pH of the external solution must be lower than pH 4.5. Maximum growth happens when the pH of the external solution is about 2.5. If the pH of the external solution is lower than 2, shrinkage happens because of the toxicity of the very low pH. The observation that pH 5 external solutions cause growth in *Avena* coleoptile segments reported by Rayle (1973) is called into question by Kutschera and Schopfer (1985a). This relates to the strong neutral buffer used to preincubate the segments in Rayle's experiments. They argued that the strong neutral buffer shifts the pH dependency of the growth to a higher pH. Several years later, Schopfer (1989) reported that the strong neutral buffers used to preincubate peeled segments inhibit the simultaneous growth burst of the segments as the result of the releasing cell tension by peeling process. Therefore, when the segments are used to examine

the effects of low pH external solutions on the growth of the segments, the external solutions release the inhibition and therefore allow the segments to grow.

The actual pH of the cell wall $_{OFS}$ is not measured yet and the pH of the external solution observed during auxin action certainly does not represent the pH of the cell walls. Because protons are pumped out from the cells to the external medium during auxin action, the pH of the cell walls is lower than the pH of the external solution. Based on the Donnan potential of the walls, Cleland (1976) estimated that the pH of the wall is 0.3 pH units lower than the pH of the external medium. In this present work, the pH of the walls, and also the change of the pH during proton extrusion, can be calculated using the WADM model for fluxes (see Chapter 5).

The elongation response due to low pH is different from the elongation response due to auxin action (Vanderhoef 1980). In this case, the acid-induced growth never shows a steady state rate; however the growth in response to auxin reaches a steady state rate and remains in this state for a long time. Probably, acid is only responsible for the initial growth. This relates to the acid effect in causing wall loosening. After that, this is followed by other complex processes necessary for growth, involving synthesis of protein and other things necessary for wall materials as suggested in the gene expression hypothesis (Key 1969).

In relation to the third prediction of the acid-growth hypothesis (Cleland 1980), the removal of cuticles is also important when the effect of neutral buffers to the auxin-induced growth of plant segments is examined because the presence of cuticles prevents the penetration of the buffers into the tissue segments. The permeability of cuticles to buffers is low or even lower than the permeability of cuticles to protons (Cleland 1980). Therefore, when the cuticles are left intact, the neutral buffers do not have much effect on the auxin-induced growth of the segments. Furthermore, in the experiments using neutral buffers, the osmolarity of the solution varies with the buffer concentration. Therefore, assessment of the results must be carried out by comparison with the effect of an unbuffered solution with the same osmolarity.

Several studies of the effects of neutral buffers on growth have been carried out and the results clearly show that neutral buffers inhibit growth (Durran and Rayle 1973, Cleland 1980). The mechanism of the inhibition is still

not clear. Cleland (1980) suggested that the inhibition is due to the buffers preventing wall acidification. This argument supports the acid-growth hypothesis. Kutschera and Schopfer (1985a) argued that if neutral buffers inhibit auxin-induced growth by preventing the acidification of the walls, the response to the auxin action must be dependent on the pH of the neutral buffers. The inhibition must be bigger when the pH of the neutral buffers is higher. However when the pH is in the range of pH 6.0 to 10.0, they found that the auxin-induced elongation is independent of the pH of the neutral buffers. Therefore, they suggested that the neutral buffers inhibit growth not by preventing the wall acidification, but probably by another mechanism.

The fourth prediction of the acid-growth hypothesis states that other agents which induce proton extrusion must cause parallel promotion of growth at a concentration which produces equal proton extrusion (Cleland 1980). Fusicoccin is found to induce proton extrusion and it is also found that fusicoccin also induces cell elongation (Cleland 1976, Kutschera and Schopfer 1985a&b, Brummer et al. 1985). However, at a concentration which produces equal proton secretion, fusicoccin is much less effective than auxin in inducing cell elongation (Kutschera and Schopfer 1985a). When the growth response of fusicoccin is compared to the growth response of acid solutions, they are similar (Kutschera and Schopfer 1985b). They are also not additive (Marrè 1979). The timing of fusicoccin-induced growth, medium acidification and membrane hyperpolarization also match well (Kutschera and Schopfer 1985b; Senn and Goldsmith 1988; Lüthen et al. 1990). Based on this evidence, it seems likely that the acid-growth hypothesis is suitable for fusicoccin action.

Sugars also induce proton excretion and the sugar-induced medium acidification is larger than the auxin-induced medium acidification (Kutschera and Schopfer 1985a). However, cell elongation induced by sugars is delayed more than 6 hours. This is in contrast to the forth prediction of the acid-growth hypothesis.

The auxin-induced cell elongation begins with a lag of about 10 minutes (Senn and Goldsmith 1988, Evans and Ray 1969, Vesper and Evans 1978). If the acid-growth hypothesis is suitable for auxin action, the timing of the auxin-induced medium acidification must be similar to the timing of the auxin-induced increase in growth rate. However, the lag of the auxin-induced medium acidification varies greatly between experiments with differing sensitivity. Senn and Goldsmith (1988) found that the medium acidification in freshly cut

sections of oats which grew in response to IAA is delayed longer than the growth. It seems that the length of the preincubation time also contributes to the size of the lag.

In relation to the time lag of the auxin-induced growth, Brummell and Hall (1987) gave an explanation in terms of Ca^{2+} as a second messenger. When auxin is taken up by the cells, auxin binds to its receptors. In the cells, auxin receptors are located in the plasma membranes, the membranes of endoplasmic reticulum (ER) and the tonoplast. In the plasma membranes, the receptors are not only in the inner face but also in the outer face (Klämbt 1990). When auxin binds to its receptors, the concentration of calcium in the cytoplasm increases. The increase is probably due to the opening of calcium channels in the plasma membranes so that wall calcium enters the cytoplasm (see Hertel in Brummell and Hall 1987) and/or due to the calcium release from ER (Brummer and Parish 1983) and vacuole (Brummell and Hall 1987) which provide stores of calcium ions.

In the cytoplasm, some of the calcium binds to a protein-response element or to the modulator protein calmodulin which also binds to the response element (see Hepler and Wayne 1985 and its references). It was suggested that this binding activates some responses necessary for growth. It was also suggested that, some cytoplasmic calcium is also taken up by mitochondria which then release protons to the cytoplasm (Brummer and Parish 1983). As a result, the pH of the cytoplasm decreases. It was suggested that to maintain the cytoplasmic pH constant, the cells then pump the protons out from the cytoplasm. One of the results is proton extrusion to the external medium.

1.5 The Unifying Hypothesis

From the discussion above, it is clear that the role of wall calcium during the early process of growth of plant cells remains controversial. This needs to be clarified since calcium is the major ion in plant cell walls. According to the calcium bridge hypothesis (Bennet-Clark 1956; Carlier and Buffel 1955), auxin releases wall calcium that has stiffened the walls by making cross-links between pectin chains of the walls (Grant et al. 1973, Rees 1977). The inhibition of the growth of plant segments caused by added calcium in the external medium supports this hypothesis (Tagawa and Borner 1957, Cleland and Rayle 1977). However, auxin does not cause any significant loss of

calcium in tissue segments with intact cuticle (Cleland 1960). It this case, if there is any loss of calcium, calcium is trapped by the cuticle. Besides, calcium itself is needed for new walls during IAA-induced growth. Calcium chelator EGTA and low pH increase the extensibility of isolated walls (Virk and Cleland 1988), but EGTA in strong buffer and another calcium chelator Quin 2 remove wall calcium at first without any increase in wall extensibility (Rayle 1989, Virk and Cleland 1990, Cleland et al. 1990).

According to the acid-growth hypothesis (Rayle and Cleland 1970, Cleland 1971; Hager et al. 1971), auxin induces medium acidification to cause growth (Durran and Rayle 1973, Cleland 1975, Cleland 1976, Cleland 1980, Lüthen and Böttger 1989). However some workers still have questions regarding the significance of the auxin-induced medium acidification to cause cell elongation (Kutschera and Schopfer 1985a, Senn and Goldsmith 1988, Schopfer 1989). It was suggested that the growth induced by medium acidification involves activation of some wall enzymes by low pH to cause wall loosening (McQueen-Mason et al. 1992).

Plant cell walls contain weak acid polymers and according to the WADM model (Richter and Dainty 1990b, Ryan, Newman and Arif 1992), wall calcium is separated into calcium condensed to the weak acids of wall polymers and calcium in the DFS. My hypothesis is that the auxin-induced wall acidification mentioned in the acid-growth hypothesis causes removal of condensed calcium in the walls as is consistent with the calcium bridge hypothesis. When the pH of the walls decreases during the auxin-induced proton extrusion, more weak acids of wall polymers are protonated by removing the condensed calcium. The removed calcium could include calcium that cross links between the wall pectins and other macromolecules and acts as the load-bearing bond of the walls. As a consequence of this proton-calcium exchange, I expect that not only protons but also calcium are extruded out to the external medium during auxin-induced wall acidification. Based on this argument, I undertook simultaneous observation of proton and calcium fluxes adjacent to the cell walls to study proton-calcium exchange during wall acidification induced by IAA or other growth substances.

The Microelectrode Ion Flux Estimation (MIFE) technique has been applied successfully to determine fluxes of particular ions in low salt solutions by measuring their electrochemical potential gradients adjacent to the tissue surfaces (Newman et al. 1987, Ryan, Newman and Arif 1992). Using the

technique, fluxes of several ions can be determined simultaneously and the flux determination can be carried out with relatively high solution/tissue volume ratio. In this study, this technique was used to test the hypothesis. Since proton extrusion induced by fusicoccin is substantial, fusicoccin was used first to investigate the possibility of the proton-calcium exchange in the walls of plant cells. After that, effect of exogenous IAA was studied. The results of the observation of proton flux also contribute in clarifying doubts about the significance and the time lag of the medium acidification to cause growth during IAA action. The fluxes of potassium and chloride were also investigated in some treatments to study their involvement in charge balancing. The membrane potential was measured using the standard technique available.

1.6 The Structure of the Thesis

Chapter 1 Describes the development of the unifying hypothesis of proton-calcium exchange in the wall when protons are extruded out during the growth of plant cells. It begins with the description of the growth of plants and the responses of growth substances. This chapter also describes the physics of the growth and the structure of the walls. Reviews about the mechanism of wall loosening that initiates the growth are then given to provide some bases for the development of the hypothesis.

Chapter 2 Describes the plant materials used in the present study. It includes the conditions used to grow the plants and the preparation of the plant segments for the measurements. The general description of the flux measurements and the membrane potential measurements is also given. The Microelectrode Ion Flux Estimation (MIFE) technique used to determine ion fluxes itself is described in Appendix A.

Chapter 3 The determination of proton flux in buffered solutions by measuring the electrochemical potential gradient of protons is in error because some of the diffusing protons are carried by the buffer. In this chapter, the analysis is carried out to calculate the error. The result is the ratio between the proton flux carried by the buffer and the apparent proton flux. This analysis also includes the error for buffers which have more than one pK value.

Chapter 4 The analysis of the WADM model for fluxes is given to describe the change of the ionic condition in the walls, as well as the ion fluxes

outside the wall, when protons are extruded from the cells to the cell walls. The WADM model for fluxes is the key issue for the present hypothesis of proton-calcium exchange in the walls during proton extrusion. This chapter also describes the effects of wall parameter uncertainties on the WADM model for fluxes.

Chapter 5 Provides the results of the simultaneous flux measurements of protons, calcium and potassium and the membrane potential measurements during fusicoccin action on oats. The WADM model for fluxes is applied on the observed fusicoccin-induced proton and calcium effluxes and the results are discussed in relation to the validity of the proton-calcium exchange in the walls. The role of condensed calcium in the walls is also discussed.

Chapter 6 The results of the flux measurements and the membrane potential measurements during IAA action on oats are presented. Discussion is also given to relate the IAA-induced proton and calcium effluxes to the proton-calcium exchange expected from the WADM model. The exchange in the walls is also discussed in relation to the different lags of the IAA-induced proton extrusion, membrane hyperpolarization and growth.

Chapter 7 The development of solid-state chloride microelectrodes is described. The microelectrodes are used to measure the chloride flux during IAA action on oats.

Chapter 8 Describes the results of the flux measurements and the membrane potential measurements during fusicoccin and IAA action on peas. In this Chapter, the WADM model for fluxes is applied on the observed fusicoccin-induced proton and calcium effluxes. It is shown that pea responses to IAA are different from oats.

Chapter 9 Provides a general conclusion that can be drawn from all results obtained in the present study. The discussion is also given to justify the validity of the hypothesis of the proton-calcium exchange when protons are extruded during the growth of plants.

<div style="text-align: center">

Chapter 2

MATERIALS AND METHODS

</div>

2.1 Plant Materials

In this thesis, study of proton-calcium exchange during the early process of growth is carried out in two different plant materials. The plant materials are oats (*Avena sativa* L.) for representing graminaceous monocots and peas (*Pisum sativum* L.) for representing dicots.

Seeds of *Avena sativa* L. cv Victory I were obtained from Svalöf AB, Svalöf, Sweden. To obtain seedlings necessary for the experiments, husks were removed from seeds and the peeled seeds were then held in individual perspex holders with filter papers (refer to Newman 1963). After that, the seeds were germinated and grown by moistening the filter papers with distilled water, in darkness. The temperature of the growing cabinet was 23-24 °C. At the beginning of the second day, the seeds were illuminated with a red light for 1 hour to slow the growth of their mesocotyl. When the growth of mesocotyl is slow, the straight hole in the holders causes the coleoptile to grow straight. As a result, after 4 days, the seedlings generally had straight coleoptiles 3-4.5 cm long. Seedlings with coleoptiles not in that range were not used.

The apical 3 mm was removed from a 4-day-old coleoptile and then a 12 mm long segment was cut. The segment was split longitudinally between vascular bundles and the primary leaf was removed. During this process, the coleoptile segments were held using fingers and cutting was carried out using new "Blue Gillette" blades. Senn and Goldsmith (1988) have shown that the auxin response of a split segment was equivalent to that from a peeled segment. The split segment was held on a plastic sponge using cotton thread and then preincubated in unbuffered solution BSM (basal salt medium) for the desired

duration. BSM contains 0.1 mole m^{-3} KCl and 0.1 mole m^{-3} CaCl$_2$ adjusted to pH 6 using NaOH (to give the final concentration of sodium ion of about 0.02 mole m^{-3}). During the preincubation, the solution was bubbled with a fine stream of air. Preincubation was essential for the split segments to diminish the wounding effect of being split. Hush et al. (1992) have shown that ion fluxes induced by wounding last for several hours. The whole preparation was performed under room illumination and room temperature (20 °C).

Seeds of *Pisum sativum* L. line 107 were obtained from Prof. J. Reid, Plant Science Department, University of Tasmania. The growth of line 107 is fast so that it is good for growth study. Seedlings were obtained in the following way. Seeds were soaked for about 24 hours in aerated buffered solution containing 1 mole m^{-3} NaCl, 1 mole m^{-3} Ca(NO$_3$)$_2$, 1 mole m^{-3} KH$_2$PO$_4$, and 0.25 mole m^{-3} MgSO$_4$, adjusted to pH 6.5 using NaOH which added sodium of about 0.7 mole m^{-3} to the solution (1x solution). After the seeds were husked, they were grown in moist vermiculite containing 1x solution in darkness. After 6-7 days, the third node of the seedlings was between 20-30 mm. When the third node was not in this range, the seedlings were excluded. The temperature of the growing cabinet was about 23 °C.

The third node was cut 3 mm below the leaf and the cuticle was peeled using a circular blade specially made from stainless steel. Using this circular blade, all cuticles around an epicotyl segment were peeled by pushing the segment through the blade. It was necessary to peel all cuticles around an epicotyl segment so that the growth of the segment was straight. Segments that had straight growth were required for flux measurements during the growth of the segments using the MIFE technique since the tips of the microelectrodes had to be placed at a certain distance close to the surface of the segments. When the segments bent because of the growth during the measurements, the distance changed and therefore it needed adjustment. The adjustment might cause some disturbance on the flux measurements. This could be avoided when segments with straight growth were used.

A 12 mm peeled segment was then cut, held on a plastic sponge using cotton thread and preincubated in aerated BSM for desired duration to reduce the effect of being peeled. This preparation was also carried out under room illumination and room temperature (20 °C).
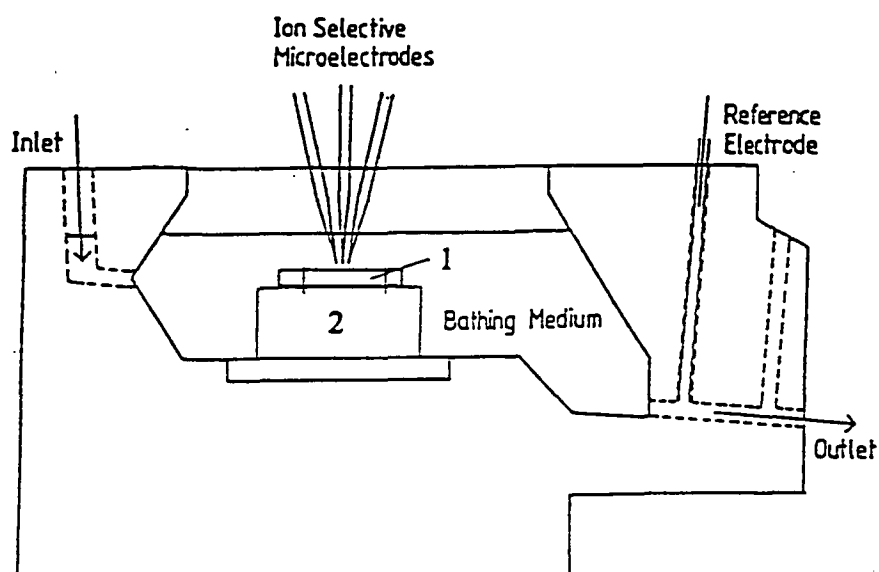
Figure 2.1

The measurement chamber. A segment (1) was held horizontally using cotton threads on a plastic sponge (2). The tips of the microelectrodes were placed 10 μm apart close to the cut surface. The chamber was designed to allow "flow through" change of solution. The volume of the solution in the chamber was about 7.5×10^{-6} m^{-3}.

2.2 Ion Flux Measurements

Fluxes of potassium, proton, and calcium were determined using the Microelectrode Ion Flux Estimation (MIFE) technique. The use of this technique for ion flux determination has been described previously (Lucas and Kochian 1986, Newman et al. 1987, Henriksen et al. 1990, Henriksen et al. 1992, Ryan et al. 1990, Ryan, Newman, Arif 1992). The liquid ion-exchange resins for potassium, protons and calcium were 60031 K^+-cocktail, 82500 H^+-cocktail, and 21048 Ca^{2+}-cocktail (Fluka Chemie AG, Buchs, Switzerland). The microelectrodes had tip diameters of about 5 μm and resistances of about 5 GΩ. In the case of measuring chloride fluxes, however, the available liquid chloride-exchange resin was not used because the selectivity of the resin to chloride was found to be not high enough. Therefore, I developed chloride selective microelectrodes using Ag/AgCl half cells. This is discussed in Chapter 7.

In our laboratory, the measurement system allows 3 microelectrodes to be mounted at a time. Therefore, it is possible to measure the fluxes of three different ions simultaneously.

The determination of ion fluxes began by measuring the Nernst slope of each ion selective microelectrode. These Nernst slopes would then be used to convert the electrochemical potentials detected by each microelectrode in a certain position to their ion activities. The flux of a particular ion was determined using Fick's law based on the measurement of the electrochemical potential gradient between two positions in the direction of the flux. (see Appendix A for further details).

The plastic sponge, with a preincubated segment held on horizontally (with the cut surface face up for split oat segments) and clamped firmly using cotton threads, was mounted in the chamber and bathed with BSM (Figure 2.1). The tissue surface was about 5 mm below the surface of the solution. The reference electrode was an Ag-AgCl electrode in a plastic tube containing 10^3 mole m^{-3} KCl (in 1% agar). This reference electrode was located in the solution at the outflow end of the chamber. The tips of the calibrated ion selective microelectrodes were than placed 10 μm apart close to the cut surface. The measurements of the ion fluxes were then started in stagnant diffusion limited solution. The measurements were carried out under room illumination and room

incandescent
temperature (20 °C). The light power was 100 watt, placed at about 1 m above
the measurement chamber.

Application of growth substances (fusicoccin and IAA, obtained from
Sigma Chemical Co., St. Louis, Mo., USA no. F-4386 and I-2886) were
carried out in two different methods. The first method of application was by
adding a small amount of very concentrated solution of the growth substance to
the chamber and mixing to give the desired concentration. In this case, the
plastic tube connected to the chamber was moved up and down several times so
that the movement of the solution between the chamber and the plastic tube gave
some mixing to the solution in the chamber. It was observed using dyes that the
mixing was almost completed after about half a minute. During this process, the
position of the microelectrode tips was not disturbed. This method was applied
for fusicoccin since fusicoccin solution was limited. In some experiments, IAA
was also applied using this method. However, most IAA experiments were
carried out using the second methods.

The second method of application was by flowing a solution containing
the growth substance with the desired concentration into the chamber at one end
while the solution in the chamber flowed out at the other end. The measurement
chamber was designed to allow "flow through" change of solution. Using a
dye-coloured solution to replace the solution in the chamber, it was observed
that the solution replacement was almost complete within less than half a
minute. The volume of the solution flowed through the chamber during the
replacement was about 30×10^{-6} m^{-3} (4 times the volume of the chamber). Before
the solution replacement was carried out, the microelectrode tips were first
moved away from the cut surface, but they were still in the solution. During the
solution replacement, the volume of the solution in the chamber was kept
constant. After the solution replacement, the tips of the microelectrodes were
again placed close to the cut surface. The whole process of these two methods
of the application of growth substance took about 3-4 minutes.

Effects of solution changing on ion flux measurements were observed
by flowing fresh solution into the chamber. After that, the measurement was
continued.

Effects of IAA action were observed by replacing solution in the
chamber with BEI (BSM + 0.01 mole m^{-3} IAA + 0.5% ethanol adjusted to pH 6
using NaOH so that the final sodium concentration was about 0.03 mole m^{-3}).

Because ethanol was used to dissolve IAA, to observe the real effect of IAA, it was necessary to carried out the measurements in BSM with the same amount of ethanol (BET) before the measurements in BSM with IAA were carried out. Therefore a typical sequence of the solution change was BSM-BSM-BET-BEI. In some experiments, the solution change effects were observed in the presence of 0.5% ethanol. Therefore, the sequence of the solution changes was BET-BET-BEI. Sometimes, the presence of ethanol is also ignored so that the IAA effects were observed by replacing BSM with BEI.

2.3. Membrane Potential Measurements

The membrane potentials of intact parenchymal cells in the cut surface of split oat segments and peeled pea segments were measured in a stagnant solution with standard microelectrodes filled with 500 mole m^{-3} M KCl. The fabrication of the microelectrodes for membrane potential measurements is described in Appendix A. A segment was mounted similarly as in ion flux measurements and bathed with BSM in the chamber. The hydraulic micromanipulator (Narishige Scientific Instrument Lab, Tokyo, Japan) together with optimum illumination allowed the tip of the electrode to be driven into the top of a chosen parenchymal cell. The measurement was started by inserting the electrode tip into the cell. While the tip was still in the cell, the solution in the chamber was altered to observe the effects of fusicoccin, IAA or solution change on the membrane potential. When the electrode bent due to growth of the segment, the hydraulic micromanipulator allowed it to be straightened with no disturbance to the membrane potential measurements.

In this study, growth not specifically measured, but it was noted that within 40 minutes, fusicoccin or IAA caused 12 mm segments of oats or peas to elongate about 1-2 mm.

Chapter 3

BUFFER EFFECTS ON

PROTON FLUX OBSERVATION

3.1 Introduction

Using the Microelectrode Ion Flux Estimation (MIFE) technique (Lucas and Kochian 1986, Newman et al. 1987, Henriksen et al. 1990, Henriksen et al. 1992, Ryan et al. 1990, Ryan, Newman, Arif 1992, see also Appendix A), the net flux of a particular ion at the surface of plant tissues in solution is determined by measuring the electrochemical potential gradient of the ion adjacent to the surface. Protons are one of the ions whose flux can be measured. In buffered solutions, any changes in pH, and thereby changes in the electrochemical potential of protons, are resisted. Therefore when protons are entering the solution at the tissue boundary, some of the diffusing protons are bound by the buffer and these protons diffuse as protonated buffer. As a result, the electrochemical gradient of protons adjacent to the surface is smaller than the gradient would be in unbuffered solution. Finally, the measurement of the true net proton flux at the boundary is underestimated using the MIFE technique. In the opposite case where protons are leaving the buffered solution at the boundary, the process is similar.

In the case where buffered solutions are deliberately used in the determination of proton flux by measuring proton electrochemical potential gradient, it is necessary to estimate the part of protons that diffuse as protonated buffer. When the measurements are carried out in unbuffered solutions, there is still buffering effect of carbonate due to carbon dioxide dissolved from the atmosphere. Water as a solvent also gives buffering effects since water acts as a

weak acid as well as a weak base. Based on this fact therefore, the buffering effects on the proton flux determination is analysed.

The protonated buffer flux, as well as the true net proton flux at the boundary, can be calculated from the measured proton flux and the buffer properties. This chapter describes the calculation and discusses some of the aspects.

3.2 The Properties of Single pK Buffers

In general, buffer action is exhibited by ions of weak acids or bases. However, practically, the best buffer action is exhibited by a mixture of a weak acid or base and its salt (White et al. 1968, Chang 1977). To begin with, buffer action exhibited by a mixture of a simple weak acid HA, that has single dissociation constant K, and its salt BA is discussed. In this case, the weak acid partially dissociates and the salt completely dissociates.

$$HA \leftrightarrow H^+ + A^-.$$ 3.1

$$BA \rightarrow B^+ + A^-.$$ 3.2

In solution, the mixture obeys the Henderson-Hasselbalch equation:

$$pH = pK + \log \frac{[A^-]}{[HA]},$$ 3.3

where $[A^-]$ and $[HA]$ are the total concentrations of A^- and HA in the solution (pH and pK have their usual definitions). In this case, the activity coefficients of A^- and HA are assumed to be the same. In dilute solution, they are near one, anyway. When a living tissue segment is placed in the solution, some of the buffer is taken up by cells in the tissue. However, the amount is very small compared to the amount of the buffer in the solution. Therefore, it is assumed that the total concentration of the buffer in the solution C ($=[A^-] + [HA]$, in mole m^{-3}) is constant everywhere. Hence, based on equation 3.3,

$$[A^-] = C \frac{10^{pH}}{10^{pH} + 10^{pK}},$$ 3.4

and

$$[HA] = C \frac{10^{pK}}{10^{pH} + 10^{pK}}.$$ 3.5

Figure 3.1 describes the relation between [HA] and [A⁻] and the pH of 10 mole m⁻³ acetate buffer (pK=4.75). It is clear that when the pH is much smaller than the pK, the buffer is mostly in the form of HA. The buffer is mostly in the form of A⁻ when the pH is much bigger than the pK. The effectiveness of a buffer is represented by the buffering capacity (β) of the buffer. β is defined as the amount of acid or base that must be added to the buffer in order to produce a unit change of pH. Therefore,

$$\beta = \frac{d[A^-]}{dpH} = -\frac{d[HA]}{dpH}.$$ 3.6

When equation 3.4 or 3.5 is substituted into this equation, the same solution for β is obtained,

$$\beta = C \ln 10 \frac{10^{pH} \, 10^{pK}}{\left(10^{pH} + 10^{pK}\right)^2}.$$ 3.7

Figure 3.2 shows the buffering capacity of 10 mole m⁻³ acetate buffer as function of pH. From this graph, it is clear that a buffer is effective at pH around the pK of the buffer. At pH far away from the pK, the buffer is no longer effective. When protons are added to the buffered solution, some of these protons bind to unprotonated buffer to form protonated buffer and the rest decreases the pH of the solution. The proportion depends on the pH of the solution and the pK of the buffer. When the pH is lower than the pK, most of the protons are for decreasing the pH of the solution. Therefore the buffering capacity is low. When the pH is around the pK, the unprotonated buffer binds most of the added protons to resist the pH of the solution to change. Therefore the buffering capacity is high. Now, when the pH is higher than the pK, most of the protons also bind to the unprotonated buffer. However, the rest of the added protons, although small, is still enough to cause a significant decrease in the pH of the solution since the amount of protons in high pH solution is very small. As a result, the buffering capacity is low.
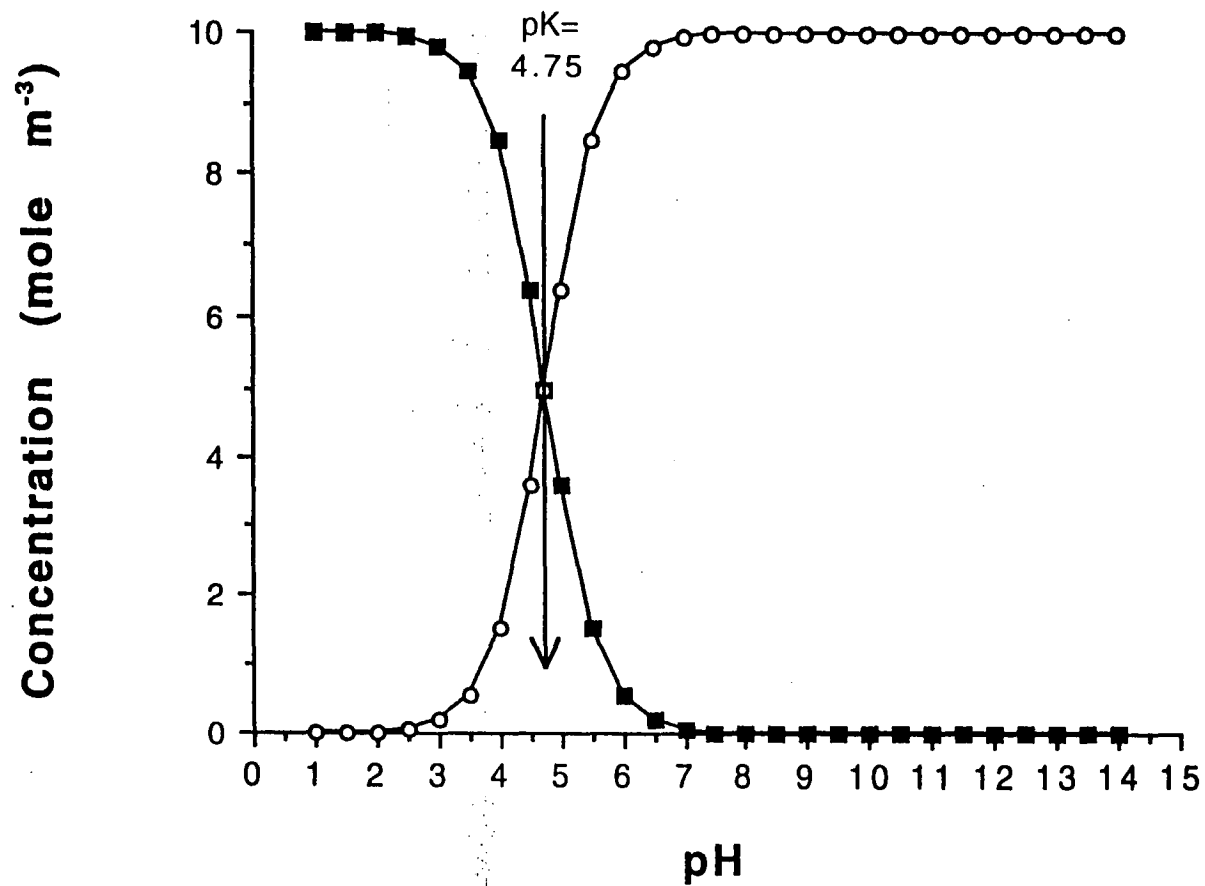
Figure 3.1

The concentration of the associated buffer [HA] (■) and the concentration of the dissociated buffer [A⁻] (O) of 10 mole m⁻³ acetate buffer (pK=4.75) at different pH values.

Figure 3.2

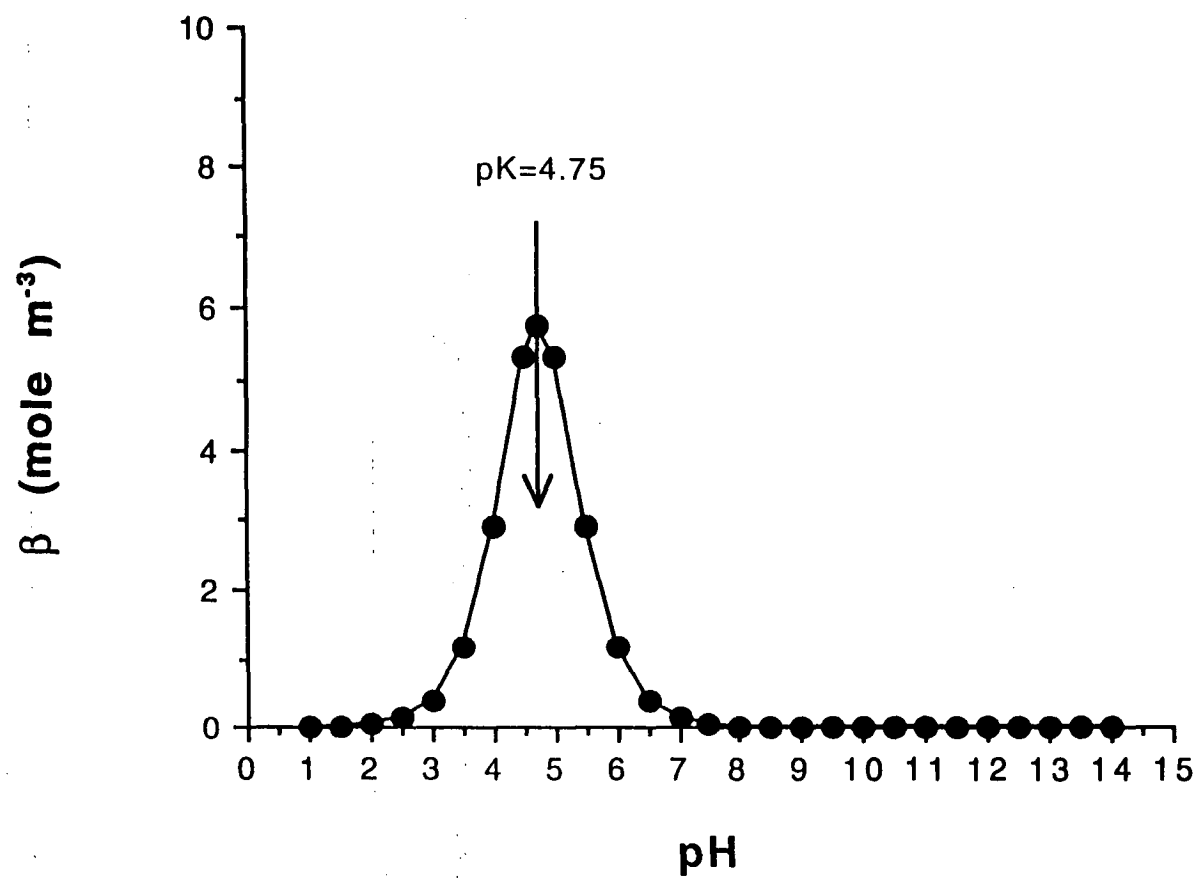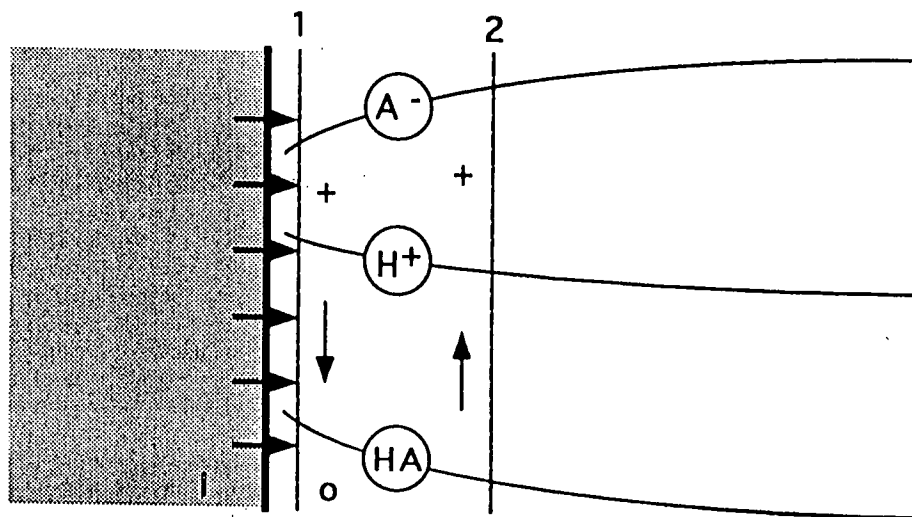The buffering capacity (β) of 10 mole m^{-3} acetate buffer at different pH values.

Figure 3.3

Diagram of concentration gradients of A⁻, H⁺ and HA close to the tissue surface when protons are extruded from the tissue to a buffered solution.

3.3 Flux Ratio Calculation

Suppose using proton selective microelectrodes, it is observed that there is proton gradient due to proton efflux from the tissue to the bathing medium which is buffered with the mixture of HA and BA. This means that the measured proton concentration at position 1 ($[H^+]_1$) is higher than at position 2 ($[H^+]_2$) (see Figure 3.3). Therefore, pH_1 is lower than pH_2. It is assumed that at any position in the solution, including the two positions, the Henderson-Hasselbalch equation (equation 3.3) is satisfied and the total concentration of the buffer C ($=[A^-] + [HA]$, in mole m^{-3}) is constant. $[HA]_1$ would therefore be bigger than $[HA]_2$. Consequently, $[A^-]_1$ would be smaller than $[A^-]_2$. As a result, the concentration gradient of A^- causes A^- to diffuse from position 2 to position 1. At position 1, A^- associates with an extruded proton to form HA. In that time, the concentration gradient of HA causes HA to diffuse from position 1 to position 2. At this position, HA dissociates a proton to form A^-. The mobilities of A^- and HA are assumed to be the same. Therefore the rate of association between A^- and the extruded protons in position 1 is the same as the rate of proton release by HA in position 2. This process keeps going unless the proton efflux stops. This explains why in buffered solutions, some of the proton efflux is represented by the "efflux" of the protonated buffer (HA). The following analysis is carried out to calculate the ratio between the protonated buffer flux and the measured proton flux.

The proton flux is given by

$$J_{H^+} = -[H^+] \, u_{H^+} \frac{d\mu_{H^+}}{dx},$$ \hfill 3.8

where $[H^+]$ is the concentration of proton ions in mole m^{-3}, u_{H^+} is the mobility of protons, and μ_{H^+} is the electrochemical potential of protons which is expressed by the following equation.

$$\mu_{H^+} = \mu_{H^+}^{ref} + R \, T \, \ln(\gamma_{H^+}[H^+]) + z_{H^+} \, F \, E.$$ \hfill 3.9

In this equation, the pressure and gravitational terms are not included because their effects on the electrochemical potential gradient are negligible. $\mu_{H^+}^{ref}$ is the reference of the electrochemical potential of protons, γ_{H^+} is the activity coefficient of protons, z_{H^+} is equal to 1, and E is the electrical potential. R, T,

and F have their usual meanings. When equation 3.9 is substituted into equation 3.8, the flux becomes

$$J_{H^+} = -u_{H^+}\left(R\,T\,\frac{d[H^+]}{dx} + [H^+]\,F\,\frac{dE}{dx}\right). \qquad 3.10$$

For flux experiments using the MIFE technique, an external electric field usually is not applied in the bathing medium. Therefore, the only electric potential gradient that may present in the medium is due to the diffusion of ions (diffusion potential). The diffusion potential depends on both the mobility difference between cations and anions and the concentration difference in the medium (Nobel 1974, p.106-108). Now we are considering a medium dominated by the bulk concentration of K^+, Ca^{2+}, Na^+, and Cl^-. These ions have similar mobilities. Their distribution in the medium is also almost uniform. Therefore, the potential gradient as the result of the diffusion of these ions should be small and negligible. As a result, we may neglect the contribution of the potential gradient on the proton flux so that the flux becomes

$$J_{H^+} = -u_{H^+}\,R\,T\,\frac{d[H^+]}{dx}. \qquad 3.11$$

Similarly, the flux of [HA] is given by

$$J_{HA} = -[HA]\,u_{HA}\,\frac{d\mu_{HA}}{dx}, \qquad 3.12$$

where u_{HA} is the mobility of the protonated buffer and μ_{HA} is its electrochemical potential which is expressed by the following equation.

$$\mu_{HA} = \mu_{HA}^{ref} + R\,T\,\ln(\gamma_{HA}\,[HA]). \qquad 3.13$$

μ_{HA}^{ref} is the reference of the electrochemical potential of the protonated buffer and γ_{HA} is its activity coefficient. The electrical term is not included here because the valency of HA is zero. Therefore, the flux of the protonated buffer becomes

$$J_{HA} = -u_{HA}\,R\,T\,\frac{d[HA]}{dx}. \qquad 3.14$$

When equation 3.5 is substituted into this equation and

$$pH = -\log\left(\gamma_{H^+}\,[H^+]\,10^{-3}\right), \qquad 3.15$$

we get the following expression for the flux of the protonated buffer.

$$J_{HA} = - u_{HA} \, R \, T \, C \, 10^{-3} \, 10^{pK} \left(\frac{10^{pH}}{10^{pH} + 10^{pK}} \right)^2 \frac{d[H^+]}{dx}.$$
3.16

Based on equation 3.11, this expression can be modified into

$$J_{HA} = \frac{u_{HA}}{u_{H^+}} C \, 10^{-3} \, 10^{pK} \left(\frac{10^{pH}}{10^{pH} + 10^{pK}} \right)^2 J_{H^+}.$$
3.17

Therefore, the ratio of the protonated buffer flux J_{HA} to the measured proton flux J_{H^+} can be obtained as

$$r = \frac{u_{HA}}{u_{H^+}} C \, 10^{-3} \, 10^{pK} \left(\frac{10^{pH}}{10^{pH} + 10^{pK}} \right)^2.$$
3.18

Figure 3.4 shows the result of flux ratio calculation using equation 3.18 when protons are extruded from tissues to 10 mM acetate buffer. It is clear from the equation and the figure that the ratio is dependent on the pH of the solution. When the pH is smaller than the pK,

$$r \approx \frac{u_{HA}}{u_{H^+}} C \, 10^{-3} \, \frac{\left(10^{pH} \right)^2}{10^{pK}}.$$
3.19

In this pH range, the ratio increases with the slope of about 2 (in log scale). The flux ratio is directly proportional to the buffer concentration. Therefore when the pH is 1 unit higher, the ratio is the same as when the buffer concentration is 100 times higher. The slope becomes smaller when the pH of the solution approaches the pK of the buffer. When the pH is larger than the pK, the ratio levels off to reach its maximum,

$$r \approx \frac{u_{HA}}{u_{H^+}} C \, 10^{-3} \, 10^{pK}.$$
3.20

The slope in this pH range is about zero. From equation 3.20, the maximum of the ratio depends on both the concentration and the pK of the buffer. In this case, the pK of the buffer has much more effect compared to the concentration of the buffer.
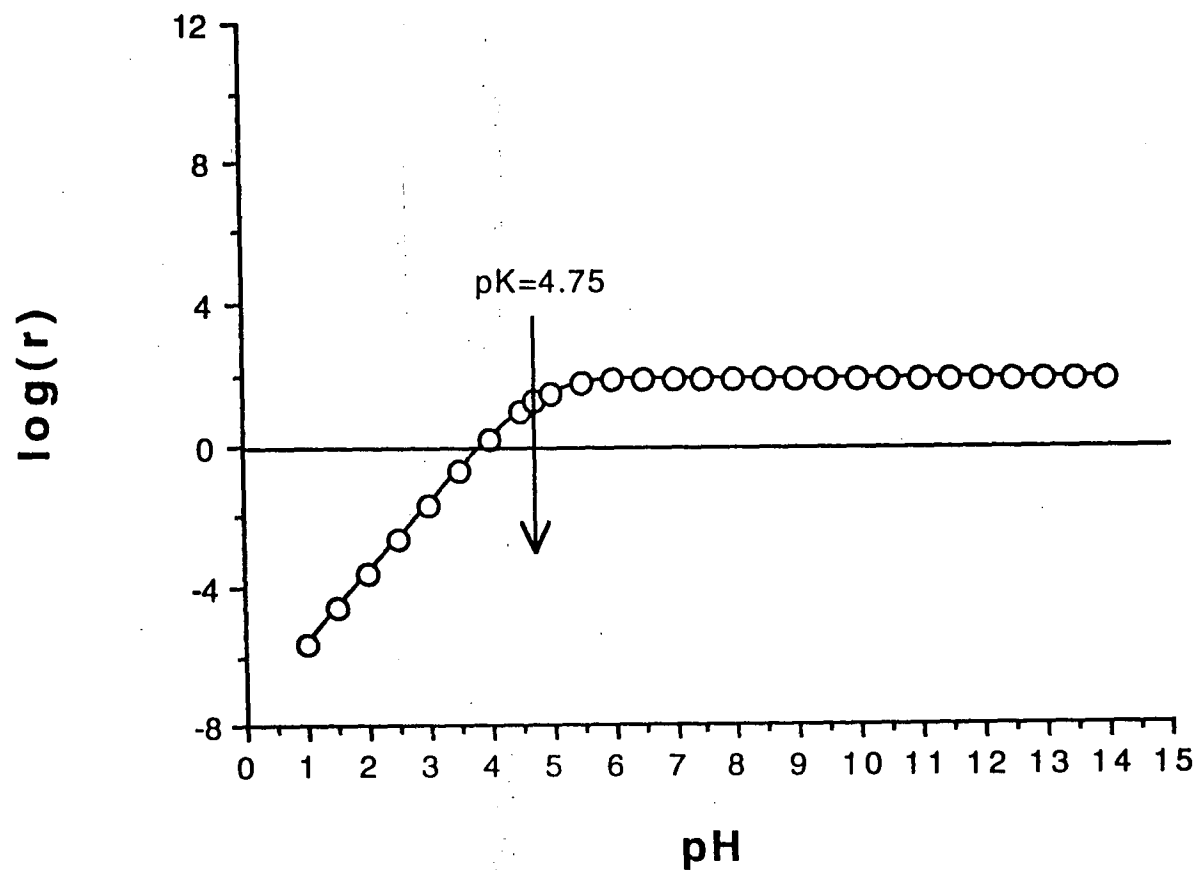
Figure 3.4

The flux ratio (r) close to the tissue surface in 10 mole m^{-3} acetate buffer at different pH values.

The mobility ratio of protonated buffer to protons is taken as 5/37.5.

Figure 3.5

The protonated buffer efflux (solid symbol) and the proton efflux (open symbol) close to the tissue surface at different pH values when 50 nmol. m^{-2} s^{-1} proton efflux presents from the tissue to 10 (□) or 0.1 (○) mole m^{-3} acetate buffer. Log_{10} scale for efflux. Mobility ratio of protonated buffer to protons is taken as 5/37.5.

It may be informative to show J_{H^+} and J_{HA} for a given proton flux at the boundary of the tissue in a buffered solution. Now, when the proton flux at the boundary $J_{H^+}^t$, is constant, where

$$J_{H^+}^t = J_{H^+} + J_{HA} = J_{H^+}(1 + r),$$ 3.21

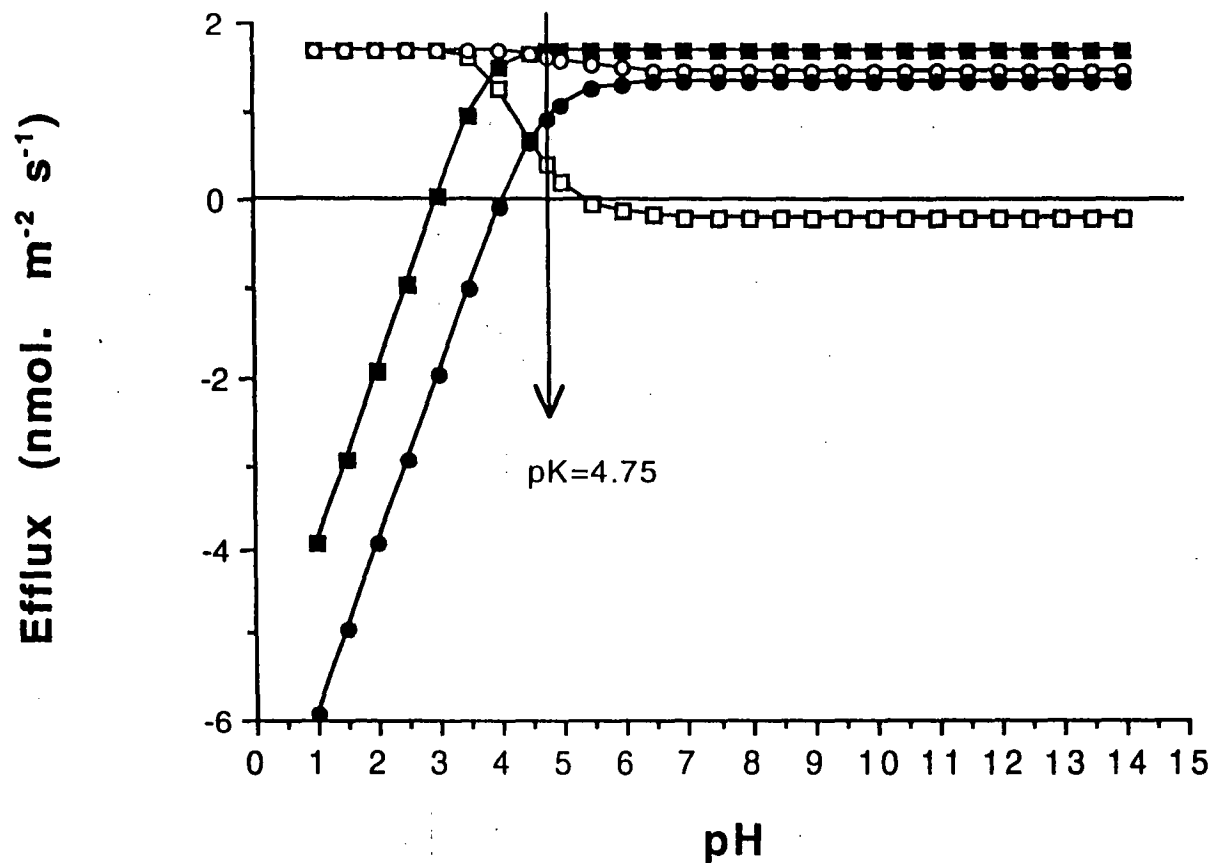the proton flux J_{H^+} and the protonated buffer flux J_{HA} expected in the solution can be represented in terms of $J_{H^+}^t$ and the pH of the solution according to the following equations.

$$J_{H^+} = \frac{J_{H^+}^t(10^{pH} + 10^{pK})^2}{\frac{u_{HA}}{u_{H^+}}C\, 10^{-3}\, 10^{pK}(10^{pH})^2 + (10^{pH} + 10^{pK})^2},$$ 3.22

$$J_{HA} = \frac{J_{H^+}^t \frac{u_{HA}}{u_{H^+}}C\, 10^{-3}\, 10^{pK}(10^{pH})^2}{\frac{u_{HA}}{u_{H^+}}C\, 10^{-3}\, 10^{pK}(10^{pH})^2 + (10^{pH} + 10^{pK})^2}.$$ 3.23

With two different concentrations of acetate buffer (10 and 0.1 mole m^{-3}), these equations are illustrated in Figure 3.5 (in log scale). At pH lower than the pK of the buffer, 50 nmol. m^{-2} s^{-1} proton efflux from tissue mostly exists as proton efflux. In this pH range, the portion of proton efflux that presents as protonated buffer efflux is small and it increases with a slope of about 2 (in log scale). At pH higher than the pK, this portion is bigger than the existing proton efflux if the flux ratio is bigger than 1. Otherwise it is smaller.

3.4 Ratio calculation in Complex Buffer Solutions

Complex buffers are defined as buffers that have more than one dissociation constant such as carbonic and phosphoric buffers. For that kind of buffer, the mathematical analysis for the flux ratio is much more complex compared to the analysis for single pK buffers. Therefore in the following calculation, numerical analysis, which is relatively easier, is used.

To begin with, we consider the proton flux (J_{H^+}) and the average pH (pH$_{av}$) between two positions (1 and 2) in buffered solution adjacent to the tissue surface (see Figure 3.3) where their magnitudes are known from the measurements. Based on equation 3.10, the proton flux is

$$J_{H^+} = - u_{H^+} \left(R T \frac{d[H^+]}{dx} + [H^+]_{av} F \frac{dE}{dx} \right), \qquad 3.24$$

where according to the definition of pH (equation 3.15), the average proton concentration (in mole m^{-3}) is

$$[H^+]_{av} = \frac{10^3}{\gamma_{H^+} 10^{pH_{av}}}. \qquad 3.25$$

Since the two positions are close enough ($\Delta x = x_2 - x_1$ is very short), equation 3.24 can be approximated as

$$J_{H^+} = - u_{H^+} \left(R T \frac{([H^+]_2 - [H^+]_1)}{\Delta x} + [H^+]_{av} F \frac{(E_2 - E_1)}{\Delta x} \right). \qquad 3.26$$

The average proton concentration can also be expressed in terms of the proton concentration in position 1 and 2 according to the following equation.

$$[H^+]_{av} = \frac{1}{2} ([H^+]_1 + [H^+]_2). \qquad 3.27$$

Therefore, when this equation is substituted into equation 3.26 to replace the proton concentration at position 2, we obtain,

$$J_{H^+} = - u_{H^+} \left(2 R T \frac{([H^+]_{av} - [H^+]_1)}{\Delta x} + [H^+]_{av} F \frac{(E_2 - E_1)}{\Delta x} \right). \qquad 3.28$$

When equation 3.25 is substituted into this equation, the proton concentration at position 1 would be

$$[H^+]_1 = \frac{10^3}{\gamma_{H^+} 10^{pH_{av}}} + \frac{\dfrac{J_{H^+} \Delta x}{u_{H^+}} + \dfrac{10^3 F (E_2 - E_1)}{\gamma_{H^+} 10^{pH_{av}}}}{2RT}. \qquad 3.29$$
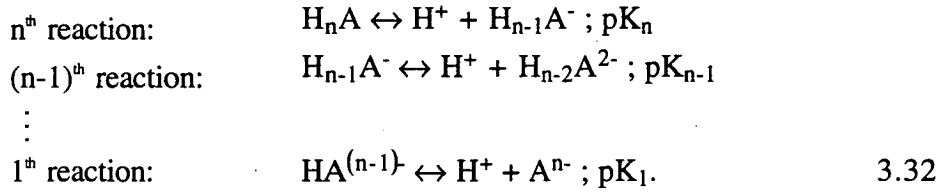
Now, based on the definition of pH (equation 3.15), this equation becomes

$$pH_1 = - \log \left(\frac{1}{10^{pH_{av}}} + \frac{\dfrac{J_{H^+} \Delta x \, \gamma_{H^+}}{u_{H^+} 10^3} + \dfrac{F (E_2 - E_1)}{10^{pH_{av}}}}{2RT} \right). \qquad 3.30$$

When equation 3.27 is substituted into equation 3.26 to replace the proton concentration at position 1, in a similar way, we also obtain

$$pH_2 = -\log\left(\frac{1}{10^{pH_{av}}} - \frac{\dfrac{J_{H^+} \Delta x \, \gamma_{H^+}}{u_{H^+} 10^3} + \dfrac{F(E_2 - E_1)}{10^{pH_{av}}}}{2RT}\right).$$ 3.31

Now, when the buffer has n pK values, there would be n reactions involved:

n^{th} reaction: $\quad H_nA \leftrightarrow H^+ + H_{n-1}A^- \; ; pK_n$

$(n-1)^{th}$ reaction: $\quad H_{n-1}A^- \leftrightarrow H^+ + H_{n-2}A^{2-} \; ; pK_{n-1}$

$\vdots$

1th reaction: $\quad HA^{(n-1)-} \leftrightarrow H^+ + A^{n-} \; ; pK_1.$ 3.32

Each reaction also obeys the Henderson-Hasselbalch equation. Therefore,

$$\frac{\left[H_{n-i}A^{i-}\right]}{\left[H_{n-i+1}A^{(i-1)-}\right]} = 10^{(pH-pK_{n-i+1})} \; ; i = 1, 2, \cdots n.$$ 3.33

In this equation, H_0A^{n-} represents A^{n-}. Based on this equation, the concentration of a particular type of the buffer can be expressed in terms of $[H_nA]$ using the following equation.

$$\left[H_{n-i}A^{i-}\right] = [H_nA] \, 10^{\sum_{k=n-i+1}^{n} (pH-pK_k)}; \; i = 1, 2, \cdots n.$$ 3.34

The total concentration of the buffer in the solution (C) is also assumed to be constant throughout. Therefore,

$$C = \sum_{i=0}^{n} \left[H_{n-i}A^{i-}\right].$$ 3.35

By expressing the concentration of every type of the buffer in this equation in terms of $[H_nA]$ using equation 3.34, we obtain

$$C = [H_nA]\left(1 + \sum_{i=1}^{n} 10^{\sum_{k=n-i+1}^{n} (pH-pK_k)}\right).$$ 3.36

Therefore,

$$[H_nA] = C \left(1 + \sum_{i=1}^{n} 10^{\sum_{k=n-i+1}^{n} (pH - pK_k)} \right)^{-1}.$$ 3.37

The total concentration of the buffer C and the pK of each reaction are given. Therefore, using equations 3.34 and 3.37, the concentration of each type of buffer can be obtained when the pH is known. Now at positions 1 and 2, the pH can be obtained from equations 3.30 and 3.31. Consequently, the concentration of each type of buffer in those positions can also be calculated. Using the same principles as used to derive equation 3.26, the flux of each type of buffer between those positions can be calculated from its concentration at those positions with the following equation.

$$J_{H_{n-i}A^{i-}} = - u_{H_{n-i}A^{i-}} R T \frac{([H_{n-i}A^{i-}]_2 - [H_{n-i}A^{i-}]_1)}{\Delta x}$$
$$- u_{H_{n-i}A^{i-}} \frac{1}{2} ([H_{n-i}A^{i-}]_2 + [H_{n-i}A^{i-}]_1) z_{H_{n-i}A^{i-}} F \frac{(E_2 - E_1)}{\Delta x};$$
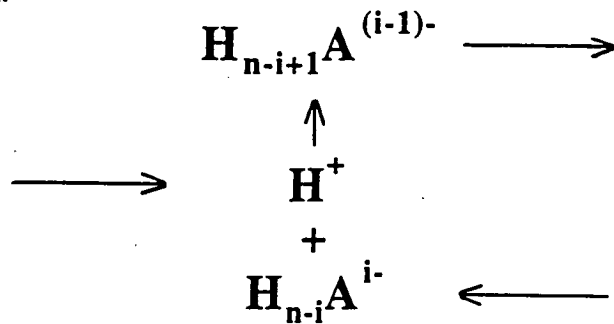$$i = 0, 1, 2, \cdots n.$$ 3.38

$z_{H_{n-i}A^{i-}}$ is equal to $-i$. Equation 3.14 is effectively a special case in relation to this equation with $i=0$. In the equation above, $J_{H_{n-i}A^{i-}}$ is not the flux of $H_{n-i}A^{i-}$, that carries protons, but this is the total flux of $H_{n-i}A^{i-}$ that diffuses to pick up a proton in $(n-i+1)^{th}$ reaction and that diffuses to release a proton in $(n-i)^{th}$ reaction (see equation 3.32 and Figure 3.6). In this case, the flux of $H_{n-i}A^{i-}$ that diffuses to release a proton in $(n-i)^{th}$ reaction is the same but in the opposite direction as the flux of $H_{n-i-1}A^{(i+1)-}$ that diffuses to pick up a proton in the same reaction. Furthermore, $J_{H_{n-i-1}A^{(i+1)-}}$ is the total flux of $H_{n-i-1}A^{(i+1)-}$ that diffuses to pick up a proton in $(n-i)^{th}$ reaction and that diffuses to release a proton in $(n-i-1)^{th}$ reaction. Based on this algorithm therefore, the flux of $H_{n-i}A^{i-}$, that carries protons is,

$$J_{H}{}_{H_{n-i-1}A^{i-}} = - \sum_{j=0}^{n-i-1} J_{H_jA^{(n-j)-}}; \quad i = 0, 1, \cdots (n-1).$$ 3.39

The total flux of protons carried by the buffer J_{HA}^h is obtained by combining the fluxes of all types of the buffer that carry protons,

$$J_{HA}^h = - \sum_{i=0}^{n-1} \sum_{j=0}^{i} J_{H_jA^{(n-j)-}}.$$ 3.40

$(n-i+1)^{th}$ reaction:

$$H_{n-i+1}A^{(i-1)-} \longrightarrow$$

$$\uparrow$$

$$\longrightarrow \quad H^+$$

$$+$$

$$H_{n-i}A^{i-} \quad \longleftarrow$$

- - - - - - - - - - - - - - - - -

$(n-i)^{th}$ reaction:

$$H_{n-i}A^{i-} \longrightarrow$$

$$\uparrow$$

$$\longrightarrow \quad H^+$$

$$+$$

$$H_{n-i-1}A^{(i+1)-} \quad \longleftarrow$$

- - - - - - - - - - - - - - - - -

$(n-i-1)^{th}$ reaction:

$$H_{n-i-1}A^{(i+1)-} \longrightarrow$$

$$\uparrow$$

$$\longrightarrow \quad H^+$$

$$+$$

$$H_{n-i-2}A^{(i+2)-} \quad \longleftarrow$$
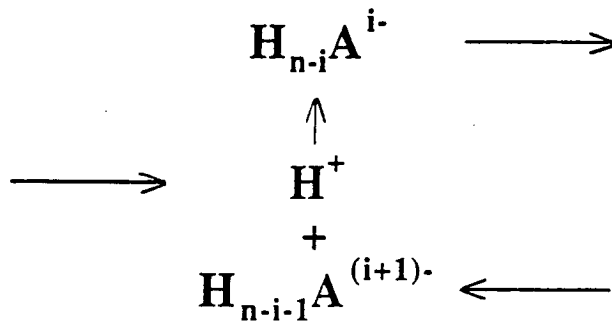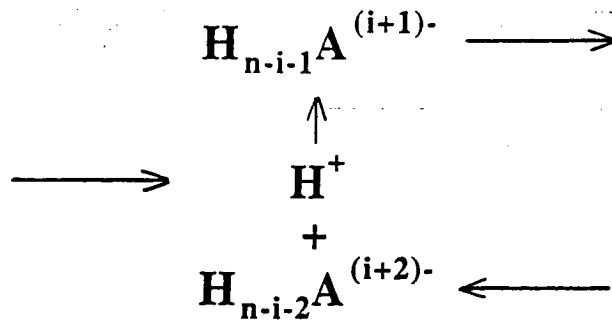
Figure 3.6

Diagram of several reactions of a complex buffer for calculating the total flux of the buffers that carry protons.
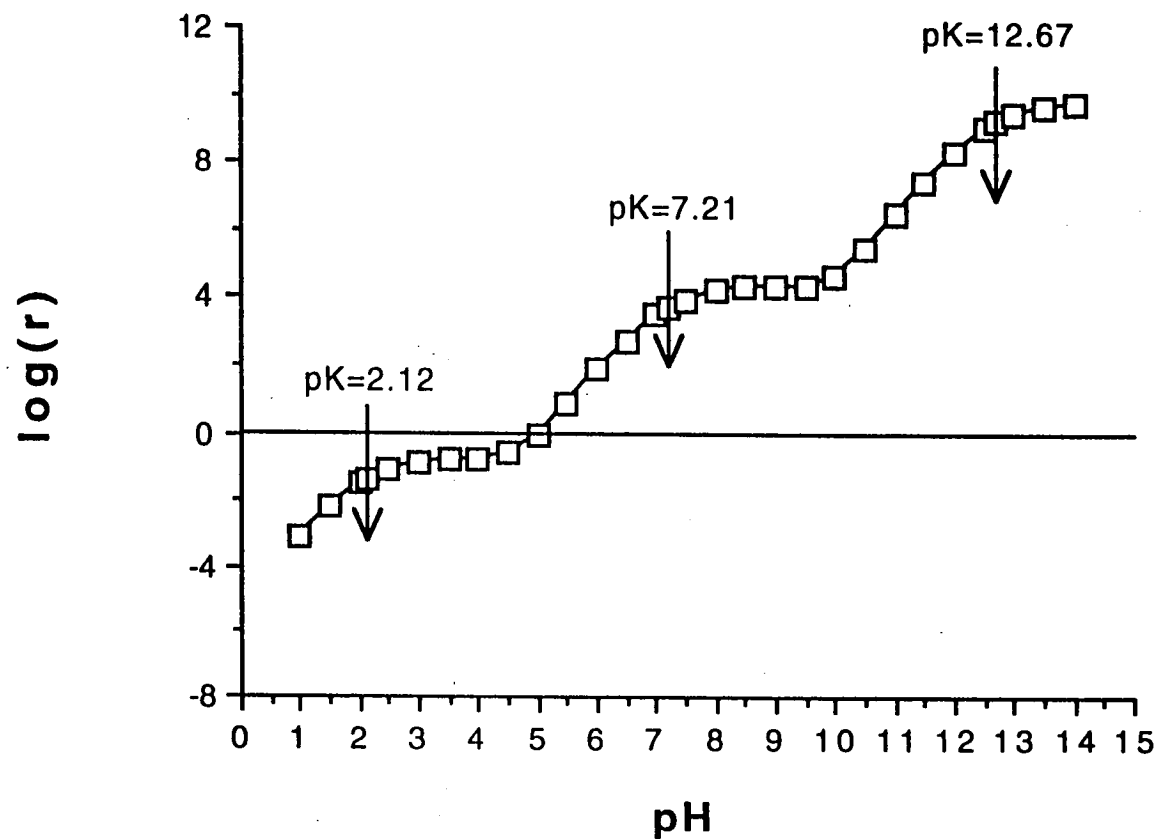
Figure 3.7

The flux ratio (r) close to the tissue surface at different pH values in 10 mole m^{-3} phosphate buffer, that has three dissociation constants (pK$_1$=12.67, pK$_2$=7.21, pK$_3$=2.12). In the flux ratio calculation, E$_2$-E$_1$ is set up to zero.

Mobility ratio of each kind of protonated buffer to protons is taken as 5/37·5.

Figure 3.8

The buffering capacity (β) of 10 mole m^{-3} phosphate buffer at different pH values. In this calculation, E_2-E_1 is set up to zero.

The ratio of the total flux of protons carried by the buffer to the measured proton flux in the buffered solution is

$$r = \frac{J_{HA}}{J_{H^+}}.$$

3.41

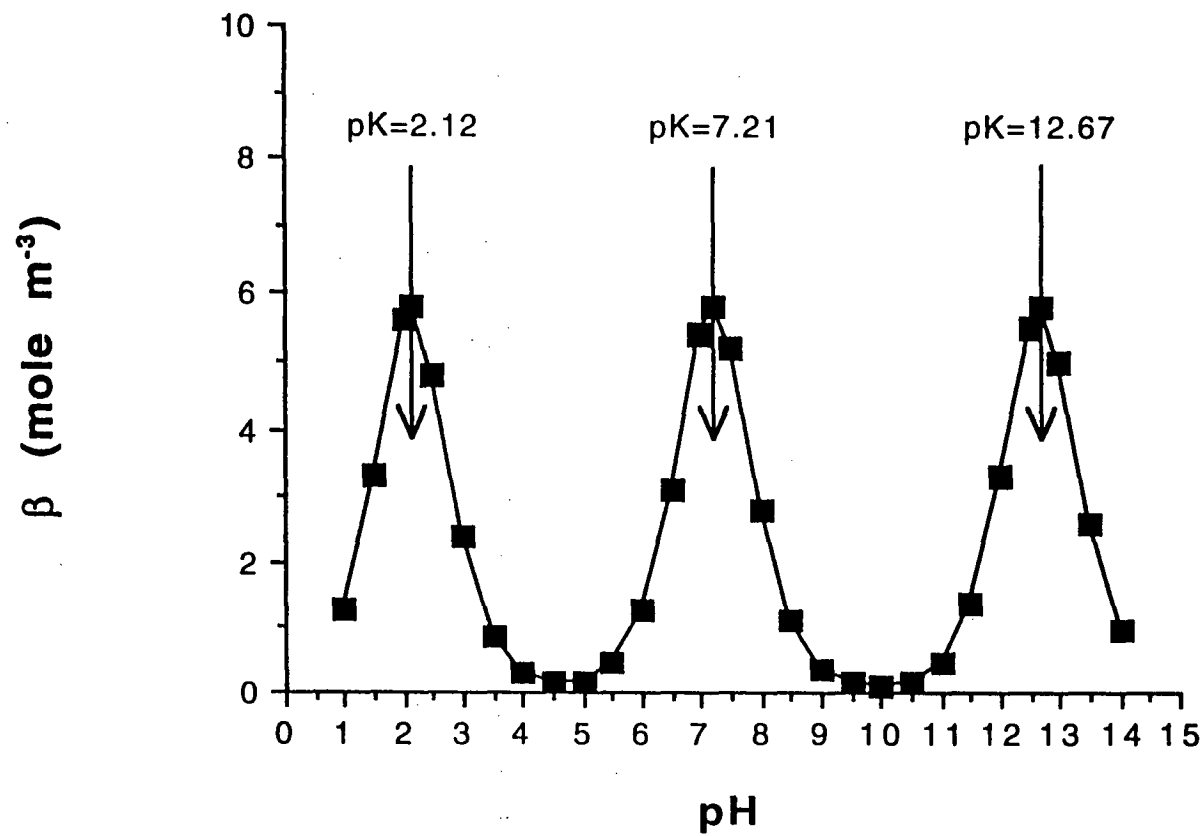Based on equation 3.6, the total buffering capacity of the buffer β can be calculated from the concentration gradient of all protonated buffer types in respect to the pH gradient between position 1 and position 2. To do this calculation, the same principle as used to derive equation 3.40 is used. Therefore,

$$\beta = \frac{\sum_{i=0}^{n-1} \sum_{j=0}^{i} ([H_j A^{(n-j)-}]_2 - [H_j A^{(n-j)-}]_1)}{pH_2 - pH_1}.$$

3.42

Now for 10 mole m^{-3} phosphate buffer with 3 dissociation constants (pK_1=12.67, pK_2=7.21, pK_3=2.12), the flux ratio and the buffering capacity calculated from the equations above are shown in Figure 3.7 and 3.8. In the calculation, E_2-E_1 is set up to zero. Comparing Figures 3.4 and 3.7, the pattern of the flux ratio is similar to the pattern of the flux ratio calculated for single pK buffer. The log of the flux ratio increases when the pH of the solution is lower than the pK. When the pH increases beyond the pK, the ratio levels off. For phosphate buffer therefore, the flux ratio increases three times. As in Figure 3.5, Figure 3.7 also shows that the maximum of the buffering capacity happens when the pH of the solution is the same as the pK of the buffer.

3.5 Effects of Water, Carbonate and Mixed Buffers

Water is always present in solution because it is used as a solvent. In solution, water behaves both as a weak acid as well as a weak base. The concentration of water in solution is also very high. Therefore the buffering effect given by water on the results of proton flux measurements must be considered. Water dissociates according to the following equation.
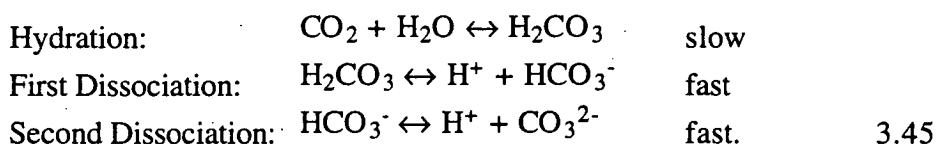
$$H_2O \leftrightarrow H^+ + OH^-.$$

3.43

The dissociation constant is defined as

$$K = \frac{[H^+][OH^-]}{[H_2O]},$$ 3.44

where at 24° C, the ionic product of water ($=[H^+][OH^-]$) is 10^{-14} (Chang 1977). The concentration of water ($[H_2O]$) is about 55.56 M. Therefore, the pK of water is about 15.75. Now if there is proton flux entering (or leaving) a neutral solution (pH=7, from equation 3.7 $\beta=2.303\times10^{-4}$ mole m^{-3}), using equation 3.18, the ratio of the flux of water molecules that carry protons to the flux of protons is about the ratio of the mobility of water molecules to the mobility of protons, which is not far from 1. Let us assume that the flux ratio at this pH is 1. Now, when the pH of the solution is 1 unit higher (pH=8), the ratio would be about 100 since the slope of the flux ratio in pH domain (in log scale) is 2. Therefore, pH 7 can be considered as the boundary above which protons in the solution start to diffuse mostly as water molecules. As a consequence, when the measurements of proton flux are made in solution without buffers but with water at pH higher than 7, the measured proton flux is expected to be small. In order to determine the proton flux in this range, measurements must be carried out on the flux of hydroxyl ions that is the same, but the opposite, as the flux of water molecules that carry most of diffusing protons. At pH 6, the ratio would be about 0.01. This means that the flux of protons carried by water molecules is very small. Therefore, the buffering effect of water on the determination of proton flux at pH 6 and below can be neglected.

Besides the buffering effect of water, the buffering effect of carbonates due to carbon dioxide dissolved from the atmosphere is also present in solution. In the earth atmosphere, there is about 0.026% (v/v) of carbon dioxide. At 20 °C, this is about 0.01067 mole m^{-3}. The equilibrium concentration of carbon dioxide in solution depends on the temperature. At 20 °C, the partition coefficient of the equilibrium concentration of carbon dioxide in the solution and in the adjacent atmospheric gas is 0.88 (Nobel 1974). Therefore at this temperature, the equilibrium concentration of dissolved carbon dioxide is 0.00939 mole m^{-3}. In the solution, the dissolved carbon dioxide reacts with water to form carbonates. The reactions are:

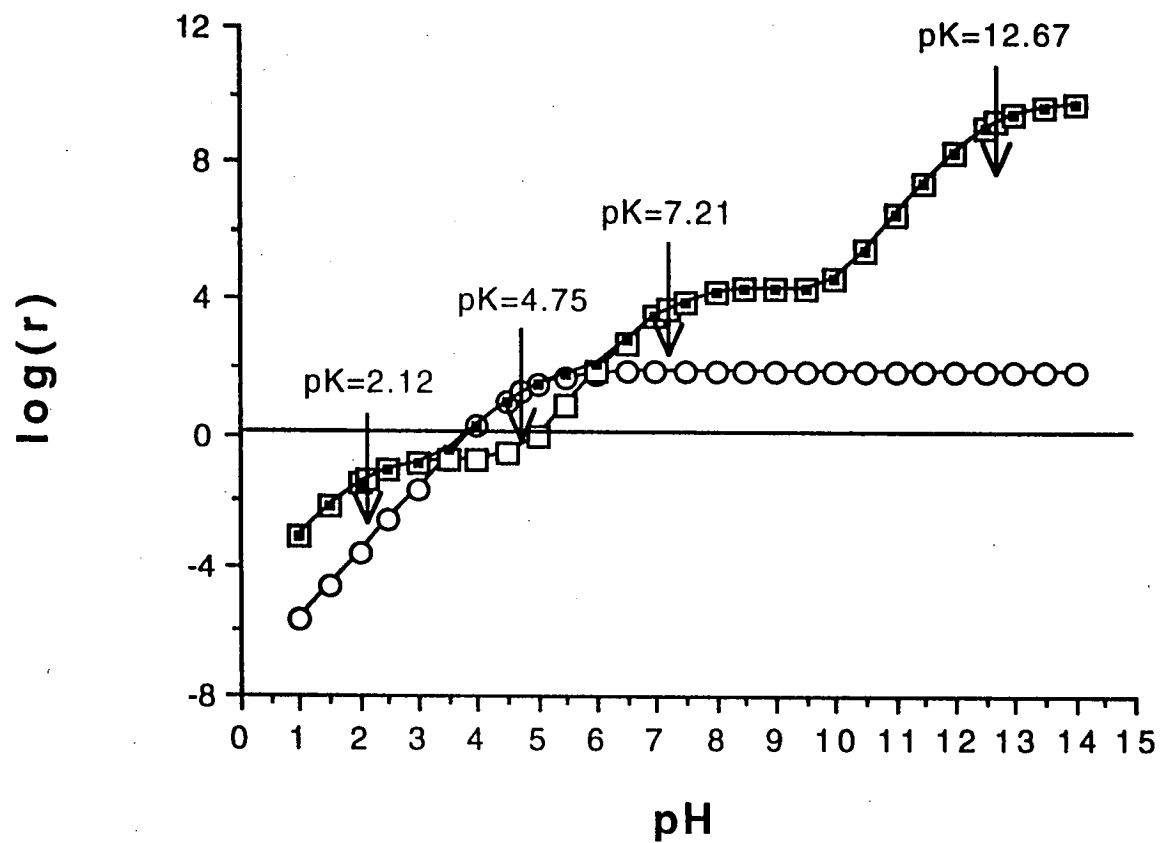|			
Hydration:	$CO_2 + H_2O \leftrightarrow H_2CO_3$	slow	
First Dissociation:	$H_2CO_3 \leftrightarrow H^+ + HCO_3^-$	fast	
Second Dissociation:	$HCO_3^- \leftrightarrow H^+ + CO_3^{2-}$	fast.	3.45

Figure 3.9

The flux ratio (r) in 10 mole m^{-3} acetate buffer (O) and in 10 mole m^{-3} phosphate buffer (□). In the calculation, E$_2$-E$_1$ is set up to zero. When both buffers are mixed, the flux ratio is shown as ■. Mobility ratios : see legends to Figs 3.4 and 3.7.

In these reactions, the equilibrium constant of the hydration reaction is 0.00258, the apparent dissociation constant of the hydration reaction and the first dissociation reaction is 4.2×10^{-7}, and the dissociation constant of the second dissociation reaction is 5.6×10^{-11}. Therefore the total concentration of carbonates due to dissolved atmospheric carbon dioxide in the solution depends on the pH of the solution. Under normal conditions, unbuffered solutions and distilled water prepared for experiments have been equilibrated with atmospheric carbon dioxide at pH around 6. These solutions have total carbonate buffer of not more than 0.004 mole m^{-3}. This concentration increases when the solutions are equilibrated at higher pH for long periods. However for short experiments, although the pH of the solutions is then changed to the desired pH, the concentration of carbonates in the solutions is almost unchanged because the hydration reaction is comparatively slow. For solutions containing 0.004 mole m^{-3} carbonates, the flux ratio calculated using equation 3.41 is about 0.003. This is much smaller than 1. This means that if there is proton flux in these solutions, the flux of protons carried by carbonates is small and therefore, the proton flux determination in these solutions at any experimental pH is almost not altered by the buffering effect of carbonates in the solutions.

Practically, several buffers are used together to obtain effective buffering effects at a certain pH range. For this kind of buffered solution, the flux ratio is additive because each buffer acts independently based on its concentration and its pK value. Complex buffers themselves in fact contain several buffers with different pK values. This means that when proton flux exists in solutions containing several different buffers, the ratio of the total flux of protons carried by the buffers to the flux of protons by themselves is the sum of the flux ratios contributed by all the buffers. For example, the buffering effects of water and carbonates due to dissolved carbon dioxide from the atmosphere are always present together in solutions. As calculated above, at pH 6, the flux ratios due to the buffering effects of water and carbonates are about 0.01 and 0.003 respectively. The sum of both flux ratios is still much less than 1. Therefore at pH 6 or less, the determination of the proton flux is ineffectively altered by their buffering effects. As another example, Figure 3.9 shows the flux ratio as function of pH in solutions containing 10 mole m^{-3} acetate buffer and 10 mole m^{-3} phosphate buffer ($E_2 - E_1$ is set up to zero). When 10 mole m^{-3} phosphate buffer is used separately, at pH 4.75, the buffer has little effect on the measurements of proton flux because the log of the flux ratio is smaller than 0. However when 10 mole m^{-3} acetate buffer is added into this phosphate

buffer, the mixture would be much more effective at pH 4.75 to reduce proton flux in the solution because the log of the total flux ratio is now bigger than 0.

3.5 Conclusion

The determination of proton flux in buffered solution by measuring the proton electrochemical potential gradient is in error because some of the protons diffuse as protonated buffer. The calculation above indicates that the ratio of the protonated buffer flux to the proton flux depends on the pH of the solution. The flux ratio rises with pH when the working pH is lower than the buffer pK and it levels off as the pH increases beyond the pK. At low pH, when protons diffuse in the solution, only small amounts of the diffusing protons are bound by the buffer. Therefore protons diffuse mostly as protons by themselves. At higher pH, more diffusing protons are bound by the buffer. However, whether the portion of protons that diffuse as protonated buffer is larger than the portion of protons that diffuse as protons by themselves depends on the buffer concentration. When the buffer concentration is low so that the flux ratio is less than 1, less protons diffuse as protonated buffer than as protons by themselves. Otherwise the portion of protons that diffuse as protonated buffer is larger.

At pH 6, the flux ratio in unbuffered solutions that always have buffering effects of water and carbonates due to carbon dioxide dissolved from the atmosphere is much smaller than 1. Therefore, measurement of proton flux by determining the electrochemical potential gradient of protons in unbuffered solutions at this pH or below is valid.

Chapter 4

THE WADM MODEL FOR FLUXES

4.1 Introduction

The plasmalemma of plant cells does not directly perceive the ionic composition of the surrounding medium because the walls of the cells modify the ionic composition of the medium at the surface of the plasmalemma (Sentenac and Grignon 1981, Richter and Dainty 1989a). The walls of plant cells contain fixed negative charges. Therefore, cations from the surrounding medium are electrostatically bound in the walls. Since the transport of ions between the cells and the medium operates under the condition of the walls, the knowledge about the ion composition of the walls, that depends on the wall parameters, is important. However direct measurements of the ionic composition of the walls are difficult to carry out. Therefore this has been studied using theoretical models (Sentenac and Grignon 1981, Richter and Dainty 1989a).

With the usual consideration that the walls are an homogenous phase, the composition of ions in the walls in response to the surrounding medium can be estimated using the classical Donnan theory. To refine the analysis, the Donnan theory has been combined with several other aspects. In this case Richter and Dainty (1989a&b, 1990a&b) proposed the Weak Acid Donnan-Manning (WADM) model to explain the ion behaviour in plant cell walls. The model describes the walls of plant cells as a system containing weak acid polymers where the interaction of ions obeys the Manning condensation theory and the Donnan theory. This model has been applied to estimate the composition of ions in the walls of *Chara* when the composition of ions in the surrounding medium was altered (Ryan, Newman, Arif 1992). In Appendix C, the equilibrium WADM model is described in detail. The application of the

model to estimate the ionic composition of the walls when tissues were bathed with BSM or BSM containing IAA, which is a weak acid, is also presented in this appendix.

The composition of ions in the walls is also altered when ions are transported across the walls. This is due to both the interaction of the transported ions with the ions in the walls and the change in the ion concentration in the surrounding medium. In plant cells, some ions are transported across the plasmalemma to or from the walls of the cells. Therefore it is useful to describe the change of the ionic composition in the walls during the transport. In this chapter, the WADM model for fluxes is developed to describe quantitatively the change of the ionic composition in the walls, as well as the ion fluxes outside the walls, when there is a proton efflux from the cell to the walls and the surrounding medium (in this case BSM).

4.2 Initial Conditions

To start with, we consider plant cells bathed with a medium containing $[K_o]$ mole m^{-3} of potassium, $[Ca_o]$ mole m^{-3} of calcium, $[Na_o]$ mole m^{-3} of sodium, $[Cl_o]$ mole m^{-3} of chloride, at pH_o. Based on the definition of pH, the concentration of protons in the medium is

$$[H_o] = \frac{10^3}{\gamma_{1o}} 10^{-pH_o} \qquad\qquad 4.1$$

where γ_{1o} is the activity coefficient of monovalent ions in the bathing medium. At t=0, it is assumed that the flux of every ion across the plasmalemma and the cell walls is zero and the equilibrium between the walls and the bathing medium has been established. In this situation, the concentration of ions in the (WFS) is ⟵ *water free space*

the same as in the bathing medium. Therefore, the initial concentration of the ions of interest in the WFS can be expressed as $[K_o](0)$, $[Ca_o](0)$, $[Na_o](0)$, $[Cl_o](0)$ and $[H_o](0)$.

When the concentration of ionisable sites in the DFS of the wall $[A_{sites}]$, the pK of the wall's weak acids (assumed to be single), and the intrinsic linear charge density parameter of the walls ξ^* (representing the property of the linear array of fixed anionic ionisable sites) are known, using the WADM model analysis, the concentrations of all ions in the DFS can be estimated based on

their concentrations in the WFS (Ryan, Newman, Arif 1992, Appendix C). These concentrations are then considered as the initial concentrations of the ions in the DFS and they can be expressed as $[K_w](0)$, $[Ca_w](0)$, $[Na_w](0)$, $[Cl_w](0)$ and $[H_w](0)$.

The WADM model analysis also provides other quantities of the wall WFS (subscript o) or the wall DFS (subscript w) such as the activity coefficient of each ion (γ, subscript 1 for monovalent ions, 2 for divalent ions) and the ionic strength (I). Furthermore, it provides the linear charge density parameter (ξ), the concentration of condensed cation in the wall's weak acids ($[Ca_{cond}]$, in this case calcium because calcium is the highest valency cation available in the walls), the concentration of dissociated ionisable sites in the DFS ($[A_{diss}]$), the concentration of the fixed negative charges available for the Donnan equilibrium ($[A_{Donn}]$), the Donnan partition coefficient (σ) and the Donnan potential of the DFS in respect to the WFS (E_{wo}).

4.3 Effects of Proton Efflux

Now, at time $0 < t \leq tm$ where tm is the length of the time under consideration, it is supposed that there is a proton efflux from the cell to the cell walls and the bathing medium that varies with time $(J_H^{cell}(t))$ in mole. $m^{-2} s^{-1}$). Transport of ions across the plasma membrane gives a net transported charge. However, this transported charge is very small compared to the individual transported ions. This must be so because the change of the membrane potential during the transport is relatively small (never exceeding 300 mV). This indicates that the transport of a particular ion across the plasma membrane is usually balanced by the transport of other ions that almost cancels all of the transported charge by the ion. Based on this argument, it is assumed that the proton efflux is balanced by the efflux of anion N^- of valency -1 with the same magnitude $(J_{N^-}^{cell}(t) = J_H^{cell}(t))$. Other ion fluxes (calcium, potassium sodium, and chloride) during this time are assumed to be zero.

When protons are extruded to the walls and the bathing medium, some of the extruded protons function to increase the concentration of protons in the DFS ($\Delta[H_w]$) and in the WFS ($\Delta[H_o]$) so that the pH of the DFS and the pH of the WFS decrease. Consequently, some of the extruded protons also protonate the wall's weak acids so that the concentration of the dissociated ionisable sites decreases (ΔA_{diss}). When condensed calcium exists on these sites in the

condensed phase of the walls, the decrease causes release of the calcium. Therefore the concentration of the condensed calcium in this part decreases ($\Delta[Ca_{cond}]$). The rest of the extruded protons diffuse to the external medium (ΔT_H^{ext} in mole. m^{-2}). In the WADM model for fluxes, all of these quantities are calculated at every small and equal time interval during the time under consideration ($\Delta t = tm/n$; n is the number of intervals). Therefore, the quantities involved in the model, including ion fluxes, are indexed from 0 to n, where index 0 is for the initial condition. In this case, the ion fluxes at every time interval are assumed to be constant.

On page 55, a paragraph "During proton extrusion from the cells to the cell walls, wall demethylation may also occur. The question now is how much extruded protons are needed to replace methyls that are covalently bound to wall polymers. Since this kind of binding is quite strong, only very small amounts of extruded protons are capable to replace methyls from the wall polymers. Based on this argumentation, the very small reduction of the amount of extruded protons for the possible demethylation process is not considered in this calculation. Besides, the replacement of methyls by extruded protons during demethylation process does not change the concentration of fixed negative ions in the walls. In this process, the ionic condition of the walls only changes slightly because of the addition of methyl ions in the walls which is little." should be added before the second paragraph.

4.3.1 Protons

The amount of extruded protons from the cell due to proton efflux $J_H^{cell}(k)$ during Δt in mole. m^{-2} is

$$\Delta T_H^{cell}(k) = J_H^{cell}(k) \, \Delta t. \tag{4.2}$$

The thickness of the wall is h in m. It is supposed that the proportion of the DFS in the walls is λ and the rest $(1-\lambda)$ is the WFS. Therefore,

$$\Delta T_H^{cell}(k) = \Delta[A_{diss}](k) \lambda h + \{\Delta[H_w](k) \lambda h + \Delta[H_o](k)(1-\lambda)h\} + \Delta T_H^{ext}(k). \tag{4.3}$$

The concentration of the dissociated ionisable sites in the DFS of the walls obeys the Henderson-Hasselbalch equation,

$$[A_{diss}](k) = [A_{sites}] \frac{10^{(pH_w(k)-pK)}}{1 + 10^{(pH_w(k)-pK)}}. \tag{4.4}$$

Using the definition of pH (see equation 4.1), this equation can be rewritten as

condensed phase of the walls, the decrease causes release of the calcium. Therefore the concentration of the condensed calcium in this part decreases ($\Delta[Ca_{cond}]$). The rest of the extruded protons diffuse to the external medium (ΔT_H^{ext} in mole. m^{-2}). In the WADM model for fluxes, all of these quantities are calculated at every small and equal time interval during the time under consideration ($\Delta t = tm/n$; n is the number of intervals). Therefore, the quantities involved in the model, including ion fluxes, are indexed from 0 to n, where index 0 is for the initial condition. In this case, the ion fluxes at every time interval are assumed to be constant.

Now let us analyse the ionic composition of the walls at $t=i\Delta t$, where i=1 to n. At this time, the change of the ionic composition of the walls from their initial ionic composition is due to all ion fluxes to and from the walls from t=0 until $t=i\Delta t$. Therefore, to obtain the complete ionic composition at $t=i\Delta t$, we must start with the initial ionic composition of the walls, not the ionic composition of the walls at $t=(i-1)\Delta t$. After that, the effect of kth ion fluxes, where k=1 to i, on the ionic composition of the walls is analysed one by one.

4.3.1 Protons

The amount of extruded protons from the cell due to proton efflux $J_H^{eff}(k)$ during Δt in mole. m^{-2} is

$$\Delta T_H^{eff}(k) = J_H^{eff}(k) \, \Delta t. \qquad\qquad 4.2$$

The thickness of the wall is h in m. It is supposed that the proportion of the DFS in the walls is λ and the rest $(1-\lambda)$ is the WFS. Therefore,

$$\Delta T_H^{eff}(k) = \Delta[A_{diss}](k) \, \lambda h + \{\Delta[H_w](k) \, \lambda h + \Delta[H_o](k)(1-\lambda)h\} + \Delta T_H^{ext}(k). \qquad 4.3$$

The concentration of the dissociated ionisable sites in the DFS of the walls obeys the Henderson-Hasselbalch equation,

$$[A_{diss}](k) = [A_{sites}] \, \frac{10^{(pH_w(k)-pK)}}{1 + 10^{(pH_w(k)-pK)}}. \qquad\qquad 4.4$$

Using the definition of pH (see equation 4.1), this equation can be rewritten as

$$[A_{diss}](k) = \frac{[A_{sites}]}{\gamma_{1w}(k)[H_w](k)\ 10^{(pK-3)} + 1}.$$ 4.5

Based on this equation, the concentration reduction of the dissociated ionisable sites in equation 4.3 can be obtained from the following equation.

$$\Delta[A_{diss}](k) = \left(\frac{[A_{sites}]}{\gamma_{1w}(k-1)[H_w](k-1)\ 10^{(pK-3)} + 1} - \frac{[A_{sites}]}{\gamma_{1w}(k)[H_w](k)\ 10^{(pK-3)} + 1}\right).$$ 4.6

The increase of proton concentration in the DFS due to $J_{ff}^{II}(k)$ during Δt is

$$\Delta[H_w](k) = [H_w](k) - [H_w](k-1),$$ 4.7

and the increase of proton concentration in the WFS is

$$\Delta[H_o](k) = [H_o](k) - [H_o](k-1).$$ 4.8

From Donnan theory, the relation between the concentration of ions in the DFS and in the WFS is

$$\gamma_{z|w}[N_w] = \sigma^z\ \gamma_{z|o}[N_o].$$ 4.9

Here, σ is the Donnan partition coefficient, γ is the activity coefficient, z is the valency of ions and N is the symbol for ions. Based on this relation, equation 4.7 becomes

$$\Delta[H_o](k) = \frac{\gamma_{1w}(k)[H_w](k)}{\sigma(k)\ \gamma_{1o}(k)} - [H_o](k-1).$$ 4.10

In Appendix B, it is shown that when the initial distribution of concentration of species j (its diffusion coefficient D_j is constant) in semi-infinite system is C_o for $0 < x \leq a$ and 0 for $x > a$ (see Figure b.3), the concentration distribution as a function of position x and time t is

$$C(x,t) = \frac{1}{2}\ C_o\left\{erfc\left(\frac{x-a}{2\sqrt{D_j\ t}}\right) - erfc\left(\frac{x+a}{2\sqrt{D_j\ t}}\right)\right\}.$$ 4.11

Based on this equation, it can be calculated that by $t=t_i$, the total amount of species j that has diffused away across the boundary at $x=a$ is

$$T_j^{x>a} = C_o \, r_j \qquad\qquad 4.12$$

where

$$r_j = a \, erfc\left(\frac{a}{\sqrt{D_j \, t_i}}\right) - \sqrt{\frac{D_j \, t_i}{\pi}}\left(1 - e^{-\left(\frac{a^2}{D_j \, t_i}\right)}\right). \qquad\qquad 4.13$$

Equations 4.11 and 4.12 are equations b.15 and b.19 in Appendix B. The amount of species j that is left in $0<x\leq a$ at this time is

$$T_j^{0<x\leq a} = C_o \, (a - r_j). \qquad\qquad 4.14$$

When this equation is substituted into equation 4.12, the amount of species j that diffuses away across the boundary $x=a$ can be expressed in terms of the amount of species j that is left in $0<x\leq a$,

$$T_j^{x>a} = T_j^{0<x\leq a}\left(\frac{r_j}{a - r_j}\right). \qquad\qquad 4.15$$

Now for proton extrusion due to a constant rate $\left(J_{ff}^{1l}(k)\right)$, during Δt, we can consider that first, all amounts of the extruded protons during the interval $\left(T_{ff}^{1l}(k)\right)$ fill the wall and become distributed only to increase the proton concentration in the DFS and in the WFS and to decrease the concentration of the dissociated ionisable sites in the DFS of the walls. At this state, the amount of the extruded protons for diffusing to the bathing medium is zero.

The increase of proton concentration in the DFS and in the WFS is considered as the driving force for the diffusion of protons from the wall to the bathing medium. In this case, the increase of the proton concentration in the DFS and in the WFS is treated as the initial concentration distribution, like C_o used to derive equation 4.11. The extruded protons that decrease the concentration of the dissociated ionisable sites in the DFS of the walls are not included as the driving force of the proton diffusion because the protons are in the form of protonated ionizable sites, not in the form of proton ions.

Now, when protons begin to diffuse from the DFS and the WFS to the bathing medium, the driving force of the diffusion starts to decrease and the pH of the DFS starts to increase. Consequently, some extruded protons that protonate the ionizable sites are released again from these sites. The released proton ions go to the DFS and the WFS and contribute to the driving force of the proton diffusion. Therefore, the decrease of the driving force of the proton diffusion from the DFS and the WFS to the bathing medium during this time is relatively slower.

The amount of the extruded protons that diffuse to the bathing medium increases with time. In this case, the amount of the extruded protons that diffuse to the bathing medium can be calculated from the total amount of the extruded protons for increasing the proton concentration in the DFS and in the WFS using equation 4.15.

The approximation above is valid to describe the interdependency of the extruded proton distribution between the DFS, the WFS, the ionizable sites and the bathing medium during proton extrusion if the time interval is small enough. Therefore in this analysis, the time interval set up is small.

At $t=i\Delta t$, the diffusion due to the kth proton efflux has happened for $(i-k+1)\Delta t$. Therefore, based on equations 4.7, 4.8, 413 and 4.15, at this time, the amount of the extruded protons that diffuse to the bathing medium due to $J_{H}^{efflux}(k)$ during Δt is

$$\Delta T_H^{ex}(k) = \{\Delta[H_w](k)\,\lambda h + \Delta[H_o](k)(1-\lambda)h\}\left(\frac{r_H((i-k+1)\Delta t)}{\lambda h - r_H((i-k+1)\Delta t)}\right), \qquad 4.16$$

where

$$r_H((i-k+1)\Delta t) = \lambda h\,\mathrm{erfc}\left(\frac{\lambda h}{\sqrt{D_H\,(i-k+1)\Delta t}}\right)$$

$$-\sqrt{\frac{D_H\,(i-k+1)\Delta t}{\pi}}\left(1 - e^{-\left(\frac{(\lambda h)^2}{D_H\,(i-k+1)\Delta t}\right)}\right). \qquad 4.17$$

In equations 4.13 and 4.15, a is replaced with the thickness of the DFS (λh) because in the wall, protons are mostly in the DFS rather than in the WFS. Therefore equations 4.13 and 4.15 become equations 4.17 and 4.16. For the same reason, the diffusion coefficient of protons in the DFS is also used for D_H

in equation 4.17. When equation 4.16 is substituted into equation 4.3, we obtain

$$\Delta T_{ff}^{II}(k) = \Delta[A_{diss}](k)\, \lambda h + \{\Delta[H_w](k)\, \lambda h + \Delta[H_o](k)\, (1-\lambda)h\} \left(\frac{\lambda h}{\lambda h - r_H((i-k+1)\Delta t)}\right).$$

4.18

When equations 4.2, 4.6, 4.7, and 4.10 are substituted into equation 4.18, a quadratic equation for the proton concentration in the DFS ($[H_w](k)$) is obtained. (The quadratic equation gives two solutions for $[H_w](k)$, one positive and the other negative. However, since concentration is always positive, the positive solution for $[H_w](k)$ is used.) This equation is long and complex. To solve this equation, the activity coefficients of monovalent ions in the DFS and in the WFS ($\gamma_{1w}(k)$, $\gamma_{1o}(k)$) and the related Donnan partition coefficient ($\sigma(k)$) are required. The previous proton concentration in the DFS ($[H_w](k-1)$) and the WFS ($[H_o](k-1)$), the kth proton efflux at the plasmalemma ($J_{ff}^{II}(k)$), the pK of the wall's weak acids and the concentration of ionizable sites in the DFS of the walls ($[A_{sites}]$) in the equation are already known.

The activity coefficient of ions with valency z in the DFS ($\gamma_{zw}(k)$) is defined as (Richter and Dainty 1990b, Ryan, Newman, Arif 1992),

$$\ln(\gamma_{z|w}(k)) = -z^2 \left(\frac{\xi^{eff}(k)\,[A_{Donn}](k)}{4\, I_w(k)}\right),$$

4.19

where the effective linear charge density parameter is

$$\xi^{eff}(k) = \frac{[A_{Donn}](k)}{[A_{sites}]}\, \xi^*.$$

4.20

and the ionic strength in the DFS is

$$I_w(k) = 0.5 \sum_{all\ N} (z_N)^2\, [N_w](k).$$

4.21

Here, $[A_{Donn}](k)$ is the concentration of the fixed anions in the walls useable for the Donnan equilibrium and N is the symbol for ions. In the WFS, the activity coefficient of ions with valency z is calculated from the Debye-Hückel expression.

$$\log(\gamma_{z|o}(k)) = -0.509\,z^2 \left\{ \frac{\sqrt{I_o(k)}}{1 + \sqrt{I_o(k)}} \right\}, \qquad\qquad 4.22$$

where the ionic strength in the WFS is

$$I_o(k) = 0.5 \sum_{\text{all } N} (z_N)^2 [N_o](k). \qquad\qquad 4.23$$

It is clear from equations 4.19 and 4.22 that the determination of $\gamma_{1w}(k)$, and $\gamma_{1o}(k)$, depends on the composition of ions in the DFS and in the WFS. However at this state, the composition of ions in the DFS and in the WFS are not known. Therefore, to begin with, starting values for $\gamma_{1w}(k)$, and $\gamma_{1o}(k)$, are needed. The Donnan partition coefficient ($\sigma(k)$) also depends on the composition of ions in the walls so that it also needs a starting value. In this case, the previous values of these quantities ($\gamma_{1w}(k-1)$, $\gamma_{1o}(k-1)$ and $\sigma(k-1)$) are used for the starting values.

After the proton concentration in the DFS ($[H_w](k)$) is obtained using the quadratic equation derived from equations 4.2, 4.6, 4.7, 4.10 and 4.18, we can calculate the proton concentration in the WFS ($[H_o](k)$) from the Donnan relation (equation 4.9), the increase of the proton concentration in the DFS ($\Delta[H_w](k)$) from equation 4.7 and the increase of the proton concentration in the WFS($\Delta[H_o](k)$) from equation 4.8. Using the increase of the proton concentration in the DFS and in the WFS, the concentration reduction of the dissociated ionisable sites due to $J_{ff}^{oll}(k)$ during Δt ($\Delta[A_{diss}](k)$) can be calculated from equation 4.18.

4.3.2 Condensation

The total concentration reduction of the dissociated ionizable sites due to proton effluxes $J_{ff}^{oll}(m)$, where m=1 to (k-1), is $\Delta[A_{diss}^T](k-1)$. Therefore, by adding the concentration reduction of the dissociated ionisable sites due to $J_{ff}^{oll}(k)$ during Δt, the present total concentration reduction of the dissociated ionizable sites is obtained.

$$\Delta[A_{diss}^T](k) = \Delta[A_{diss}^T](k-1) + \Delta[A_{diss}](k). \qquad\qquad 4.24$$

In this case, $\Delta[A_{diss}^T](0)=0$. The concentration of the dissociated ionizable sites can be calculated from its initial concentration using the following equation.

$$[A_{diss}](k) = [A_{diss}](0) - \Delta[A_{diss}^T](k).$$ 4.25

We may calculate the concentration of the dissociated ionizable sites using equation 4.4 by calculating first the pH of the DFS from the proton concentration in the DFS. However using this equation, the concentration of dissociated ionizable sites is sensitive to the change of the pH, and I found that the limitation of the computer in handling high precision values affects the calculation. Therefore the concentration of the dissociated ionizable sites is calculated using equation 4.25, not using equation 4.4. After the concentration of the dissociated ionizable sites is obtained from equation 4.25, the linear charge density parameter can be calculated using the following equation (see equation c.2 in Appendix C).

$$\xi(k) = \frac{[A_{diss}](k)}{[A_{sites}]} \xi^*.$$ 4.26

When condensed calcium exists on the dissociated ionizable sites in the walls, the concentration reduction of the dissociated ionizable sites causes concentration reduction of the condensed calcium on these sites. Consequently, the total concentration reduction of the condensed calcium, caused by the total concentration reduction of the dissociated ionizable sites, can not exceed the initial concentration of the condensed calcium available on these sites ($[Ca_{cond}](0)$). In this case, when half of the total concentration reduction of the dissociated ionizable sites ($\frac{1}{2}\Delta[A_{diss}^T](k)$) is still less than $[Ca_{cond}](0)$, the total concentration reduction of the condensed calcium is half of the total concentration reduction of the dissociated ionizable sites.

$$\Delta[Ca_{cond}^T](k) = \frac{1}{2}\Delta[A_{diss}^T](k).$$ 4.27

However, when $\frac{1}{2}\Delta[A_{diss}^T](k)$ is equal or higher than $[Ca_{cond}](0)$, the total concentration reduction of the condensed calcium is forced to be $[Ca_{cond}](0)$. Therefore,

$$\Delta[Ca_{cond}^T](k) = [Ca_{cond}](0).$$ 4.28

For both conditions, the concentration reduction of the condensed calcium due to $J_{ff}^{cell}(k)$ during Δt is obtained using the following equation.

$$\Delta[Ca_{cond}](k) = \Delta[Ca^T_{cond}](k) - \Delta[Ca^T_{cond}](k-1). \qquad 4.29$$

For this equation, $(\Delta[Ca^T_{cond}](0) = 0)$. Now, the concentration of condensed calcium can be calculated from its previous concentration using the following equation.

$$[Ca_{cond}](k) = [Ca_{cond}](k-1) - \Delta[Ca_{cond}](k). \qquad 4.30$$

The concentration of the fixed anions in the DFS of the walls useable for the Donnan equilibrium is determined by subtracting the concentration of the dissociated ionizable sites with the concentration of the sites occupied by the condensed calcium.

$$[A_{Donn}](k) = [A_{diss}](k) - 2\{[Ca_{cond}](0) - \Delta[Ca^T_{cond}](k)\}. \qquad 4.31$$

The result must be the same as the one that is obtained from the following equation used in Appendix C (see equation c.3).

$$[A_{Donn}](k) = \xi^{eff}(k)\frac{[A_{sites}]}{\xi^*}. \qquad 4.32$$

4.3.3 Calcium

Although it has been assumed that the calcium flux at the plasmalemma is zero, for general consideration let us include an efflux of calcium at the plasmalemma in the calculation below. Therefore, the amount of calcium transported from the cell due to calcium efflux $J_{Ca}^{cell}(k)$ during Δt in mole. m^{-2} is

$$\Delta T_{Ca}^{cell}(k) = J_{Ca}^{cell}(k)\,\Delta t. \qquad 4.33$$

(In the case when the calcium flux is an influx, the amount of calcium transported from the cell is negative. When there is no calcium flux at the plasmalemma as assumed, the amount of calcium transported from the cell is zero.) The calcium from the cell and the calcium released from the walls due to $J_{ff}^{cell}(k)$ during Δt are the sources of calcium entering the DFS, the WFS and the

bathing medium. Therefore similar to equations 4.18, 4.7, 4.8, 4.10 and 4.17, for calcium at $t=i\Delta t$, we obtain

$$\Delta T_{Ca}^{cell}(k) + \Delta[Ca_{cond}](k)\,\lambda h = \{\Delta[Ca_w](k)\,\lambda h + \Delta[Ca_o](k)\,(1-\lambda)h\}$$

$$\times \left(\frac{\lambda h}{\lambda h - r_{Ca}((i-k+1)\Delta t)}\right) \qquad 4.34$$

where

$$\Delta[Ca_w](k) = [Ca_w](k) - [Ca_w](k-1), \qquad 4.35$$

$$\Delta[Ca_o](k) = [Ca_o](k) - [Ca_o](k-1) = \frac{\gamma_{2w}(k)\,[Ca_w](k)}{(\sigma(k))^2\,\gamma_{2o}(k)} - [Ca_o](k-1), \qquad 4.36$$

and

$$r_{Ca}((i-k+1)\Delta t) = \lambda h\; erfc\left(\frac{\lambda h}{\sqrt{D_{Ca}\,(i-k+1)\Delta t}}\right)$$

$$- \sqrt{\frac{D_{Ca}\,(i-k+1)\Delta t}{\pi}}\left(1 - e^{-\left(\frac{(\lambda h)^2}{D_{Ca}\,(i-k+1)\Delta t}\right)}\right). \qquad 4.37$$

In equation 4.34, $\Delta[Ca_{cond}](k)$ is obtained from equation 4.29. In equations 4.34 and 4.37, the thickness of the DFS (λh) is used to substitute a (see equations 4.15 and 4.13) because most of the calcium in the walls is in the DFS. Here, D_{Ca} is the diffusion coefficient of calcium in the DFS.

When equations 4.33, 4.35 and 4.36 are substituted into equation 4.34, an expression for the calcium concentration in the DFS ($[Ca_w](k)$) is obtained. To calculate $[Ca_w](k)$ using this expression, the activity coefficients of divalent ions in the DFS and in the WFS ($\gamma_{2w}(k)$, $\gamma_{2o}(k)$), which depend on the composition of other ions in the DFS and in the WFS (see equations 4.19 and 4.22), are also required. Therefore, we need the starting values not only for the activity coefficient of monovalent ions in the DFS and in the WFS and the Donnan activity coefficient, but also for the activity coefficient of divalent ions in the DFS and in the WFS. In this case, the previous values of these quantities ($\gamma_{2w}(k-1)$ and $\gamma_{2o}(k-1)$) are used for the starting values. After $[Ca_w](k)$ is obtained, we can calculate the calcium concentration in the WFS ($[Ca_o](k)$) from the Donnan relation (equation 4.9), the increase of the calcium concentration in

the DFS ($\Delta[Ca_w](k)$) from equation 4.35 and the increase of the calcium concentration in the WFS($\Delta[Ca_o](k)$) from equation 4.36.

4.3.4 Non-Condensed Monovalent Ions

In this analysis, the non-condensed monovalent ions (N, z=±1) under consideration are potassium, sodium, chloride and the negative ion transported to balance the transport of protons across the plasmalemma (N$^-$). For these ions, the amount of the ions transported from the cell due to efflux $J_N^{cell}(k)$ during Δt in mole. m^{-2} is

$$\Delta T_N^{cell}(k) = J_N^{cell}(k)\, \Delta t. \qquad\qquad 4.38$$

(For potassium, sodium and chloride, it has been assumed that their fluxes across the plasmalemma are zero. Therefore the amount for these ions transported from the cell is zero. For N$^-$, the efflux across the plasmalemma is the same as the efflux of protons.) Since there is not condensation of these ions in the walls, the walls do not release these ions during proton extrusion. Therefore the only source of the ions entering the DFS, the WFS and the bathing medium is the ions from the cell. Similar to equations 4.18, 4.7, 4.8, 4.10 and 4.17, for the ions at t=iΔt, we obtain

$$\Delta T_N^{cell}(k) = \{\Delta[N_w](k)\,\lambda h + \Delta[N_o](k)(1-\lambda)h\}\left(\frac{a}{a - r_N((i-k+1)\Delta t)}\right), \qquad 4.39$$

where

$$\Delta[N_w](k) = [N_w](k) - [N_w](k-1), \qquad\qquad 4.40$$

$$\Delta[N_o](k) = [N_o](k) - [N_o](k-1) = \frac{\gamma_{1w}(k)\,[N_w](k)}{(\sigma(k))^z\,\gamma_{1o}(k)} - [N_o](k-1); \qquad 4.41$$

and

$$r_N((i-k+1)\Delta t) = a\,\mathrm{erfc}\left(\frac{a}{\sqrt{D_N\,(i-k+1)\Delta t}}\right)$$

$$- \sqrt{\frac{D_N\,(i-k+1)\Delta t}{\pi}}\left(1 - e^{-\left(\frac{a^2}{D_N\,(i-k+1)\Delta t}\right)}\right). \qquad 4.42$$

For monovalent cations (potassium and sodium), a in equations 4.39 and 4.42 is substituted with the thickness of the DFS (λh) because in the walls, cations are mostly in the DFS. For monovalent anions (chloride and N^-), a is substituted with the thickness of the WFS ($(1-\lambda)h$) because in the walls, anions are mostly in the WFS. With the same reason, for cations, D_N in equation 4.42 is the diffusion coefficient of the cations in the DFS. For anions, D_N in equation 4.42 is the diffusion coefficient of the anions in the WFS.

For N^- (which is probably organic anion, possibly malate?), its initial concentration should be very small in the DFS and small in the WFS. Therefore $[N_w^-](0)$ and $[N_o^-](0)$ are assumed to be zero. Because N^- is not known, for the present calculations, its diffusion coefficient is assumed to be the same as the diffusion coefficient of chloride. The uncertainty in the diffusion coefficient of N^- has little effect on the results because as an anion, N^- is excluded from the walls so that its concentration in the walls is small and changes little during the flux.

With the same principle as used for calcium, we can substitute equations 4.38, 4.40 and 4.41 into equation 4.39 to calculate the concentrations of potassium, sodium, chloride and N^- in the DFS ($[K_w](k)$, $[Na_w](k)$, $[Cl_w](k)$ and $[N_w^-](k)$). After that, their concentrations in the WFS ($[K_o](k)$, $[Na_o](k)$, $[Cl_o](k)$ and $[N_o^-](k)$), the increase of their concentration in the DFS ($\Delta[K_w](k)$, $\Delta[Na_w](k)$, $\Delta[Cl_w](k)$ and $\Delta[N_w^-](k)$) and the increase of their concentration in the WFS ($\Delta[K_o](k)$, $\Delta[Na_o](k)$, $\Delta[Cl_o](k)$ and $\Delta[N_o^-](k)$) can be calculated from equations 4.9, 4.40 and 4.41.

4.3.5 Donnan Considerations

In the DFS, electric neutrality must be satisfied. Therefore,

$$[A_{Donn}](k) + [N_w^-](k) + [Cl_w](k) = [H_w](k) + [K_w](k) + [Na_w](k) + 2[Ca_w](k).$$
$$4.43$$

Here, $[A_{Donn}](k)$ is obtained from equation 4.31. Since ions from the cell and ions released from the walls enter the DFS and the WFS and increase the concentration of the ions in both compartments, it is necessary to express the DFS concentration of each ion in equation 4.43 in terms of the increase of the

ion concentration and the previous ion concentration in both compartments. Therefore for the involved ions, we have

$$[N_w](k) = \frac{(\sigma(k))^z \gamma_{z|o}(k)}{\gamma_{z|w}(k) + (\sigma(k))^z \gamma_{z|o}(k)} \{\Delta[N_w](k) + \Delta[N_o](k) + [N_w](k-1) + [N_o](k-1)\}.$$

4.44

Here, N is either protons, calcium, potassium, sodium, chloride or N⁻. z is the valency of the ions. When equation 4.44 is applied on all these ions, and then the results are substituted into equation 4.43, a polynomial of degree 4 to solve for the Donnan partition coefficient $\sigma(k)$ is obtained. Using a standard routine, the roots of this polynomial can be found. In this case, the positive root of the polynomial is selected for $\sigma(k)$ because the Donnan partition coefficient must be positive.

Based on the calculated Donnan potential $\sigma(k)$, we can recalculate the concentrations of all the involved ions in the DFS using equation 4.44. After that, their concentrations in the WFS can be calculated using the Donnan relation (equation 4.9). Based on these concentrations, the ionic strength in the DFS and in the WFS can be calculated using equations 4.21 and 4.23. Finally, the activity coefficients of ions in the DFS and in the WFS can also be calculated from equation 4.19 and 4.22. In equations 4.19 and 4.20, $[A_{Donn}](k)$ is obtained from equation 4.31.

Using the calculated Donnan partition coefficient and the calculated activity coefficients of ions in the DFS and in the WFS, the calculation above, that begins from equation 4.2 until equation 4.44, is carried out again so that new values for the Donnan partition coefficient and the activity of ions in the DFS and in the WFS are obtained. These values are then used in the calculation again so that other new values of the quantities are obtained. This iterative process is continued until these values approach a steady state. At this state, the iteration to obtain the ionic composition of the walls for k^{th} ion fluxes at $t=i\Delta t$ has been completed.

Here, k is from 1 to i. Therefore, there would be i iterations that must be completed to obtain the complete ionic composition of the walls at $t=i\Delta t$. After that, the Donnan potential, the potential of the DFS in respect to the WFS, can be calculated from $\sigma(k=i)$ using the following equation.

$$E_{wo}(i) = -\frac{RT}{F} \ln(\sigma(k=i)).$$ 4.45

R, T, F have their usual definitions.

To analyse all the change of the ionic composition of the walls during the time under consideration (tm), the analysis is carried out at every time interval (t=iΔt, where i is from 1 to n). The flux of ions from the walls to the bathing medium at t=iΔt is defined as the difference between the total amount of the ions that diffuse from the wall to the external medium at t=(i-1)Δt and at t=iΔt divided by the time difference,

$$J_N^{ext}(i) = \frac{T_N^{ext}(i) - T_N^{ext}(i-1)}{\Delta t}.$$ 4.46

Here, the total amount of the ions that have diffused from the wall to the external medium at t=iΔt is

$$T_N^{ext}(i) = \sum_{k=1}^{i} (\Delta[N_w](k) + \Delta[N_o](k)) \frac{r_N((i-k+1)\Delta t)}{a - r_N((i-k+1)\Delta t)},$$ 4.47

and N is either protons, calcium, potassium, sodium, chloride or N$^-$. $r_N((i-k+1)\Delta t)$ is according to equation 4.42. In equations 4.47, for cations (protons, calcium, potassium and sodium), a is substituted with the thickness of the DFS (λh). For anions (chloride and N$^-$), a is substituted with the thickness of the WFS (($1-\lambda$)h). In equation 4.42, for cations, D_N is the diffusion coefficient of the cations in the DFS. For anions, D_N is the diffusion coefficient of the anions in the WFS. In the WADM model for fluxes above, the small concentration of fixed positive charges that exist in the walls is ignored.

4.4 Effects of Wall Parameter Uncertainties

Beside the composition of ions in the external solution, several parameters of the walls are needed in the analysis of the WADM model for fluxes: the concentration of ionisable sites ([A$_{sites}$]), the pK of the wall's weak acids, the intrinsic linear charge density parameter (ξ^*), the thickness of the walls (h), the portions of the DFS and the WFS in the walls (λ and $1-\lambda$) and the diffusion coefficient of cations in the DFS. The values of these parameters are different between plants. In *Chara*, Ryan, Newman, Arif (1992) used 800 mole

m^{-3} for the concentration of ionisable sites and 2.2 for the pK based on the report of Dainty et al. (1960). In *Sphagnum russowii*, Richter and Dainty (1989a) found two classes of wall's weak acids, one of them has a pK between 2 and 4. Richter and Dainty (1990a) also reported that the walls of *Sphagnum* have an intrinsic linear charge density parameter of about 0.71. The thickness of the primary walls also varies around 1.0 μm and it was reported for *Chara* (Dainty and Hope 1959) that half of the walls is the DFS (λ=0.5). The diffusion coefficient of cations in the DFS is not known. Because the DFS contains more ions and the movement of ions in this region has contorted pathways, the diffusion coefficient of ions in the DFS should be smaller than in open water. In the WFS, the movement of ions is also contorted. But the composition of ions in the WFS is similar to that in open water Therefore, the diffusion of ions in the WFS is assumed to be the same as in open water (9.17×10^{-9} m^2 s^{-1} for protons, 1.99×10^{-9} m^2 s^{-1} for calcium, 1.9×10^{-9} m^2 s^{-1} for potassium, 1.28×10^{-9} m^2 s^{-1} for sodium, 1.93×10^{-9} m^2 s^{-1} for chloride). In this section, the effects of altering the values of the parameters in the analysis of the WADM model for fluxes are presented.

To begin with, we consider a tissue which has 10 cells in its thickness. It is assumed that the concentration of the ionisable sites of the cell walls is 800 mole m^{-3}, the pK of the wall's weak acids is 3.0, the intrinsic linear charge density parameter is 0.71, the wall thickness of each cell is 1.0 μm, the portion of the DFS in the walls (λ) is 0.5 and the diffusion coefficient of cations in the DFS is 1/5 of that in open water. The bathing medium contains 0.1 mole m^{-3} potassium, 0.1 mole m^{-3} calcium, 0.02 mole m^{-3} sodium, 0.3 mole m^{-3} chloride at pH 6. Now it is assumed that there is a proton efflux at the plasmalemma described by the following equation (in nmol m^{-3} s^{-1}, influx positive).

$$\left(J_H^{pell}(t)\right) = -300 \left(1 - e^{-\left(\frac{t}{5}\right)}\right).$$ 4.48

Here, t is in minutes. This exponential proton efflux is selected because the real proton efflux is mostly exponential. The selected magnitude of the proton efflux (300 nmol m^{-3} s^{-1}) and the selected time constant (t_o=5 minutes) are also reasonable. In this case, the length of the time under consideration is 40 minutes. Figure 4.1 shows this proton efflux as function of time. The efflux increases to approach 300 nmol m^{-3} s^{-1}. The proton efflux is balanced by the efflux of N^-. The fluxes of calcium potassium, sodium and chloride at the plasmalemma are assumed to be zero.
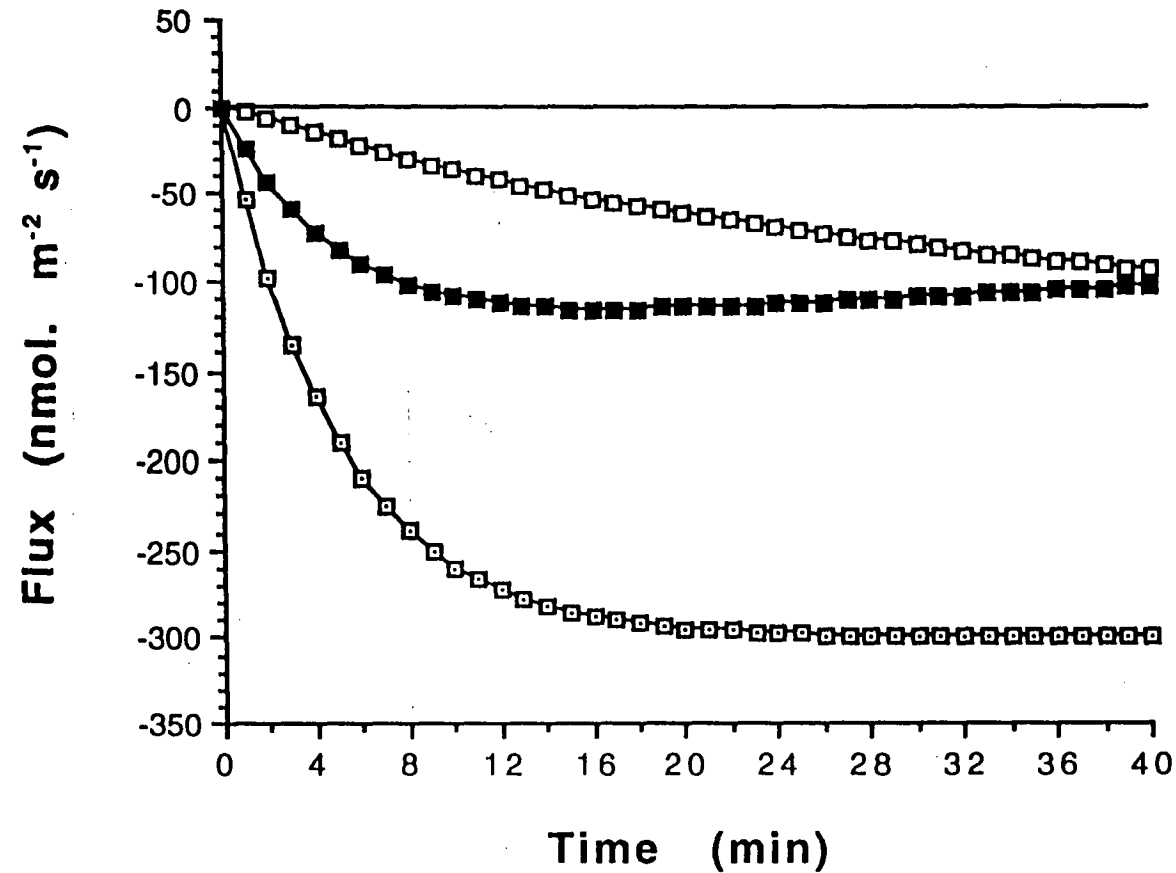
Figure 4.1

The proton efflux at the plasmalemma (◫) and the proton (□) and calcium (■) effluxes outside the walls calculated using the WADM model for fluxes. The proton efflux at the plasmalemma is the total efflux from 10 cells in the thickness of a tissue. The wall thickness of each cell is 1.0 μm, half is the DFS and the rest is the WFS. The concentration of the ionisable sites in the DFS of the walls is 800 mole m^{-3}, the pK of the wall's weak acids is 3.0, the intrinsic linear charge density parameter is 0.71, and the diffusion coefficient of cations in the DFS is 1/5 of that in the WFS. The external medium contains 0.1 mole m^{-3} potassium, 0.1 mole m^{-3} calcium, 0.02 mole m^{-3} sodium, 0.3 mole m^{-3} chloride at pH 6.
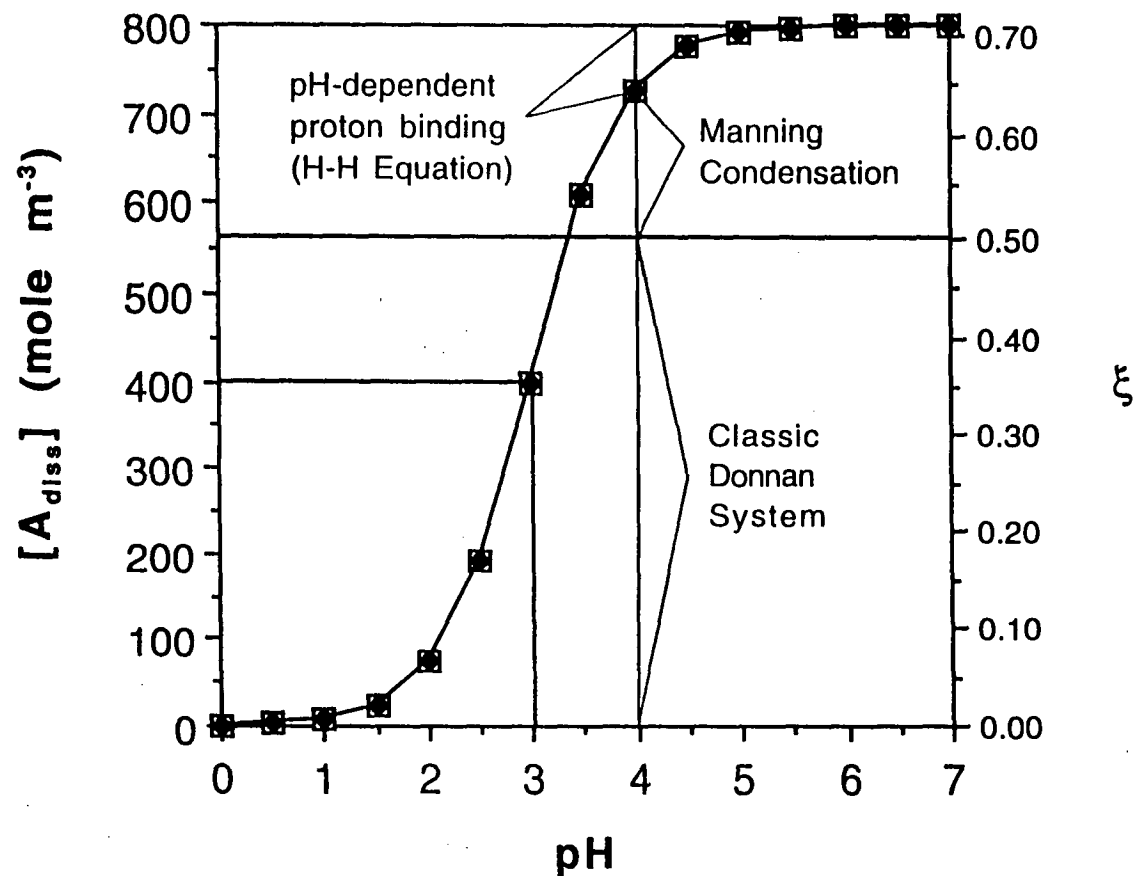
Figure 4.2

The concentration of the dissociated ionizable sites $[A_{diss}]$ (□) and the linear charge density parameter ξ (●) as function of pH when the concentration of the ionisable sites in the DFS of the walls is 800 mole m^{-3}, the pK of the wall's weak acids is 3.0 and the intrinsic linear charge density parameter is 0.71. Calcium (valency 2) is the highest valency cation in the walls.
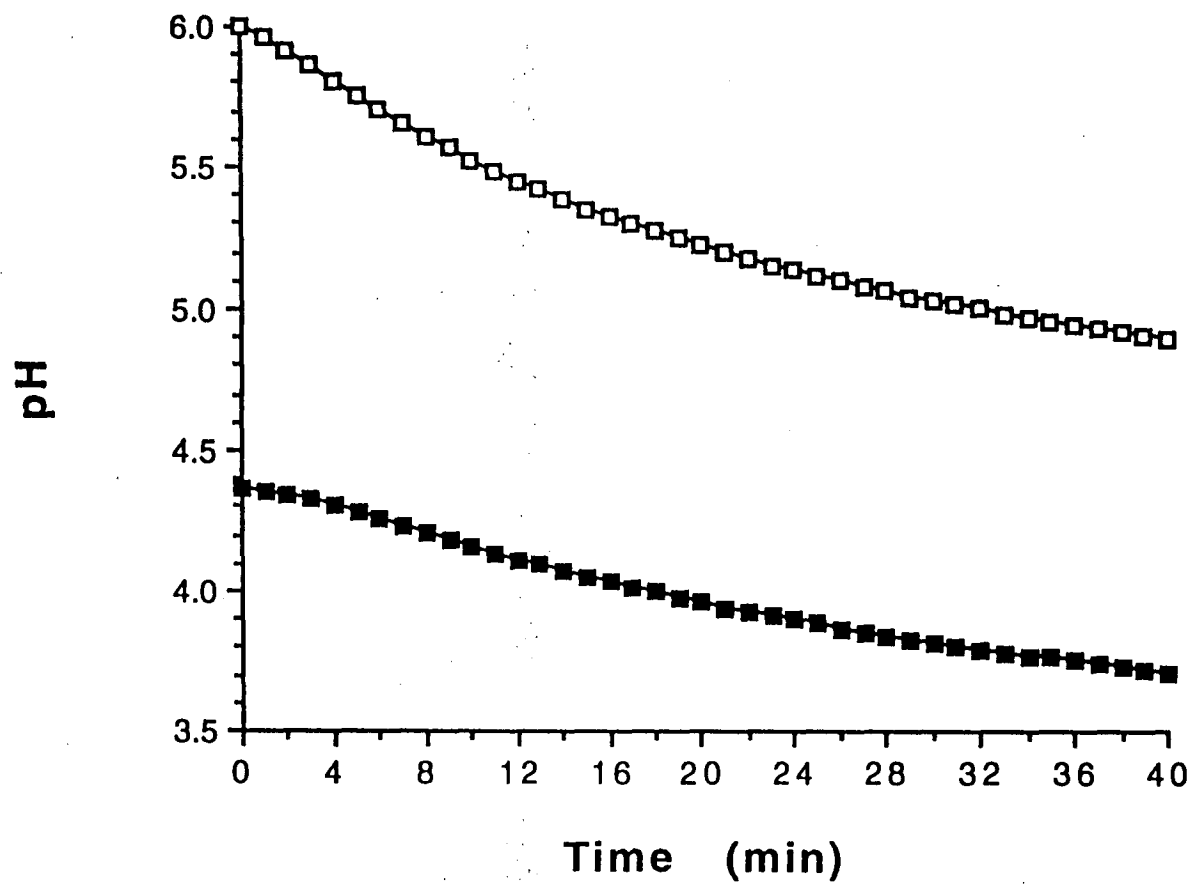
Figure 4.3

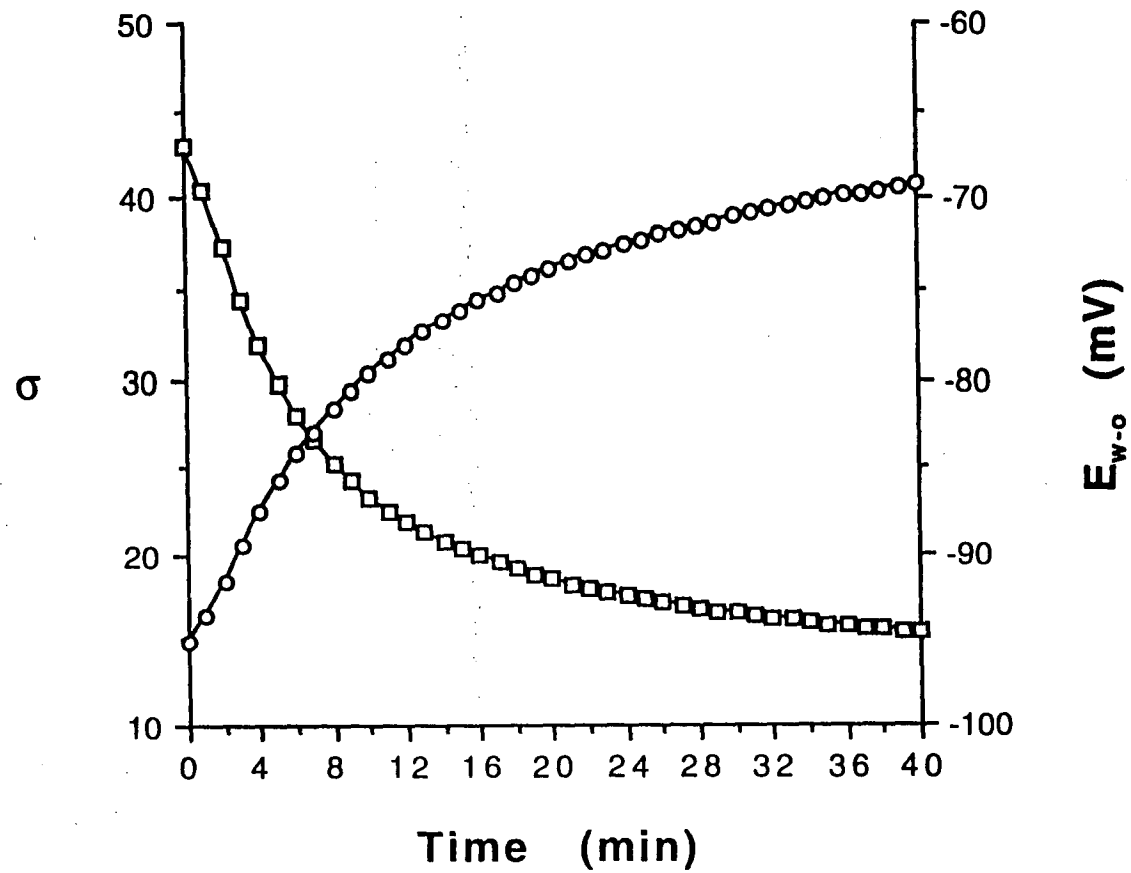The pH of the DFS (■) and the WFS (□) for the condition used in Figure 4.1.

Figure 4.4

The Donnan partition coefficient σ (□) and the Donnan potential $E_{w\text{-}o}$ (O) for the condition used in Figure 4.1.
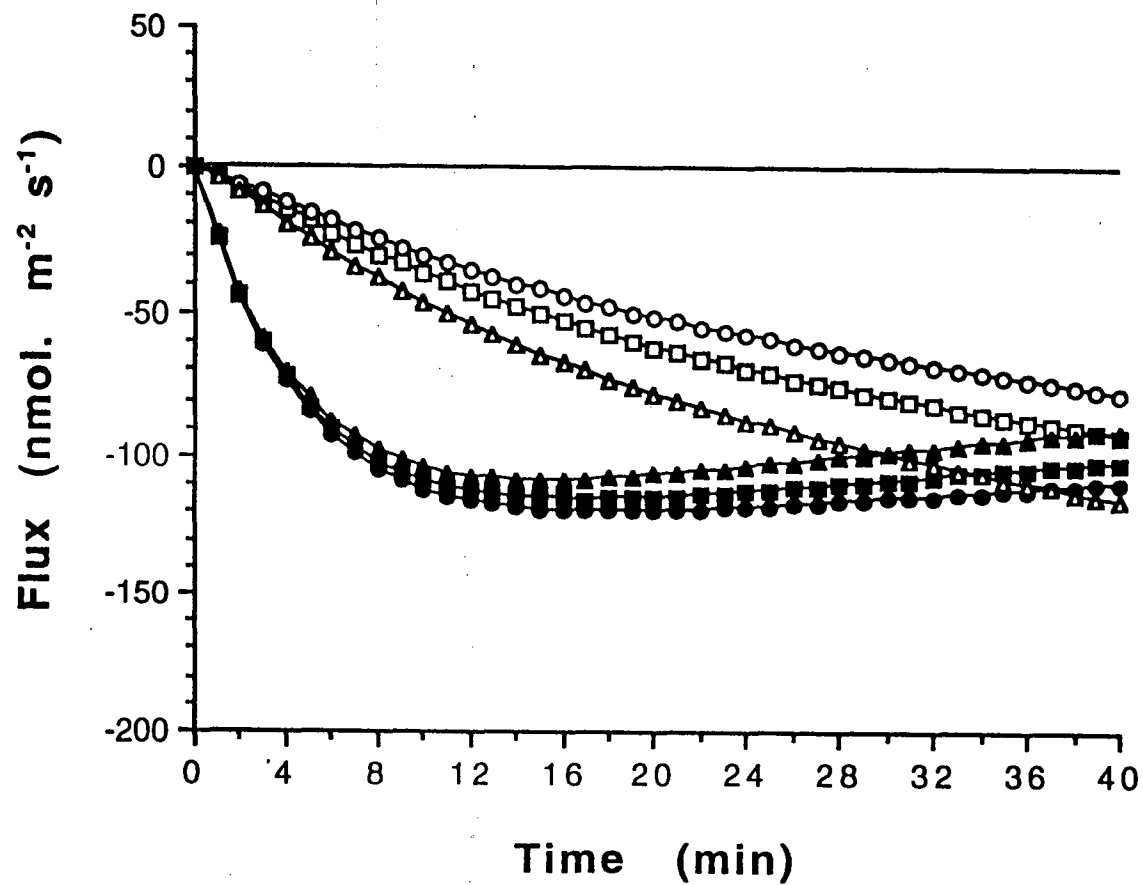
Figure 4.5

The calculated proton (open symbol) and calcium (solid symbol) effluxes using the WADM model for fluxes when the concentration of the ionisable sites in the DFS of the walls is 600 (Δ), 800 ($\square$) or 1000 (O) mole m^{-3}. Other details are the same as in Figure 4.1.

Figure 4.6

The calculated proton (open symbol) and calcium (solid symbol) effluxes using the WADM model for fluxes when the pK of the wall's weak acids is 2.0 (Δ), 3.0 (□) or 3.5 (O). Other details are the same as in Figure 4.1.
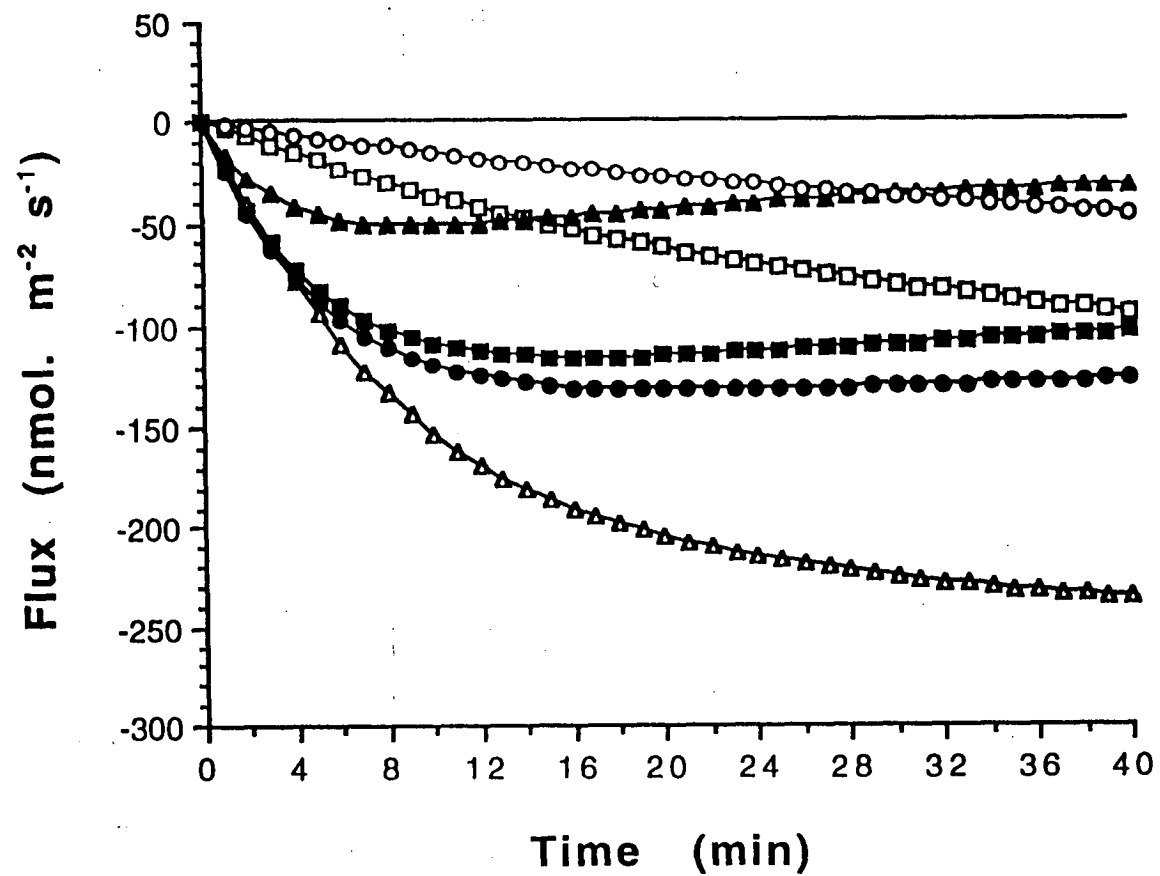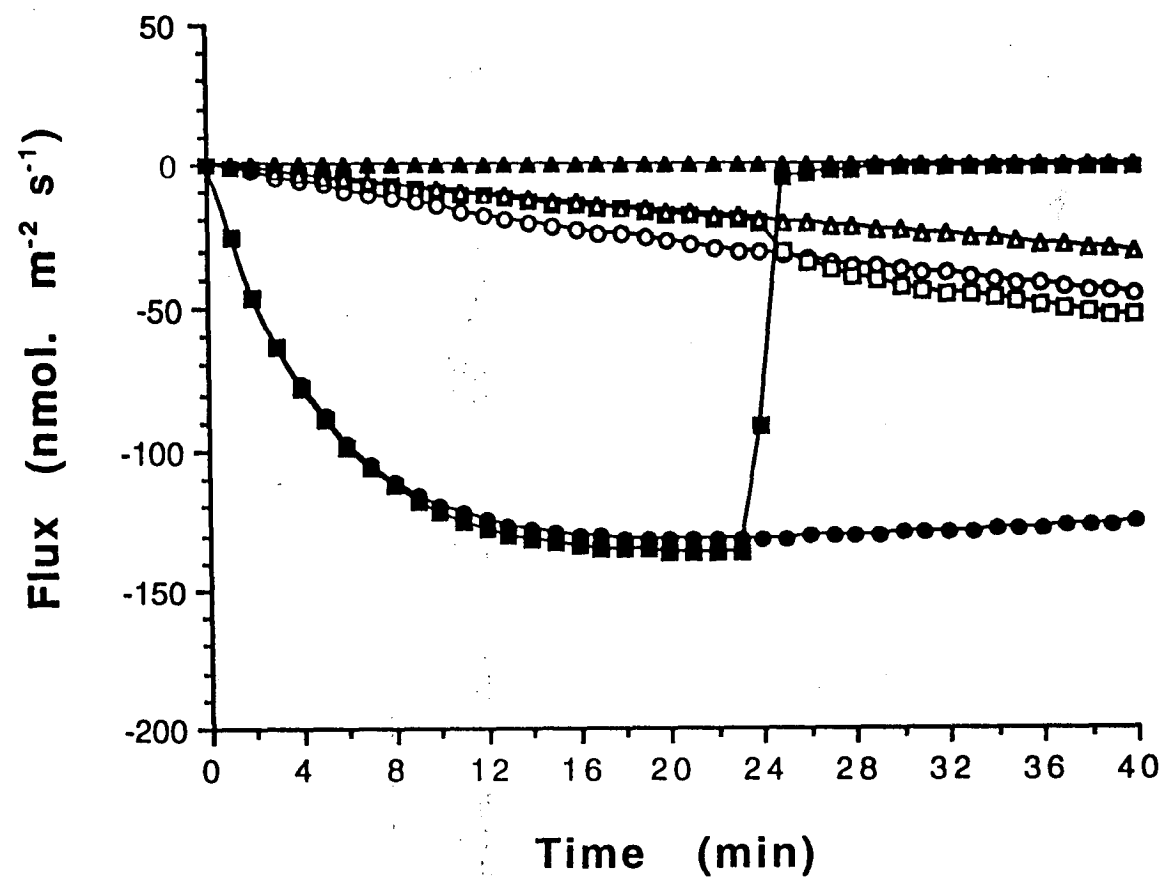
Figure 4.7

The calculated proton (open symbol) and calcium (solid symbol) effluxes using the WADM model for fluxes when the pK of the wall's weak acids is 3.5 (O), 3.8 (□) or 4.0 (△). Other details are the same as in Figure 4.1.

Figure 4.8

The calculated proton (open symbol) and calcium (solid symbol) effluxes using the WADM model for fluxes when the intrinsic linear charge density parameter is 0.61 (Δ), 0.71 ($\square$) or 0.81 (O). Other details are the same as in Figure 4.1.
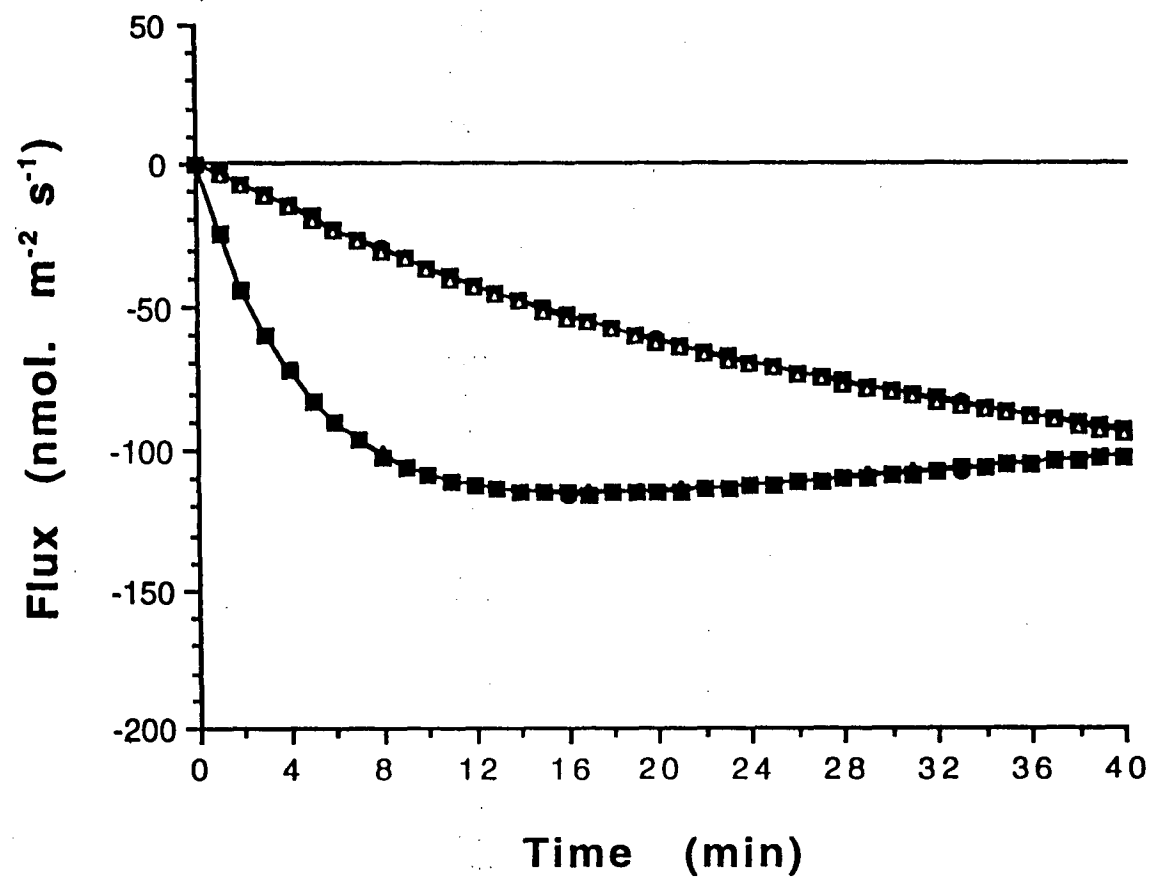
Figure 4.9

The calculated proton (open symbol) and calcium (solid symbol) effluxes using the WADM model for fluxes when the intrinsic linear charge density parameter is 0.50 (□), 0.53 (○) or 0.61 (△). Other details are the same as in Figure 4.1.

Figure 4.10
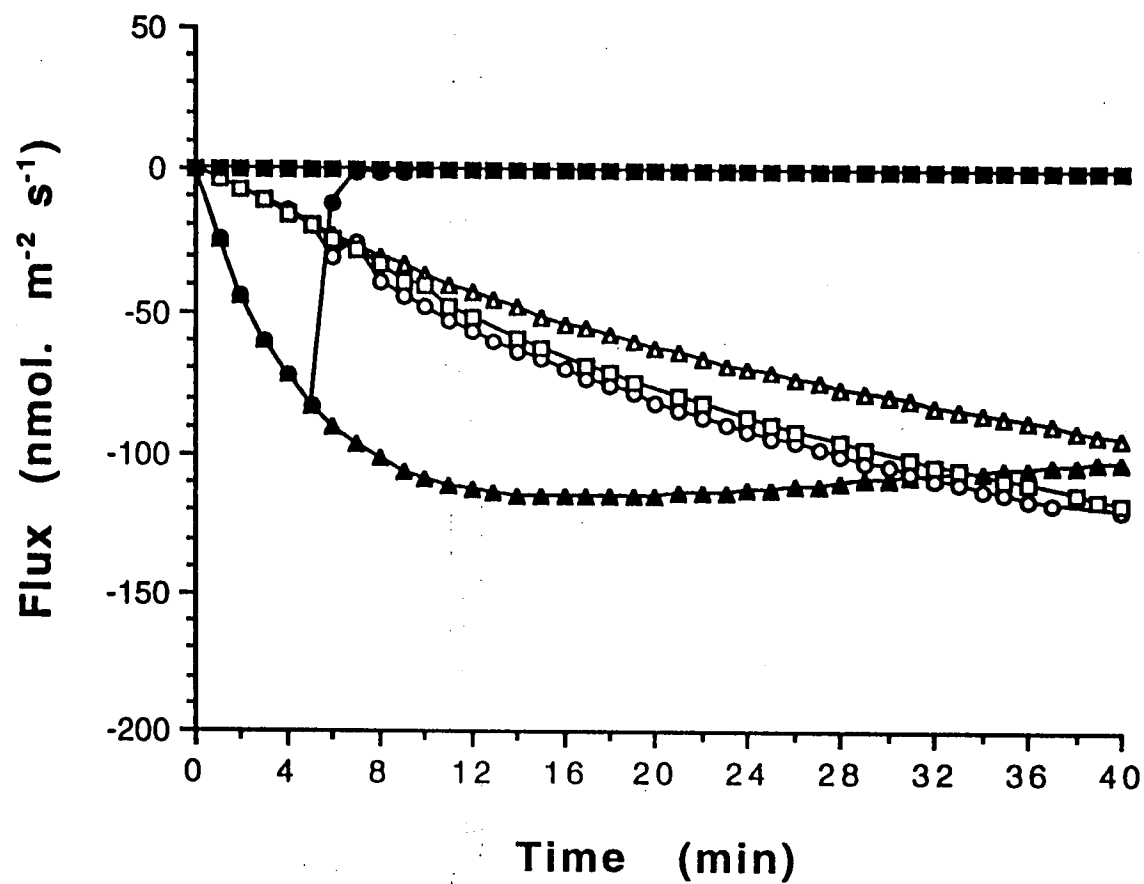
The calculated proton (open symbol) and calcium (solid symbol) effluxes using the WADM model for fluxes when the wall thickness of each cell is 0.5 (△), 1.0 (□) or 2.0 (○) μm. Other details are the same as in Figure 4.1.
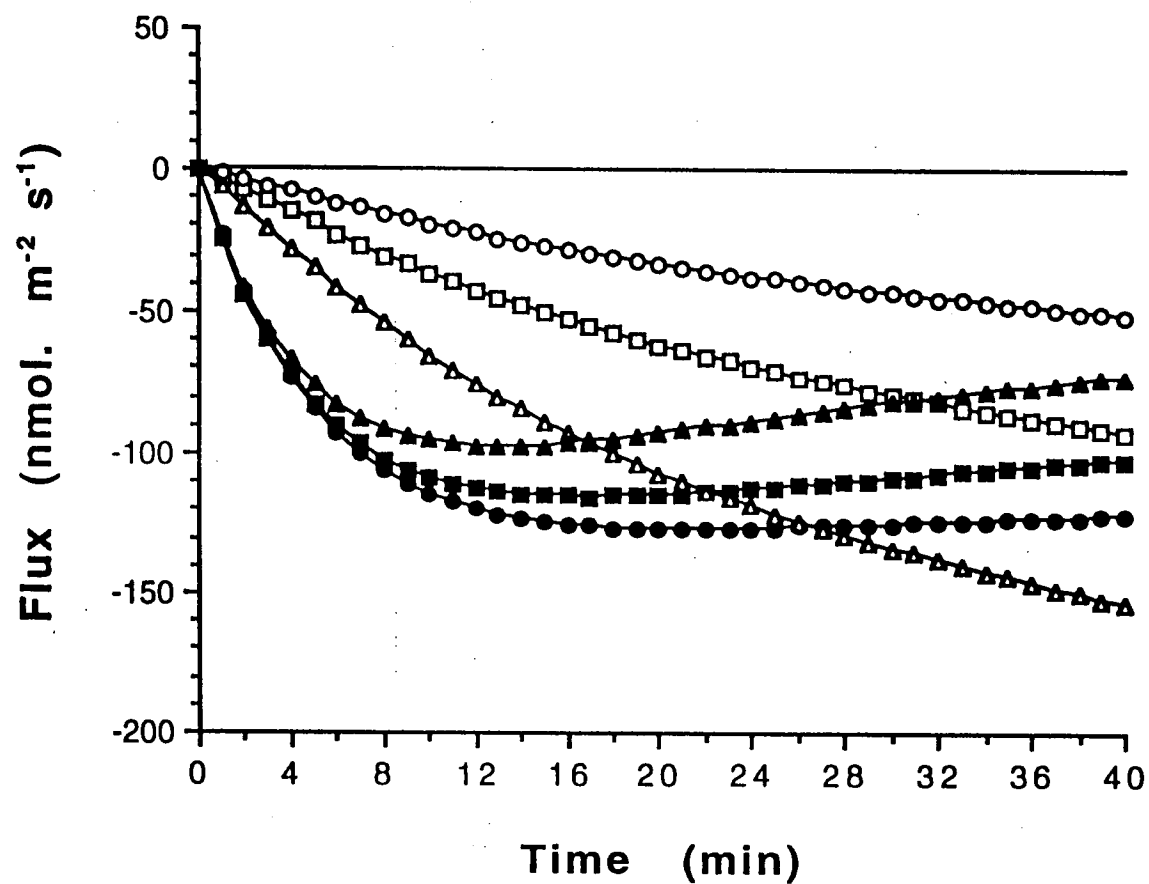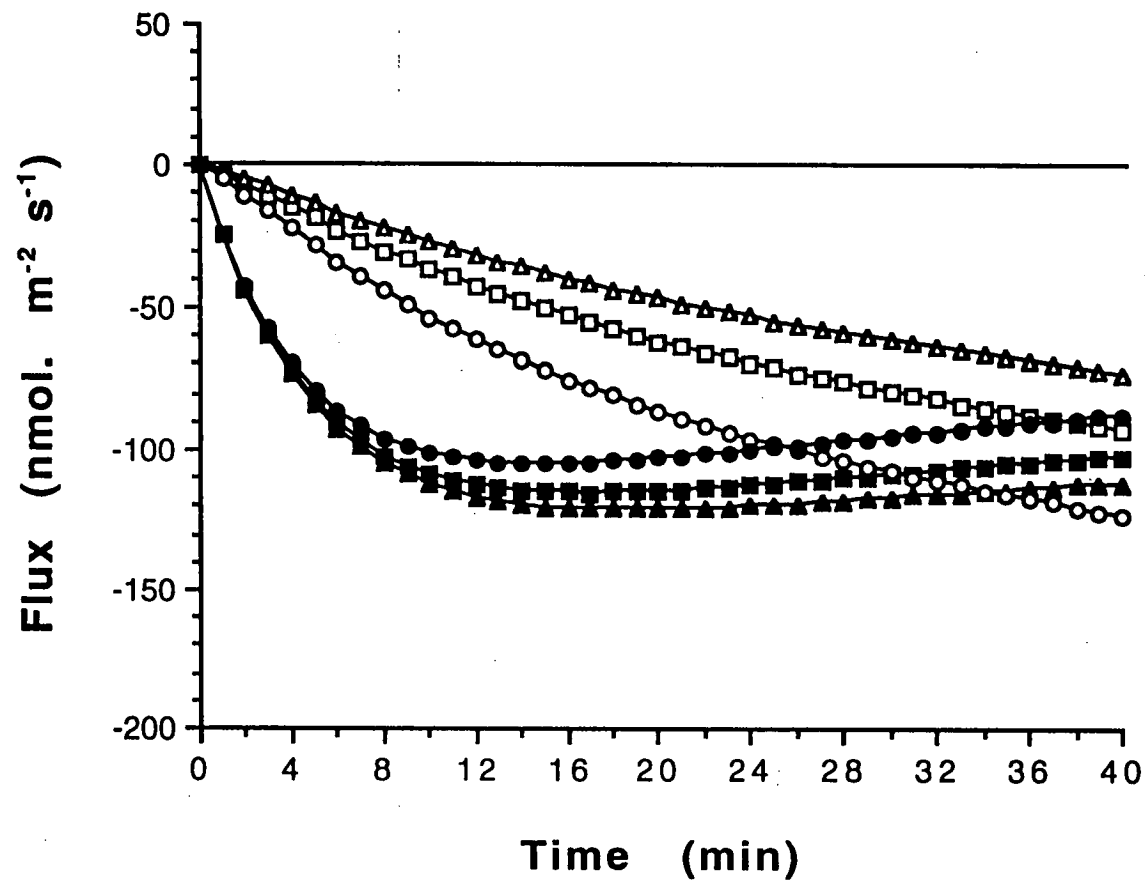
Figure 4.11

The calculated proton (open symbol) and calcium (solid symbol) effluxes using the WADM model for fluxes when the diffusion coefficient of cations in the DFS is 0.1 (Δ), 0.2 ($\square$) or 0.5 ($\bigcirc$) of that in the WFS. Other details are the same as in Figure 4.1.

When the analysis of the WADM model for fluxes is applied on these data, it is found that the calculated proton and calcium effluxes from the walls to the external medium increase (see Figure 4.1). This indicates that there is calcium release from the condensed phase in the walls by some of the extruded protons. The fluxes of potassium, sodium and chloride are zero and the efflux of N⁻ (not shown) is the same as its efflux at the plasmalemma. In fact, it is not exactly the same because some of the extruded N⁻ ions are left in the walls to increase the concentration of the N⁻ ions in the DFS and in the WFS. However the amount is small compared to the amount of the extruded N⁻ ions transported to the bathing medium.

In the beginning, the increase of calcium efflux is faster than the proton efflux. After the proton efflux at the plasmalemma levels off, the calculated calcium efflux starts to decrease. Meanwhile, the calculated proton efflux still increases. According to the WADM model, when the pH of the DFS is decreased to approach the pK of the wall's weak acids, the same pH decrease causes more calcium release (see Figure 4.2). Therefore the decrease of the calculated calcium efflux, when the proton efflux in the plasmalemma levels off, indicates that a constant proton efflux across the plasmalemma does not decrease the pH of the DFS linearly. In this case, the rate of the decrease becomes smaller. This is shown in Figure 4.3. The pH of the DFS decreases from about 4.4 to 3.7 and the pH of the WFS decreases from 6.0 to about 4.9.

The Donnan partition coefficient and the Donnan potential during the proton extrusion are shown in Figure 4.4. The Donnan partition coefficient decreases from about 43 to about 15. Meanwhile the Donnan potential depolarizes from about -95 to about -69. The calcium efflux does not drop to zero during this time. This indicates that some condensed calcium in the walls is still available at 40 minutes. In this condition, the concentration of the dissociated ionisable sites useable for the Donnan equilibrium has not been altered. Meanwhile, some of the extruded protons, the extruded N⁻ ions and the released calcium increase the ionic strength of the DFS and the WFS in the walls. Therefore the Donnan partition coefficient decreases and the Donnan potential increases. For potassium, sodium and chloride that do not have any sources in the walls, the decrease of the Donnan partition coefficient relates to the decrease of the ion concentration in the DFS and the increase of the ion concentration in the WFS. In this case, the decrease of the ion quantity in the DFS is the same as the increase of the ion quantity in the WFS. Therefore, there

are not fluxes of those ions from the walls to the bathing medium (see equation 4.46).

In the absence of calcium flux at the plasmalemma, the source of calcium entering the DFS, the WFS and the bathing medium is the calcium released from the condensed phase of the walls during proton extrusion. However, if Manning condensation is not considered in this model of the walls so that condensed calcium in the walls does not exist, there would be not calcium release during proton extrusion. In this case, as with other ions that do not have any sources in the walls, changes of Donnan equilibrium during proton extrusion only cause exchange of calcium between the DFS and the WFS within the walls. Therefore there would be not calcium efflux from the walls to the bathing medium. This is not what many people expect. In conclusion, Manning condensation must be included in the model of walls in order to allow calcium efflux from the walls to the bathing medium during proton extrusion. *See Chapter 4 and attached note.*

In conventional Donnan model, proton entry to cell walls reduces the concentration of the dissociated ionisable sites which is also considered as the fixed charge concentration in the DFS. Consequently, the Donnan partition coefficient decreases. the calcium concentration in the DFS decreases and the calcium concentration in WFS increases. The total amount of calcium that increases the calcium concentration on the WFS is the same as the amount of calcium that reduces the calcium concentration in the DFS (In both DFS and WFS, there is no net addition of calcium). The increase of calcium concentration in the WFS *does not* cause diffusion of calcium from the WFS to the external medium because if it does, the diffusion will result in reduction of the new calcium concentration in the DFS (which means moving away from the equilibrium condition of the calcium concentration in the DFS). In this case, to think the process of the diffusion from the walls, we should consider driving force of diffusion caused not only by the calcium concentration difference from the equilibrium calcium concentration *in the WFS* but also by the calcium concentration difference from the equilibrium calcium concentration *in the DFS*. This is what many people usually forget to do. Since with conventional Donnan model on the walls, proton entry does not cause any net addition of calcium in both DFS and WFS, calcium efflux from the walls to the bathing medium can not be expected.

When Manning condensation is included in the model of walls, proton entry to cell walls reduces the concentration of the dissociated ionisable sites of the walls. However it will not alter the concentration of the fixed negative charges in the DFS available for the Donnan equilibrium when the linear charge density parameter ξ has not dropped below 0.5 (there is still calcium condensation in the walls). The Donnan partition coefficient still decreases but it is not as much as when the fixed negative charge concentration decreases. In this case, the decrease of the Donnan partition coefficient is only caused by the increase of the ionic strength of the DFS and the WFS in the walls. The reduction of the concentration of the dissociated ionisable sites in the walls by proton entry results in the reduction of the condensed calcium concentration in the walls. The released condensed calcium goes to the DFS and the WFS of the walls and therefore in both DFS and WFS, there is net addition of calcium. This will act as the driving force of calcium diffusion from the walls to the bathing medium.

are not fluxes of those ions from the walls to the bathing medium (see equation 4.46).

In the absence of calcium flux at the plasmalemma, the source of calcium entering the DFS, the WFS and the bathing medium is the calcium released from the condensed phase of the walls during proton extrusion. However, if Manning condensation is not considered in this model of the walls so that condensed calcium in the walls does not exist, there would be not calcium release during proton extrusion. In this case, as with other ions that do not have any sources in the walls, changes of Donnan equilibrium during proton extrusion only cause exchange of calcium between the DFS and the WFS within the walls. Therefore there would be not calcium efflux from the walls to the bathing medium. This is not what many people expect. In conclusion, Manning condensation must be included in the model of walls in order to allow calcium efflux from the walls to the bathing medium during proton extrusion. See Chapter 4 and attached note.

To study the effects of the ionisable sites in the walls, three different values of the concentration of the ionisable sites in the DFS of the walls (600, 800 and 1000 mole m^{-3}) are used in the analysis of the WADM model for fluxes. Figure 4.5 shows the results of the analysis. The patterns of the calculated proton and calcium effluxes from the walls to the external medium are the same. The higher concentration of the ionisable sites causes bigger calcium effluxes and smaller proton effluxes. The changes to the effluxes are not linearly dependent on the concentration. In this case, the increase of the concentration from 800 to 1000 mole m^{-3} causes a smaller increase of the calcium efflux and a smaller decrease of the proton efflux than from 600 to 800 mole m^{-3}. According to the Henderson-Hasselbalch equation (see also Figure 4.2), for the same pH decrease in the DFS, the higher concentration of the ionisable sites causes a bigger increase of the calcium release, thereby causing a bigger increase of the calcium efflux from the walls. Therefore, the smaller increase of the calcium efflux indicates that the pH decrease for the increase of the concentration of the ionizable sites from 800 to 1000 mole m^{-3} is smaller than the pH decrease for the increase of the concentration of the ionisable sites from 600 to 800 mole m^{-3}.

Now when the pK of the wall's weak acids is altered, the position of the working pH of the DFS relative to the pK is also changed. In Figure 4.2, this pK change shifts the curve. When the pK is increased so that it becomes closer

to the working pH, the same pH decrease caused by proton extrusion causes a larger calcium release. Therefore, the calculated calcium efflux from the cells to the bathing medium is bigger and the calculated proton efflux is smaller. Figure 4.6 shows the calculated proton and calcium effluxes when the pK of the wall's weak acids is 2.0, 3.0 and 3.5. From this figure, it is clearly shown that the calcium efflux is bigger when the pK is higher. Meanwhile, the proton efflux is smaller. When the pK is increased further so that the available initial condensed calcium in the walls is less (see Figure 4.2), after some time, the extruded protons release all of the condensed calcium. After this happens, the calcium efflux would be zero because there is not any calcium release from the walls. In Figure 4.7, when the pK is 3.8, all of the condensed calcium has been released after about 24 minutes. After this time, some extruded protons are still needed to decrease the concentration of the dissociated ionisable sites during the decrease of the pH of the DFS. Therefore the proton efflux does not increase to approach the proton efflux in the plasmalemma although the calcium efflux drops to zero. The small increase of the proton efflux at this time is due to the decrease of the concentration of the ionisable sites useable for the Donnan equilibrium. When the pK is 4.0, the initial concentration of the condensed calcium in the walls is zero (see Figure 4.2 when the curve central is shifted to 4.0 while the initial pH of the DFS is about 4.4). In this condition, proton extrusion from the cell to the cell walls does not cause any calcium release from the walls. The proton extrusion only causes an exchange of calcium between the DFS and the WFS within the walls. Therefore, there is no calcium efflux from the walls to the bathing medium.

When the intrinsic linear charge density parameter of the walls ξ^* is altered, the boundary at $\xi=0.5$ in Figure 4.2 is shifted (the maximum scale of the linear charge density parameter ξ is the new ξ^*). However, the curve is still the same. Therefore when ξ still does not drop below 0.5 during proton extrusion, the resulting proton and calcium effluxes from the walls to the bathing solution are the same. In Figure 4.8, it is shown that for different values of ξ^* (0.81, 0.71 and 0.61), the calculated proton and calcium effluxes are the same. When ξ drops below 0.5 during proton extrusion, there is not any condensed calcium in the walls to be released. Therefore the calcium efflux drops to zero. In Figure 4,9, when ξ^* is 0.53, the calcium efflux drops to zero after about 5 minutes. This indicates that at this time, ξ drops below 0.5. At this time, the concentration of the dissociated ionisable sites useable for the Donnan equilibrium also decreases so that the proton efflux increases. When ξ^* is ≤ 0.50, the initial concentration of the condensed calcium in the walls is zero.

Therefore the walls can be considered as a classic Donnan system only. In this condition, the calculated calcium efflux is zero and the calculated proton efflux is bigger than the proton efflux when there is still condensed calcium in the walls. However, the calculated proton efflux from the walls to the bathing medium is not the same as the proton efflux at the plasmalemma because some of the extruded protons are still needed to protonate the dissociated ionisable sites in the walls and to increase the proton concentration in the DFS and in the WFS.

To study the effects of the thickness of the walls, three different values of wall thickness (0.5, 1.0, 2.0 μm) are used in the analysis. In Figure 4.10, it is shown that when the walls are thinner, the calcium efflux is smaller and the proton efflux is bigger. When the cells have thinner walls, the extruded protons travel in the walls in a shorter time. During this time , the interaction between the extruded protons and the condensed calcium in the walls only causes a smaller amount of calcium release. Therefore for thinner walls, the extruded protons diffuse out from the walls more as proton efflux than as calcium efflux.

Similarly, when the diffusion coefficient of cations in the DFS is higher, the cations diffuse in the walls faster and the time for the interaction between the extruded protons and the condensed calcium is shorter. As a result, the proton efflux is bigger and the calcium efflux is smaller. Figure 4.11 shows the results of the WADM model analysis for fluxes when the diffusion coefficient of cations in the DFS is 0.5, 0.2 and 0.1 times that of in the WFS.

4.5 Conclusion

The WADM model for fluxes provides a quantitative analysis to estimate the wall's quantities and the ion fluxes from the walls to the bathing medium during proton extrusion. It is shown that the proton extrusion causes effluxes of both protons and calcium. This indicates that the WADM model for fluxes is successful in describing the proton-calcium exchange in the walls expected during proton extrusion. Meanwhile the fluxes of potassium, sodium and chloride are zero. The estimated pH of both the DFS and the WFS, and the estimated Donnan partition coefficient decrease. The estimated Donnan potential depolarizes.

Beside the composition of ions in the external solution, the results of the WADM model for fluxes also depend on the wall's parameters: the concentration of the ionisable sites, the pK of the wall's weak acids, the wall thickness, and the diffusion coefficient of cations in the DFS. When the linear charge density parameter is still higher than the reciprocal of the highest valency of the involved cations (in this case 0.5 for calcium), the results do not depend on the intrinsic linear charge density parameter.

When the intrinsic linear charge density parameter is ≤0.5, the WADM model prevents calcium condensation in the walls. Therefore the walls can be considered as a classic Donnan system only. With this special case of the WADM model, proton extrusion across the plasmalemma to the walls does not cause any calcium release from the walls. The proton extrusion only causes an exchange of calcium between the DFS and the WFS within the walls. Therefore there is not calcium efflux from the walls to the bathing medium during proton extrusion. This indicates that Manning condensation must be included in the model of walls to allow calcium release from the walls by extruded protons.

Chapter 5

FUSICOCCIN EFFECTS ON OATS

5.1 Introduction

The fungal toxin fusicoccin (FC) is well known as a tool in plant physiology since it affects many physiological processes in higher plants (Marrè 1979). Some of the effects mimic the effects of natural plant growth substances such as cell enlargement, medium acidification and membrane hyperpolarization (Cleland 1976, Kutschera and Schopfer 1985a&1985b, Bertl and Felle 1985, Felle et al. 1986, Senn and Goldsmith 1988, Brummer et al. 1985, Lüthen and Böttger 1989, Lüthen et al. 1990, Schulz et al. 1990). Fusicoccin also causes uptake of potassium and other solutes, seed germination and stomatal opening (Marrè 1979, Blatt 1988, Blatt and Clint 1989, Clint and Blatt 1989). However evidence for calcium transport during fusicoccin action is still lacking.

The growth response of fusicoccin is similar to the growth response of acid solutions (Kutschera and Schopfer 1985b). Their responses are immediate and also not additive (Marrè 1979, Kutschera and Schopfer 1985a&1985b). This indicates that the growth mechanism induced by fusicoccin and acid solutions may be the same, i.e. by wall acidification. Therefore it was suggested that the acid-growth theory is suitable for fusicoccin-induced growth (Kutschera and Schopfer 1985b).

When fusicoccin causes medium acidification, the walls also become acid. In this thesis, the hypothesis is that when the wall pH decreases as the result of proton extrusion induced by particular treatments, some of the condensed wall calcium is released from the walls by exchange with the extruded protons. The argument of this hypothesis is based on the WADM model (Richter and Dainty 1990b, Ryan, Newman and Arif 1992). In this

chapter, the hypothesis is tested for the acidification of the walls induced by fusicoccin.

Fusicoccin is useful in studying the possibility of proton-calcium exchange in the walls during wall acidification because medium acidification induced by fusicoccin happens immediately (Cleland 1976, Brummer et al. 1985, Kutschera and Schopfer 1985a&1985b). If the medium acidification is delayed, any other processes that involve calcium release from the cells and/or the walls during the delay would interfere with the detection of the expected proton-calcium exchange in the walls. The fusicoccin-induced medium acidification is also substantial (Brummer et al. 1985, Kutschera and Schopfer 1985a&1985b). If proton-calcium exchange happens during this time, the amount of calcium released from the walls would be substantial too. Therefore the detection of calcium release would be clear.

Proton extrusion, membrane hyperpolarization, and uptake of solutes including potassium during fusicoccin action are sensitive to metabolic blockage and ATPase inhibitors. Based on this evidence, it was argued that during fusicoccin action, the ATPase in the plasma membranes is activated to cause proton extrusion and that changes in the transport of other solutes are the results of the increased proton electrochemical potential gradient and the membrane hyperpolarization (Marrè, 1979). However fusicoccin binding on oat root membranes was found in membrane proteins that are distinct from H^+-ATPase (Stout and Cleland, 1980). During fusicoccin-induced membrane hyperpolarization on guard cells of *Vicia faba* L., the enhancement of the pump current is limited and the membrane conductance decreases (Blatt 1988). In guard cells where the primary proton pump shows little activity and potassium efflux contributes largely to charge balance maintaining membrane potential, tracer study shows that fusicoccin, like the K^+-channel blocker tetraethylammonium (TEA), reduces the potassium efflux; fusicoccin increases potassium influx but the influx is insensitive to the K^+-channel blocker (Clint and Blatt 1989). Furthermore, measurements under voltage clamp show that outward-directed K^+-channel current that contributes to charge balance maintaining membrane potential is inactivated during fusicoccin action (Blatt and Clint 1989). These indicate that potassium uptake during fusicoccin action is not only the result of the secondary transport related to the change of the protons concentration gradient, but also the result of the inactivation of the outward-directed K^+-channel current. In relation to this argument, the effect of fusicoccin on potassium transport in oat coleoptile segments is also studied by

simultaneously measuring potassium flux with proton and calcium fluxes. The results of membrane potential measurements during fusicoccin action in this study are also presented and discussed

A 12-mm-long split segment of a 4-day-old oat coleoptile, cut 3 mm below the apex, was put on a plastic sponge with the cut surface face up and pretreated for 4.5 hours in aerated standard unbuffered solution (BSM) containing 0.1 mole m^{-3} KCl and 0.1 mole m^{-3} $CaCl_2$ adjusted to pH 6 using NaOH. It is assumed that preincubation in the aerated solution for 4.5 hours is adequate to eliminate most of the effects of splitting. As described in Chapter 3, the unbuffered solution in fact still has buffering effects of water and carbonates due to carbon dioxide dissolved from the atmosphere. However at pH 6, the calculated flux ratio between the protonated buffers and the protons in the presence of these buffering effects is much less than 1. Therefore in these experiments, using the solution at pH 6, the results of the proton flux measurements are assumed not to be altered by the buffering effects.

Proton, potassium and calcium fluxes close to the cut tissue surface in diffusion limited solution were determined simultaneously using the MIFE technique described in Chapter 2 and Appendix A (see also Newman et al. 1987, Ryan et al. 1990). As a control, the fluxes were measured in the absence of fusicoccin for about 40 minutes. Fusicoccin was then applied by adding a small amount of very concentrated fusicoccin solution to the measurement chamber to give the desired final concentration (see Chapter 2 for details). In this case, to study the relation between the magnitude of the responses and the fusicoccin concentration, four different concentrations of fusicoccin (10^{-2}, 10^{-3}, 5×10^{-4} and 10^{-4} mole m^{-3}) were used. The flux measurements in the presence of fusicoccin were carried out every minute for about 40 minutes.

I decided to limit the length of the flux measurements to study proton-calcium exchange during fusicoccin or IAA action to 40 minutes because the wall loosening as the result of wall acidification that initiates the growth (acid-growth) happened in the first half hour after the application of the growth substances. This process was indicated by the increase of growth rate during this time (Vanderhoef 1980). I expected that proton-calcium exchange takes place during this time causing wall loosening. After the first half hour, growth still occurs but it was suggested that other complex processes are involved (gene expression hypothesis). Proton-calcium exchange may still take place

during these processes, however in the present work, it was not studied. Therefore the flux measurements were not carried out for a longer time.

The membrane potential of parenchymal cells in the segments were measured using the method described in Chapter 2 and Appendix A. The treatment was similar to the treatment in the flux measurements. The concentration of fusicoccin were 10^{-3}, 5×10^{-4} and 10^{-4} mole m^{-3}.

5.2 Results

The results of the flux measurements for each concentration of fusicoccin are presented in Figures 5.1, 5.2, 5.3 and 5.4. For membrane potential measurements, the results are presented in Figures 5.5, 5.6 and 5.7. For comparison, the results of proton flux, calcium flux, potassium flux, pH and membrane potential are combined in Figures 5.8, 5.9, 5.10, 5.11 and 5.12 respectively.

5.2.1 Ion Fluxes

Using the MIFE technique, segments of oat coleoptiles preincubated for 4.5 hours show a net proton efflux of about 15 nmol. m^{-2} s^{-1} in BSM (Figure 5.8). Fusicoccin, in the concentration range between 10^{-2}-10^{-4} mole m^{-3}, increases the proton efflux immediately. The increase is transient. The efflux reaches its maximum at about 15 minutes. The magnitude of the maximum is different for different applied concentrations of fusicoccin. For 10^{-2}, 10^{-3}, 5×10^{-4} and 10^{-4} mole m^{-3} fusicoccin, the maxima of the efflux are about 130, 130, 100 and 70 nmol. m^{-2} s^{-1} respectively. This suggests that the increase of proton efflux induced by fusicoccin is saturated at 10^{-3} mole m^{-3} fusicoccin.

In BSM, the flux of calcium varies between experiments from 10 nmol. m^{-2} s^{-1} influx to 30 nmol. m^{-2} s^{-1} efflux (Figure 5.9). The flux also shows slow fluctuations. After the addition of fusicoccin, the calcium flux clearly becomes an efflux and the change is immediate. The calcium efflux is also transient with the maximum reached at about 25 minutes from the fusicoccin application. The calcium effluxes induced by 10, 1, 0.5 and 0.1 μM fusicoccin are almost the same, that is about 120 nmol. m^{-2} s^{-1}. This indicates that the fusicoccin-induced

calcium efflux does not depend on the concentration of fusicoccin, at least in the range of 10^{-2}-10^{-4} mole m^{-3}.

The 4.5 h preincubated segments in BSM showed an initial potassium efflux of about 30 nmol. $m^{-2} s^{-1}$ (Figure 5.10). After application of fusicoccin, the potassium efflux increases immediately. The increase is transient and the maximum is reached at about 13 minutes. At this time, the effluxes are 160, 160, 110, 40 nmol. $m^{-2} s^{-1}$ respectively for 10^{-2}, 10^{-3}, 5×10^{-4} and 10^{-4} mole m^{-3} fusicoccin. Similar to the fusicoccin-induced proton efflux, the fusicoccin-induced potassium efflux is saturated at 10^{-3} mole m^{-3} fusicoccin.

During the determination of proton fluxes using the MIFE technique, the average pH of the solution adjacent to the tissue surface can also be estimated. In these experiments of fusicoccin action on split oat segments, the pH before fusicoccin application varies with the experiments, in the range of 5.4-5.55 (Figure 5.11). The pH drop in the start of the graphs indicates that proton concentration gradient is being established after the solution is stirred up during the preparation. Just after the application of fusicoccin, there is a transient increase in pH, presumably as the result of the removal of the proton concentration gradient during the mixing to apply fusicoccin. After the transient, the pH decreases and in 20-25 minutes it starts to level off. During this time, the pHs for 10^{-2}, 10^{-3}, 5×10^{-4} and 10^{-4} mole m^{-3} fusicoccin are about 5.25, 5.25, 5.25 and 5.38 respectively.

5.2.2 Membrane Potential

In BSM, the initial membrane potential is between -70 to -60 mV (Figure 5.12). After application of fusicoccin, the membrane potential hyperpolarizes (negative going) immediately. Within 15-25 minutes, the membrane hyperpolarization levels off. For 10^{-3}, 5×10^{-4} and 10^{-4} mole m^{-3} fusicoccin, the new membrane potentials are -143, -140 and -110 mV. This indicates that the fusicoccin-induced membrane hyperpolarization depends on the concentration of fusicoccin.

In last paragraph on page 89, "The membrane potential of that magnitude is relatively small compared to the expected membrane potential observed in plant cells (smaller than -100 mV). Since the measured membrane potential was obtained from healthy parenchymal cells, there should be some explanation regarding the smallness of the measured membrane potential. Perhaps this is related to a different composition of ion concentration inside the parenchymal cells of oat coleoptiles. This needs some clarification." should be added just before sentence "After application of fusicoccin ...".
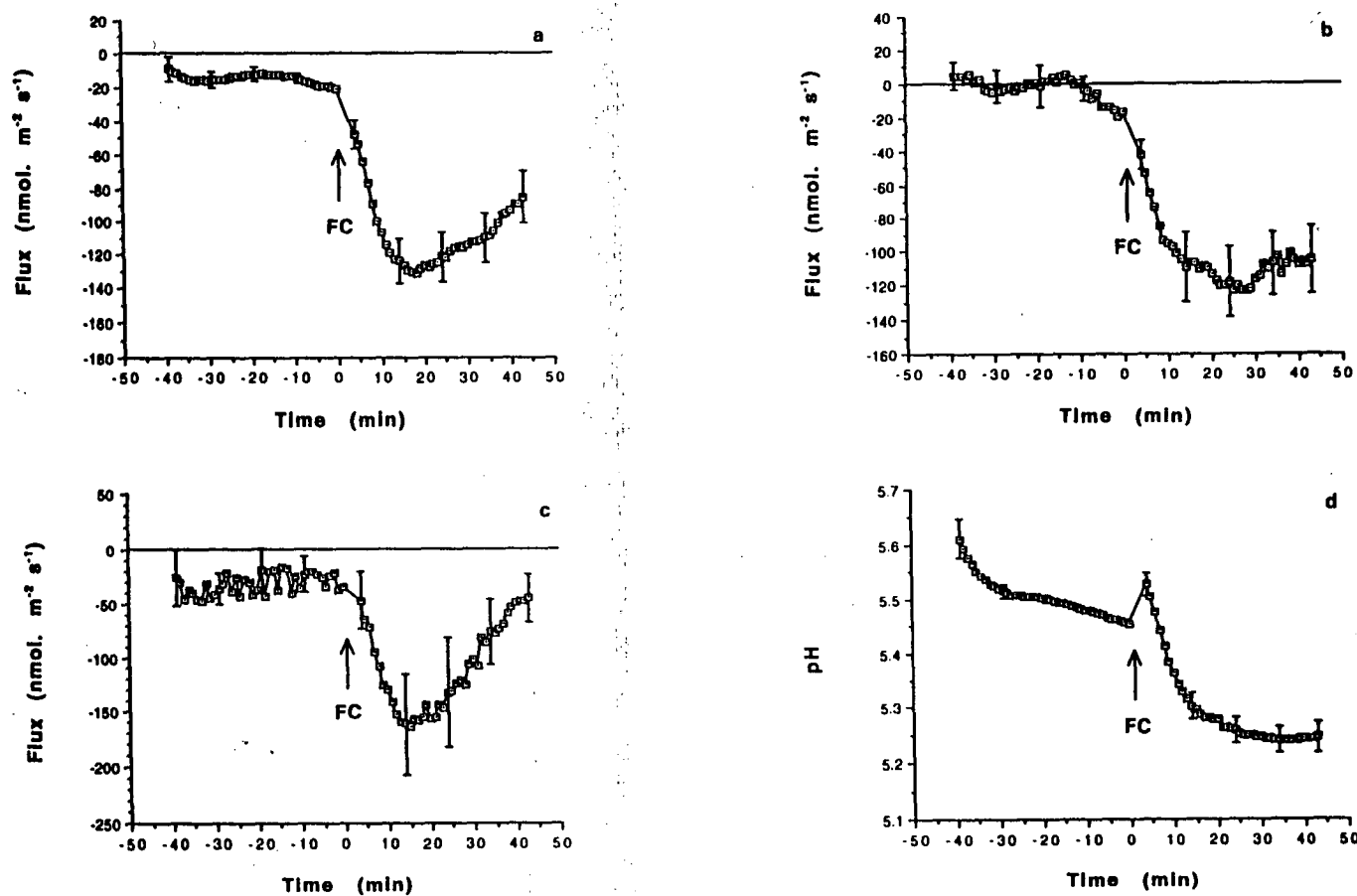
Figure 5.1

Effects of 10^2 mole m^3 fusicoccin (FC) on proton (a), calcium (b) and potassium (c) net fluxes (efflux negative) and pH (d) adjacent to the cut tissue surface of 4-day-old split oat coleoptile segments preincubated in BSM for 4.5 hours. Upward arrow indicates application of fusicoccin. Each mean of fifteen plants is calculated relative to the value obtained just before the application of fusicoccin. Bars show representative SE.
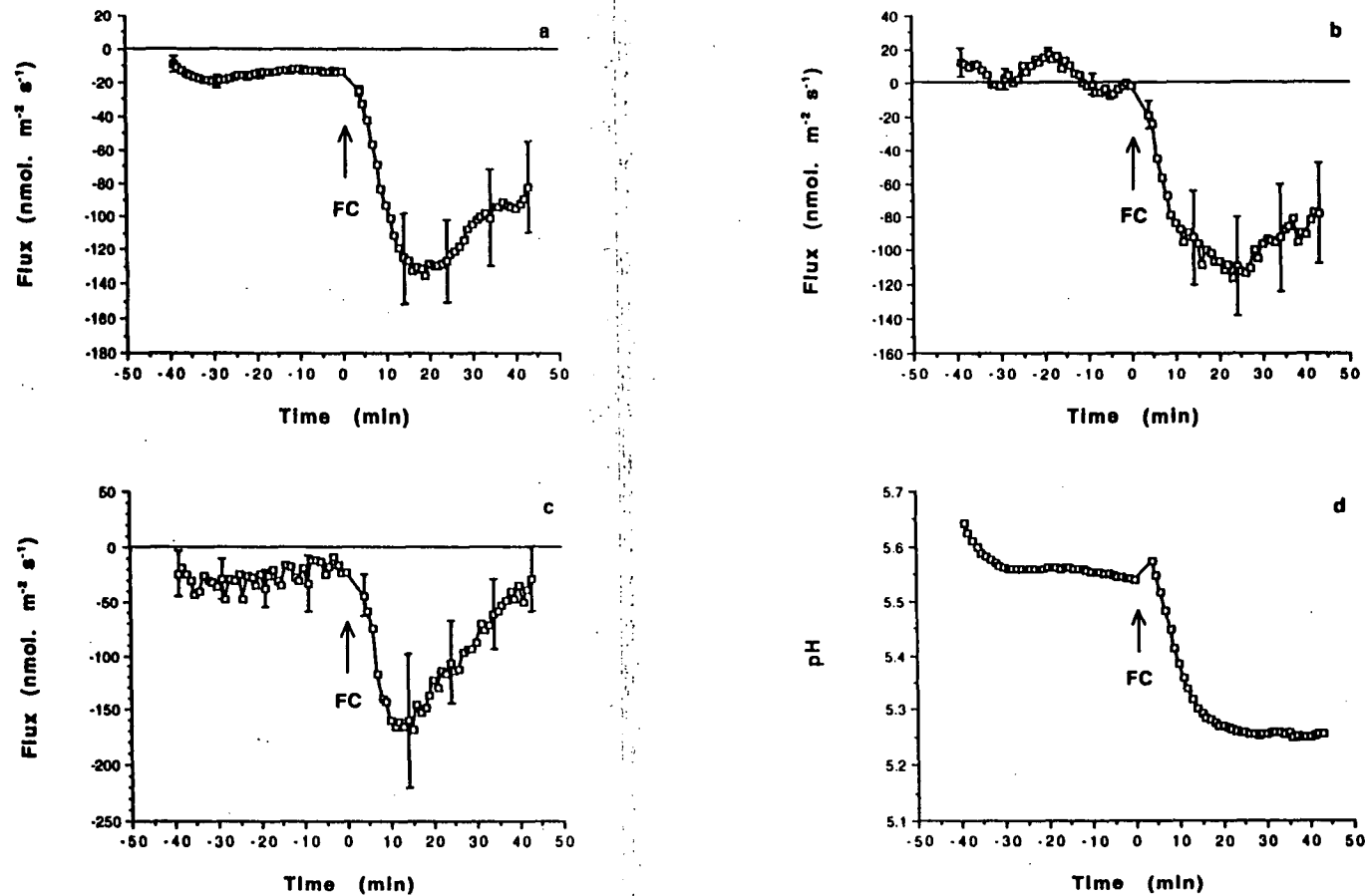
Figure 5.2

Effects of 10^{-3} mole m^{-3} fusicoccin (FC) on proton (a), calcium (b) and potassium (c) net fluxes (efflux negative) and pH (d) adjacent to the cut tissue surface of 4-day-old split oat coleoptile segments preincubated in BSM for 4.5 hours. Upward arrow indicates application of fusicoccin. Each mean of nine plants is calculated relative to the value obtained just before the application of fusicoccin. Bars show representative SE.

Figure 5.3

Effects of 5×10^{-4} mole m^{-3} fusicoccin (FC) on proton (a), calcium (b) and potassium (c) net fluxes (efflux negative) and pH (d) adjacent to the cut tissue surface of 4-day-old split oat coleoptile segments preincubated in BSM for 4.5 hours. Upward arrow indicates application of fusicoccin. Each mean of nine plants is calculated relative to the value obtained just before the application of fusicoccin. Bars show representative SE.
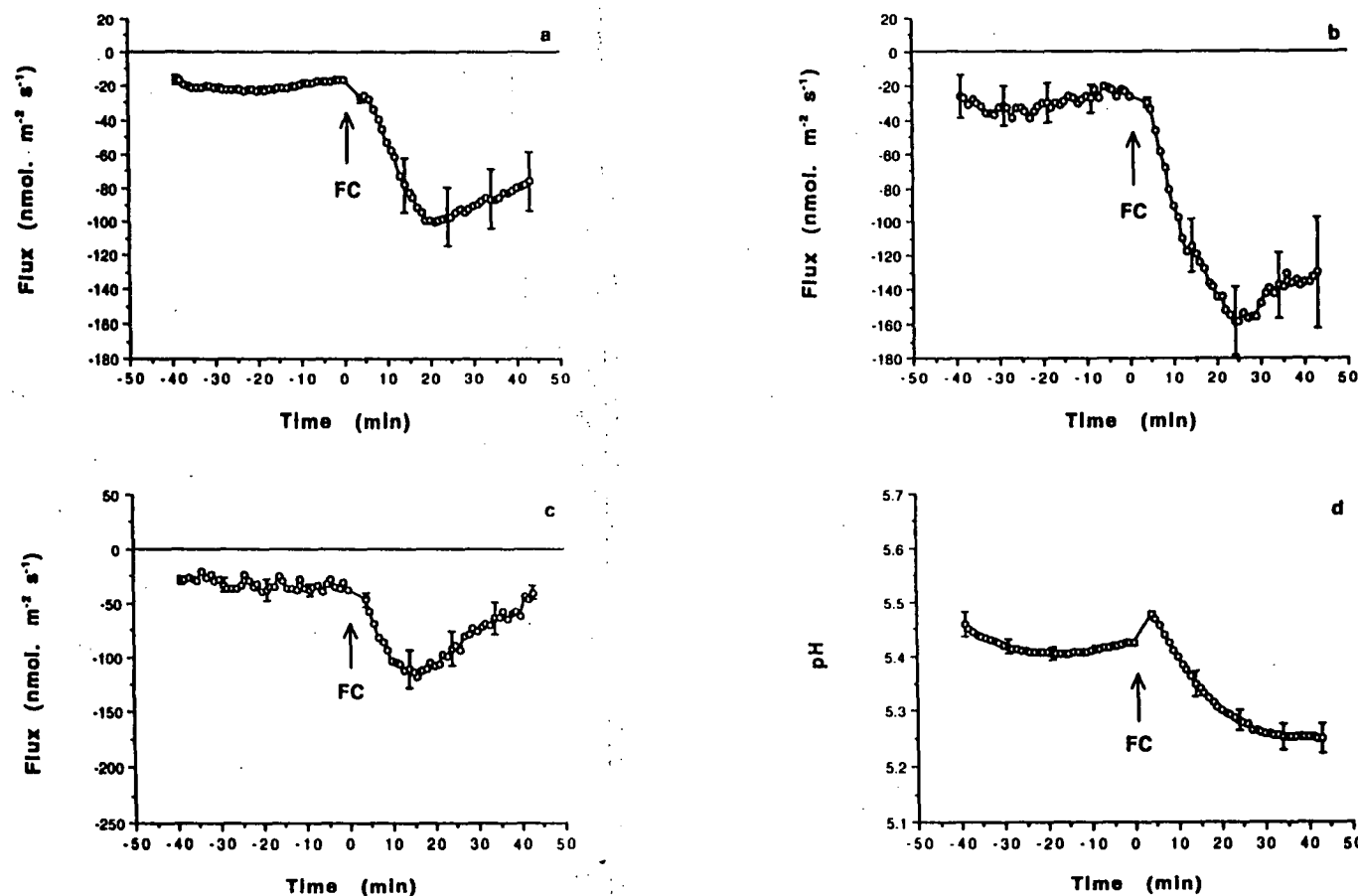
Figure 5.4

Effects of 10^{-4} mole m^{-3} fusicoccin (FC) on proton (a), calcium (b) and potassium (c) net fluxes (efflux negative) and pH (d) adjacent to the cut tissue surface of 4-day-old split oat coleoptile segments preincubated in BSM for 4.5 hours. Upward arrow indicates application of fusicoccin. Each mean of nine plants is calculated relative to the value obtained just before the application of fusicoccin. Bars show representative SE.
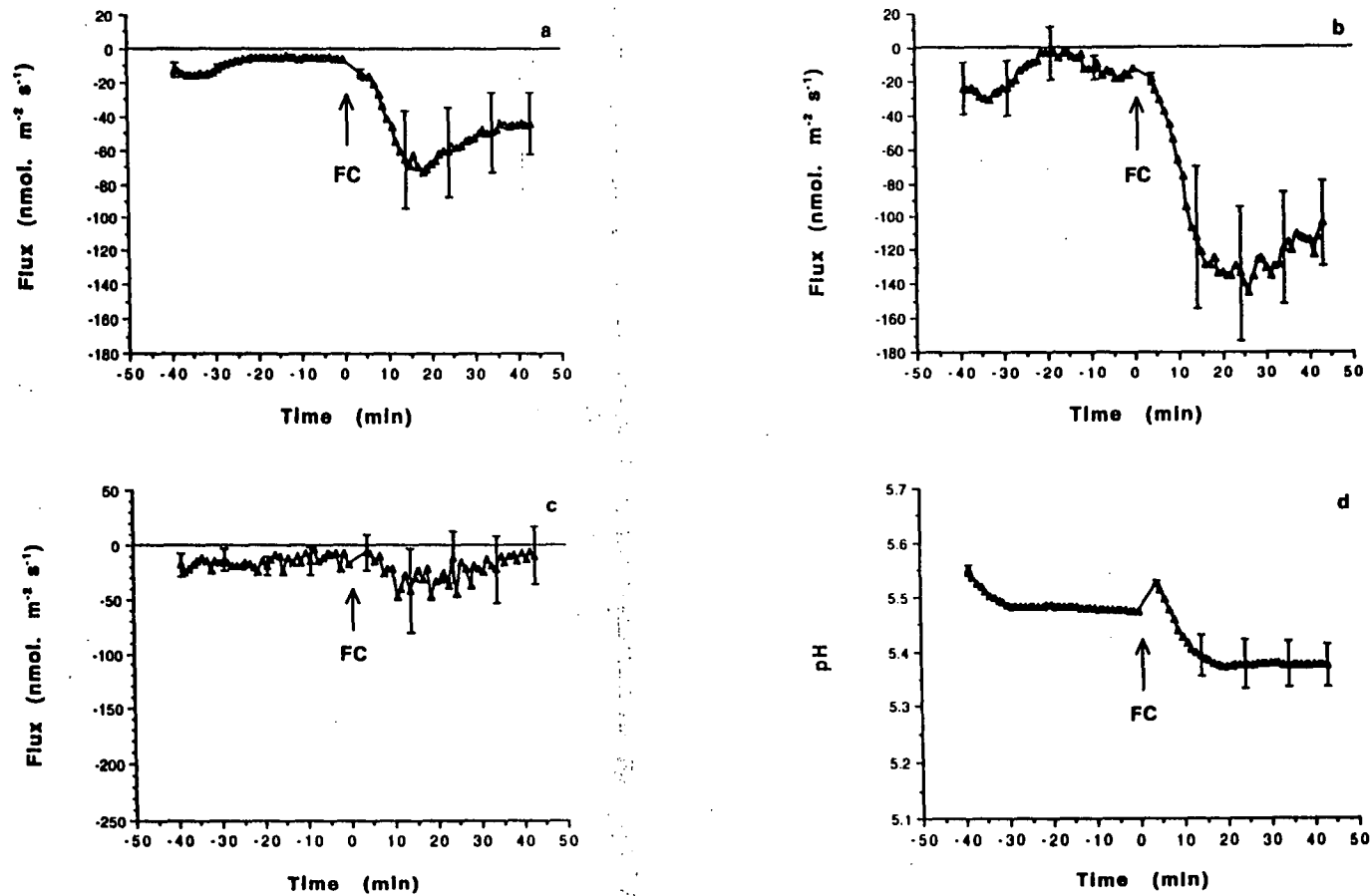
Figure 5.5

Effects of 10^3 mole m^{-3} fusicoccin (FC) on membrane potential (PD) of parenchymal cells in 4-day-old split oat coleoptile segments preincubated in BSM for 4.5 hours. Upward arrow indicates application of fusicoccin. Each mean of eight plants is calculated relative to the value obtained just before the application of fusicoccin. Bars show SE.

Figure 5.6

Effects of 5×10^{-4} mole m^{-3} fusicoccin (FC) on membrane potential (PD) of parenchymal cells in 4-day-old split oat coleoptile segments preincubated in BSM for 4.5 hours. Upward arrow indicates application of fusicoccin. Each mean of three plants is calculated relative to the value obtained just before the application of fusicoccin. Bars show SE.
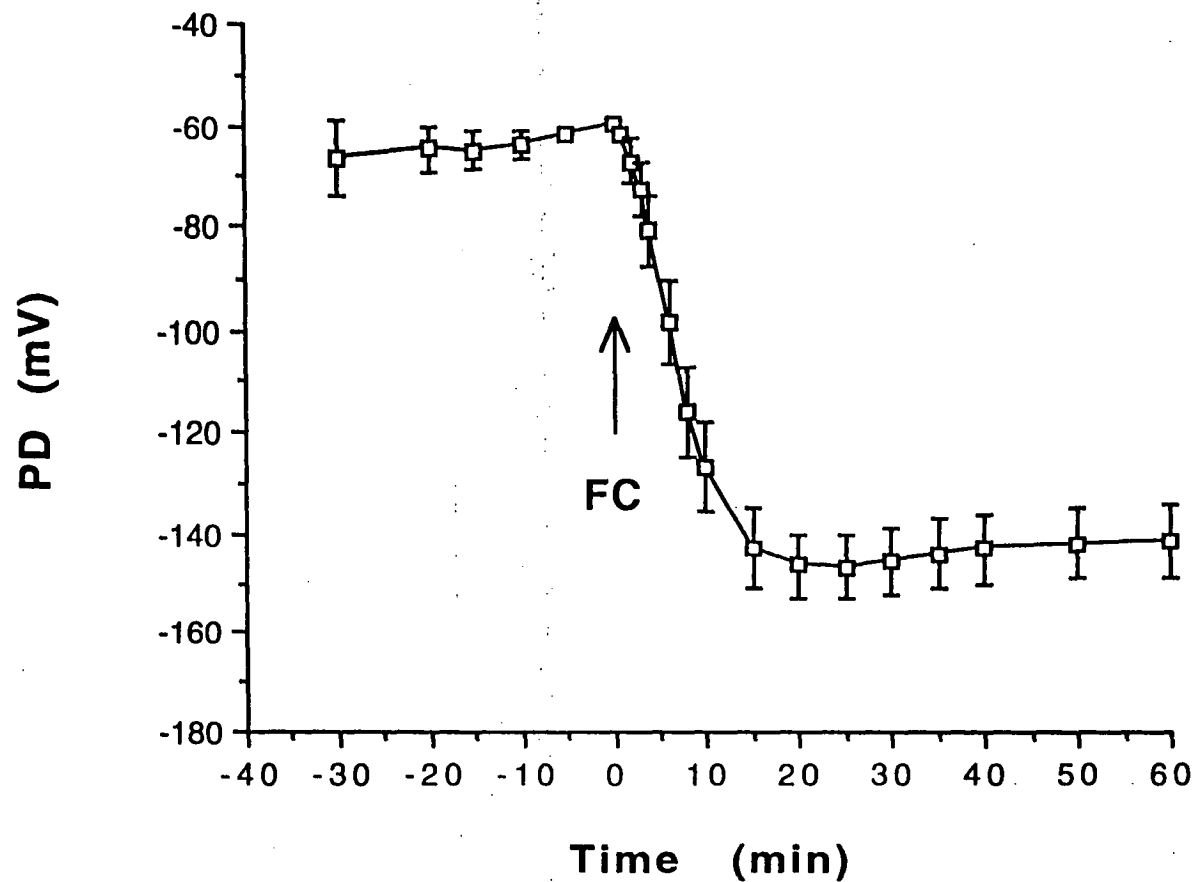
Figure 5.7

Effects of 10^{-4} mole m^{-3} fusicoccin (FC) on membrane potential (PD) of parenchymal cells in 4-day-old split oat coleoptile segments preincubated in BSM for 4.5 hours. Upward arrow indicates application of fusicoccin. Each mean of six plants is calculated relative to the value obtained just before the application of fusicoccin. Bars show SE.
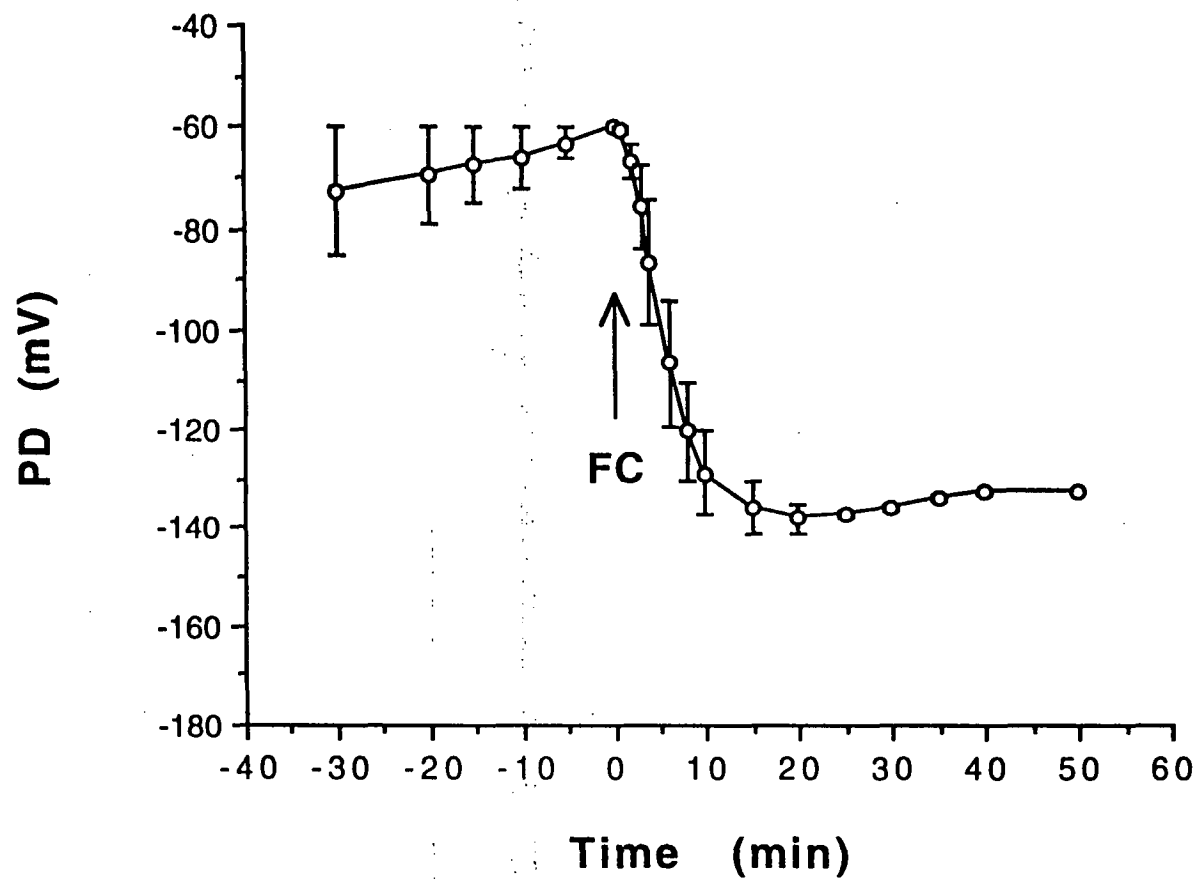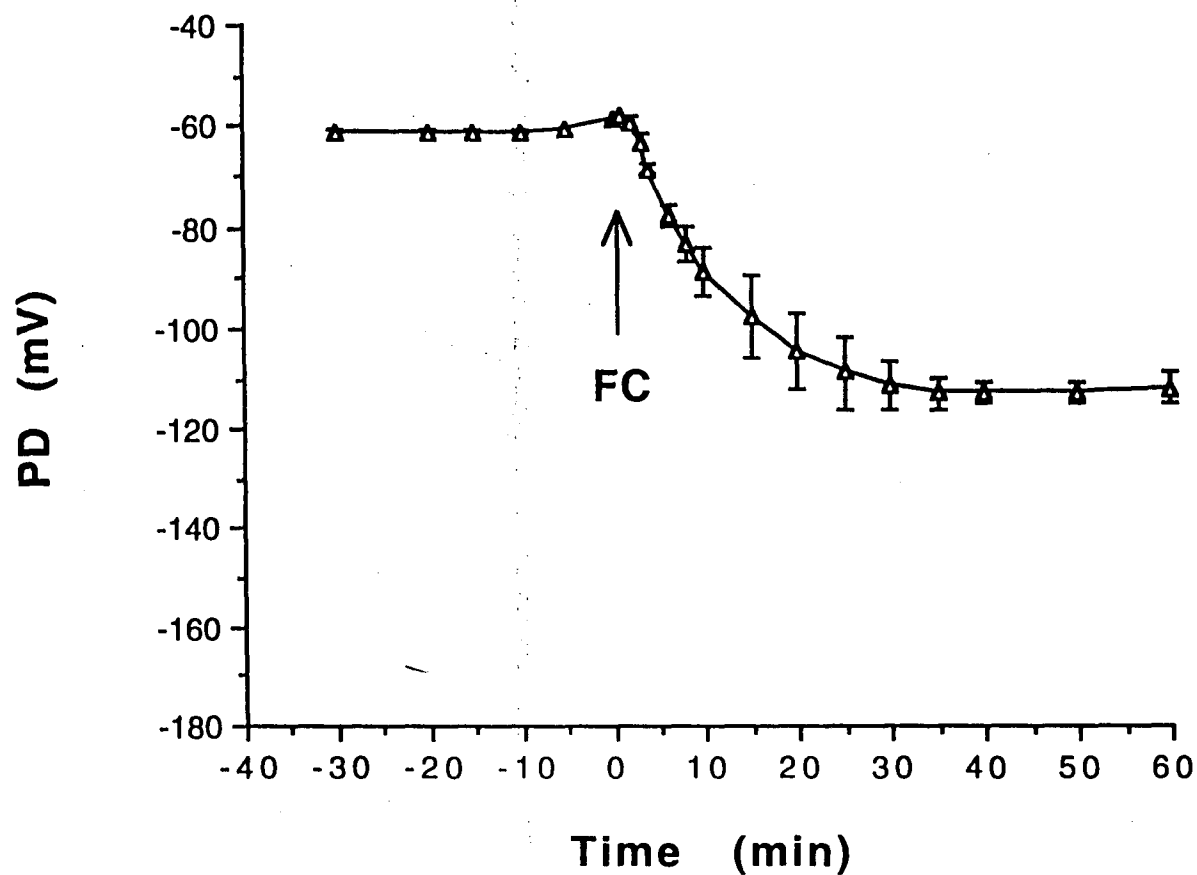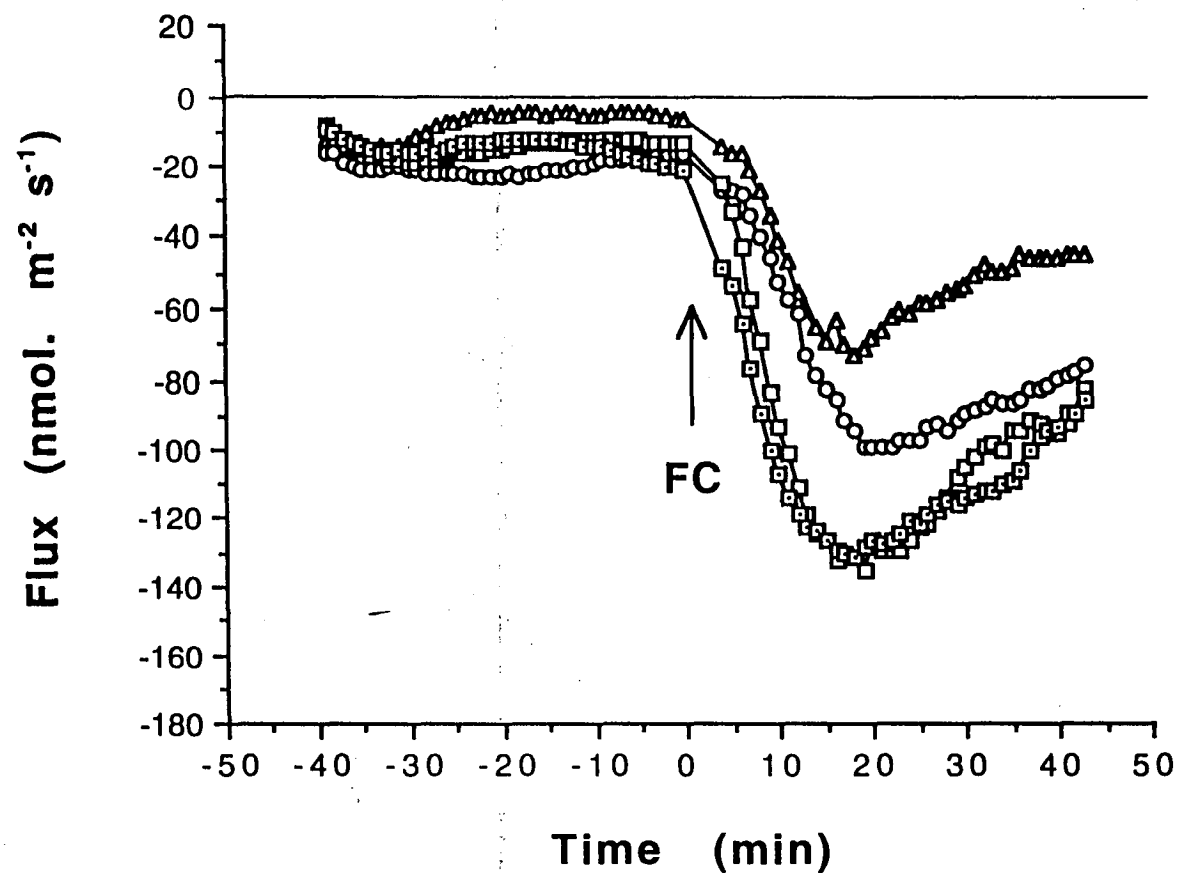
Figure 5.8

Effects of 10^{-2} (▣), 10^{-3} (□), 5×10^{-4} (○) or 10^{-4} (△) mole m^{-3} fusicoccin (FC) on proton net flux (efflux negative) adjacent to the cut tissue surface of 4-day-old split oat coleoptile segments preincubated in BSM for 4.5 hours. Upward arrow indicates application of fusicoccin.

Figure 5.9

Effects of 10^{-2} (▣), 10^{-3} (☐), 5×10^{-4} (○) or 10^{-4} (△) mole m^{-3} fusicoccin (FC) on calcium net flux (efflux negative) adjacent to the cut tissue surface of 4-day-old split oat coleoptile segments preincubated in BSM for 4.5 hours. Upward arrow indicates application of fusicoccin.
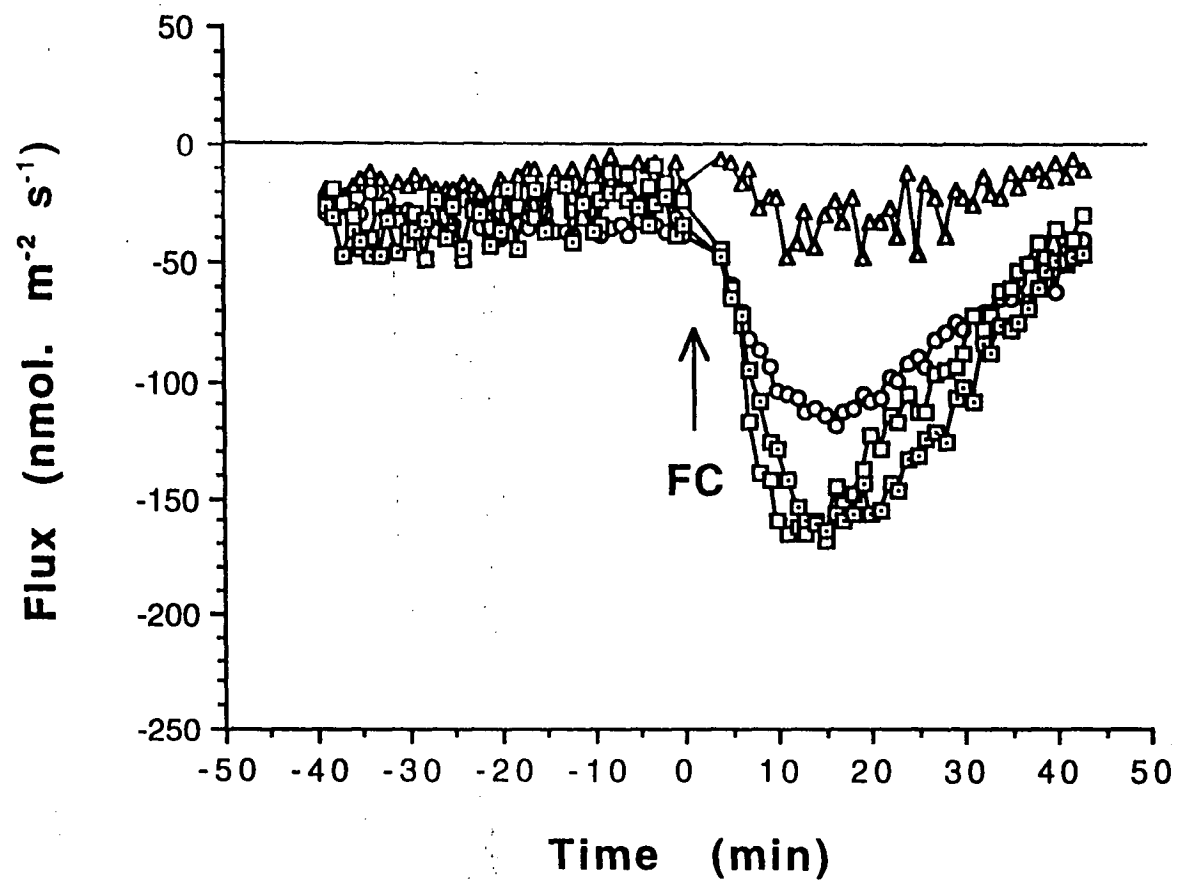
Figure 5.10

Effects of 10^{-2} (⊟), 10^{-3} (□), 5×10^{-4} (○) or 10^{-4} (△) mole m^{-3} fusicoccin (FC) on potassium net flux (efflux negative) adjacent to the cut tissue surface of 4-day-old split oat coleoptile segments preincubated in BSM for 4.5 hours. Upward arrow indicates application of fusicoccin.
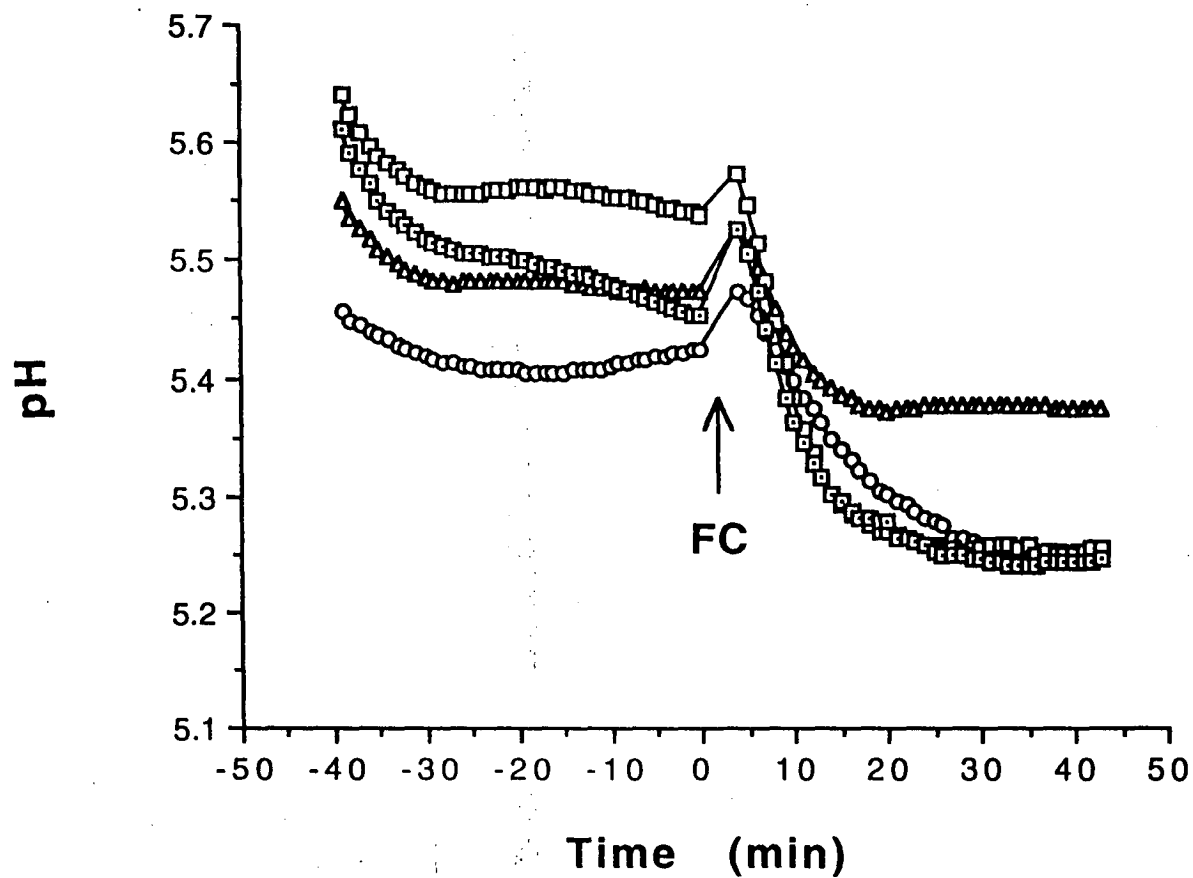
Figure 5.11

Effects of 10^{-2} (▣), 10^{-3} (□), 5×10^{-4} (○) or 10^{-4} (△) mole m^{-3} fusicoccin (FC) on pH adjacent to the cut tissue surface of 4-day-old split oat coleoptile segments preincubated in BSM for 4.5 hours. Upward arrow indicates application of fusicoccin.
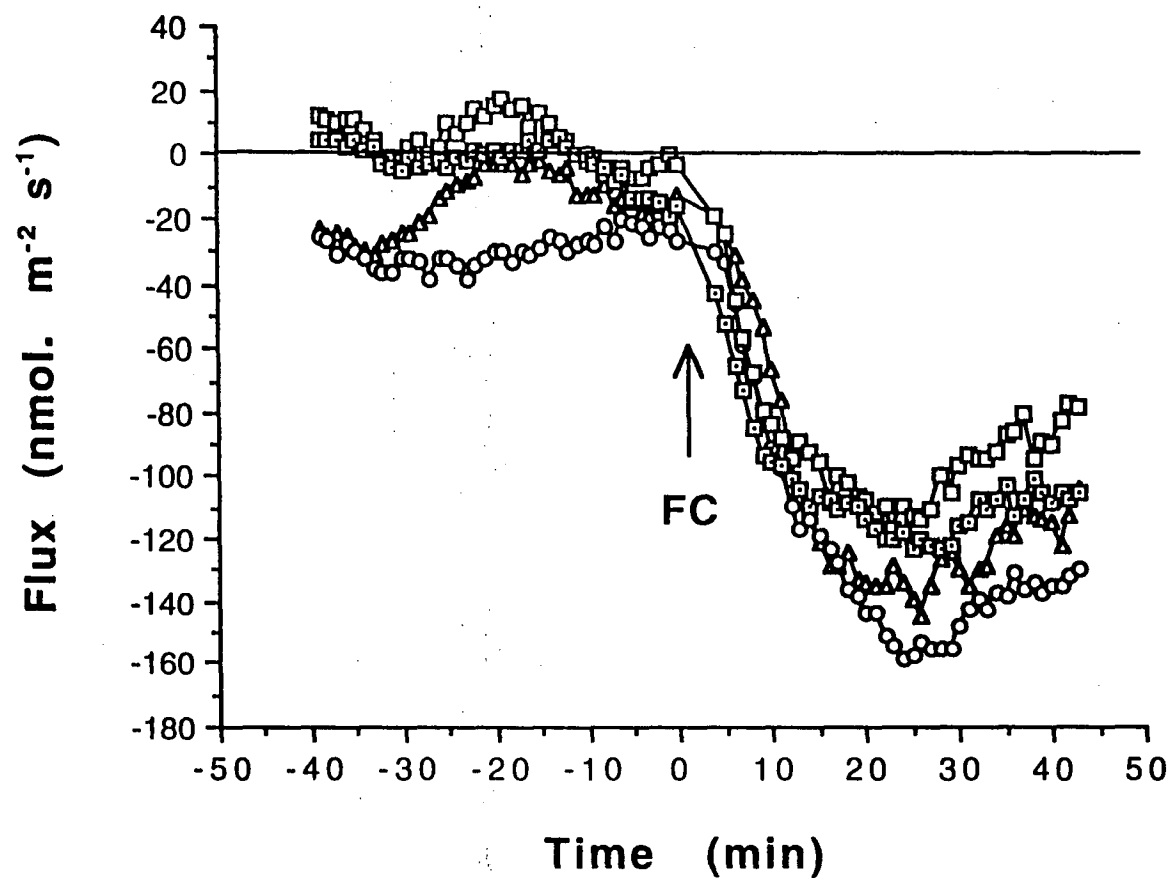
Figure 5.12

Effects of 10^{-3} (□), 5×10^{-4} (○) or 10^{-4} (△) mole m^{-3} fusicoccin (FC) on membrane potential (PD) of parenchymal cells in 4-day-old split oat coleoptile segments preincubated in BSM for 4.5 hours. Upward arrow indicates application of fusicoccin.

5.3 Discussion
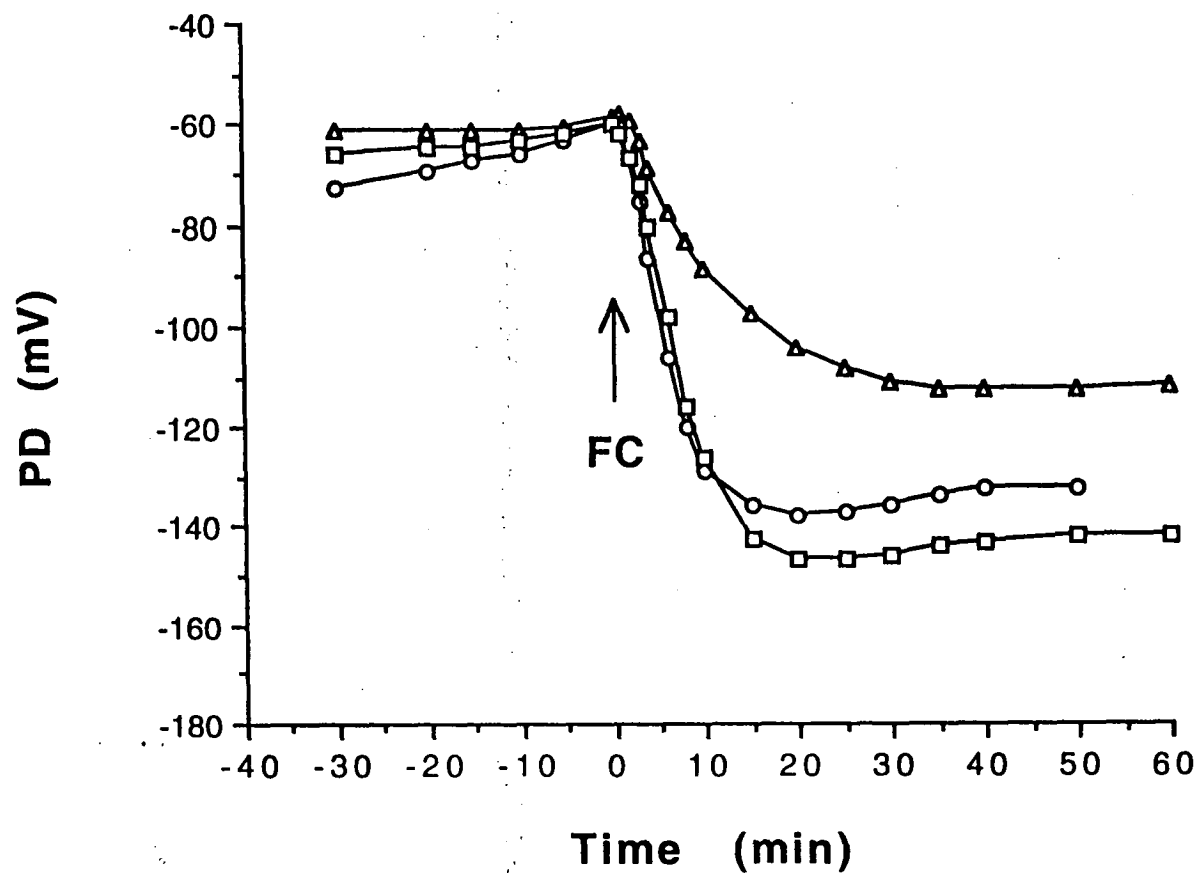
It has been widely reported that during fusicoccin action, the bathing medium becomes acid (Cleland 1976, Marrè 1979, Brummer at al. 1985, Kutschera and Schopfer 1985a&1985b). In this present work, the observation of proton flux using the MIFE technique clearly shows that fusicoccin induces proton efflux. This is consistent with the early reported fusicoccin-induced medium acidification. The proton efflux is also immediate and substantial as the medium acidification. Furthermore, fusicoccin hyperpolarizes the membrane potential. This membrane hyperpolarization is also observed previously (Kutschera and Schopfer 1985b, Bertl and Felle 1985, Felle et al. 1986, Senn and Goldsmith 1988, Brummer et al. 1985). However the observed calcium efflux that goes with the proton efflux during fusicoccin action has not previously been reported. In contrast to the widely reported potassium uptake (Marrè 1979, Blatt 1988, Blatt and Clint 1989, Clint and Blatt 1989), the observed transient potassium efflux in the first 40 minutes of the action also needs some discussion.

5.3.1 The Source of the Calcium Efflux

Since the observations of the fluxes using the MIFE technique were carried out in places adjacent to the surface of the tissues, any measured ion efflux must be from the tissues. This means that the possible sources of the extruded calcium are vacuole, cytoplasm or walls of the cells in the tissues. From Figures 5.1b, 5.2b, 5.3b and 5.4b, the total amounts of calcium extruded from the tissues can be estimated by calculating the area above the curves. From this calculation, the estimated total amounts of calcium extruded from the tissues within 40 minutes are in the range between 0.21 to 0.19 mmol m^{-2}. What is the source of the fusicoccin-induced calcium efflux?

The cells in the tissue are generally cylindrical, and for a cell, more than 95% of the cell volume is occupied by the vacuole and the rest is occupied by the cytoplasm and the cell walls in which their proportions are approximately the same. Therefore it can be assumed that the proportion between the total thicknesses of the vacuole, the cytoplasm and the walls across the side of a cylindrical cell is 100:1:1. Now it is also assumed that there are 10 cells in the thickness of the tissue, each of which has vacuole, cytoplasm, and walls of

100, 1 and 1 μm thickness respectively. Based on this assumption, every mmol m^{-2} of the amount of extruded ion from the tissue would cause a consequent reduction in the concentration of the ion in the vacuole by 1 mole m^{-3}, or in either the cytoplasm or the cell walls by 100 mole m^{-3}. Therefore, when the amount of the extruded calcium is about 0.2 mmol m^{-2}, the consequent reduction of free calcium concentration in the vacuole, in the cytoplasm, or in the cell walls would be 0.2, 20 or 20 mole m^{-3} respectively. Under normal conditions, the concentration of free calcium is about 10 mole m^{-3} in the vacuole, 10^{-3} mole m^{-3} in the cytoplasm, and 4×10^2 mole m^{-3} in the cell walls. From this approximation, it is not likely that the extruded calcium only comes from the cytoplasm, unless there is a lot of bound calcium in the cytoplasm released during this time. However there is no evidence that a lot of free calcium is produced in the cytoplasm during this time. Moreover, it has been reported that in algae, the substantial increase in cytoplasmic calcium concentration stops cytoplasmic streaming that is important for the cells (Tominaga and Tazawa 1981).

The extruded calcium may also come from the vacuole. However, the calcium transport from the vacuole can affect the concentration of free calcium in the cytoplasm. Therefore, although some of the extruded calcium may come from inside the cells, a more likely source of the extruded calcium is the cell walls. The release of calcium from the walls during fusicoccin-induced proton efflux has been expected, based on the analysis of the WADM model for fluxes in Chapter 4. Now, the analysis is applied to the measured proton and calcium effluxes obtained using the MIFE technique during fusicoccin action on oat coleoptile segments.

5.3.2 Proton-Calcium Exchange

The flux observation using the MIFE technique only provides the fluxes of protons and calcium in the places adjacent to the tissue surface. It does not provide the proton efflux at the plasmalemma. The WADM model for fluxes described in Chapter 4 needs the information of this proton efflux so that the fluxes of protons and calcium outside the walls as the result of proton-calcium exchange in the walls can be estimated. By assuming that part of the extruded protons retained for acidifying the walls is relatively small and all of the extruded calcium is from the walls, the efflux of protons at the plasmalemma can be estimated from the total charge transported out by the observed effluxes

of both protons and calcium. The charges transported by the observed fusicoccin-induced potassium efflux are not included because the extruded potassium is not the result of potassium release from the walls by extruded protons. In the walls, there is not potassium condensation. Therefore if there is potassium efflux outside the walls during proton extrusion, the transported potassium is from the cell, not from the walls. If there is not potassium efflux at the plasmalemma, proton extrusion only causes potassium exchange between the DFS and the WFS without any potassium loss from the walls to the bathing medium (see Chapter 4 for detail discussion).

Beside proton efflux at the plasmalemma, wall parameters of oats necessary for the WADM model such as the concentration of ionisable sites $[A_{sites}]$, the pK of the wall's weak acids, the intrinsic linear charge density parameter ξ^* and the wall thickness are also not available. In the absence of reliable knowledge, the values of these parameters for other plants were used. Ryan, Newman and Arif (1992) have used $[A_{sites}]=800$ mole m^{-3} for *Chara*. In the present analysis for oats, this value was used again. For the pK of the wall's weak acids, I used pK 3 since the pK of the wall's weak acids of *Sphagnum russowii* is between 2 and 4 (Richter and Dainty 1989a). The intrinsic linear charge density parameter of *Sphagnum russowii* of 0.71 was also used in the present analysis (Richter and Dainty 1990a). The thickness of the walls (including secondary walls) varies with cell type, from 0.1 to 10 μm (Nobel 1974). However for primary walls, that are the walls present in the growing parenchymal cells, the thickness is about 0.5-1 μm (M.J. Canny, personal communication). Therefore I used 1 μm for the thickness of the walls in this analysis. It was also assumed that the portion of the DFS and the WFS in the walls is half each (Dainty and Hope 1959).

The diffusion coefficients of cations in the DFS are also required for the analysis of the WADM model for fluxes. However, they are not known. Since they must be smaller that those in open water, it was assumed that they are 1/5 of those in open water. For anions, their diffusion coefficients in the WFS are required. In this case, they are assumed to be the same as those in open water.

Now, using the concentration of the ions in BSM and its pH as the initial condition for the external solution and assuming that the initial condition in the WFS is the same as in the external solution, the initial condition of the DFS was obtained using the same method as used by Ryan, Newman and Arif (1992). The WADM model for fluxes was then applied to estimate proton and

calcium effluxes outside the walls as the results of proton-calcium exchange in the walls when the proton efflux happens from the cells to the cell walls. The observed potassium efflux was not included in the analysis because it only causes a small effect on the analysis. In the walls, there is not potassium condensation. Therefore when the observed potassium efflux is included in the analysis, the calculated potassium efflux is simply a bit smaller than the observed potassium efflux at the plasmalemma. Figures 5.13, 5.14, 5.15 and 5.16 show both the observed effluxes and the calculated effluxes of protons and calcium for every concentration of applied fusicoccin.

From these figures, the calculated effluxes of both protons and calcium are similar to the observed effluxes but they are not exactly the same. In the beginning, the calculated calcium efflux always increases faster than the calculated proton efflux. However, the increase on the calculated proton efflux continues with the rate becoming smaller. Meanwhile, the calculated calcium efflux decreases again after it reaches its maximum. These circumstances are aspects of the WADM model for fluxes.

Basically when protons are extruded from the cells to the cell walls, part of the protons are for lowering the pH of the DFS of the walls. In this case, the magnitude of the pH decrease depends on both the rate of the extruded protons and the position of the pH with respect to the pK of the wall's weak acids. At the beginning, the pH of the walls is higher and far from the pK of the wall's weak acids. With this condition, the buffering capacity is low. Therefore the extruded proton can easily lower the pH of the walls. The proton efflux at the plasmalemma also increases at this time. Therefore the pH decrease is substantial. At this pH, the amount of released calcium per unit pH is small (see Figure 4.2). However, when the pH decrease is substantial, the amount of the calcium released from the walls would also be substantial. Therefore at this time, the calculated calcium efflux outside the walls increases faster than the calculated proton efflux. As the pH of the walls decreases further, the buffering capacity becomes higher so that attempts to lower the pH by extruded protons has more resistance. Beside that, the increase of the proton efflux at the plasmalemma is slower. Consequently, the magnitude of the pH decrease is smaller. However, at lower pH, the amount of released calcium per unit pH is higher. Therefore the amount of the calcium released from the walls at this time may still be substantial.

Figure 5.13

Proton (a) and calcium (b) net fluxes (efflux negative) during 10^{-2} mole m^{-3} fusicoccin (FC) action. Solid symbols (■) represent the outputs of the "weak acid Donnan Manning" (WADM) model for fluxes. Wall quantities used in the model: $[A_{sites}]$ = 800 mole m^{-3}, pK = 3.0, ξ^* = 0.71, h = 1.0 μm and λ = 0.5. The diffusion coefficients of cations in the DFS is 1/5 of those in the WFS. The external medium is BSM. It was assumed that there are 10 cells in the thickness of a tissue.

Figure 5.14

Proton (a) and calcium (b) net fluxes (efflux negative) during 10^{-3} mole m^{-3} fusicoccin (FC) action. Solid symbols (■) represent the outputs of the "weak acid Donnan Manning" (WADM) model for fluxes. Other details are as in Figure 5.13.

Figure 5.15

Proton (a) and calcium (b) net fluxes (efflux negative) during 5×10^{-4} mole m^{-3} fusicoccin (FC) action. Solid symbols (●) represent the outputs of the "weak acid Donnan Manning" (WADM) model for fluxes. Other details are as in Figure 5.13.
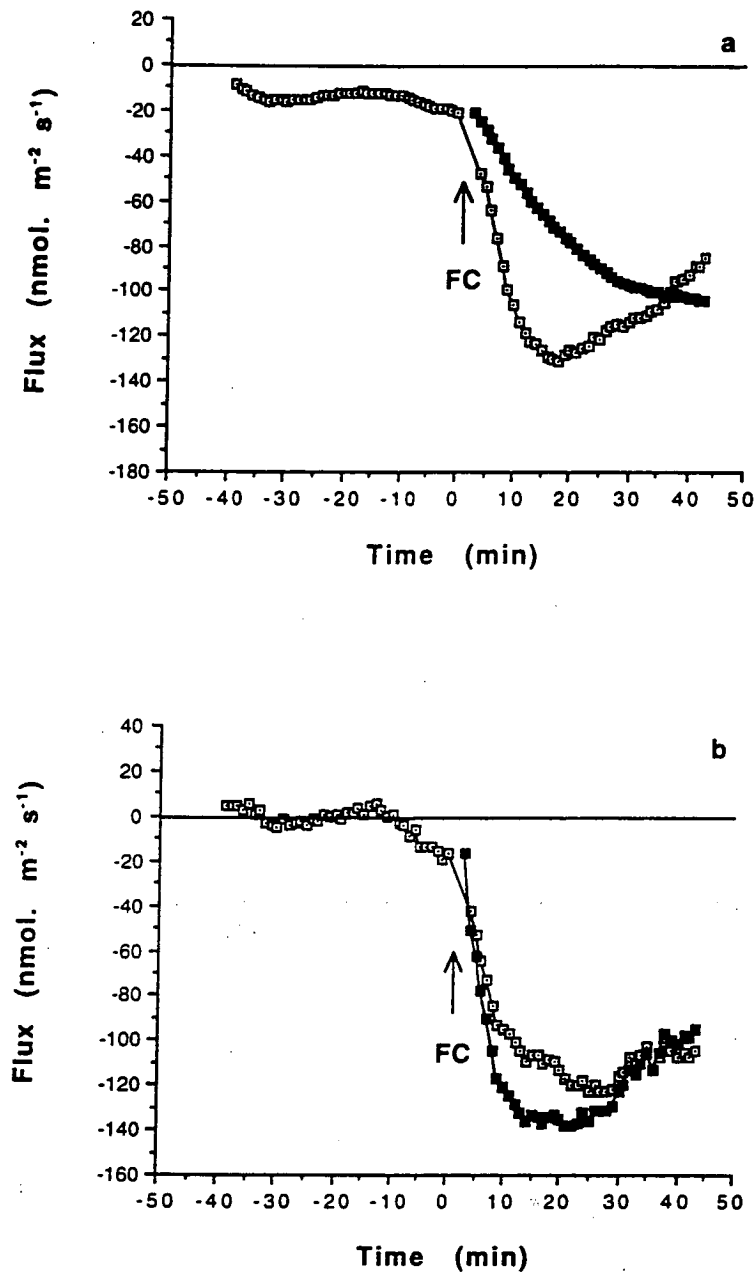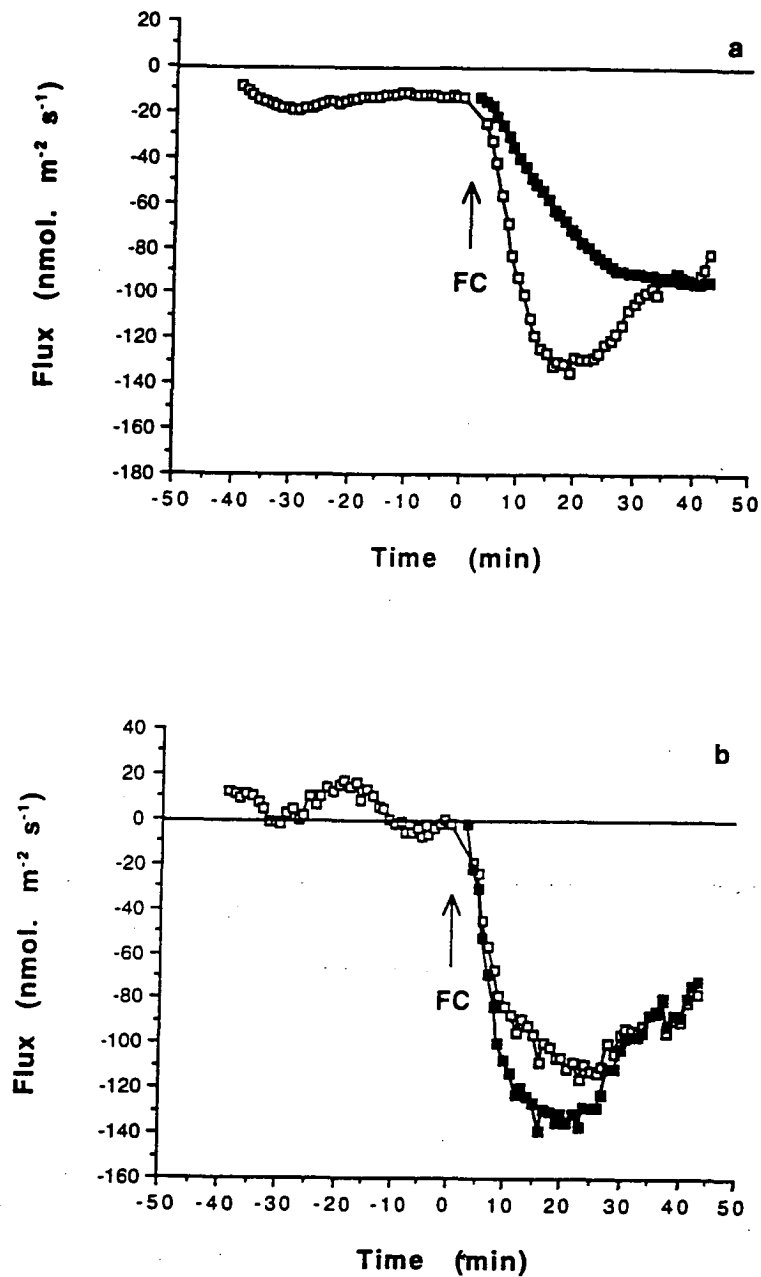
Figure 5.16

Proton (a) and calcium (b) net fluxes (efflux negative) during 10^{-4} mole m^{-3} fusicoccin (FC) action. Solid symbols ($\blacktriangle$) represent the outputs of the "weak acid Donnan Manning" (WADM) model for fluxes. Other details are as in Figure 5.13.
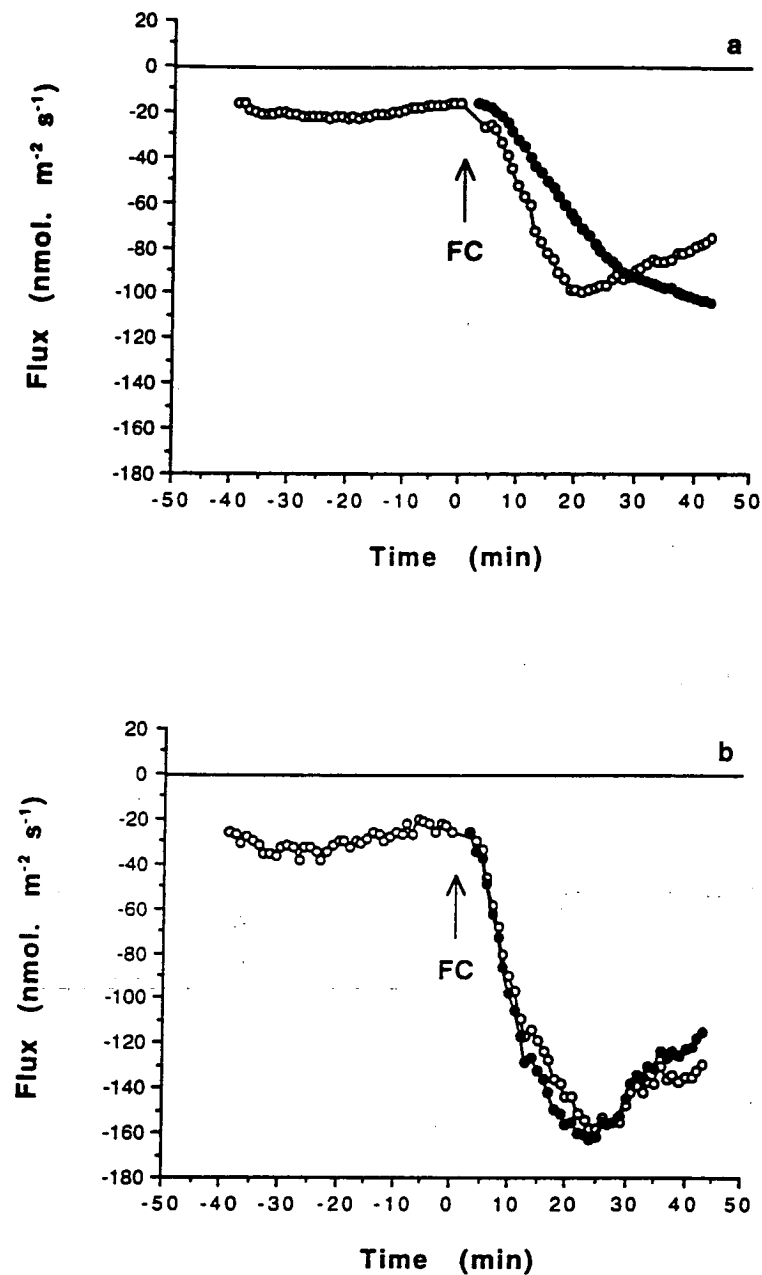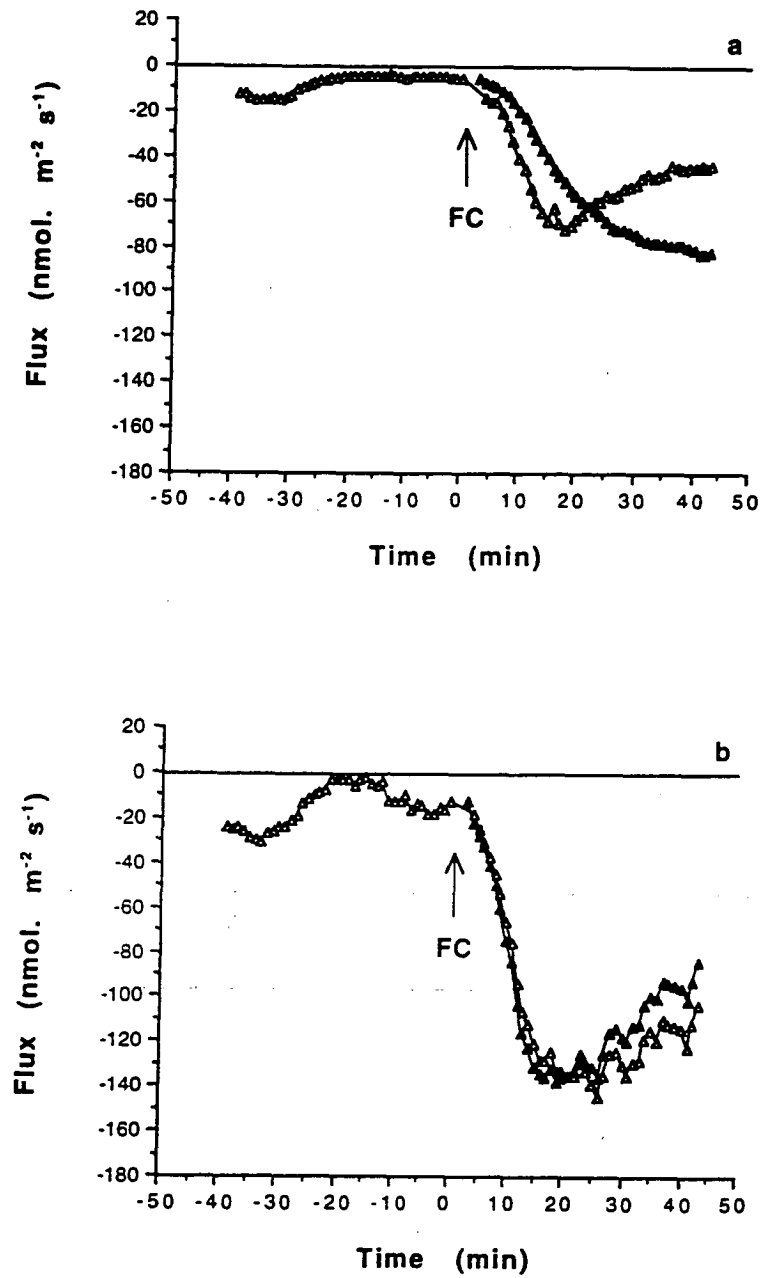
Now when the pH becomes closer to the pK of the wall's weak acids, the buffering capacity is much higher. The proton efflux at the plasmalemma also decreases at this time. Therefore the decrease of the pH is even smaller. With this condition, although the amount of released calcium per unit pH is higher, the amount of the calcium released from the walls will be less. Therefore the calculated calcium efflux decreases to approach zero flux and the calculated proton efflux tends to approach the source proton efflux at the plasmalemma. Meanwhile the pH of the walls approaches a constant value. The curves of the calculated calcium efflux, the calculated proton efflux and the proton efflux at the plasmalemma will meet each other when the proton efflux at the plasmalemma is zero. This indicates that the calculated proton efflux does not always increase. It may also decrease to approach a decreasing proton efflux at the plasmalemma.

The similarity of the observed and calculated effluxes strongly supports the WADM model of proton-calcium exchange in the walls during proton extrusion. The question now is why the observed proton and calcium effluxes increase almost at the same time but the model shows the calcium efflux first. Does the process of proton-calcium exchange need time? If the exchange between extruded protons and wall calcium needs time before the process happens, the extruded protons will diffuse earlier and the diffusion of the released wall calcium happens later. Besides, certain explanations as to why the

In 2nd paragraph page 110, "Another question is why the observed calcium effluxes for different fusicoccin concentration are almost the same while the related observed proton effluxes are different (Figures 5.1, 5.2, 5.3, 5.4). The WADM for fluxes model predicts that the calcium efflux from the wall is proportional to the related proton efflux. It is shown in Figures 5.13, 5.14, 5.15 and 5.16 in which the calculated calcium and proton effluxes are proportional. Does some mechanism regarding saturation involve in the proton-calcium exchange process in the wall? If it involves, the mechanism should be added to the model." should be added just before sentence "Besides, certain explanations as ...".

The acid-growth theory predicts that wall loosening which initiates the growth of plant cells is the result of wall acidification caused by proton extrusion (Rayle and Cleland 1970, Hager et al. 1971). It has been reported that the growth response of fusicoccin and acid solutions is similar and not additive (Marrè 1979, Kutschera and Schopfer 1985b). The timing of the growth response, the fusicoccin-induced medium acidification and membrane hyperpolarization also match well. This indicates that the acid-growth theory is suitable for the fusicoccin-induced growth. The observation of the pH of the solution adjacent to the tissue surface in the present work shows that fusicoccin decreases the pH significantly (Figure 5.11). The final pH at about 20 minutes

Now when the pH becomes closer to the pK of the wall's weak acids, the buffering capacity is much higher. The proton efflux at the plasmalemma also decreases at this time. Therefore the decrease of the pH is even smaller. With this condition, although the amount of released calcium per unit pH is higher, the amount of the calcium released from the walls will be less. Therefore the calculated calcium efflux decreases to approach zero flux and the calculated proton efflux tends to approach the source proton efflux at the plasmalemma. Meanwhile the pH of the walls approaches a constant value. The curves of the calculated calcium efflux, the calculated proton efflux and the proton efflux at the plasmalemma will meet each other when the proton efflux at the plasmalemma is zero. This indicates that the calculated proton efflux does not always increase. It may also decrease to approach a decreasing proton efflux at the plasmalemma.

The similarity of the observed and calculated effluxes strongly supports the WADM model of proton-calcium exchange in the walls during proton extrusion. The question now is why the observed proton and calcium effluxes increase almost at the same time but the model shows the calcium efflux first. Does the process of proton-calcium exchange need time? If the exchange between extruded protons and wall calcium needs time before the process happens, the extruded protons will diffuse earlier and the diffusion of the released wall calcium happens later. Besides, certain explanations as to why the observed proton efflux also decreases sooner than the calculated proton efflux are still needed. It seems likely that proton-calcium exchange is not the only process that happens during fusicoccin-induced proton extrusion.

5.3.3 Calcium Release and Acid Growth

The acid-growth theory predicts that wall loosening which initiates the growth of plant cells is the result of wall acidification caused by proton extrusion (Rayle and Cleland 1970, Hager et al. 1971). It has been reported that the growth response of fusicoccin and acid solutions is similar and not additive (Marrè 1979, Kutschera and Schopfer 1985b). The timing of the growth response, the fusicoccin-induced medium acidification and membrane hyperpolarization also match well. This indicates that the acid-growth theory is suitable for the fusicoccin-induced growth. The observation of the pH of the solution adjacent to the tissue surface in the present work shows that fusicoccin decreases the pH significantly (Figure 5.11). The final pH at about 20 minutes

from the application of fusicoccin is about 5.25. Since protons are extruded out during this time, the pH of the wall must be lower than 5.25.

The analysis of the WADM model for fluxes can also provide an estimate of the average pH of the walls. For the initial conditions used in these experiments, the estimated pH of the WFS and the DFS is 6.0 and 4.36 respectively. For example, after the addition of 10^{-3} mole m^{-3} fusicoccin, the estimated pH of the WFS and the DFS becomes 5.22 and 3.94 at 20 minutes and 4.92 and 3.728 at 40 minutes respectively (see also Arif and Newman 1993). This indicates that after 20 minutes, the pH of the WFS decreases still further. However in the observation of the pH adjacent to the tissue surface, the pH decreases little. This is probably due to the applied small tissue/solution volume ratio in the observation. Therefore the extruded protons keep diffusing out to the bulk solution. The estimated pH of the WFS is lower than the pH observed at places adjacent to the tissue surface using the MIFE technique. This suggests that to compare the growth effects of acid solutions and growth substances, the pH of the applied acid solutions must be lower than the pH of the external solution obtained during the growth induced by the substances.

The acid-growth theory predicts that during acid-induced growth, wall acidification will activate some enzymes to break bonds between growth restrictive polysaccharides, so that the walls become loosened. This has been favoured recently by the finding that two cell-wall associated proteins induce extension of heat-inactivated cell walls (McQueen-Mason et al. 1992). Furthermore, the involvement of enzymatic processes in acid-induced wall loosening is also supported by the report of the inhibition of wall loosening, and thereby cell elongation, by glucanase and xyloglucan antibodies during auxin-induced medium acidification (Hoson et al. 1991, Inouhe and Nevins 1991). In the present work, it has been shown that the process of calcium exchange by extruded protons also happens during wall acidification. Since this calcium is displaced from wall's weak acids including cell wall's proteins and wall's polymers, the exchange may interact with the enzymatic processes of wall loosening.

The involvement of calcium bonds in the walls to cause wall stiffening has long been considered (Bennet-Clark 1956). However this has been put into question because calcium chelator EGTA in strong buffer and another calcium chelator Quin 2 cause calcium removal without an increase in wall extensibility (Virk and Cleland 1990, Cleland et al. 1990). The wall extensibility starts to

increase when more than 60-70% of the wall calcium has been removed from the walls. The use of EGTA in strong buffer and Quin 2 is to avoid the change of the wall pH during the treatments. Therefore if there is any change in the transport of ions, in this case calcium, it is not the result of wall acidification. According to the WADM model, calcium in the walls is separated between calcium bound to wall's weak acids and calcium in the DFS. When the pH of the walls decreases, some calcium bound to wall's weak acids is replaced by protons. However when calcium is removed from the walls by calcium chelator EGTA in strong buffer or Quin 2 in which the pH of the walls is kept constant, the calcium release should be from the DFS, not from the wall's weak acids. Because calcium in the DFS is not expected to cause wall stiffening, the loss of calcium from the DFS does not cause any increase of wall extensibility.

The result of the analysis using the WADM model on cell walls with the parameters I have used and BSM as the external solution, shows that the total concentration of wall calcium is about 380 mole m^{-3}. The concentration of calcium in the DFS is about 270 mole m^{-3}. This is about 70% of the total calcium concentration in the walls. Therefore it seems likely that the calcium chelators used by Virk and Cleland (1990) and Cleland et al (1990) act first on calcium in the DFS. During this time the wall extensibility does not increase. After all the calcium in the DFS is removed, the calcium chelators then start to remove calcium bound to the wall's weak acids. The function of calcium bound to wall's weak acids is not specified in the WADM model. However since the wall extensibility increases when more than 60-70% of total wall calcium is removed, the removal of calcium bound to wall's weak acids may relate to the process of wall loosening. This associates condensed calcium (cross-link) with wall stiffening directly.

5.3.4 Fusicoccin-Induced Potassium Efflux

It has been shown for guard cells with little primary proton pump activity that outward-directed K^+ channel current contributed appreciably to charge balance maintaining the membrane potential (Clint and Blatt 1989). In my experiments on oat coleoptile segments, the potassium efflux contributed for the charge balancing is about 30 nmol. m^{-2} s^{-1} (Figure 5.10). With 0.1 mole m^{-3} concentration of external potassium, the Nernst potential of potassium should *and assuming the cytoplasmic concentration is 100 md m⁻³,* be about -175 mV. Measurements of the membrane potential showed that the initial membrane potential is about -65 mV (Figure 5.12) which is higher than

the Nernst potential of potassium. In this situation, the electrochemical potential of potassium inside the cell is higher than outside the cell. Therefore potassium transported from the cell to the external medium is energetically downhill.

According to the WADM model for fluxes, any potassium efflux through cell walls changes only slightly the conditions in the walls since potassium is not a cation that is bound to wall's weak acids. This slight change is due to the little change of potassium concentration in the walls during the efflux. Therefore the Donnan partition coefficient and the distribution of other ions between the DFS and the WFS also change little.

Fusicoccin was reported to induce potassium uptake in higher plant cells and it was suggested that the uptake is part of the secondary transport, stimulated during the increase of the cation driving force due to the fusicoccin-induced membrane hyperpolarization (Marrè 1979). In addition, based on the evidence of cells with little proton pump activity, it was also suggested that part of the potassium uptake is due to the fusicoccin-induced inactivation of the outward-directed K^+ channel current that contributes to charge balance maintaining the membrane potential (Blatt 1988, Clint and Blatt 1989, Blatt and Clint 1989). In my experiments, fusicoccin clearly hyperpolarizes the membrane potential and the membrane hyperpolarization is immediate (Figures 5.5, 5.6 and 5.7). However, the flux measurements show that during fusicoccin-induced membrane hyperpolarization, the potassium efflux increases immediately and the increase is transient (Figures 5.1c, 5.2c, 5.3c and 5.4c). This increase is surprising because it was expected that fusicoccin would decrease the initial potassium efflux. Based on the WADM model, the fusicoccin-induced potassium efflux does not come from the cell walls. It should come from inside the cells. It is also clear that the efflux is not part of the secondary transport due to the fusicoccin-induced membrane hyperpolarization because it even contributes to cause membrane hyperpolarization. The increase of the potassium efflux also suggests that the outward-directed K^+ channel current to maintain charge balancing on oat coleoptile cells is not inactivated by fusicoccin.

On page 113 before the last paragraph, "The fusicoccin induced immediate and transient potassium efflux is a new information for fusicoccin action. The question is now by what mechanism this response happens. Since the extruded potassium is from inside the cells, possibly fusicoccin has an initial effect which opens more potassium channels in the plasmalemma. Therefore the energetically downhill potassium efflux increases. However, this is followed by other processes including the suggested inactivation of the outward-directed K^+ channel current (Blatt 1988, Clint and Blatt 1989, Blatt and Clint 1989). As a result, the initially increased potassium efflux decreases again. The possible mechanism above is still uncertain and needs further studies." should be inserted as a new paragraph.

the Nernst potential of potassium. In this situation, the electrochemical potential of potassium inside the cell is higher than outside the cell. Therefore potassium transported from the cell to the external medium is energetically downhill.

According to the WADM model for fluxes, any potassium efflux through cell walls changes only slightly the conditions in the walls since potassium is not a cation that is bound to wall's weak acids. This slight change is due to the little change of potassium concentration in the walls during the efflux. Therefore the Donnan partition coefficient and the distribution of other ions between the DFS and the WFS also change little.

Fusicoccin was reported to induce potassium uptake in higher plant cells and it was suggested that the uptake is part of the secondary transport, stimulated during the increase of the cation driving force due to the fusicoccin-induced membrane hyperpolarization (Marrè 1979). In addition, based on the evidence of cells with little proton pump activity, it was also suggested that part of the potassium uptake is due to the fusicoccin-induced inactivation of the outward-directed K^+ channel current that contributes to charge balance maintaining the membrane potential (Blatt 1988, Clint and Blatt 1989, Blatt and Clint 1989). In my experiments, fusicoccin clearly hyperpolarizes the membrane potential and the membrane hyperpolarization is immediate (Figures 5.5, 5.6 and 5.7). However, the flux measurements show that during fusicoccin-induced membrane hyperpolarization, the potassium efflux increases immediately and the increase is transient (Figures 5.1c, 5.2c, 5.3c and 5.4c). This increase is surprising because it was expected that fusicoccin would decrease the initial potassium efflux. Based on the WADM model, the fusicoccin-induced potassium efflux does not come from the cell walls. It should come from inside the cells. It is also clear that the efflux is not part of the secondary transport due to the fusicoccin-induced membrane hyperpolarization because it even contributes to cause membrane hyperpolarization. The increase of the potassium efflux also suggests that the outward-directed K^+ channel current to maintain charge balancing on oat coleoptile cells is not inactivated by fusicoccin.

Fusicoccin-induced potassium uptake was generally observed using tracer studies. These studies were usually carried out over a long period (much more than 1 hour). Using the MIFE technique, the flux measurements can be carried out every minute immediately after the treatment. From the measurements, it was shown that the fusicoccin-induced potassium efflux is

transient and lasts about 40 minutes. After this time, the efflux may become an influx. If this happens for a longer time, it will allow potassium uptake as observed by tracer studies. Observation of potassium flux for longer periods during fusicoccin action using the MIFE technique may clarify this possibility. In the present work, this observation was not carried out because this is not one of the aims of the study.

5.3.5 Effects of Fusicoccin Concentration

From Figures 5.8, 5.9, 5.10, 511 and 5.12, it is clearly shown that several responses to fusicoccin, i.e. proton efflux, potassium efflux, medium acidification and membrane hyperpolarization, depend on the fusicoccin concentration. In this case, it seems likely that 10^{-3} mole m^{-3} is the maximum concentration that can be applied to saturate the responses. The response of calcium efflux to fusicoccin is similar for different fusicoccin concentrations between 10^{-2}-10^{-4} mole m^{-3}.

5.4 Conclusion

Using the MIFE technique, it has been confirmed that fusicoccin induces proton extrusion and acidification of the medium around the tissues. The fusicoccin-induced proton efflux is immediate and transient. The pH adjacent to the tissue surface is about 5.25. During fusicoccin action, the membrane potential also hyperpolarizes.

Fusicoccin also induces calcium efflux. It was expected that during fusicoccin-induced proton extrusion, some of the extruded protons would replace calcium bound to wall's weak acids, and the replaced calcium then would diffuse from the walls to the external medium. The MIFE technique provides simultaneous observation of proton and calcium effluxes during fusicoccin action. The analysis of the WADM model for fluxes on the observed proton and calcium effluxes confirms that proton-calcium exchange happens in the walls during fusicoccin-induced proton extrusion. There is still some refinement of the model needed to address minor discrepancy between the observed and the calculated proton and calcium effluxes.

The analysis of the WADM model for fluxes also provides an estimate of the wall pH during this time. It shows that the wall pH decreases, and is lower than the pH of the medium around the tissue.

Fusicoccin causes transient potassium efflux. This has been difficult to discuss since fusicoccin has been reported to cause potassium uptake when it was studied using tracer. Probably the fusicoccin-induced transient potassium efflux observed using the MIFE technique will become an influx over a longer period.

10^{-3} mole m^{-3} fusicoccin is sufficient to cause maximum proton and potassium effluxes, membrane hyperpolarization and medium acidification.

Chapter 6

IAA EFFECTS ON OATS

6.1 Introduction

A clear indication has been found of the proton-calcium exchange in cell walls during fusicoccin-induced substantial proton extrusion and growth. The process is also expected to happen during the growth induced by natural growth hormone IAA. In this chapter, the hypothesis is tested using the same plant material (oats).

In Chapter 1, it is mentioned that IAA is one of the natural growth hormones found in plants. Description of the transport of IAA in plants and the IAA responses is also presented. As with fusicoccin, IAA causes cell enlargement, thereby cell elongation and growth. While the fusicoccin-induced growth is immediate, the growth induced by IAA has a lag of several minutes. During IAA-induced growth, the surrounding medium becomes more acid and the membrane potential hyperpolarizes. It was suggested that these responses are related to the activation of proton pumps in the plasmalemma (Cleland 1980). According to the WADM model (Richter and Dainty 1990b, Ryan, Newman, Arif 1992, Chapter 4, Appendix C), any proton extrusion to the walls of plant cells that contain weak acids, causes wall acidification and calcium release from the condensed phase of the walls. Therefore the IAA-induced proton extrusion is also expected to cause calcium release from the walls. In this chapter, the results of the simultaneous measurements of proton and calcium fluxes during IAA action using the MIFE technique are presented. There is indication that proton-calcium exchange in the walls also takes place during IAA-induced proton extrusion.

The measurement of proton flux during IAA-action using the MIFE technique also provides the time sequence of the IAA-induced proton extrusion. The time sequence, together with the significance of the IAA-induced medium acidification, has recently become a major issue concerning the validity of the acid-growth theory (Cleland 1975, Cleland 1976, Jacobs and Ray 1976, Evan and Vesper 1980, Kutschera and Schopfer 1985a, Senn and Goldsmith 1988, Schopfer 1989, Lütten and Böttger 1989, Lütten et al. 1990, Cleland et al. 1991, see also Chapter 1). IAA-induced proton extrusion was usually observed by measuring the pH of the surrounding medium. In the case that the net proton flux is initially an influx, the IAA-induced medium acidification is not readily observed until the influx becomes an efflux. By measuring the proton electrochemical potential gradient using the MIFE technique, a change in proton flux is directly observable.

Study of calcium transport during IAA-induced growth is still lacking. The involvement of wall calcium during growth has been mentioned in the calcium bridge hypothesis (Bennet-Clark 1959). Calcium is also suggested to have an important role inside the cells during IAA action (Brummer and Parish 1983, Hepler and Wayne 1985, Brummell and Hall 1987), however this has been difficult to demonstrate experimentally. There is also evidence that the IAA-induced medium acidification and growth depend on the presence of calcium in the external medium (Cohen and Nadler 1976, Hasenstein and Evan 1986) and that the cytoplasmic free calcium increases during IAA action (Felle 1988). The results of the calcium flux observation using the MIFE technique obtained in this present work offer some information on the possible transport and role of calcium during IAA action.

Regarding the change of potassium flux during fusicoccin action, potassium flux was also measured simultaneously with proton and calcium fluxes during IAA action using the MIFE technique. As IAA induced membrane hyperpolarization, the membrane permeability to potassium and hence the potassium flux were expected to change. In this chapter, the results of the potassium flux measurements are presented. From the results, it seems likely that potassium flux does not change during this time.

The flux measurements of the ions were begun in BSM (see Chapter 2 for the detail preparation of the flux measurements). After 10 minutes, the solution in the chamber was replaced with fresh BSM to observe the effect of solution change. The result was used as a control for the observation of IAA

effect where IAA was applied by replacing the solution in the chamber with solution containing IAA (BEI). BEI is BSM containing 10^{-2} mole m^{-3} IAA and 0.5% ethanol. Therefore before the observation of IAA effect in BEI was carried out, BSM in the chamber was first replaced with BET, which is BSM with the same amount of ethanol as BEI, but without IAA. In this case, the solution replacement was carried out 10 minutes after the solution change. To observe the effect of IAA, 20 minutes after this solution replacement, BEI was added to the chamber to replace BET. The observation in BEI was carried out for about 40 minutes.

Senn and Goldsmith (1988) also reported that the medium acidification during IAA action depends on the preincubation time of split segments before they were used in experiments. This may relate to the time required to recover from injury caused by splitting. Injury was found to cause changes in net ion current around a plant tissue (Hush and Overall 1989, using vibrating probes), and the changes are related to the changes of some ion fluxes including proton flux (Gronewald and Hanson 1980, Rincon and Hanson 1986, Hush et al. 1992 using the MIFE technique). Based on these reports, in the present work, the ion flux measurements during IAA action were carried out on segments with several different preincubation times. The preincubation times were 4.5, 3.5, 2.25 and 1 hour. Unlike on segments preincubated for 4.5, 2.25 and 1 hour, the flux measurements on segments preincubated for 3.5 hours were started when a preincubated segment was directly bathed in BET. After 10 minutes, the solution was refreshed to observe the effect of solution change. 30 minutes after the refreshment, the effect of IAA was then observed by flowing BEI to the chamber to replace BET.

There is evidence that strong neutral buffered solutions inhibit spontaneous growth and that the inhibition is released by distilled water (Schopfer 1989). Therefore, buffering of the solution during preincubation was not carried out.

To study the net ionic current across the membranes during IAA action, the membrane potential was also measured. It was reported that during IAA action, the membrane potential depolarizes slightly and then hyperpolarizes with a lag similar to the lag of the IAA-induced growth (Cleland et al. 1977, Bates and Goldsmith 1983, Senn and Goldsmith 1988). Within 20-25 minutes, the membrane potential is about 25 mV more negative than the initial level. In this

chapter, it is confirmed that IAA hyperpolarizes the membrane potential after a brief and transient depolarization.

The membrane potential was observed in a stagnant (diffusion limited) solution because the ion flux measurements needed to be carried out under such conditions. In order to compare results with those of other workers, some observations of the membrane potential were also carried out in flowing solution.

During the measurements of membrane potential, the microelectrode tip was inserted into a parenchymal cell in the cut surface of a split segment while the segment was bathed with BSM. After about 10 minutes, the solution was refreshed to observe the effect of solution change. After the cells had recovered from the effect of solution change (within 20 minutes), observation of the IAA effect on membrane potential was begun by replacing BSM with BEI. The measurements of membrane potential were carried out on segments preincubated for 4.5, 2.25 or 1 hour. When measurements of the membrane potential were carried out in flowing solution, the solution flowed into the measurement chamber at one end and out at the other end at a rate of about 5 cm^3/minute. The volume of the solution in the chamber was kept constant at 7.5 cm^3. The measurements in running solution were carried out only on segments preincubated for 4.5 hours.

6.2 Results

The results of the measurements of proton, calcium and potassium net fluxes and pH adjacent to the cut tissue surface of 4-day-old split oat coleoptile segments during IAA action for each preincubation time are presented in Figures 6.1, 6.2, 6.3 and 6.4. For membrane potential, the results of the measurements are presented in Figures 6.5, 6.6, 6.7 and 6.8. For comparison, the results of proton flux, calcium flux, potassium flux, pH and membrane potential are combined in Figures 6.9, 6.10, 6.11, 6.12 and 6.13.
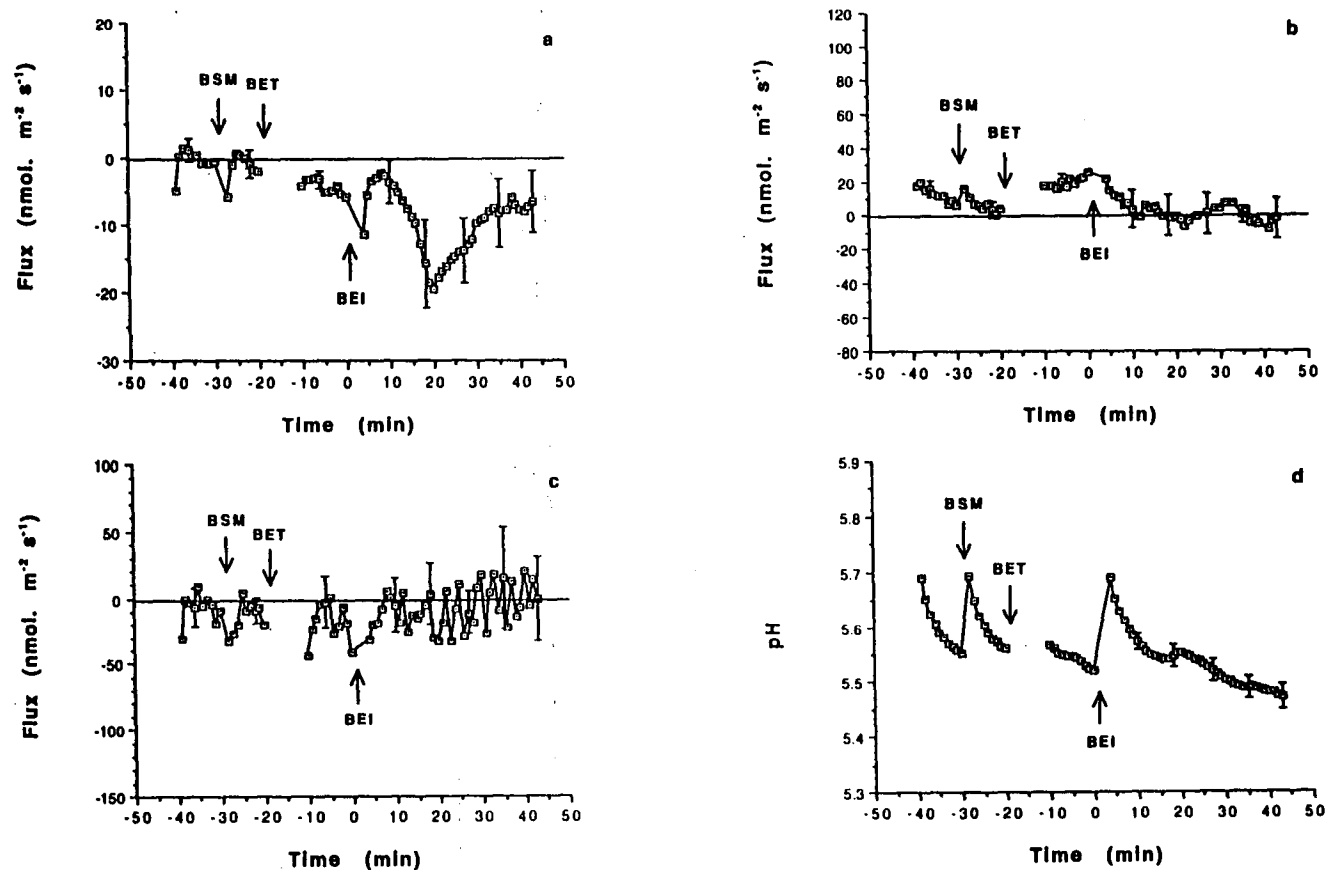
Figure 6.1

The responses of 4.5 hour preincubated segments of 4-day-old split oat coleoptiles to 10^{-2} mole m^{-3} IAA: proton (a), calcium (b) and potassium (c) net fluxes (efflux negative) and pH (d) adjacent to the cut tissue surface. First downward arrow indicates the solution replacement with the same solution (BSM) to study the effect of solution change. Second downward arrow indicates the solution replacement with the solution containing the same amount of ethanol (BET) as BEI. Upward arrow indicates the solution replacement with BEI to apply IAA. Each mean of ten plants is calculated relative to the value obtained just before the solution replacement with BSM or BEI. Bars show representative SE.

Figure 6.2

The responses of 3.5 hour preincubated oat coleoptile segments to 10^{-2} mole m^{-3} IAA: proton (a) and calcium (b) net fluxes (efflux negative) and pH (c) adjacent to the cut tissue surface. Downward arrow indicates the solution replacement with the same solution (BET) to study the effect of solution change. Each mean of six plants is calculated relative to the value obtained just before the solution replacement with BET or BEI. Other details are as in Figure 6.1.
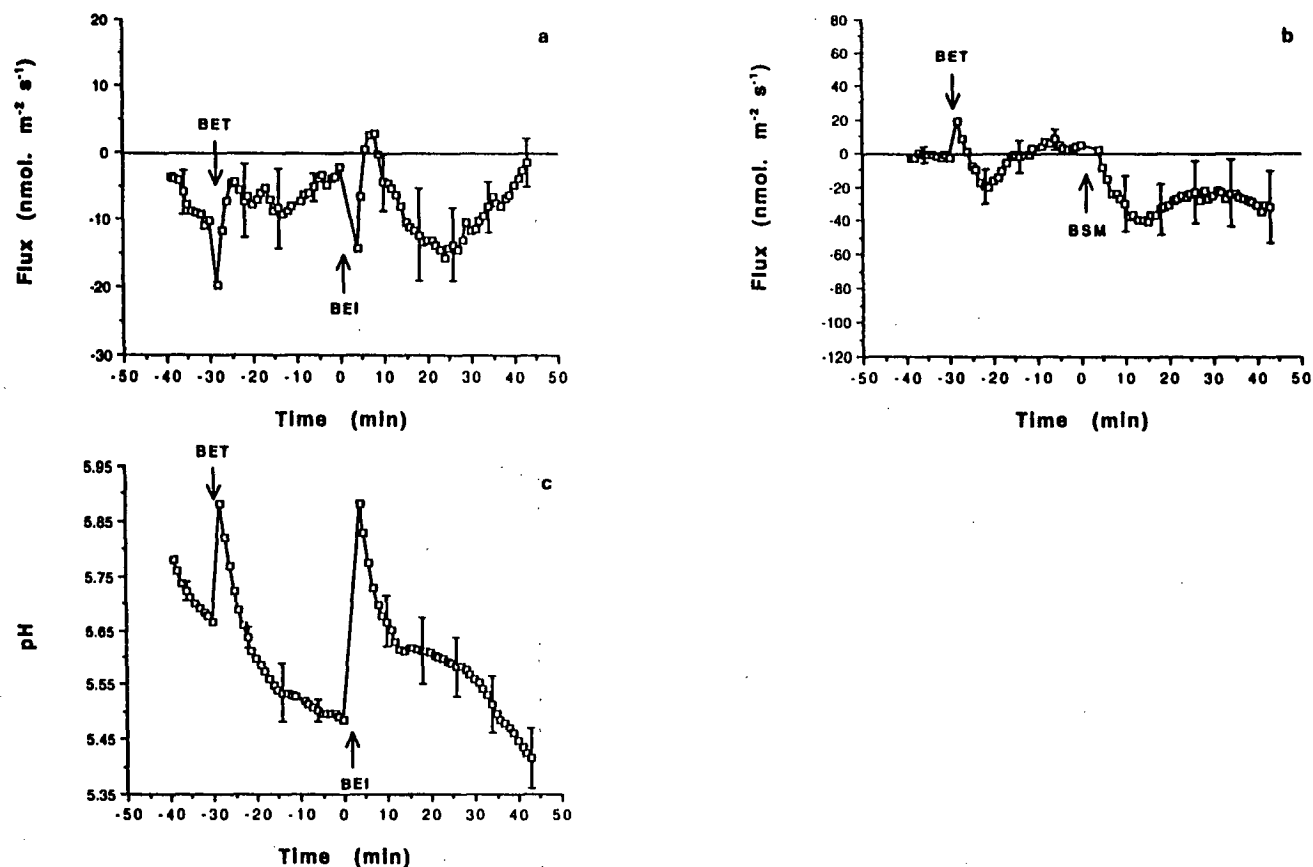
Figure 6.3

The responses of 2.25 hour preincubated oat coleoptile segments to 10^2 mole m^{-3} IAA: proton (a), calcium (b) and potassium (c) net fluxes (efflux negative) and pH (d) adjacent to the cut tissue surface. Each mean is from ten plants. Other details are as in Figure 6.1.
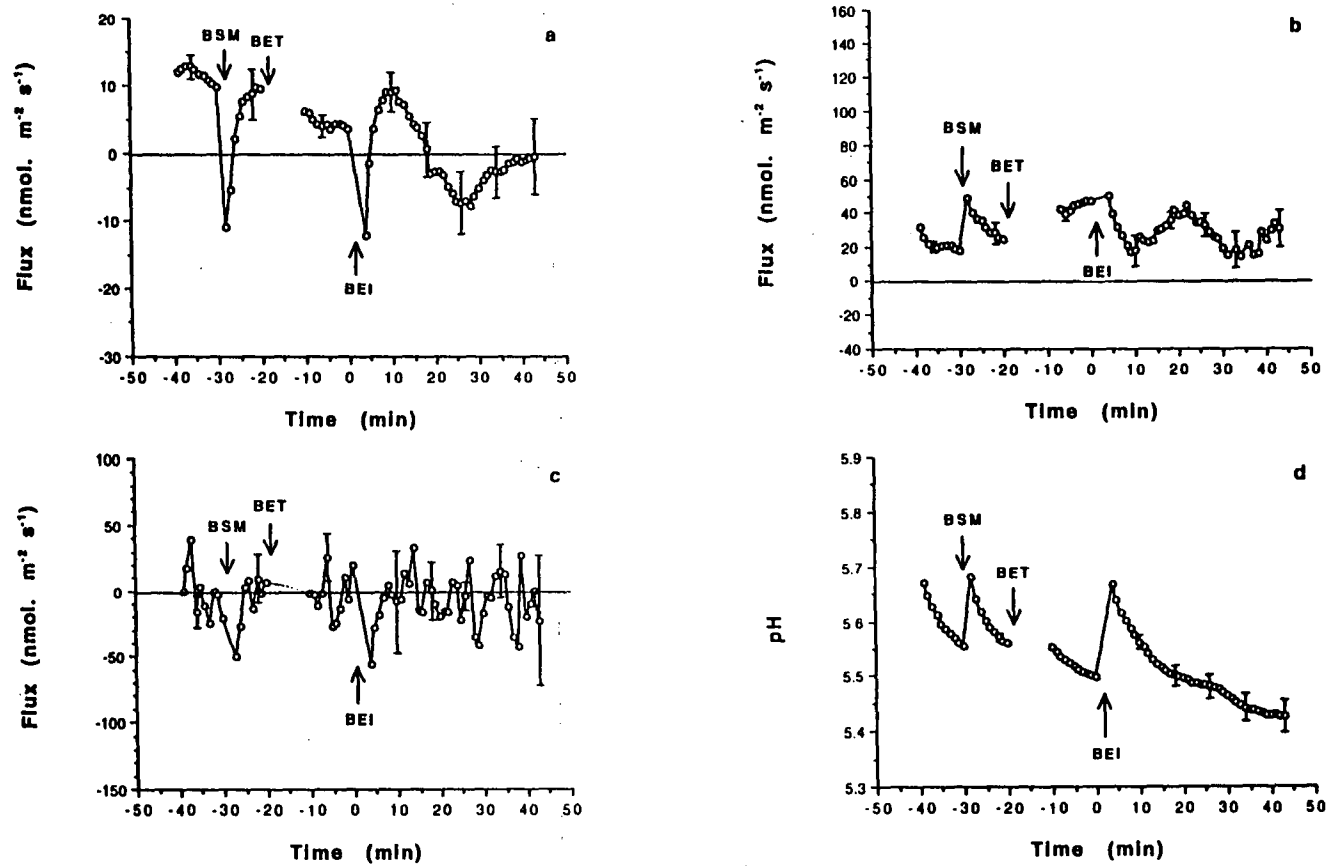
Figure 6.4

The responses of 1 hour preincubated oat coleoptile segments to 10^{-2} mole m^{-3} IAA: proton (a), calcium (b) and potassium (c) net fluxes (efflux negative) and pH (d) adjacent to the cut tissue surface. Each mean is from ten plants. Other details are as in Figure 6.1.
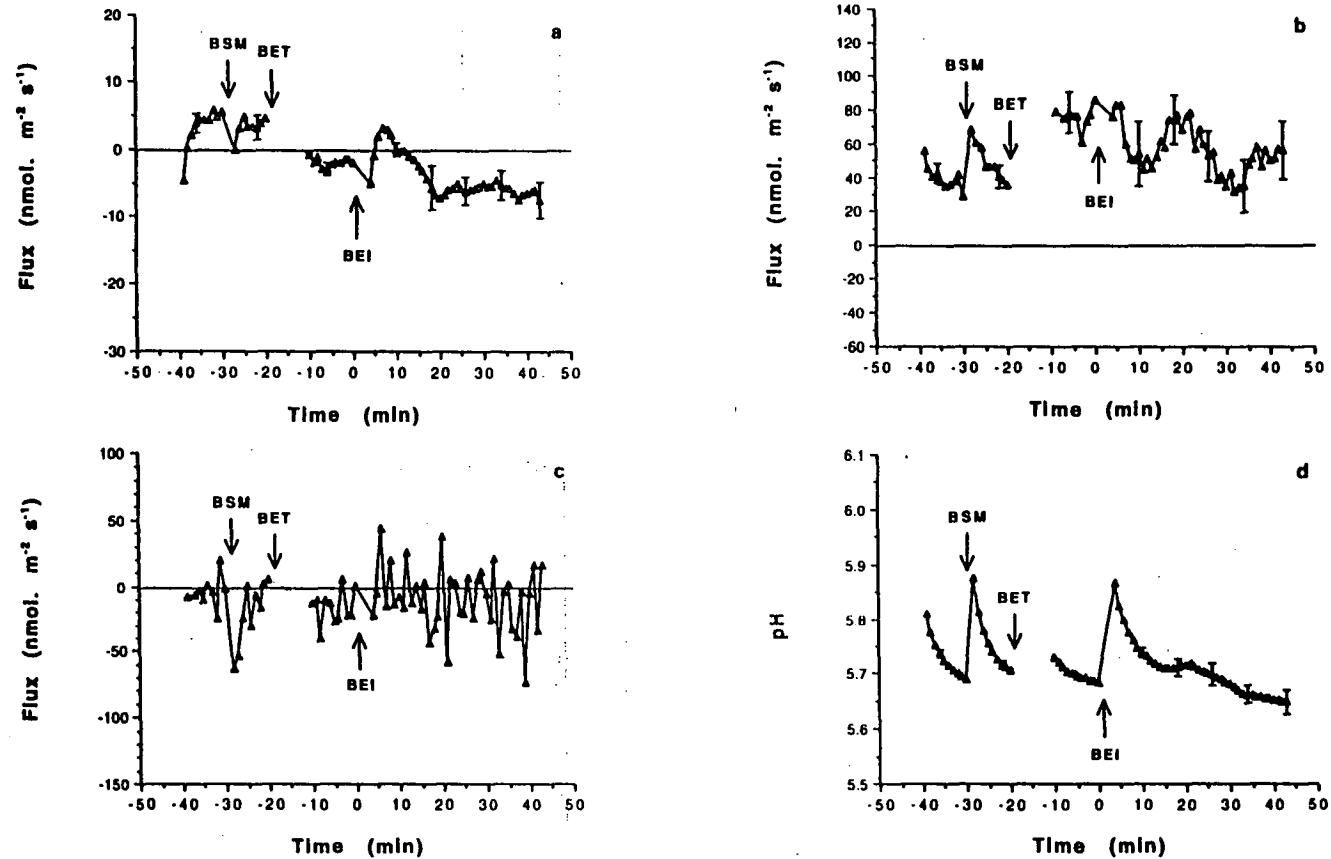
Figure 6.5

The membrane potential (PD) of parenchymal cells in 4.5 hour preincubated segments of 4-day-old split oat coleoptiles in response to 10^{-2} mole m^{-3} IAA. The measurements were carried out in stagnant solution. Downward arrow indicates the solution replacement with the same solution (BSM) to study the effect of solution change. Upward arrow indicates the solution replacement with BEI to apply IAA. Each mean of eleven plants is calculated relative to the value obtained just before the solution replacement with BSM or BEI. Bars show SE.
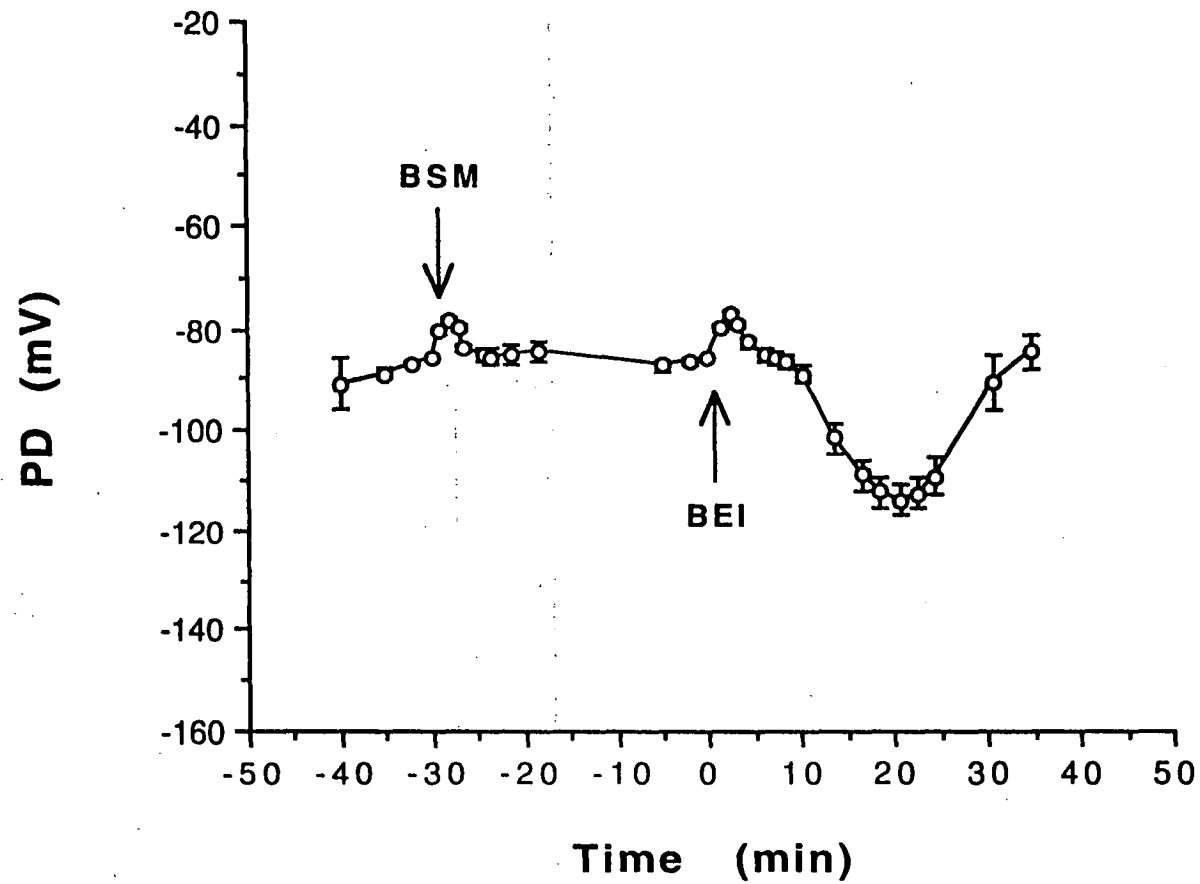
Figure 6.6

The membrane potential (PD) of parenchymal cells in 2.25 hour preincubated oat coleoptile segments in response to 10^{-2} mole m^{-3} IAA. Each mean is from eight plants. Other details are as in Figure 6.5.
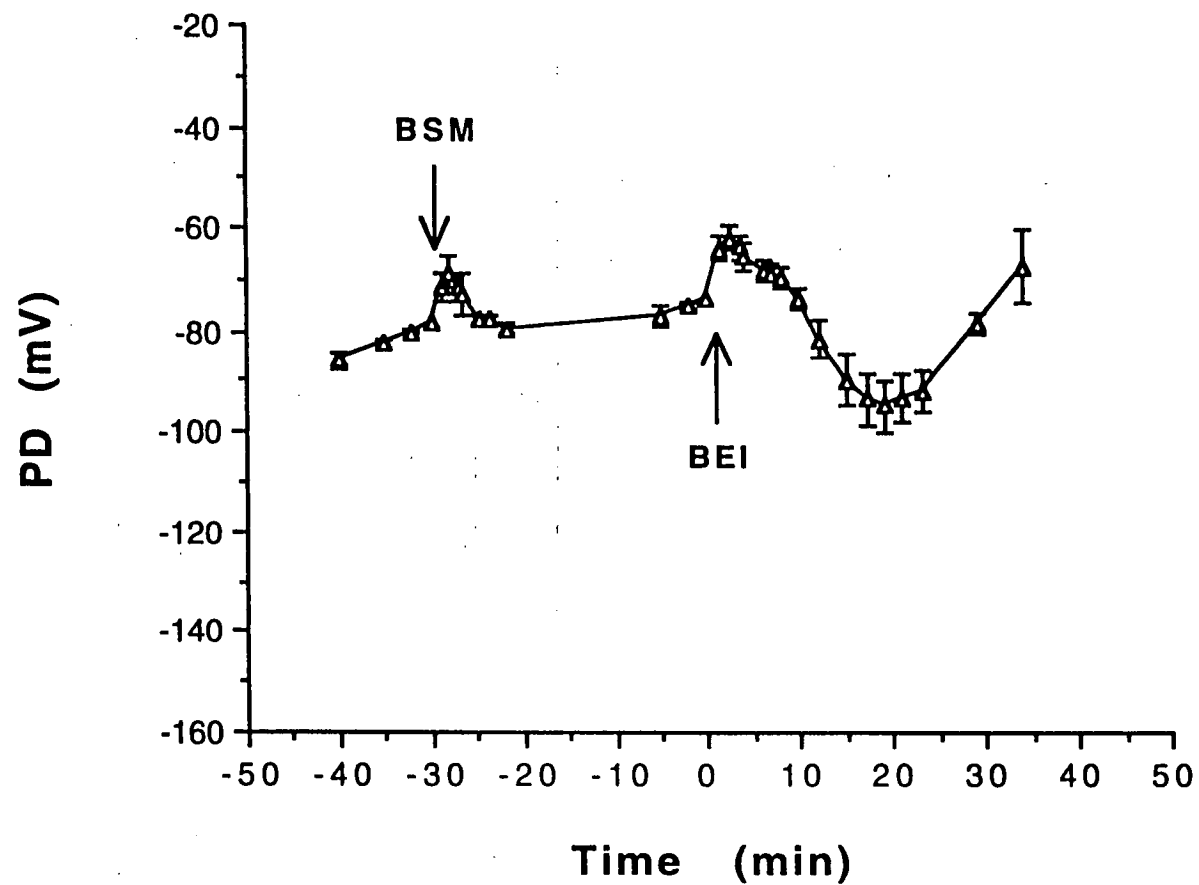
Figure 6.7

The membrane potential (PD) of parenchymal cells in 1 hour preincubated oat coleoptile segments in response to 10^{-2} mole m^{-3} IAA. Each mean is from seven plants. Other details are as in Figure 6.5.
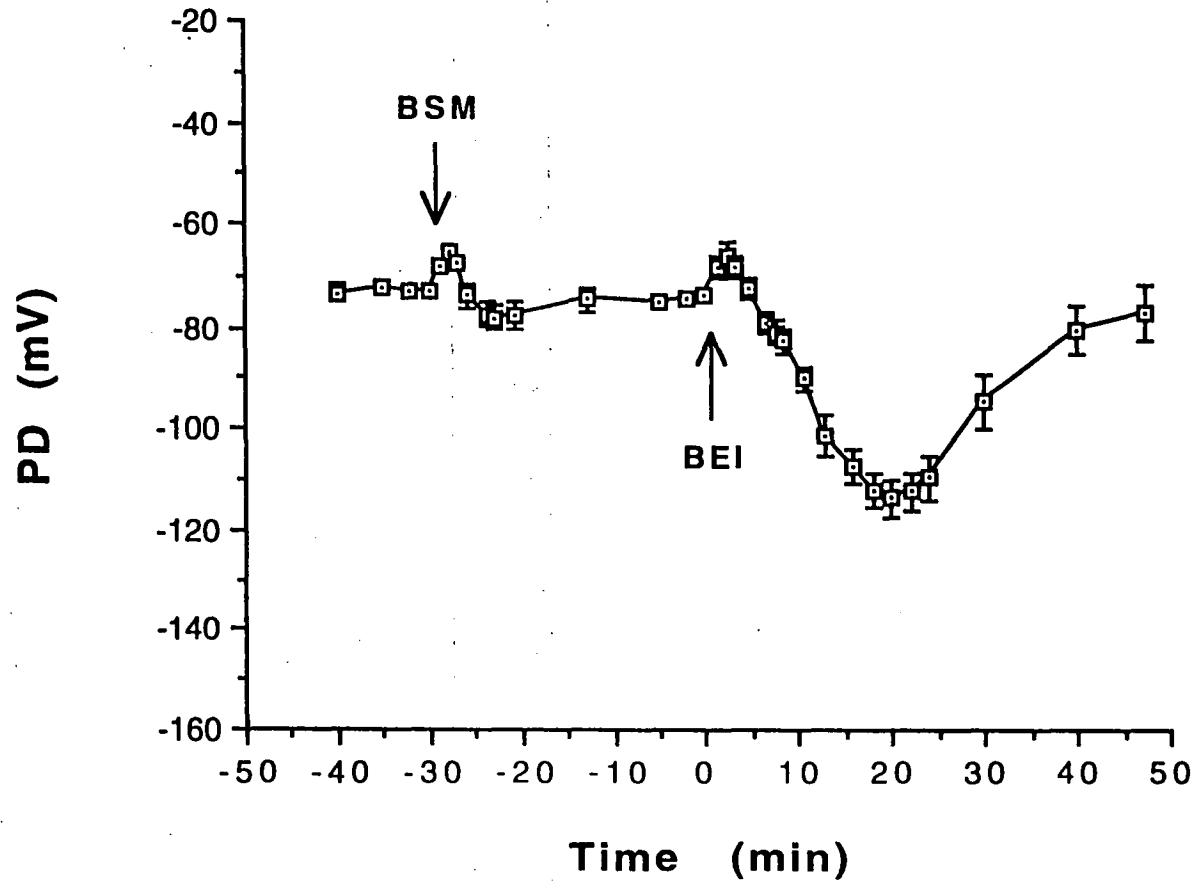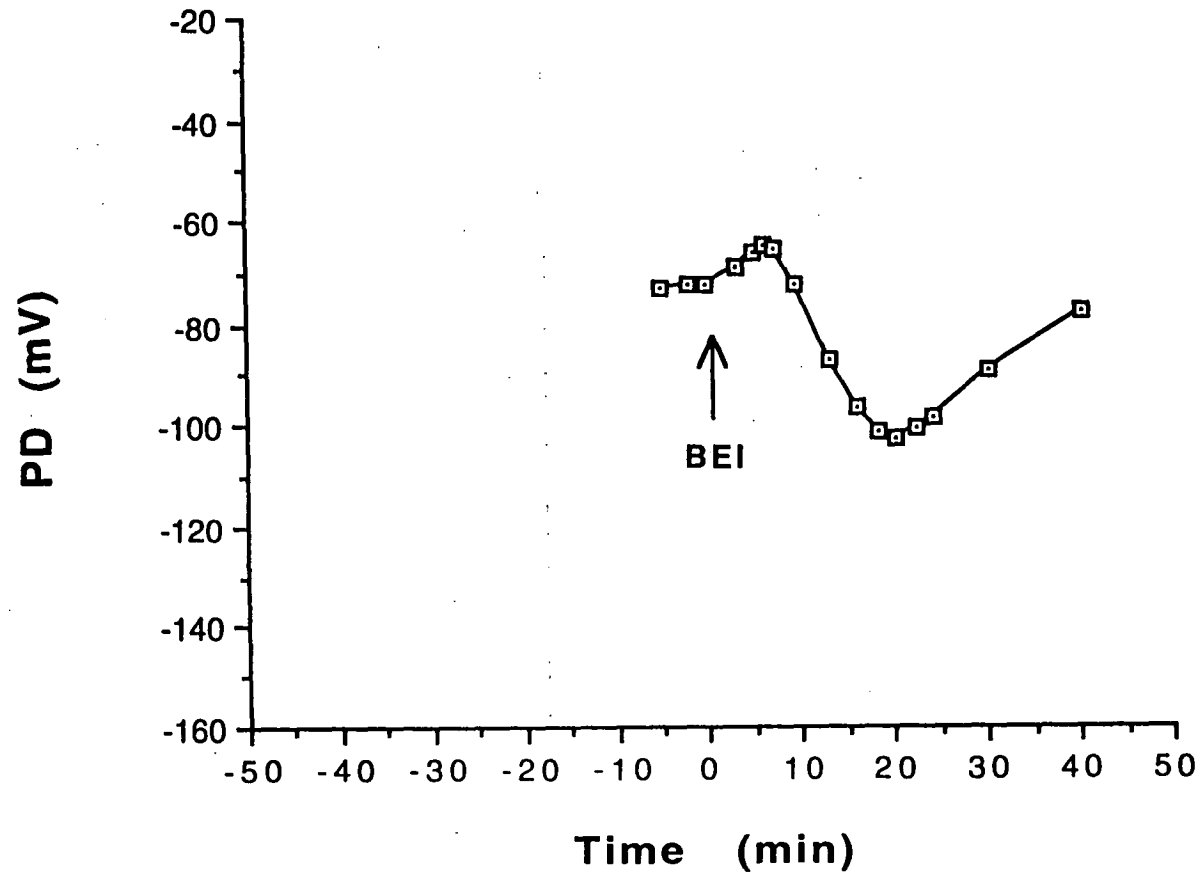
Figure 6.8

The membrane potential (PD) of parenchymal cells in 4.5 hour preincubated segments of 4-day-old split oat coleoptiles in response to 10^2 mole m^{-3} IAA. The measurements were carried out in flowing solution. Upward arrow indicates the solution replacement of BSM with BEI to apply IAA. Each mean of six plants is calculated relative to the value obtained just before the solution replacement. Bars show SE.

Figure 6.9

The mean proton net flux in response to 10^{-2} mole m^{-3} IAA observed in the solution adjacent to the cut tissue surface of 4.5 (▣), 3.5 (▢), 2.25 (○) or 1 (△) hour preincubated segments of 4-day-old split oat coleoptiles. For 4.5, 2.25 and 1 hour preincubation, first downward arrow indicates the solution replacement with BSM and second downward arrow indicates the solution replacement with BET. For 3.5 hour preincubation, first downward arrow indicates the solution replacement with BET and it is without second downward arrow. Upward arrow indicates the solution replacement with BEI to apply IAA. (see also Figures 6.1, 6.2, 6.3, 6.4).
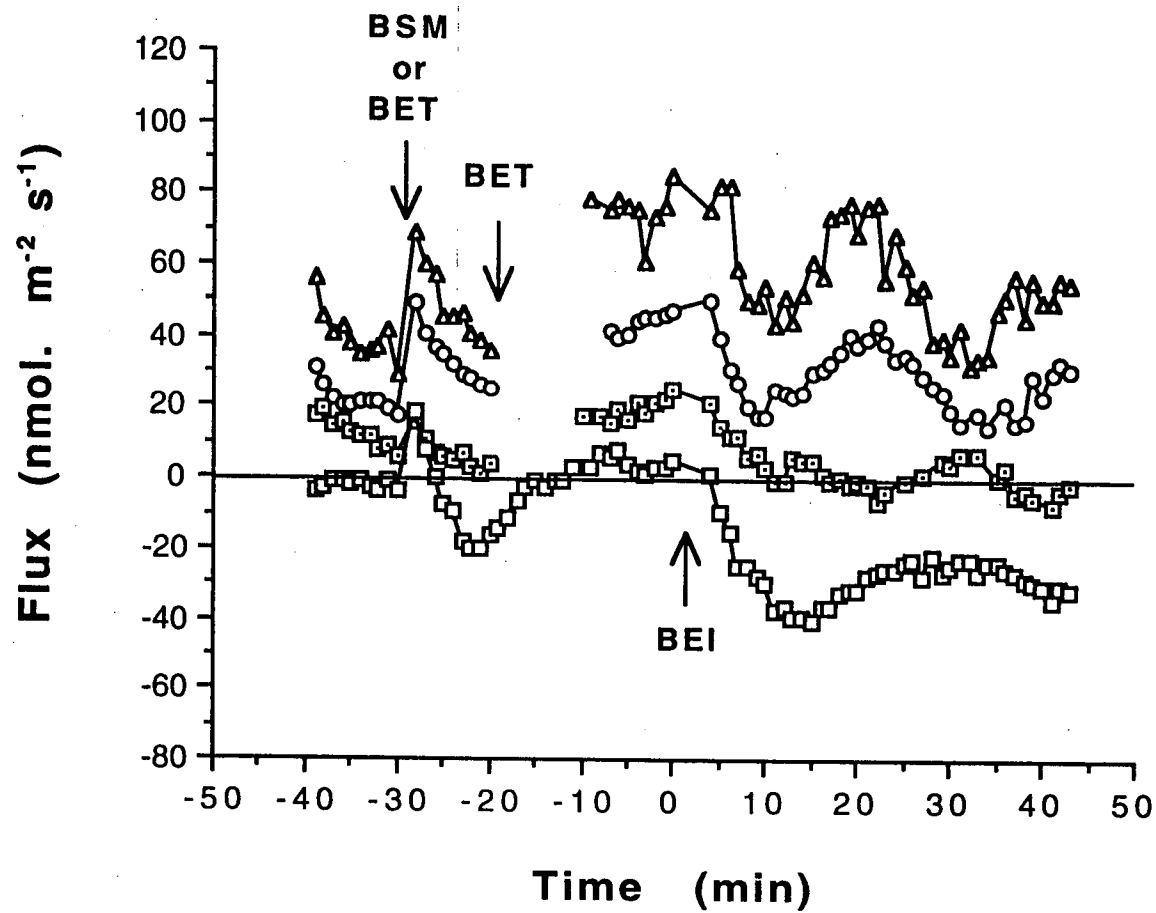
Figure 6.10

The mean calcium net flux in response to 10^{-2} mole m^{-3} IAA observed in the solution adjacent to the cut tissue surface of 4.5 (▣), 3.5 (▢), 2.25 (○) or 1 (△) hour preincubated segments of 4-day-old split oat coleoptiles. Other details are as in Figure 6.9.
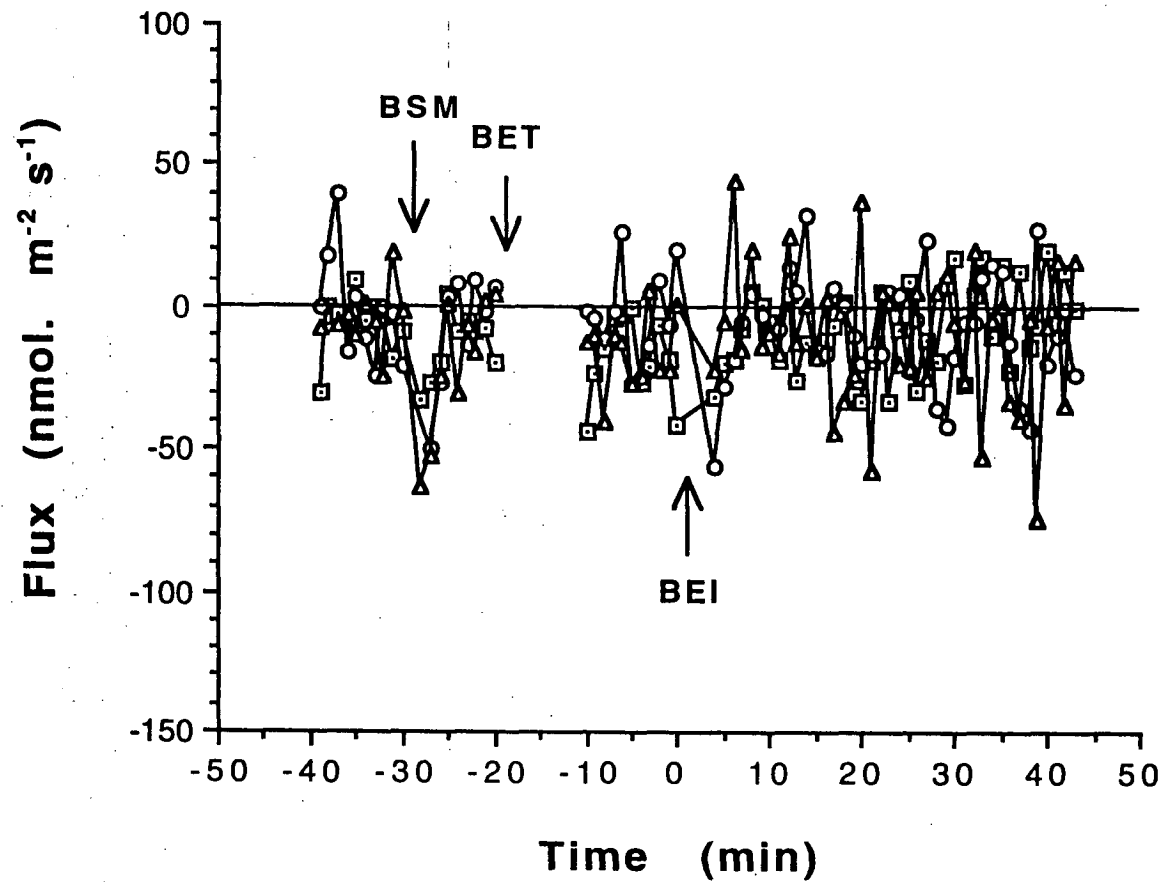
Figure 6.11

The mean potassium net flux in response to 10^{-2} mole m^{-3} IAA observed in the solution adjacent to the cut tissue surface of 4.5 (◻), 2.25 (○) or 1 (△) hour preincubated segments of 4-day-old split oat coleoptiles. First downward arrow indicates the solution replacement with BSM and second downward arrow indicates the solution replacement with BET. Upward arrow indicates the solution replacement with BEI to apply IAA. (see also Figures 6.1, 6.3, 6.4).
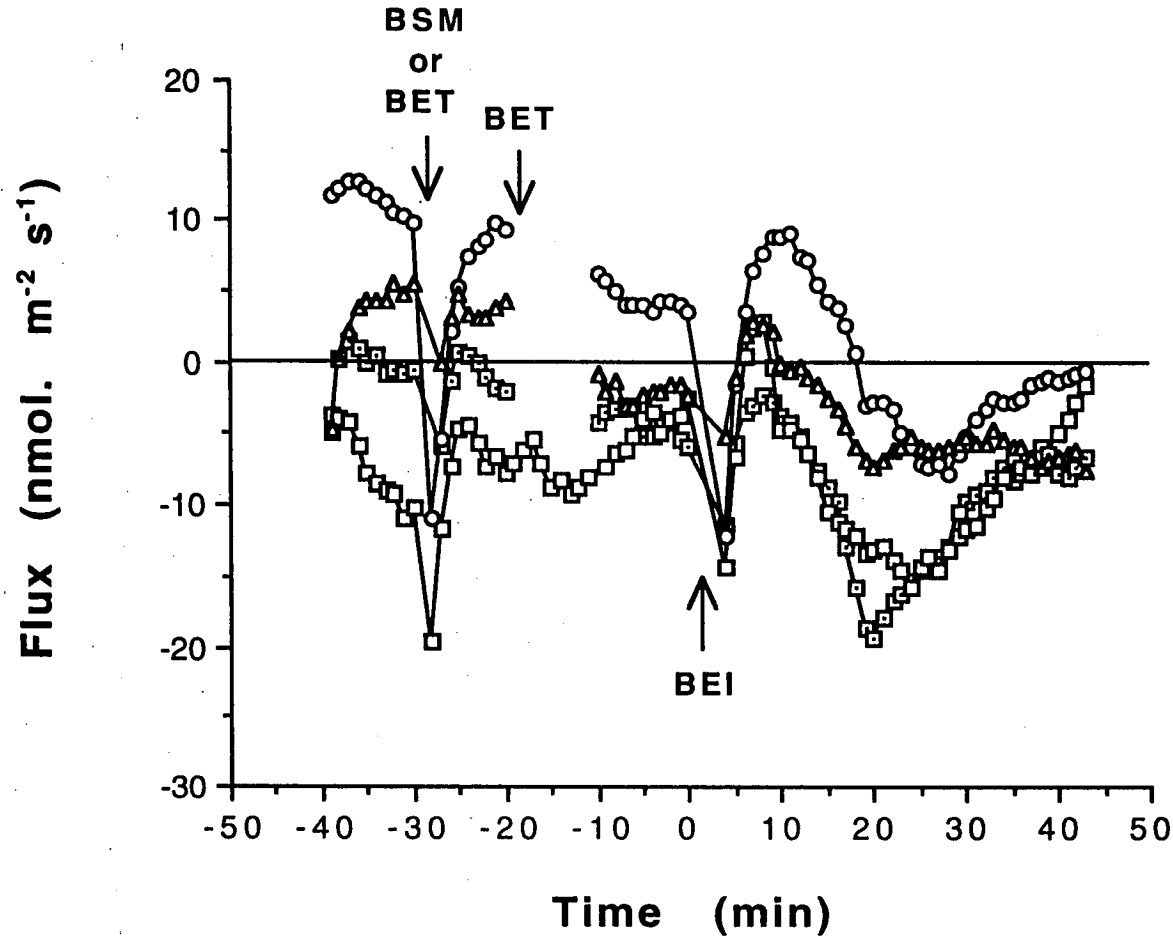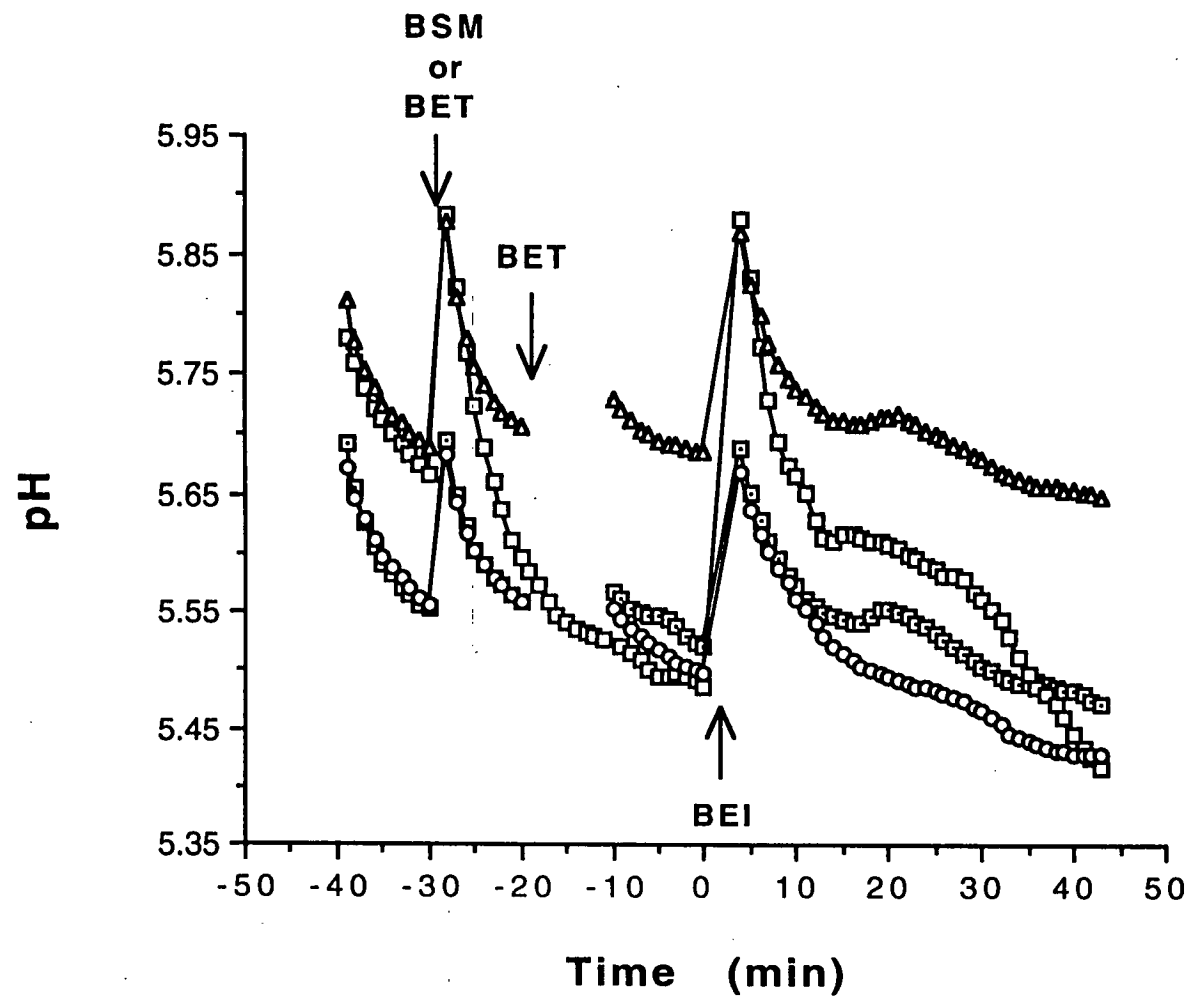
Figure 6.12

The mean pH in response to 10^{-2} mole m^{-3} IAA observed in the solution adjacent to the cut tissue surface of 4.5 (▣), 3.5 (❑), 2.25 (O) or 1 (△) hour preincubated segments of 4-day-old split oat coleoptiles. Other details are as in Figure 6.9.

Figure 6.13

The mean membrane potential of parenchymal cells in response to 10^{-2} mole m^{-3} IAA observed in 4.5 (▣), 2.25 (O) or 1 (△) hour preincubated segments of 4-day-old split oat coleoptiles. Downward arrow indicates the solution replacement with BSM. Upward arrow indicates the solution replacement with BEI to apply IAA. (see also Figures 6.5, 6.6, 6.7).

6.2.1 Ion Fluxes

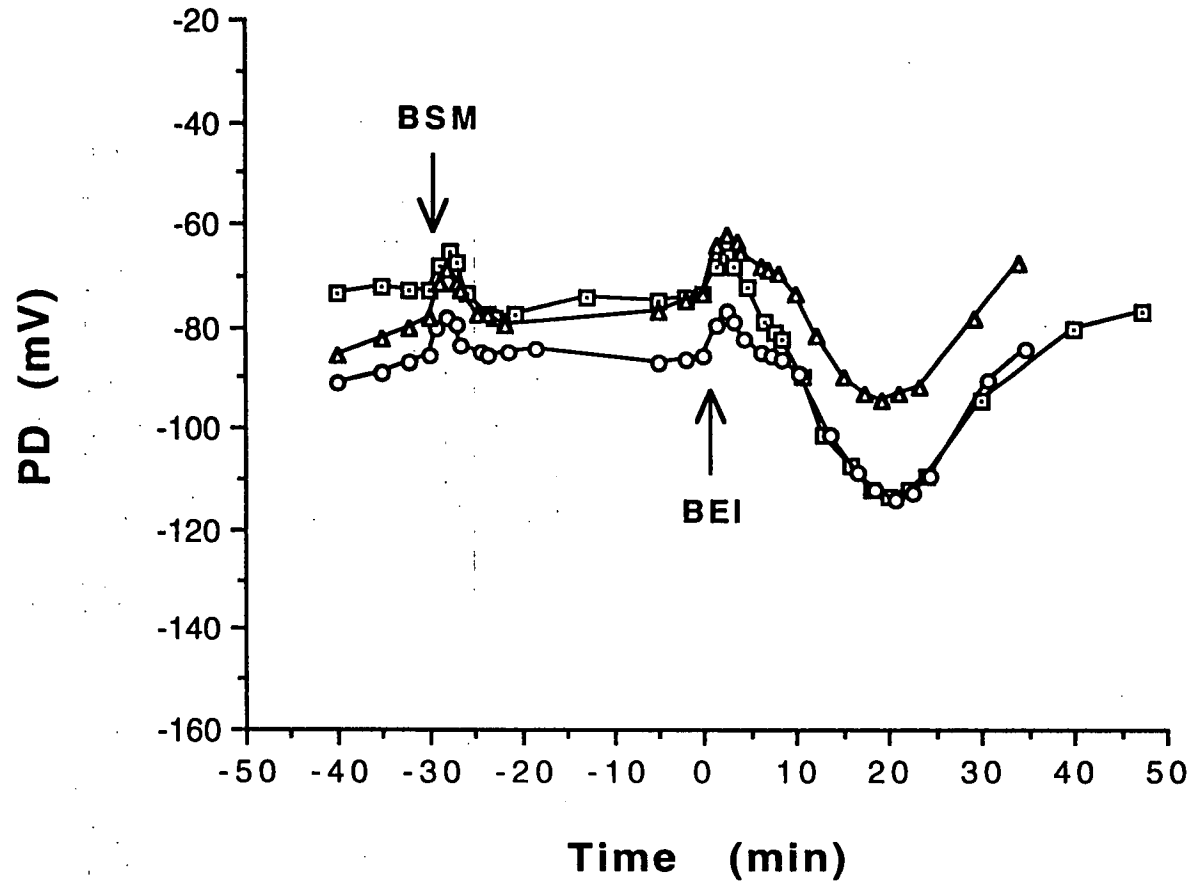Before observing the effect of solution change, the proton flux (in BSM or BET) varied with the experiments, between -10 to 10 nmol. m^{-2} s^{-1} (Figure 6.9). The solution refreshment caused a transient proton efflux. When BSM was replaced with BET (Figures 6.1a, 6.3a and 6.4a), 0.5% ethanol caused a small shift of proton efflux in addition to the solution change effect. (The results of the replacement from BSM to BET are not shown since the purpose of the replacement from BSM to BET was to bathe first the tissue segment in the chamber with solution containing the same amount of ethanol as BEI before the real effect of IAA was observed by applying BEI. The effect of the replacement from BSM to BET was not intentionally studied.) Just before the IAA application, the mean proton flux was -4, -3, 5 and -2 nmol. m^{-2} s^{-1} respectively for 4.5, 3.5, 2.25 and 1 hour preincubation. When BET was replaced with BEI to observe the effect of IAA, the replacement also showed a similar transient proton efflux. In this case, the transient proton efflux was followed by a small transient proton influx. About 13 minutes from IAA application the flux fell below its pre-BEI value, to reach its minimum at 20-25 minutes. The mean minima were -20, -15, -7 and -7 nmol. m^{-2} s^{-1} respectively for 4.5, 3.5, 2.25, and 1 hour preincubation. The proton flux then tended toward its pre-BEI value. The error bars are large because of the large variation in the magnitude of the responses in the plants. The relatively smooth changes in the mean values show that plants were consistent in the trend of the responses.

In BSM or BET, the pH close to the cut surface decreased, with the rate decreasing as a function of time (Figure 6.12). The refreshment of the solution increased the pH suddenly after which it decreased again. Just before the replacement of BET with BEI, the pH was 5.53, 5.48, 5.5, 5.7 for 4.5, 3.5, 2.25 and 1 hour preincubation respectively. The replacement caused a sudden increase in pH followed by pH decreasing. At 20-30 minutes after IAA addition, the decrease of the pH stopped transiently and after that, the pH began to decrease again. Within 40 minutes after the IAA addition, the pH was about 5.48, 5.4, 5.42, and 5.64 for 4.5, 3.5, 2.25 and 1 hour preincubation respectively.

Before the observation of the solution change effect, the calcium flux (in BSM or BET) was 10, 0, 20 and 40 nmol. m^{-2} s^{-1} respectively for 4.5, 3.5, 2.25, and 1 hour preincubation (Figure 6.10). When the solution was refreshed, the calcium influx increased transiently and recovered within 5

minutes. The solution replacement from BSM to BET caused an upward shift of calcium influx (Figures 6.1b, 6.3b and 6.4b). Before the IAA application, the calcium influx was 20, 0, 40 and 80 nmol. $m^{-2} s^{-1}$ respectively for 4.5, 3.5, 2.25, and 1 hour preincubation. After the replacement of BET with BEI was carried out, the expected transient calcium influx due to the solution change did not appear. In this case, the calcium flux decreased directly. For 4.5, 3.5, 2.25, and 1 hour preincubation, the minimum of the flux was reached at about 20, 15, 10 and 10 minutes respectively. The minima were 0, -40, 20 and 50 nmol. $m^{-2} s^{-1}$ respectively. The calcium flux rose and then fell again. For 2.25 and 1 hour preincubation, the second minimum of 15 and 40 nmol $m^{-2} s^{-1}$ was reached at about 35 and 30 minutes respectively. The mean value changes were relatively smooth. This indicates that the trend of the responses for all segments was consistent and that the large error bars were due to large variation in the magnitude of the responses from different plants.

In BSM, the potassium flux showed a wide variability throughout the experimental time for every preincubation (Figure 6.11). Based on this finding, in the last experiment which was for 3.5 hour preincubation, the observation of potassium flux was not carried out. The average potassium flux was a small efflux. It seems that the solution change from BSM to BET or from BET to BEI caused some transient increase in potassium efflux and then approached its previous level. From the results of the experiments for 4.5 hour preincubation, it was found that IAA itself might eventually cause a small potassium influx. However for other preincubation time, the effect of IAA on potassium flux was more unclear.

6.2.2 Membrane Potential

In stagnant BSM, the membrane potential was in the range between -75 and -90 mV (Figures 6.5, 6.6, 6.7 and 6.13). Solution change depolarized the membrane potential so that within about 2 minutes, the membrane potentials for segments preincubated for 4.5, 2.25 and 1 hours were about 7, 8 and 10 mV less negative than their initial values. The membrane potentials then repolarized with a small overshoot to approach their initial value within 20 minutes. When BSM was replaced with BEI to observe the effect of IAA, a similar effect of solution change in the first 7 minutes was also present: the solution replacement caused the membrane potentials to depolarize about 7.5, 9 and 12 mV respectively for 4.5, 2.25 and 1 hour preincubation, at about 2.5 minutes and

then the membrane potentials recovered. However, as they approached their initial value, about 7.5 minutes after the addition of IAA, the membrane potentials began to hyperpolarize faster. The hyperpolarization continued so that at about 20 minutes, the membrane potentials reached their minima. For 4.5, 2.25 and 1 hour preincubation, the minima were about 40, 28 and 21 mV more negative than their initial values.

In a flowing solution following 4.5 h preincubation, the replacement of BSM with BEI also caused the membrane potential to depolarize first (Figure 6.8). In this case, the membrane depolarization reached its maximum, which was 8 mV less negative than its initial value of -75 mV, within 6 minutes. This is much later than the 2 minute response of the stagnant solution-change artefact. The stagnant solution-change artefact would not be present in these conditions. The membrane depolarization was then followed by a recovery. The membrane become hyperpolarized without any indication of slowing down, so that at about 20 minutes the membrane potential was 31 mV more negative than the initial value. The membrane potential then depolarized again to approach the initial value.

With both conditions (stagnant solution and flowing solution), the magnitude of the membrane potential in BSM was relatively small compared to the usual membrane potential observed in plants (more than 100 mV). Since it was also observed in flowing solution, the small membrane potential is not due to the slightly unaerobic condition which was present in experiments with stagnant solution. The membrane potential was obtained from parenchymal cells of oats coleoptiles with respect to BSM containing 0.1 mole m^{-3} KCl + 0.1 mole m^{-3} CaCl$_2$ at pH 6. Perhaps, the ionic composition inside the parenchymal cells and in BSM was not so different. This still needs some explanation.

6.3 Discussion

6.3.1 Effects of Solution Change

When bathing solution was replaced during the experiments, the process of solution change clearly caused a transient efflux of protons, a transient influx of calcium, a transient efflux of potassium, a transient increase of external pH close to the tissue surface and a transient membrane depolarization (Figures 6.9, 6.10, 6.11, 6.12 and 6.13). During the process, the ion concentration gradient

region established close to the tissue surface was removed. The process also gave some stimuli to the tissue. Therefore, any responses that appeared after this process, were due to both the removal of the region and the stimuli.

The flux of an ion from a tissue to the bathing solution establishes a concentration gradient region of the ion in the solution adjacent to the tissue. The resultant concentration gradient region of all ions in this area also sets up a potential difference. When the solution is replaced with a new solution, the process removes the region. This also changes the potential difference. After the process is completed, a new concentration gradient region is established. The thickness of the new concentration gradient region increases with time. For example, to establish a proton concentration gradient region which has a thickness of 1 mm, the required time is about 4 minutes, based on the proton diffusion coefficient of 10^{-9} m^2 s^{-1} (see Appendix B). Now, if the bulk concentration of the ion is the same before and after the solution change, the concentration gradient of the ion in solution adjacent to the tissue just after the solution change would be larger than the gradient before the solution change. At this time, the concentration of the ion in this area itself depends on the ion flux before the solution change. When the flux is an influx, the concentration of the ion just after the solution change is bigger than before the solution change. Based on the definition of the ion flux therefore, the influx of the ion at this time would be bigger too. When the flux is an efflux, the concentration of the ion in solution adjacent to the tissue just after the solution change is smaller than before the solution change. In this case, the efflux just after the solution change is bigger if the magnitude of the decrease in the ion concentration due to the solution change is smaller than the magnitude of the increase in the ion concentration gradient. Otherwise, the efflux is smaller. With time, the ion flux changes to approach the ion flux before the solution change. When it happens, it indicates that the effect of solution change has gone.

Solution change may also cause some stimuli to the tissue. It has been reported that actions such as cutting, rubbing, chilling, heating and acydifying on living tissues cause an increase of proton influx, calcium influx, potassium efflux and membrane depolarization (Gronewald and Hanson 1980, Chastain and Hanson 1982, Rincon and Hanson 1986). Solution change is not one of the actions. However, solution change also disturbs the normal condition of the tissues which were always kept in stagnant solution during the experiments. Therefore solution change may cause similar effects.

The observed responses after the solution change: the transient proton efflux, calcium influx, potassium efflux, pH increase and membrane depolarization (Figures 6.9, 6.10, 6.11, 6.12 and 6.13) are consistent with the description of the effects of solution change above. In this case, the final responses observed after the solution change are the resultant effects of both the removal of the ion concentration gradient region and the stimulation given to the cells.

It is also interesting to realise that the observed proton flux is not always an efflux (Figures 6.9) although the observed pH close to the tissue surface always decreases (Figures 6.12). The transient increase of the pH close to the tissue surface after the solution change is consistent with the efflux of protons. Is the flux of protons shifted up? This still needs some explanation. The diffusion pattern around the tissue may not be as simple as assumed.

6.3.2 The effects of IAA

When BET is replaced with BEI to apply IAA, the transient proton efflux due to solution change is also present (Figure 6.9). The subsequent responses, a transient proton influx followed by a bigger transient proton efflux, are attributed to the effect of IAA. Apparently, IAA stimulates other intracellular processes before IAA-induced proton efflux begins. The transient proton influx is explained below in relation to the early processes of IAA action. The lag of the IAA-induced proton efflux (from pre-BEI value) is about 13 minutes. The lag is longer than the lag of the IAA-induced growth and membrane hyperpolarization (Cleland 1976, Cleland 1980, Kutschera and Schopfer 1985a, Senn and Goldsmith 1988). However, in the proton-calcium exchange section, it is explained that the lag of the IAA-induced proton efflux across the plasmalemma is shorter than the lag in external flux and is similar to the lag of the IAA-induced growth and membrane hyperpolarization (as reported by Cleland 1976, Cleland 1980, Kutschera and Schopfer 1985a, Senn and Goldsmith 1988). Therefore this supports the suggestion that during the IAA-induced growth, protons are extruded from the cells.

The transient increase in pH close to the cut surfaces is attributed to the effect of solution change (Figure 6.12). About 20 minutes after the solution-change transient, the pH starts to decrease further in response to IAA. The gentle change in slope and the long delay are due to the large solution/tissue volume ratio applied in these experiments. With a quite small solution/tissue

volume ratio, it was reported that the lag was observed much sooner, less than 10 minutes (Cleland 1980, Senn and Goldsmith 1988).

The calcium influx decreases immediately after the replacement of BET with BEI (Figure 6.10). The expected transient increase of calcium influx due to solution change is not present. This indicates that IAA causes an immediate calcium efflux which swamps the solution change influx. This is discussed below.

and small

IAA causes two processes of transient calcium efflux in sequence (Figure 6.10). In the experiments with 3.5 and 4.5 h preincubation, the second transient has not been completed within 40 minutes. The second transient calcium efflux may relate to the second increase of the IAA induced-growth rate observed by others (Vanderhoef 1980, Brummell and Hall 1987). During the second increase of IAA induced-growth rate, it has been widely interpreted that new wall materials are synthesised as a result of the activation of protein kinases. This activation depends much on the level of calcium in the cytoplasm. Perhaps, the second transient calcium efflux is due to the regulation of the calcium concentration in the cytoplasm during this process. However, it is still difficult to describe the mechanism.

The transient potassium efflux due to solution change also takes place after the replacement of BET with BEI to study the effect of IAA. Apparently, IAA itself does not have a significant effect on the potassium flux during a 40 minute period (Figure 6.11). In fact, it is difficult to study the effect of IAA on potassium flux since the variability in the flux is big. The variability is much bigger than the noise level of the measurement system in this laboratory. Therefore, the highly variable potassium flux is due to the behaviour of the plants. There is no good explanation yet of why cells give the highly variable potassium efflux and it may be interesting to study whether there is a pattern in this variability. It has been suggested that potassium efflux decreases in response to IAA (Haschke and Lüttge 1977a&b). This is based on the possibility that the antiports between K^+ and H^+ are involved in the IAA induced-proton extrusion to maintain electroneutrality. Although this has been criticised based on the finding that IAA induces membrane hyperpolarization (Cleland 1976, Cleland et al. 1977, Cleland 1980, Senn and Goldsmith 1988), a fine balance of charges is still required to prevent volt-change during the IAA-induced proton efflux. Therefore, there is still a possibility that potassium efflux decreases. If it is the case, the change in the potassium fluxes should be about

10 nmol m^{-2} s^{-1}, and, this would be lost in the observed potassium variability. However, it seems unlikely that the potassium fluxes rise at this time because their average remains at the same level before and after the IAA addition. Therefore, the IAA-induced proton efflux must be accompanied by transport of other ions so that the membrane does not hyperpolarize massively during IAA action.

When BSM is replaced with BEI to observe the effect of IAA, the resultant transient membrane depolarization, lasting about 7.5 minutes, is slightly bigger than the transient membrane depolarization due to solution change (Figure 6.13). It seems likely that IAA also causes a small and transient membrane depolarization that is combined with the transient membrane depolarization due to solution change. This is consistent with the results of the experiments in flowing solutions: a transient depolarization, lasting about 7 minutes (Figure 6.8). Similar results of experiments in flowing solutions were also obtained by others (Cleland et al. 1977, Bates and Goldsmith 1983, Senn and Goldsmith 1988). In their case, the transient depolarization lasted 7-12 minutes. It is discussed below that the depolarization in the first 7 minutes during IAA action is due to calcium transport from cell walls into the cells.

About 7.5 minutes after IAA addition, IAA causes the membrane potential to hyperpolarize further reaching its minimum at about 20 minutes. The membrane potential then recovers again. It has been suggested widely that the IAA-induced membrane hypepolarization is due to the activation of proton pumps in the plasmalemma (Cleland et al. 1977, Bates and Goldsmith 1983, Senn and Goldsmith 1988). If it is the case, the IAA-induced proton efflux across the plasmalemma should have a similar lag. The observation of proton flux during IAA action shows that the lag of the IAA-induced proton efflux adjacent to the tissue surface (13 minutes) is longer than the lag of the IAA-induced membrane hyperpolarization (7-10 minutes). This indicates that there are other processes that take place in the walls of the cells in the tissues during the delay. This is discussed in the following section.

6.3.3 Proton-Calcium Exchange

Based on the WADM model, when the IAA-induced proton efflux begins, calcium is released from the walls by some of the extruded protons and the released calcium diffuses to the bathing solution. The measurements of the

calcium flux show that IAA causes an immediate calcium efflux. It seems likely that besides the delayed calcium release due to the IAA-induced proton efflux, there is also other calcium release from the cells or walls that starts earlier. This is discussed below. The observed calcium efflux after the IAA application is the sum of all the calcium released. Now in order to quantitatively examine proton-calcium exchange during the IAA-induced proton efflux, the calcium efflux due to the IAA-induced proton efflux needs to be separated. This is difficult to carry out and for this reason, the quantitative analysis using the WADM model for fluxes is not applied to the IAA data.

In the absence of the result of the quantitative analysis, the decrease of the calcium influx observed after the IAA application can still be used to show qualitatively that the expected proton-calcium exchange takes place during IAA-induced proton efflux. In the first transient decrease of the calcium influx, the amount of the extruded calcium is between 12-37.5 μmole m^{-2}. As explained in Chapter 5, for this amount, the most likely source of the extruded calcium is the cell walls. If it is assumed that the thickness of the cell walls is about 1 μm (M.J. Canny, personal communication) and there are about 10 cells in the thickness of the split segments, the cell walls lose 1.2-3.75 mole m^{-3} of calcium. This is small compared to the calcium concentration in the cell walls (380 mole m^{-3}).

During the process of proton-calcium exchange in the walls, some of the extruded protons from the cells decrease the pH of the walls. However, this amount of protons is relatively small compared to the total amount of protons extruded from the cells. Therefore it can be considered that the IAA-induced proton efflux at the plasmalemma is the same as the sum of the observed IAA-induced proton efflux adjacent to the tissue surface and the calcium efflux due to the exchange. However, the calcium efflux is mixed up with the earlier calcium efflux due to other processes. Therefore the lag of the calcium efflux due to the exchange can not be obtained from the observed calcium efflux. According to the WADM model for fluxes, the observed proton efflux will rise more slowly than the proton efflux at the plasmalemma. Therefore the lag of the proton efflux at the plasmalemma could be the same as the lag of the IAA-induced growth and membrane hyperpolarization. This supports the suggestion that the IAA-induced growth, membrane hypepolarization and proton extrusion take place at the same time.

The question is now why the calcium influx should decrease immediately after the IAA application while the IAA-induced proton efflux and membrane hyperpolarization are delayed several minutes. Does IAA interact first with wall calcium (not load-bearing) and release it from the walls (Arif and Newman 1993)? If it is the case, it is likely that the released calcium diffuses to the bathing solution without delay. It was also observed in these experiments that during the lag, there is a small transient proton influx. This may be simply in charge-balance exchange for the released calcium diffusing initially from the walls to the bathing solution. Since the IAA bindings to the receptors in the plasmalemma may also open calcium channels (Brummell and Hall 1987), some of the calcium released in these first minutes may enter the cells. This calcium influx across the plasmalemma (at the same time as it is also diffusing to the bathing medium) is consistent with the observed transient membrane depolarization during the lag (Fig 6.13, Felle 1988, Senn and Goldsmith 1988). The calcium influx could also provide the increase of the concentration of free calcium in the cytoplasm that begins less than 5 minutes (Felle 1988). Furthermore, it was suggested that the increase of the free calcium concentration in the cytoplasm stimulates proton production in the cytoplasm that leads to the activation of the proton pumps in the plasmalemma (Hepler and Wayne 1985, Brummer and Parish 1983, Brummell and Hall 1987). This process may explain why IAA induced growth has a lag, but fusicoccin- or acid-induced growth is immediate.

6.3.4 Effects of Preincubation Time

The responses of proton fluxes to solution change following the four different preincubation times are also similar (Figure 6.9). However, their responses to IAA show that the increase of proton efflux is bigger when the segments are preincubated longer. From the areas enclosed by the graphs, it can be estimated that within 40 minutes, the total extruded protons are about 9, 12, 18, and 18 μmole m^{-2} for 1, 2.25, 3.5 and 4.5 hour preincubation respectively. This is consistent with the evidence that the medium acidification is more effective with longer preincubated segments when the solution/tissue volume ratio is small (Senn and Goldsmith 1988). Although the proton extrusion is more effective with longer preincubation, the time lag of the increase of the proton efflux from its pre-BEI value is similar (about 13 minutes) following each of the four preincubation times. Senn and Goldsmith (1988) reported that for shorter preincubation, there is a small basification of the medium before

medium acidification is started during IAA action. Therefore, the IAA-induced medium acidification appears to have a longer lag. Based on this evidence, they raised a question over the acid-growth theory. By measuring proton fluxes close to the cut surface of split segments during IAA action, it is now shown that the lag of the IAA-induced proton efflux does not depend on the length of preincubation, including 1 hour preincubation. The small basification observed by Senn and Goldsmith (1988) is probably due to the initial proton influx as observed in the present experiments with 1 hour preincubation where the effects of splitting are still present.

The length of the preincubation time does not have a consistent effect on the pH adjacent to the cut surfaces of split segments (Figure 6.12). (The pH observation following 3.5 hour preincubation was carried out in a different external medium (BET)). The responses of the pH to solution change and to IAA are similar following the four preincubation times. With relatively small solution/tissue volume ratio, it has been reported that the pH drop following longer preincubation is bigger than the pH drop following shorter preincubation during IAA action (Senn and Goldsmith 1988). With a big solution/tissue volume ratio such as I used, more protons are needed to decrease the external pH. Therefore, to cause a clear difference in the rate of the external pH drop, many more protons must be supplied. In this case, the IAA-induced extruded protons following the four preincubation times are not significant enough to cause a clear difference in the rate of the external pH drop.

The observation of calcium fluxes following 4.5, 2.25 and 1 hour preincubation shows that the initial calcium influx in BSM is generally smaller when the preincubation time is longer (Figure 6.10). The result of the calcium flux observation following 3.5 hour preincubation is not included in this comparison because the observation has been carried out in a different bathing medium (BET). It has been reported that injuries such as cutting increase the calcium influx and time is required to recover the influx in corn roots (Rincon and Hanson 1986) and in pea roots (Hush and Overall 1989, Hush et al. 1992). Therefore, the smaller influx observed following the longer preincubation time is probably due to the process of recovery from being injured during the preparation of the split segments. When the bathing medium was refreshed, the transient increase of the influx is also smaller for longer preincubation time. Just after the solution refreshment, the calcium concentration close to the tissue increases suddenly to approach the calcium concentration in the bathing medium. Therefore the calcium concentration gradient also increases. The

increase of the concentration and the gradient is bigger when the initial influx is bigger. This explains why the observed calcium influx increases suddenly after solution refreshment and the magnitude of the increase depends on the magnitude of the initial influx.

The responses of calcium fluxes to IAA following all preincubation times are different. Following 1 hour preincubation, the calcium influx has the first minimum at about 10 minutes. The occurrence of the first minimum of the influx is more delayed when the preincubation time is prolonged so that for 4.5 hour preincubation, the first minimum happens about 20 minutes after IAA addition. It is clear that the responses are due to IAA. However, the mechanism is still not clear.

In Figure 6.11, it is shown that the length of the preincubation time does not have an effect on potassium fluxes. The responses of potassium fluxes to solution change and to IAA following 4.5, 2.25 and 1 hour preincubation are similar. Gronewald and Hanson (1980) have observed the effects of cutting on potassium fluxes in corn roots. They reported that cutting reduced potassium influx and the influx recovered when the root segments were bathed in dilute, aerated $CaCl_2$ solution. The recovery time depended on the length of the root segments, i.e. the time was longer when the length was shorter. For 2 cm segments, the influx almost recovered after about 1 hour in the bathing medium. In my experiments, with 1.2 cm split segments of oat coleoptiles, it has been observed that the potassium fluxes following 4.5, 2.25 and 1 hour preincubation were similar. This indicates that the potassium fluxes in oat coleoptiles had recovered by 1 hour.

In Figure 6.13, it is shown that the magnitude of the transient membrane depolarization after solution change (BSM-BSM and BSM-BEI) is smaller for longer preincubation time. The IAA-induced membrane hyperpolarization itself is larger with longer preincubation (21, 28, 40 mV for 1, 2.25 and 4.5 hour preincubation respectively). This may relate to the recovery process from being split.

6.4 Conclusion

The solution change is clearly responsible for the transients of proton efflux, calcium influx, potassium efflux, the jump in the pH adjacent to the

tissue surface and membrane depolarization observed after the replacement of the solution in the measurement chamber. This is due to the removal of the concentration gradient region of ions in that place and some stimuli given to the cells during the process.

IAA itself causes a small transient proton influx followed by a bigger but transient proton efflux. The lag of the IAA-induced proton efflux does not depend on the length of the preincubation time. However, the IAA-induced decrease in pH close to the cut tissue surface depends on the initial proton flux and the length of the preincubation time. This confirms that the timing of the IAA-induced proton efflux is better than the pH change to indicate the timing of the IAA-induced proton extrusion. IAA also induces immediate calcium efflux which has a biphasic shape. This result has not been provided before for the IAA-action. It is likely that most of the calcium efflux is due to the release of wall calcium by protons extruded from the cells during the IAA action. The expected proton-calcium exchange in the walls based on the WADM model, also happens during the IAA-induced proton extrusion. The proton-calcium exchange provides an explanation that IAA always induces proton efflux from inside the cell at the time when the IAA-induced growth and membrane hyperpolarization begin. IAA also causes membrane hyperpolarization as reported by others. But there is no effect of IAA on potassium fluxes during a 50 minute period.

The length of the preincubation time does clearly affect the magnitude of the IAA-induced proton efflux and membrane hyperpolarization. It also affects the shape of the IAA-induced calcium efflux. This indicates that the recovery process of the segments from being cut needs time.

Chapter 7

CHLORIDE FLUXES

DURING IAA ACTION

7.1 Introduction

Few studies of chloride transport have been done in relation to the process of growth in plant cells during IAA action. In fusicoccin action that causes growth, it was reported that chloride is one of the anions that is transported into the cells as a consequence of the primary direct activating effect on the proton extrusion and on the membrane hyperpolarization (Marrè 1979). It was interpreted that the uptake of anions involves symport with protons, utilising the electrochemical potential gradient as energy source. In Characean cells, it was found that other treatments (ammonia, methylamine, chloride starvation) also cause chloride influx (Smith and MacRobbie 1981, Smith and Whittington 1988) and that in perfused cells, the influx was not affected by metabolic inhibitors (Reid and Walker 1984). This leads to the same interpretation that the chloride influx occurs by cotransport with protons. Since the transport gave an excess of positive charge into the cells (Sanders 1980) and depolarized the membrane potential (Smith and MacRobbie 1981), it was suggested that the stoichiometry of the transport is $2H^+:1Cl^-$. This had been suggested earlier by Smith and Walker (1976). Using voltage-clamp studies in Characean cells, it was also reported that at hyperpolarized levels, a voltage-dependent Cl^- leak (chloride efflux) occurred (Tyerman et al. 1986, Coleman 1986).

It is shown in the previous chapter, that IAA also induces proton efflux and membrane hyperpolarization. Similar to the suggestion for fusicoccin action, this may also provide energy source for the cotransport of chloride with

protons into the cells. Evidence for this transport during IAA-induced growth has not been provided. Therefore in this present work, I have measured the flux of chloride during IAA action in *Avena sativa* split coleoptile segments. The results of the measurements using solid-state chloride microelectrodes are presented in this chapter. Evidence for chloride transport during fusicoccin action has been provided by others (see Marrè 1979). Therefore chloride flux measurements during fusicoccin action have not been carried out in the present study. The transport of chloride, and other anions, is only a consequence of the proton extrusion and the membrane hyperpolarization and does not have a direct relation to the main hypothesis of this thesis (the proton-calcium exchange in the walls) during the growth of plant cells.

As in the previous chapter, to study the chloride flux during the recovery process of the segments after being split (Gronewald and Hanson 1980), the flux measurements were carried out on segments with 4 different preincubation times (4.5, 3.5, 2.25 and 1 hours).

7.2 Materials and Methods

There are two kinds of electrodes commonly used for measuring chloride activity, these are chloride liquid ion-exchange membranes and chlorided silver wires. The liquid chloride microelectrodes that use chloride liquid ion exchanger can be made to have very small tip diameters. The fabrication of these is similar to the fabrication of the microelectrodes with other ion selective liquid membranes already discussed (see Appendix A). However, the selectivity of the liquid chloride microelectrodes with the available chloride liquid ion exchanger is still poor (the slope is less than 50). Their resistances are also much higher (about 100 GΩ). Therefore, people are still improving the chloride liquid ion exchanger. The fabrication of the liquid chloride microelectrodes is easier than the fabrication of solid-state chloride microelectrodes, and the tips can be made as small as possible (less than 1 μm) so that intracellular chloride activity could be measured. With the available chloride liquid ion exchangers, people have measured the chloride activity in epithelial cells (Baumgarten and Fozzard 1981, Sounders and Brown 1977).

The available chloride liquid ion exchangers are Corning 477315 and Corning 477913. The latter is an improvement of the previous one. For Corning 477913, the concentration of the organophilic ligand is increased so

that the resistance decreases (Baumgarten 1981a&b). The slope is also improved. However, the resistance and the slope are still not as good as for the ion exchangers for protons, potassium, and calcium. Therefore, in the present work, measurements of the chloride fluxes were carried out using solid state chloride microelectrodes.

Solid-state chloride microelectrodes have been made from Ag/AgCl wires sealed in glass pipettes. The slope is close to the Nernst value and the resistance is much smaller. The problems are that the tips are usually large, and they are difficult to make. Now, the tips of solid-state chloride microelectrodes have been improved to be much smaller (less than 1 μm) so that they can be used to measure the intracellular chloride activity such as in epithelial cells (Saunders and Brown 1977, Neild and Thomas 1973, Armstrong et al. 1977). However, the response of these microelectrodes is slow (about 1 minute). Armstrong et al. (1977) have improved the response to about 10 seconds. However, the resistance becomes much higher (80 GΩ). In the measurements of ion fluxes with our system, microelectrodes with a fast response are needed. The slow response obtained by Saunders and Brown (1977) is probably caused by the longer time needed for diffusion of the ions to equilibrate the solution inside the tips of the microelectrodes. Therefore, for measuring chloride fluxes in the present study, I developed solid-state chloride microelectrodes with the tips of Ag/AgCl wires slightly exposed outside the tips of the glass pipettes. Therefore the tips of Ag/AgCl wires are directly in contact with the chloride ions in the solution. As a result, the response is fast and the resistance of the microelectrodes is low. For measuring chloride fluxes just outside the cut tissue, the tips of the microelectrodes need not be less than 1 μm. The important thing is that the diameter of the tips is much less than the 40 μm which is the separation of the two positions where the chloride activity is measured for flux calculation.

The fabrication of a chloride microelectrode was started with a teflon coated silver wire (AG-10T, purchased from Clark Electromedical Instruments), 0.175 mm in diameter, 6 cm in length. The teflon was removed 0.5 cm from both ends of the wire. One of the open ends of the wire was then electrolysed under microscope observation (with 100 times magnification) in 2000 mole m^{-3} NaCN with the wire positive to sharpen the wire. For a fast process, a potential of about 9 volts was first applied. After the tip of the wire was about 25 μm in diameter, a potential of about 1.5 volts was then applied. The process was continued until the diameter of the tip was about 1 μm. The tip

of the wire was rinsed in distilled water and then dried to evaporate the water left on the surface of the wire.

A small amount of wax (embedding paraffin purchased from Peel-A-Way Scientific USA, melting point 56-58 °C) was placed on the wire close to the tip (but the wax did not cover the tip) by melting the wax above the wire. In this process, it had to be ensured that the wax coated wire could still go into a glass pipette that has an inner diameter of about 0.75 mm.

A glass pipette was pulled from a glass tube (GC150-10, purchased from Clark Electromedical Instruments) as in the making of microelectrodes with ion selective liquid membranes (see Appendix A). The glass pipette was clamped on a holder and cut 4 cm from its tip. The wax coated silver wire was then placed carefully into the glass pipette through the end opposite the tip. The tip of the glass pipette was broken so that the tip of the wax coated silver wire could pass through the glass tip until a small part of the wire tip was exposed outside the glass tip.

The wax on the wire was then melted by placing a hot copper wire coil around the glass so that the wax filled the glass tip. When the coil was removed, the wax firmly clamped the silver wire tip inside the glass tip. During this process, the melting wax sometimes seeped out of the glass tip and covered the wire tip exposed outside the glass tip. When this happened, the coated wax was removed by applying a wax solvent, chloroform, to the wax-coated wire so that the wire tip was exposed again.

Sometimes the exposed silver wire tip was long so that it needed to be shortened. In this case, the tip was shortened by electrolysis. A potential of about 1.5 volts was applied with the wire positive while the exposed silver wire tip was immersed bit by bit into 0.5 M NaCN solution. After the exposed silver wire tip had become nearly level with the glass tip, the electrolysis process was stopped. The following electrolysis was carried out to coat the exposed silver wire tip with AgCl. A potential of about 1.5 volts was applied with the wire positive while the exposed silver wire tip was immersed in 0.1 M HCl solution for about 30 seconds. Longer immersions gave coatings that were too bulky. Finally, the back of the microelectrode was sealed with wax to clamp the silver wire in the glass pipette firmly. The microelectrode was then mounted in an electrode holder, connected to the measurement system, and ready to be calibrated.
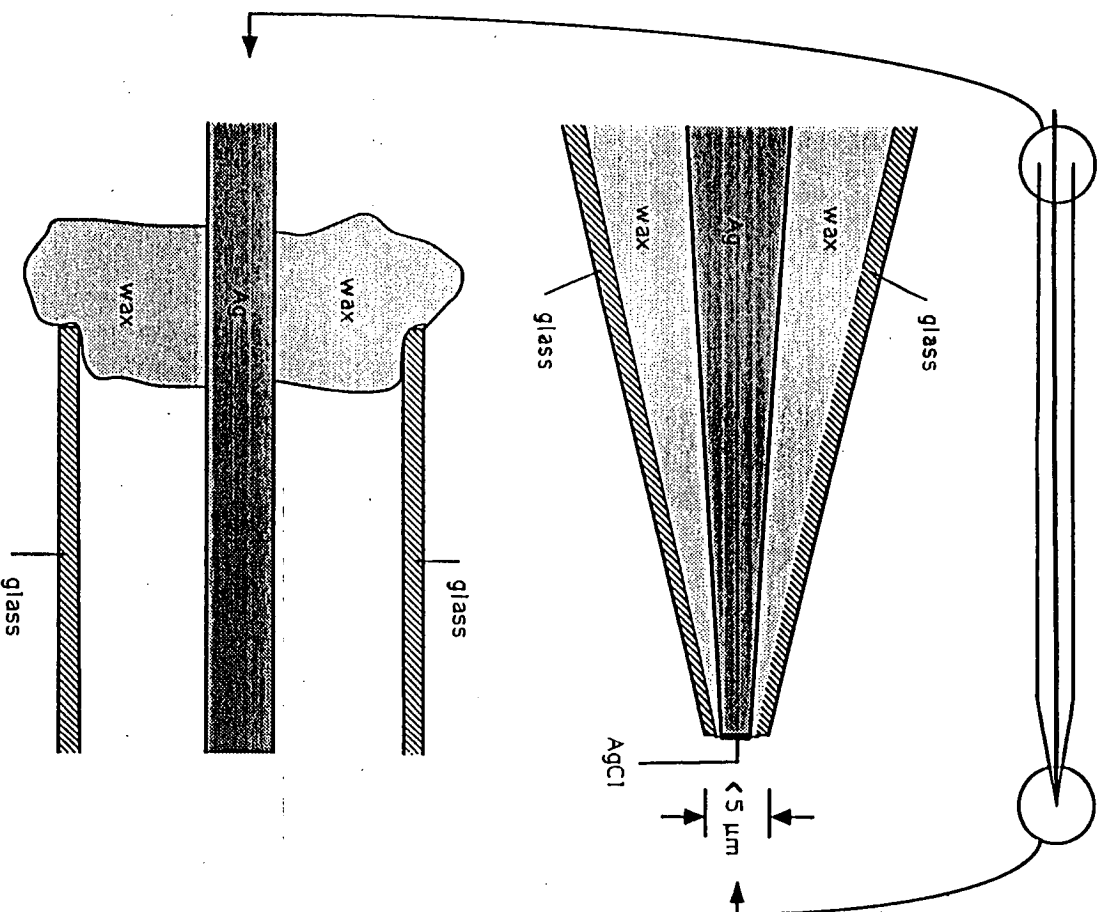
Figure 7.1

Description of the solid-state chloride microelectrode.

Figure 7.2

Chloride net flux (efflux negative) adjacent to the cut tissue surface of 4.5 hour preincubated segments of 4-day-old split oat coleoptiles in response to 10^2 mole m^3 IAA. Downward arrow indicates the solution replacement with the same solution (BET) to study the effect of solution change. Upward arrow indicates the solution replacement with BEI to apply IAA. Each mean of ten plants is calculated relative to the value obtained just before the solution replacement with BET or BEI. Bars show representative SE.

Figure 7.3

Chloride net flux (efflux negative) adjacent to the cut tissue surface of 3.5 hour preincubated oat coleoptile segments to 10^{-3} mole m^{-3} IAA. Other details are as in Figure 7.2.
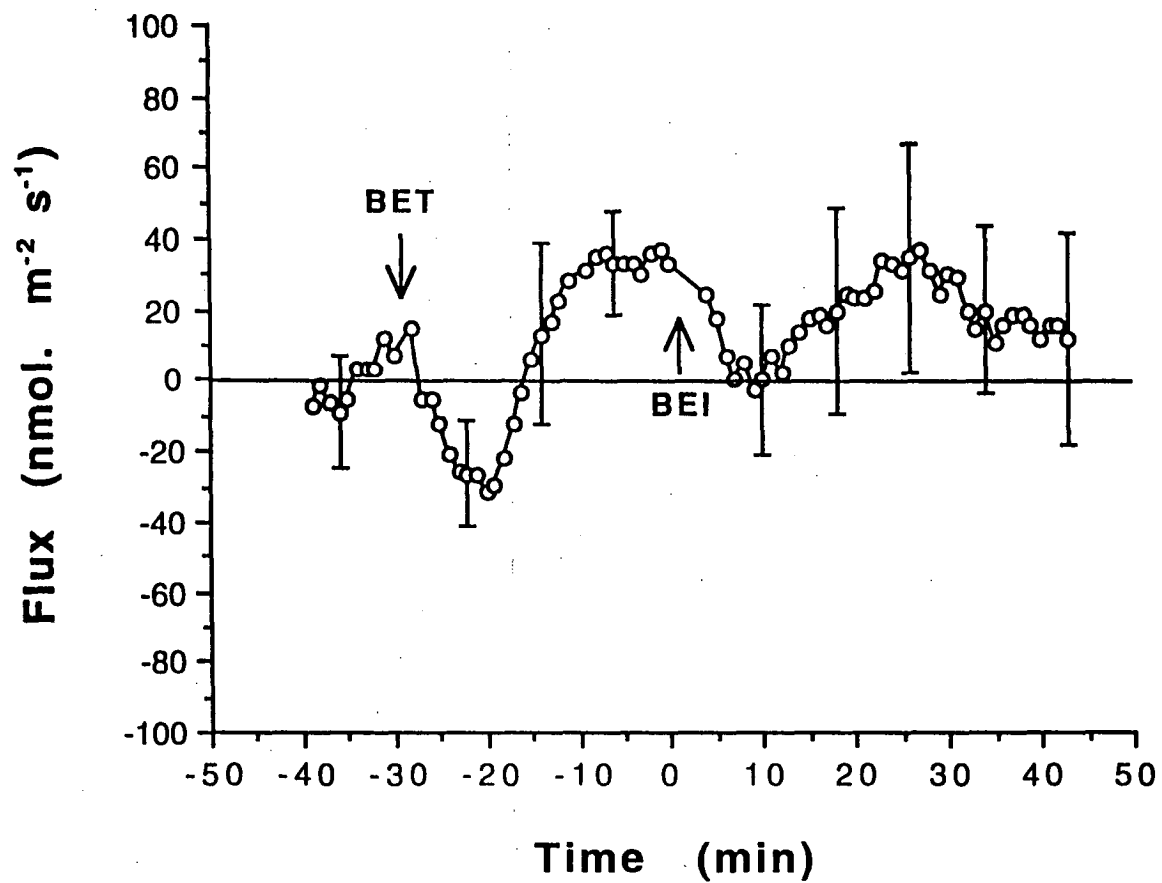
Figure 7.4

Chloride net flux (efflux negative) adjacent to the cut tissue surface of 2.25 hour preincubated oat coleoptile segments to 10^{-2} mole m^{-3} IAA. Other details are as in Figure 7.2.
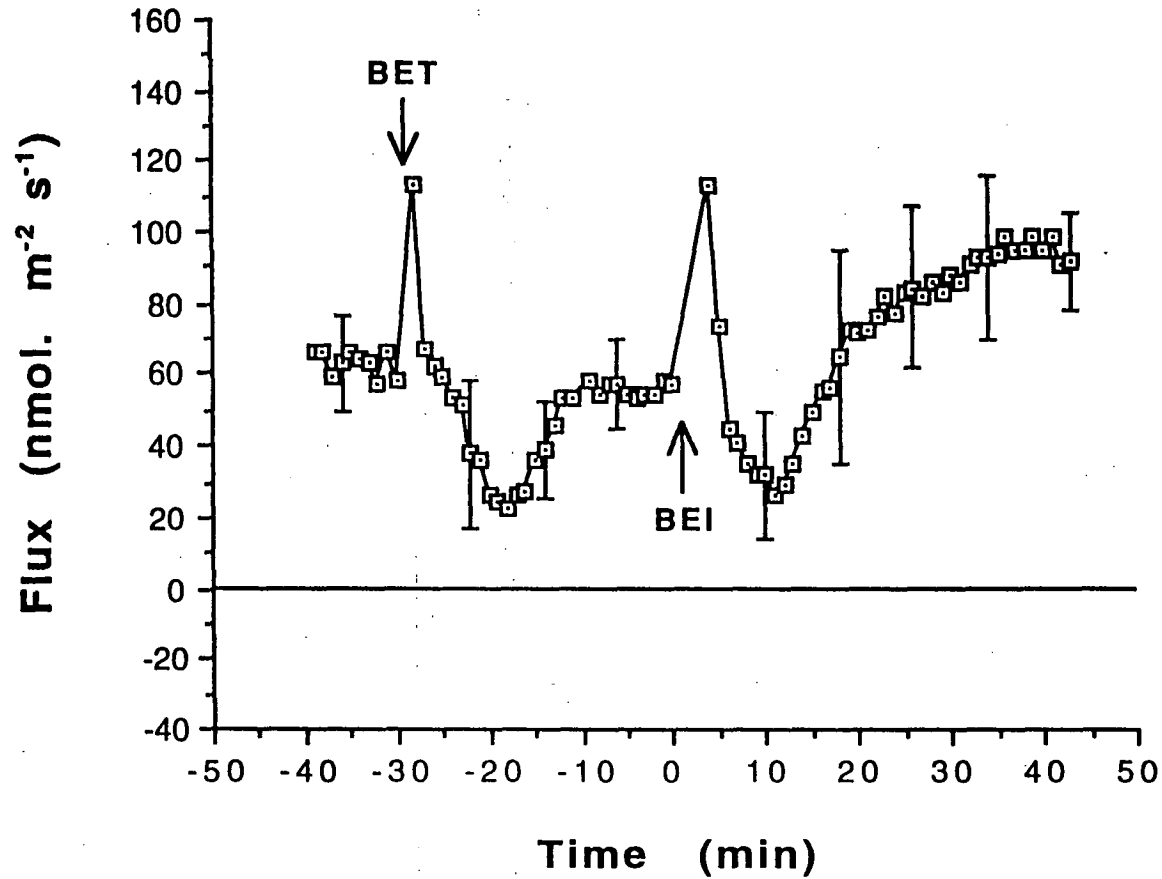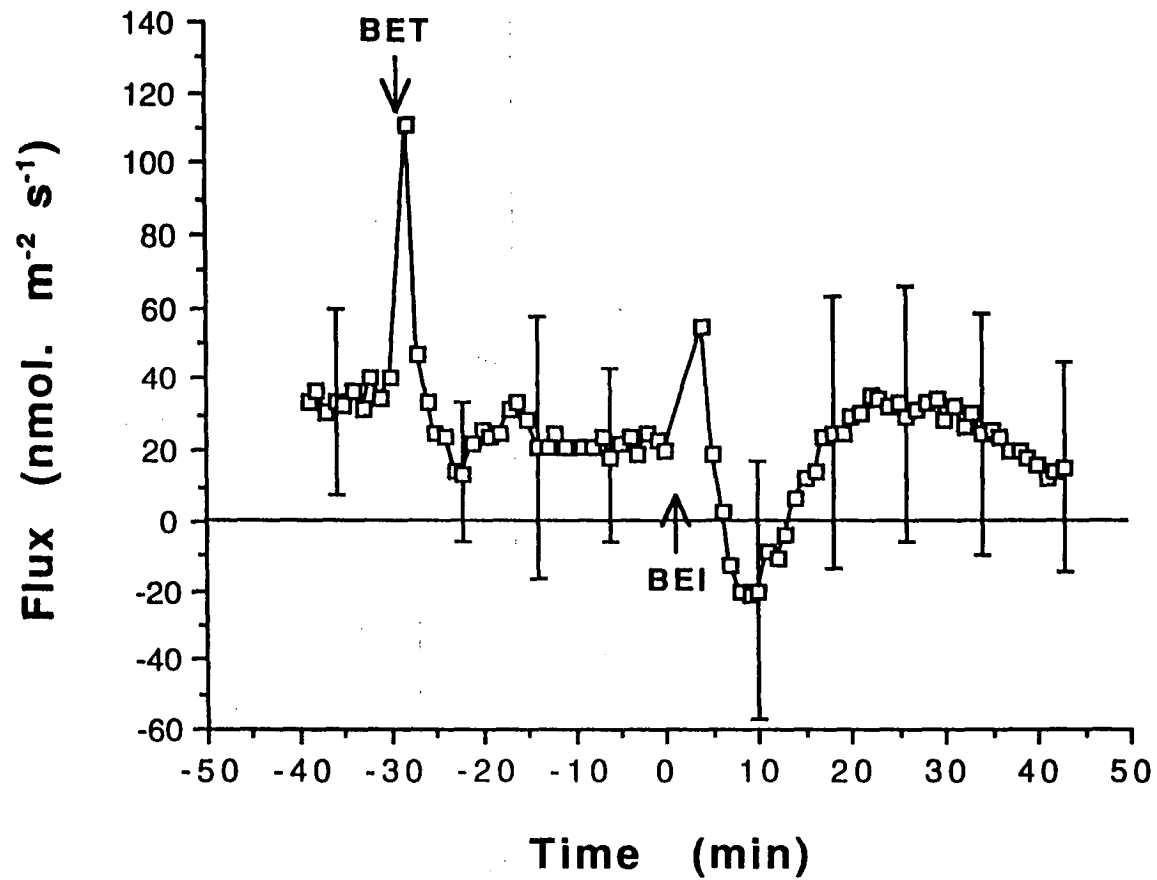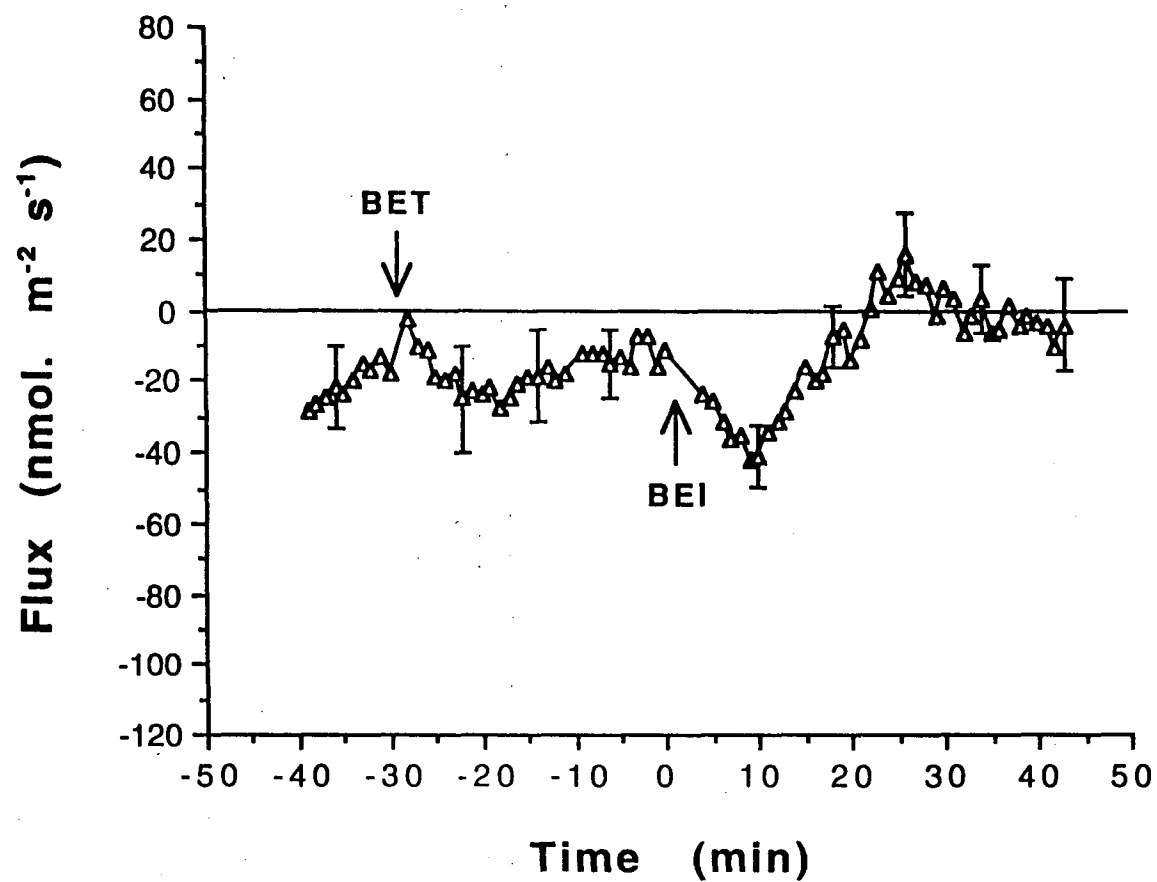
Figure 7.5

Chloride net flux (efflux negative) adjacent to the cut tissue surface of 1 hour preincubated oat coleoptile segments to 10^{-2} mole m^{-3} IAA. Other details are as in Figure 7.2.
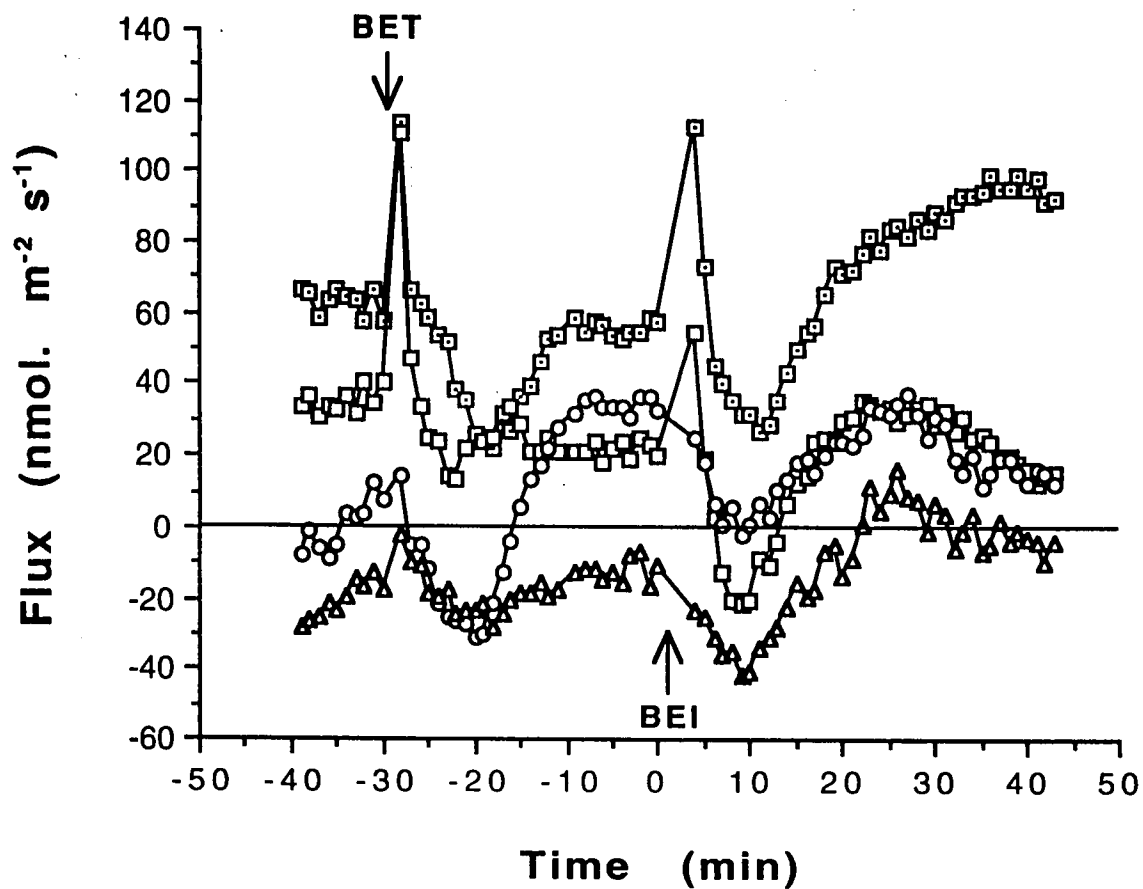
Figure 7.6

Chloride net flux (efflux negative) in response to 10^{-2} mole m^{-3} IAA observed in the solution adjacent to the cut tissue surface of 4.5 (▣), 3.5 (▢), 2.25 (O) or 1 (Δ) hour preincubated segments of 4-day-old split oat coleoptiles. Downward arrow indicates the solution replacement with the same solution (BET) to study the effect of solution change. Upward arrow indicates the solution replacement with BEI to apply IAA. (see also Figures 7.2, 7.3, 7.4, 7.5).

The developed chloride microelectrode is described in figure 7.1. The tip was less than 5 μm. Calibration results showed that the slope was 51-59, the response was fast (less than 1 second), and the resistance was about 0.5 GΩ. The response had a small drift of about 2 mV up and down in 3 hours.

As in flux measurements of other ions, after a coleoptile segment was split between vascular bundles, the split segment was held on a plastic holder and preincubated in BSM for 4.5, 3.5, 2.25, or 1 hours. The preincubated segment together with the holder was then mounted in the measurement chamber and bathed with BET. The tip of the chloride microelectrode was then placed close to the cut surface and the flux measurements were carried out. After 10 minutes, the solution was refreshed to observe the effect of solution change. About 30 minutes after the solution refreshment, BET was replaced with BEI to observe the effect of IAA for about 45 minutes.

7.3 Results

The results of the chloride flux measurements following 4.5, 3.5, 2.25 and 1 hour preincubation are presented in Figures 7.2, 7.3, 7.4 and 7.5. For comparison, these figures are combined in Figure 7.6.

In BET, the chloride flux started with an influx of about 60 nmol m^{-2} s^{-1} following 4.5 hour preincubation (Figure 7.2). The influx increased transiently when the solution was refreshed. After about 10 minutes, the influx had then decreased to a minimum of about 25 nmol m^{-2} s^{-1}. The influx recovered to its initial level at about 20 minutes after the solution change. When BET was replaced with BEI, the same sequence of transients was observed. There is a suggestion of rise in chloride influx after 20 minutes that could be due to IAA itself.

Following 3.5 hour preincubation, the chloride flux in BET started with a smaller influx of about 30 nmol m^{-2} s^{-1} (Figures 7.3 and 7.6). The refreshment of the solution also caused similar transients as were observed for 4.5 hour preincubation. However, for 3.5 preincubation, the chloride efflux, that happened after the transient chloride influx, was smaller. When BET was replaced with BEI, the observed responses were similar as for 4.5 hour preincubation. But there is no evidence for any IAA effect. With segments preincubated in BSM for 2.25 hours, the chloride influx in BET was about zero

(Figure 7.4). The influx drifted up with time. Similar transients were also observed after the BET solution change and the BEI solution change. In the experiments following 1 hour preincubation, similar but smaller transients were observed (Figure 7.5). The chloride flux in BET was an efflux of about 20 nmol m^{-2} s^{-1} in BET. Again, for both 2.25 and 1 hour preincubation, there is also no evidence for any effect of IAA.

7.4 Discussion

In Figure 7.6, it is clearly shown that the chloride influx in BET was bigger when the preincubation time was longer. It has been reported that in corn roots, cutting causes a rapid reduction in chloride influx (Gronewald and Hanson 1980). This explains why in the present study the chloride influx depended on the preincubation time. During the preparation of the coleoptile split segments, the cutting and splitting processes presumably caused the normal chloride influx to decrease. The influx then recovered during the preincubation time.

Following the four preincubation times, the responses of the chloride influx to the solution change were similar, a transient chloride influx followed by a 15 minute chloride efflux. As discussed in Chapter 6, the responses were due to the removal of the chloride concentration gradient region and the stimuli given to the cells during the solution change. The effect of the removal of the concentration gradient region should have diminished fast. However, the graphs show that the responses of the chloride flux due to solution change took place over about 20 minutes. This indicates that the effect of the stimuli given to the cells during solution change lasted about this length of time, and the effect was loss of chloride.

The responses in the first 20 minutes after the replacement of BET with BEI were due to the solution change because the responses were similar to the responses to the solution refreshment. There is no clear evidence for any effect of IAA on chloride fluxes (Figure 7.6). IAA induces chloride influx after 20 minutes as suggested by the results of the experiments with 4.5 hour preincubation. However, the evidence is very weak. For 3.5, 2.25 and 1 hour preincubation, there is even no indication of the IAA-induce chloride influx. If the influx is present, it must be very small.

On page 156 after the last paragraph, "The absence of IAA effect on chloride fluxes suggests that chloride is not the ion for charge balancing during the IAA-induced proton extrusion. Now, what is the counterion during the proton extrusion? It is good when the counterion can be identified. Therefore it is suggested for further studies." should be inserted as a new paragraph.

Based on the evidence obtained during fusicoccin action on Characean cells (Smith and Walker 1976, Marrè 1979, Smith 1980, Sanders 1980, Smith and MacRobbie 1981, Reid and Walker 1984, Smith and Whittington 1988), it was expected that cotransport of chloride with protons as the result of increasing proton electrochemical potential gradient also happens during IAA action. In this case, the chloride influx should happen after the IAA-induced proton efflux and membrane hyperpolarization. If the chloride influx after 20 minutes as suggested in the results of the experiments with 4.5 hour preincubation was really the IAA effect, this happened after the IAA-induced proton efflux and membrane hyperpolarization. Therefore this would support the theory of cotransport of chloride with protons during IAA action.

The WADM model for fluxes requires the information about the magnitude of the total proton flux in the plasmalemma, not the magnitude of each component of proton flux at the plasmalemma. If there are several components of proton fluxes at the plasmalemma during treatments such as the above proton influx cotransport with chloride influx during IAA action, only the sum of the proton fluxes is accounted for in the analysis. Therefore the result of the analysis is inaffected whether the cotransport of chloride with protons is present or not.

Chapter 8

FUSICOCCIN AND IAA EFFECTS

ON PEAS

8.1 Introduction

In the process of growth of plant cells, the cell walls play an important role. During the process, the condition of the walls is modified so that the walls have the ability to extend irreversibly. Details of cell wall make up affect growth responses.

The walls of dicot and monocot cells are different. For example, the walls of dicot cells have more xyloglucans and uronic acids than the walls of monocot cells (Hoson et al. 1991, Virk and Cleland 1990). Therefore it was expected that the growth responses of dicots and monocots are different.

In dicots, study of fusicoccin and IAA effects on medium acidification, cell enlargement and membrane hyperpolarization is lacking. Fusicoccin induces both medium acidification and cell enlargement (Marrè et al. 1974, Talbott et al. 1988, see also Marrè 1979). IAA induces cell enlargement (Jacobs and Ray 1976, Terry and Jones 1981, Reddy et al. 1988, Rayle et al. 1991). Some workers have reported that IAA also induces medium acidification (Durand and Rayle 1973, Jacobs and Ray 1976, Talbott et al. 1988). However others have reported that the IAA-induced medium acidification is not enough to cause growth (Terry and Jones 1981, see also Cleland 1980).

In Chapters 5 and 6, it is shown that both fusicoccin and IAA induce proton efflux in oat coleoptile segments. The induced proton efflux is accompanied by the efflux of calcium from the tissue. This supports the present

hypothesis expressed in the WADM model for fluxes: during proton extrusion from the cell to the cell wall, proton-calcium exchange takes place in the condensed phase of the walls. In the present work, the net fluxes of protons and calcium during fusicoccin and IAA action on pea epicotyl segments are also measured simultaneously using the MIFE technique to study the possibility of the proton-calcium exchange during the action on dicots. It is shown that the exchange clearly takes place during fusicoccin action. The indication of the exchange during IAA action is less clear.

As in experiments for oats, net potassium flux was also measured simultaneously with the fluxes of protons and calcium. The membrane potential of parenchymal cells during fusicoccin and IAA action on peas was also measured.

A 12-mm-long peeled segment of the third node of a 6- to 7-day-old pea epicotyl was held on a plastic sponge using cotton thread and pretreated for 4.5 hours in aerated BSM. The growth conditions and the segment preparation are described in Chapter 2. It is assumed that preincubation in the aerated BSM for 4.5 hours is adequate to eliminate most of the effects of peeling. Other workers preincubated the segments for about 1 hour (Terry and Jones 1981, Reddy et al. 1988).

Proton, calcium and potassium fluxes close to the cut tissue surface in diffusion limited solution were determined simultaneously using the MIFE technique described in Chapter 2 and Appendix A. As a control, the fluxes were measured in BSM for about 40 minutes. Fusicoccin or IAA was then applied by adding a small amount of very concentrated fusicoccin (0.2 mole m^{-3}) or IAA (2 mole m^{-3}) solution to the measurement chamber to give the desired final concentration. In this case, before the solution was added to the solution in the chamber, the fusicoccin or IAA stock solution was mixed first to remove any precipitation. Since IAA is an acid, the IAA addition to the solution in the chamber will slightly decrease the pH of the solution. In this present work, the effects of 10^{-2} and 10^{-3} mole m^{-3} fusicoccin and 10^{-2} mole m^{-3} IAA were studied. For the same reason as mentioned in Chapter 5, the flux measurements in the presence of fusicoccin or IAA were carried out every minute for only 40 minutes. For membrane potential measurements of parenchymal cells in the segments, the treatment was similar to the treatment in the flux measurements.

Figure 8.1

Effects of 10^{-2} mole m^{-3} fusicoccin (FC) on proton (a), calcium (b) and potassium (c) net fluxes (efflux negative) and pH (d) adjacent to the cut tissue surface of 6- to 7-day-old peeled pea epicotyl segments preincubated in BSM for 4.5 hours. Upward arrow indicates application of fusicoccin. Each mean of eleven plants is calculated relative to the value obtained just before the application of fusicoccin. Bars show representative SE.

Figure 8.2

Effects of 10^{-3} mole m^{-3} fusicoccin (FC) on proton (a), calcium (b) and potassium (c) net fluxes (efflux negative) and pH (d) adjacent to the cut tissue surface of 6- to 7-day-old peeled pea epicotyl segments preincubated in BSM for 4.5 hours. Upward arrow indicates application of fusicoccin. Each mean of ten plants is calculated relative to the value obtained just before the application of fusicoccin. Bars show representative SE.
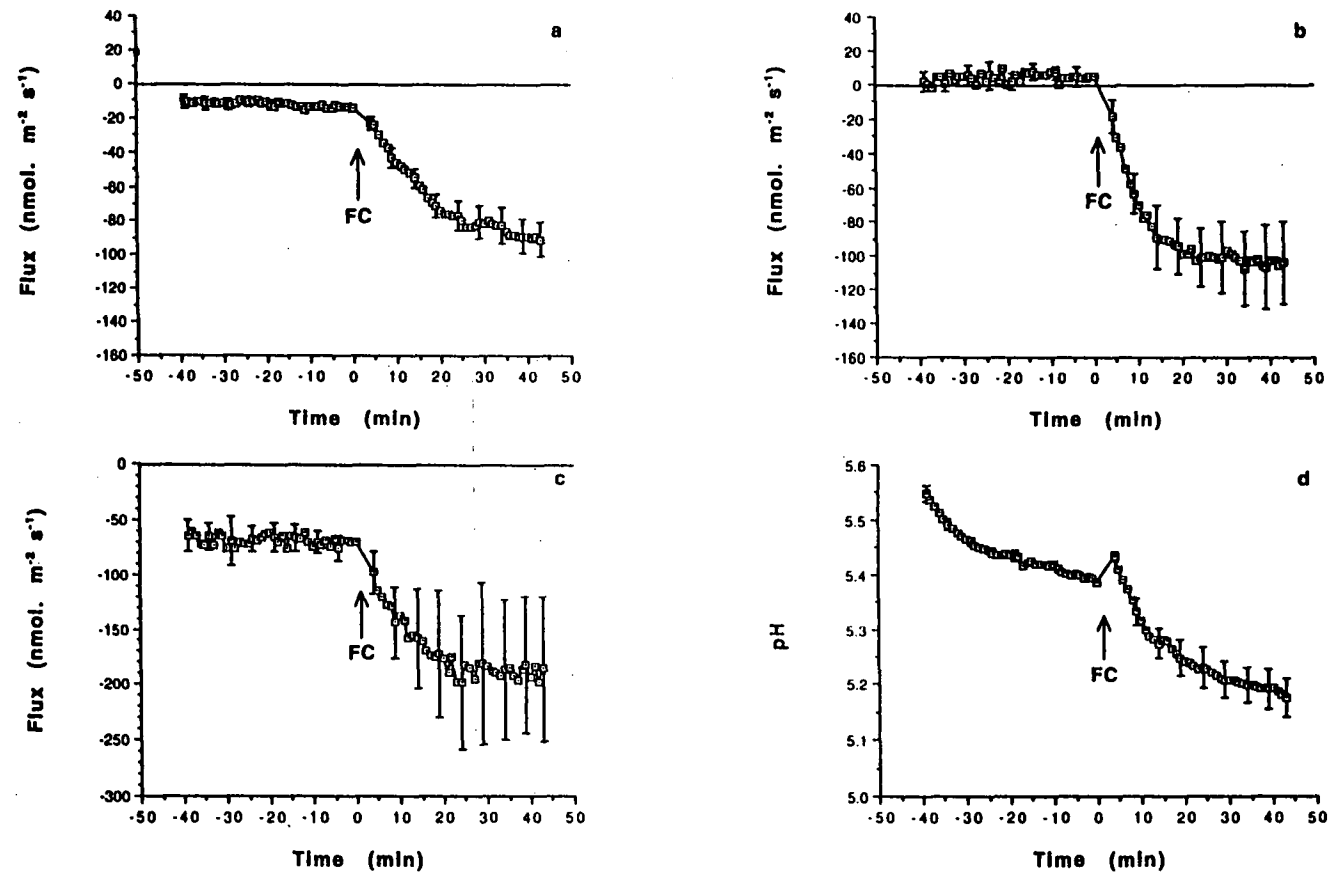
Figure 8.3

Effects of 10^{-2} mole m^{-3} IAA (FC) on proton (a), calcium (b) and potassium (c) net fluxes (efflux negative) and pH (d) adjacent to the cut tissue surface of 6- to 7-day-old peeled pea epicotyl segments preincubated in BSM for 4.5 hours. Upward arrow indicates application of IAA. Each mean of eleven plants is calculated relative to the value obtained just before the application of IAA. Bars show representative SE.
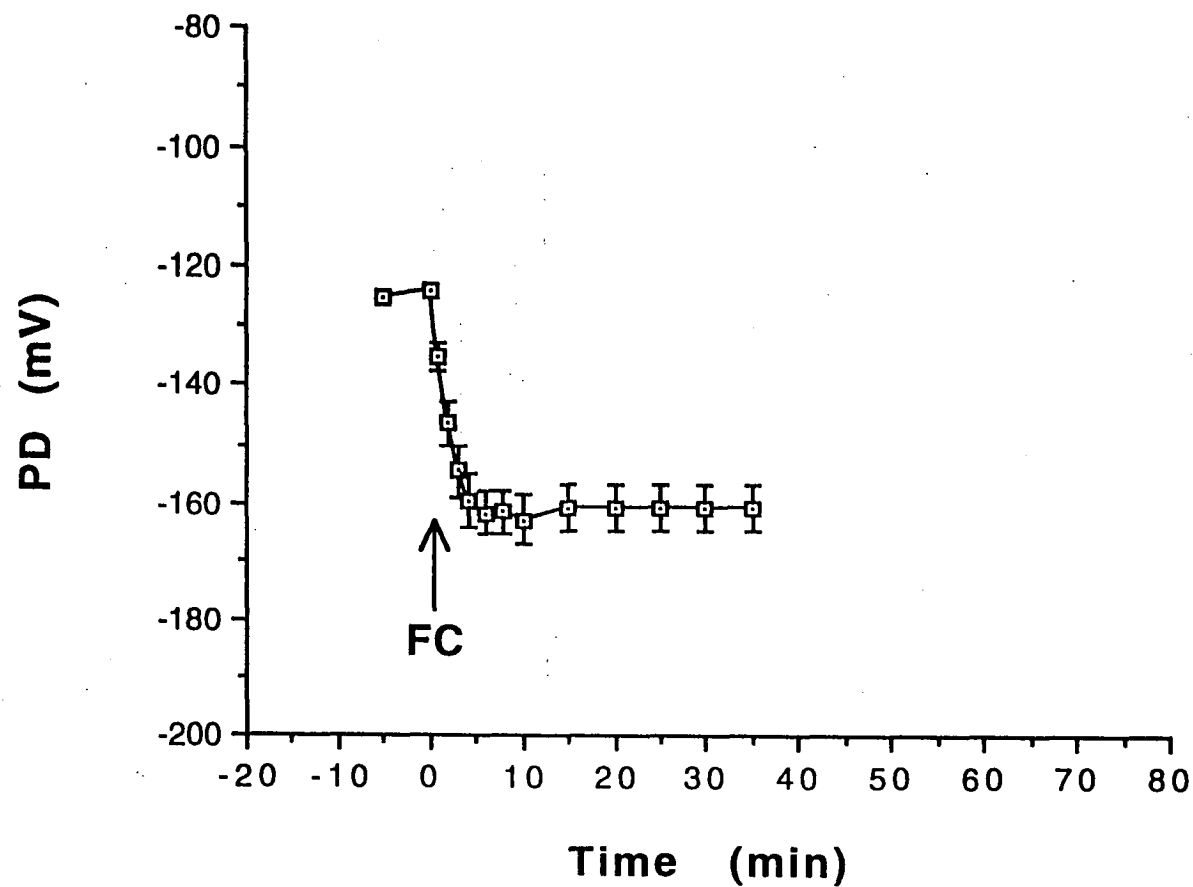
Figure 8.4

Effects of 10^{-2} mole m^{-3} fusicoccin (FC) on membrane potential (PD) of parenchymal cells in 6- to 7-day-old peeled pea epicotyl segments preincubated in BSM for 4.5 hours. Upward arrow indicates application of fusicoccin. Each mean of six plants is calculated relative to the value obtained just before the application of fusicoccin. Bars show SE.

Figure 8.5

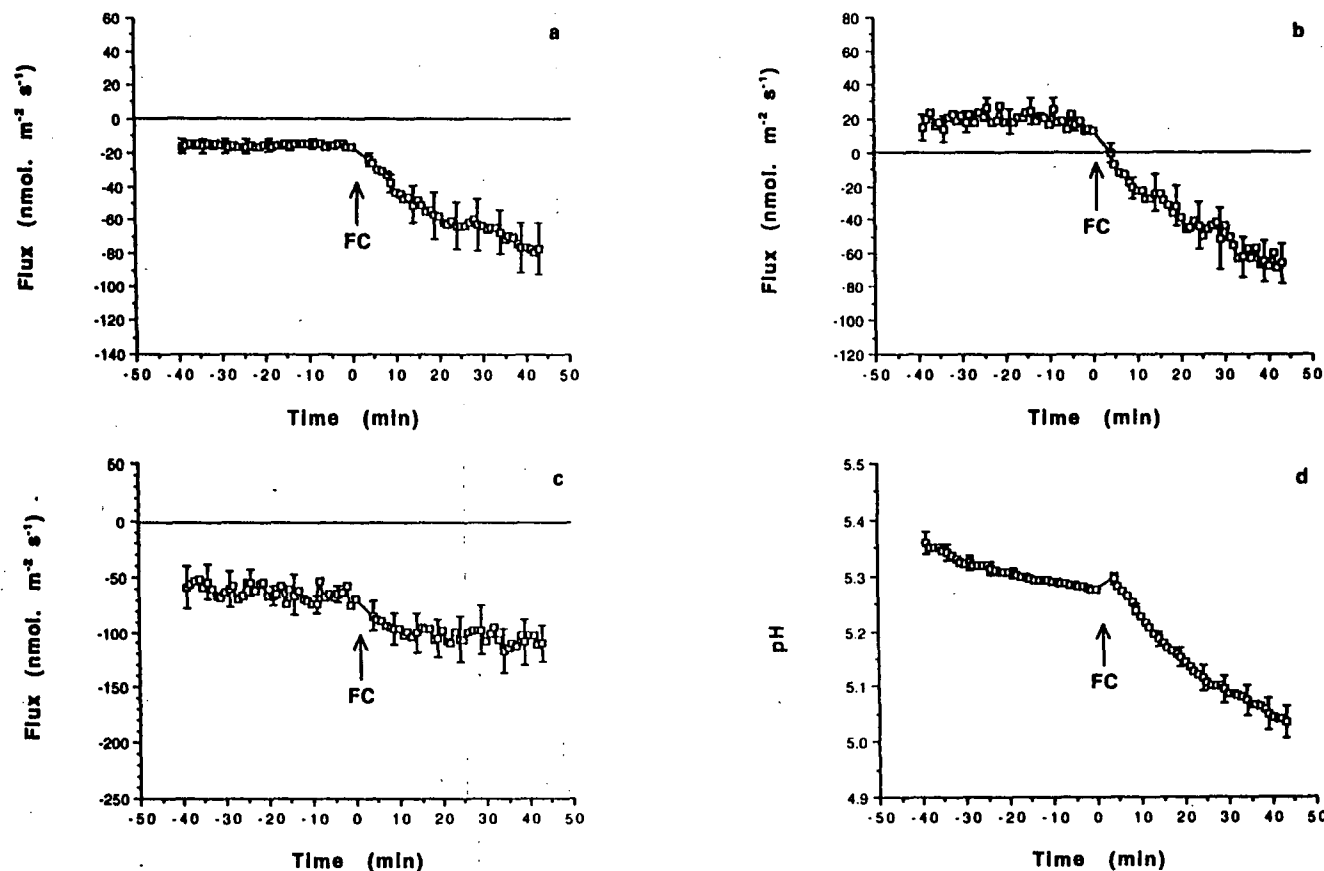Effects of 10^{-3} mole m^{-3} fusicoccin (FC) on membrane potential (PD) of parenchymal cells in 6- to 7-day-old peeled pea epicotyl segments preincubated in BSM for 4.5 hours. Upward arrow indicates application of fusicoccin. Each mean of seven plants is calculated relative to the value obtained just before the application of fusicoccin. Bars show SE.
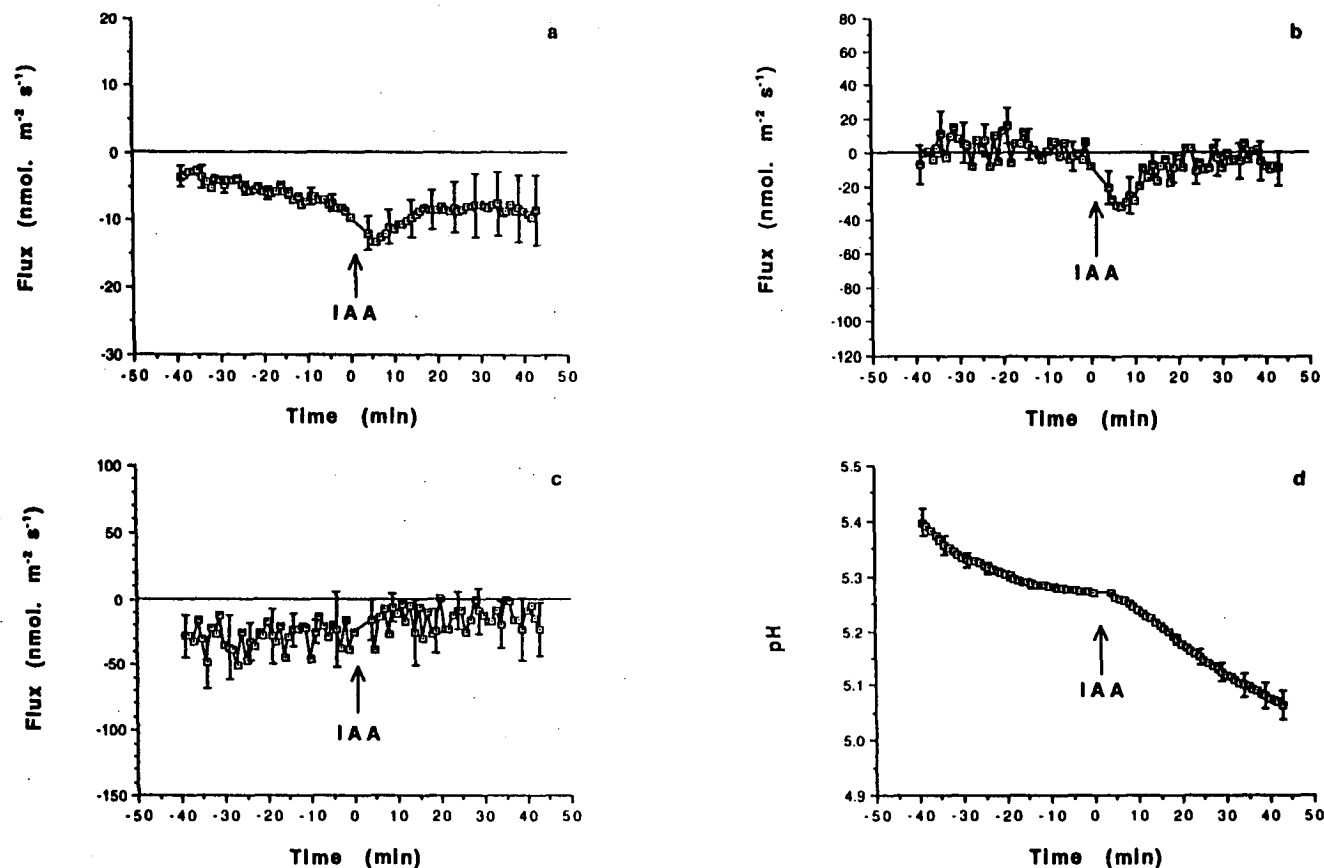
Figure 8.6

Effects of 10^{-2} mole m^{-3} IAA (FC) on membrane potential (PD) of parenchymal cells in 6- to 7-day-old peeled pea epicotyl segments preincubated in BSM for 4.5 hours. Upward arrow indicates application of IAA. Each mean of seven plants is calculated relative to the value obtained just before the application of IAA. Bars show SE.
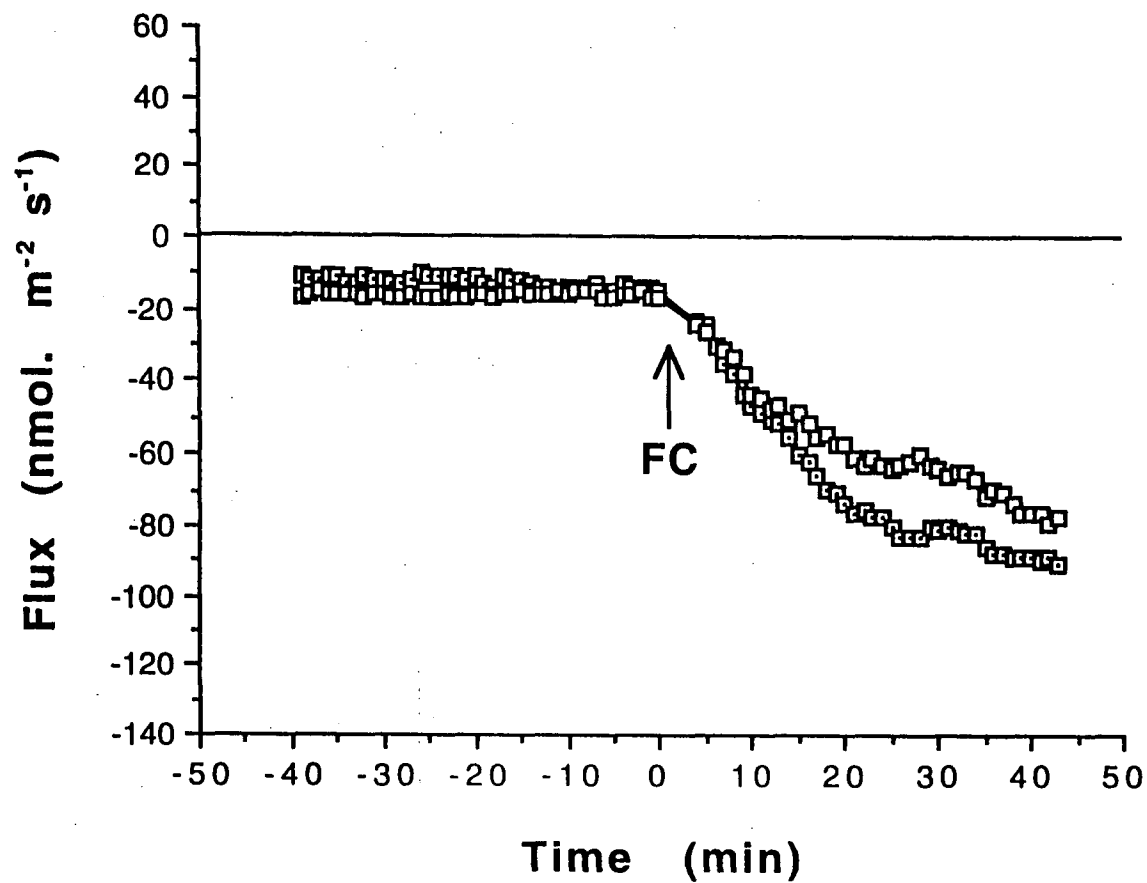
Figure 8.7

Effects of 10^{-2} (▣) and 10^{-3} (▢) mole m^{-3} fusicoccin (FC) on proton net flux (efflux negative) adjacent to the cut tissue surface of 6- to 7-day-old peeled pea epicotyl segments preincubated in BSM for 4.5 hours. Upward arrow indicates application of fusicoccin.
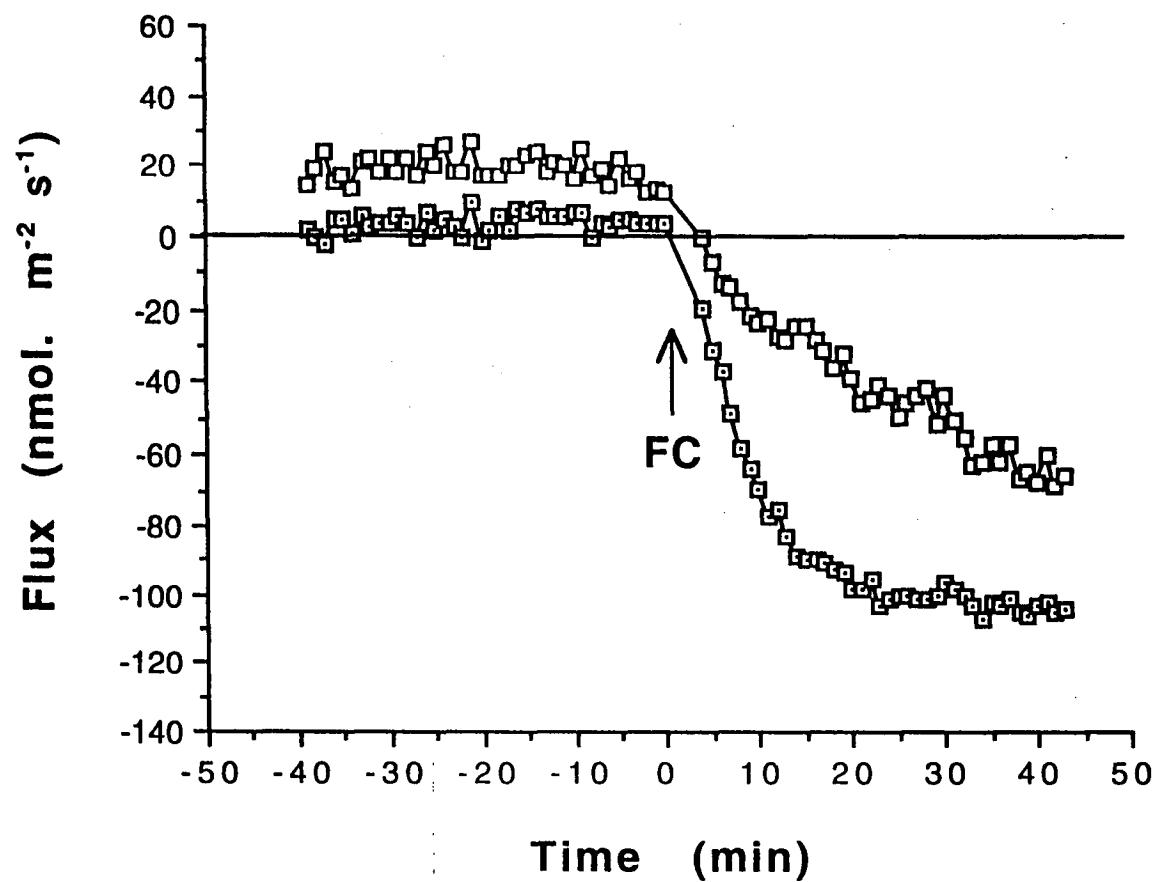
Figure 8.8

Effects of 10^2 (◨) and 10^3 (◻) mole m^3 fusicoccin (FC) on calcium net flux (efflux negative) adjacent to the cut tissue surface of 6- to 7-day-old peeled pea epicotyl segments preincubated in BSM for 4.5 hours. Upward arrow indicates application of fusicoccin.
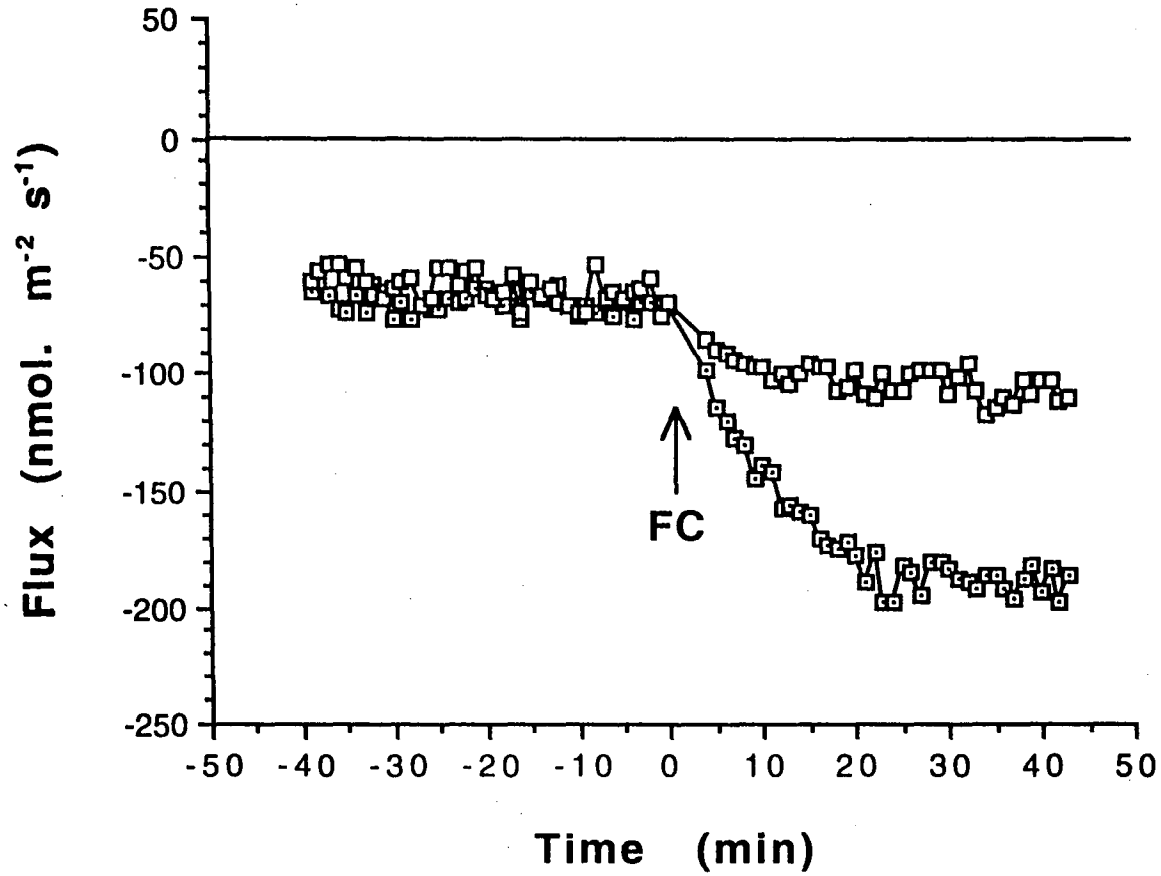
Figure 8.9

Effects of 10^2 (▣) and 10^3 (▢) mole m^{-3} fusicoccin (FC) on potassium net flux (efflux negative) adjacent to the cut tissue surface of 6- to 7-day-old peeled pea epicotyl segments preincubated in BSM for 4.5 hours. Upward arrow indicates application of fusicoccin.
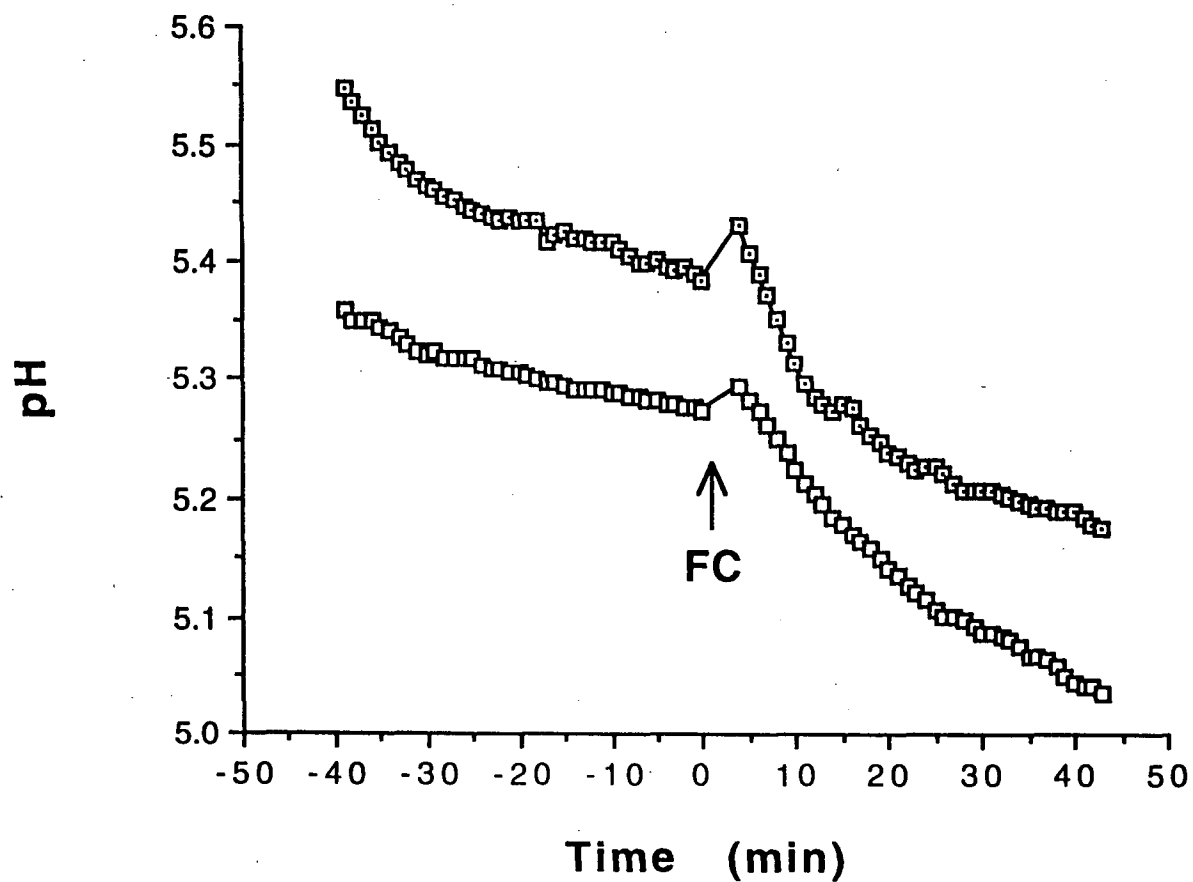
Figure 8.10

Effects of 10^{-2} (◙) and 10^{-3} (□) mole m^{-3} fusicoccin (FC) on pH adjacent to the cut tissue surface of 6- to 7-day-old peeled pea epicotyl segments preincubated in BSM for 4.5 hours. Upward arrow indicates application of fusicoccin.
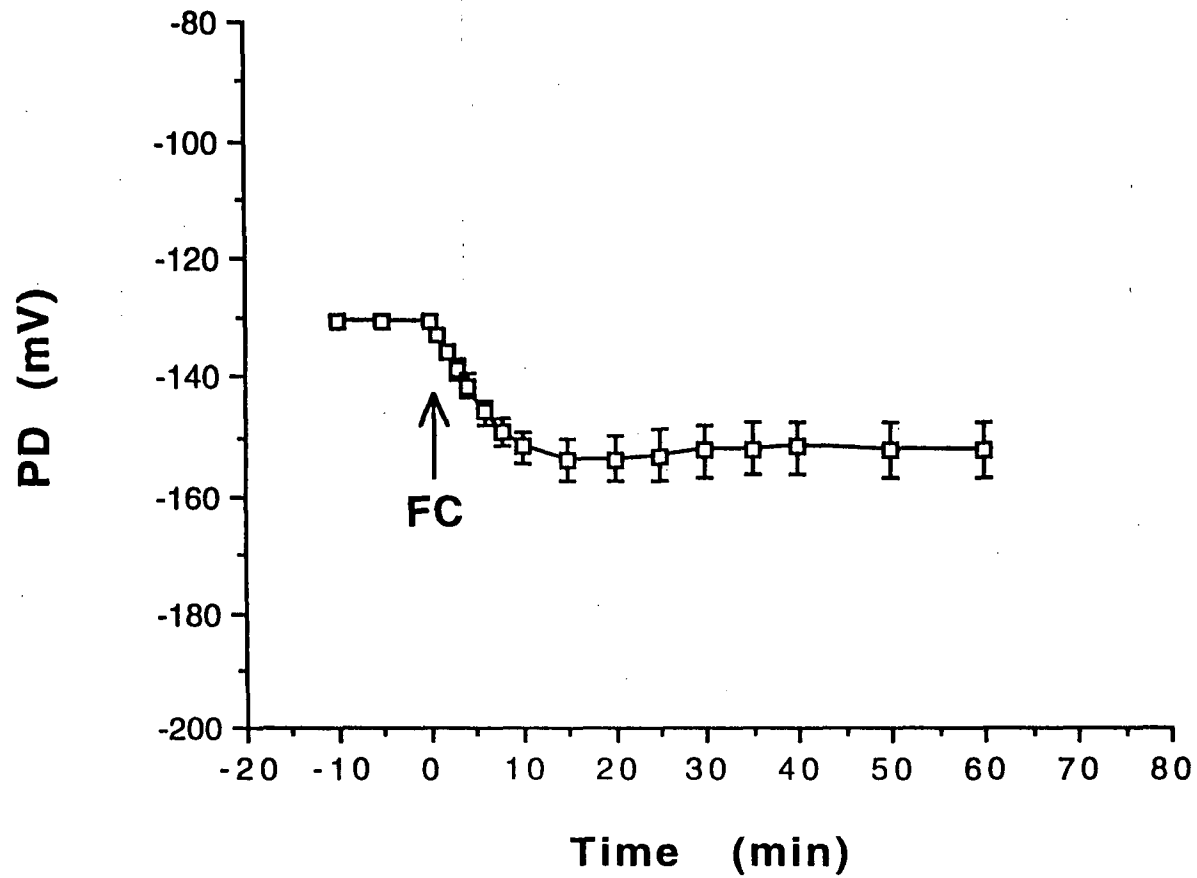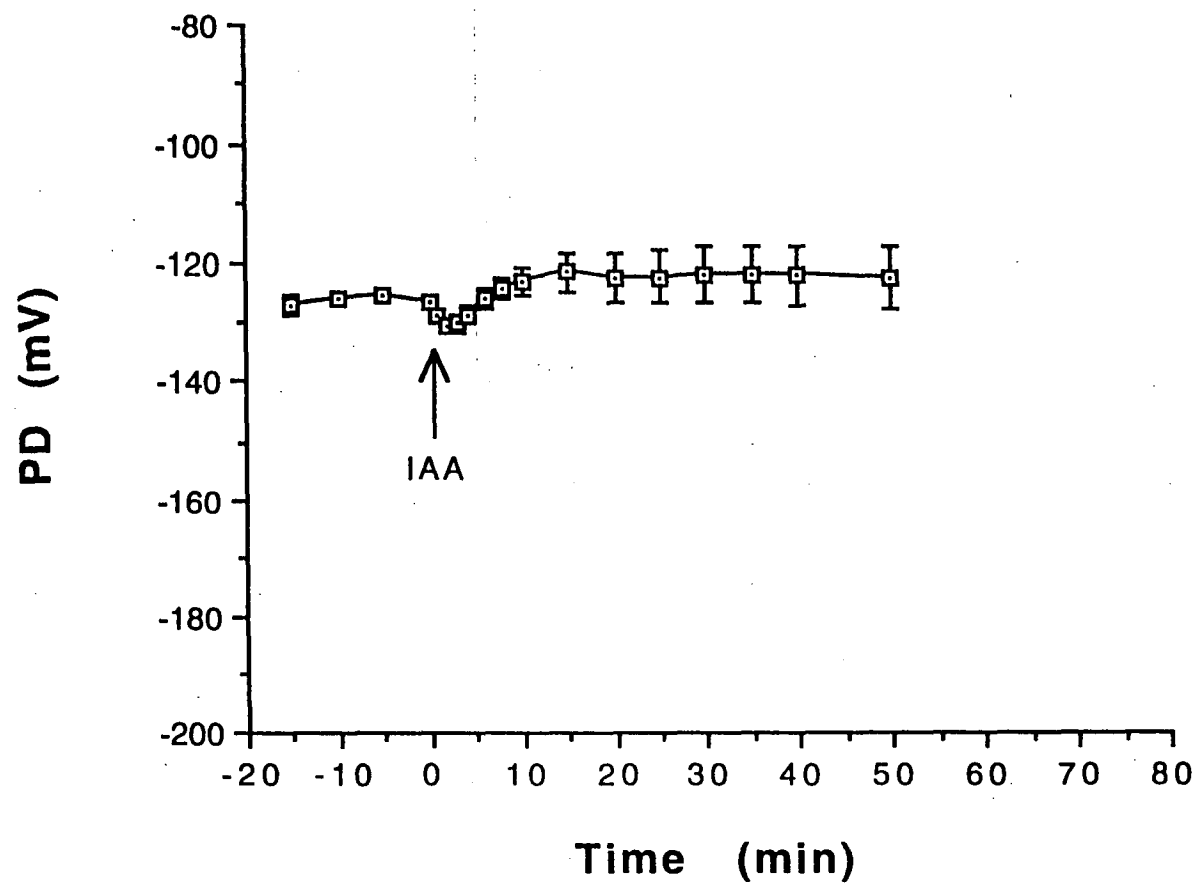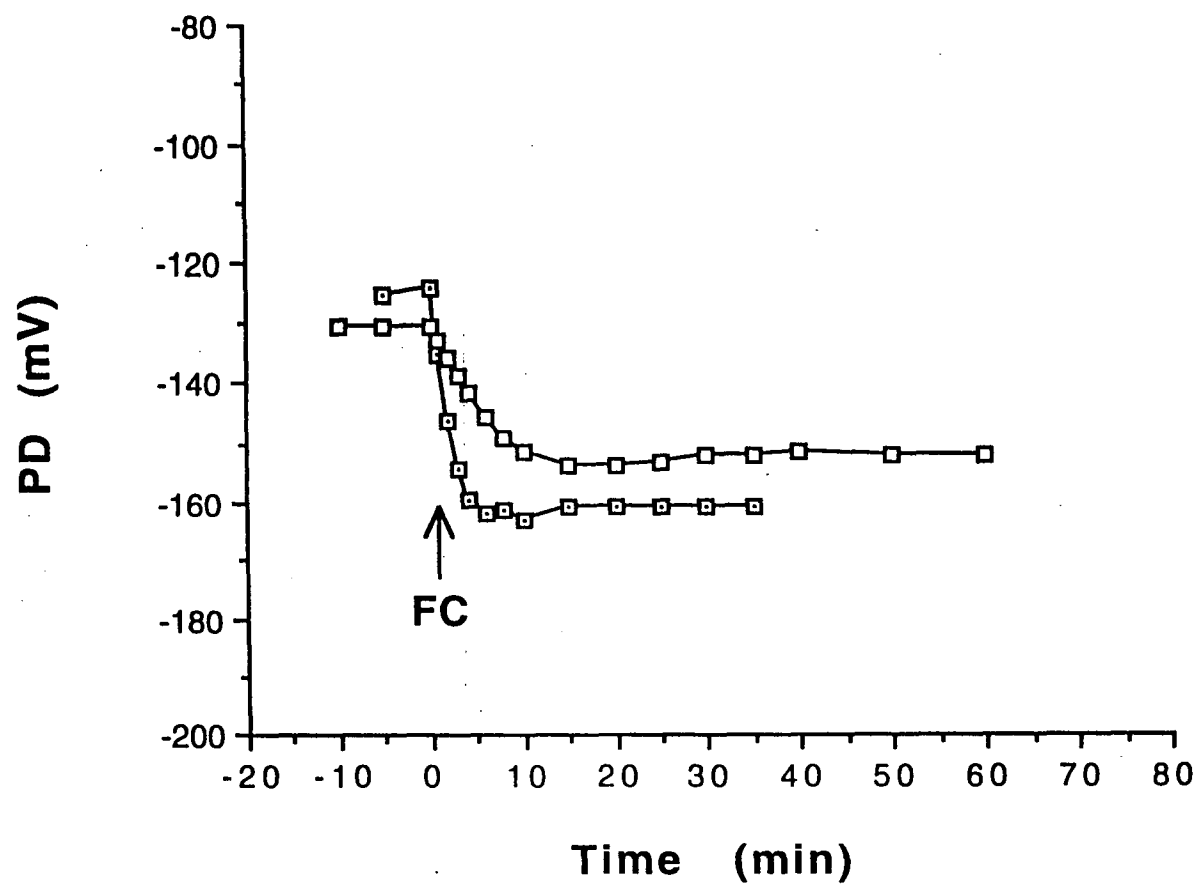
Figure 8.11

Effects of 10^{-2} (⊡) and 10^{-3} (▢) mole m^{-3} fusicoccin (FC) on membrane potential (PD) of parenchymal cells in 6- to 7-day-old peeled pea epicotyl segments preincubated in BSM for 4.5 hours. Upward arrow indicates application of fusicoccin.

Figure 8.12

Proton (a) and calcium (b) net fluxes (efflux negative) during 10^{-2} mole m^{-3} fusicoccin (FC) action on 6- to 7-day-old peeled pea epicotyl segments preincubated in BSM for 4.5 hours. Solid symbols (■) represent the outputs of the "weak acid Donnan Manning" (WADM) model for fluxes. Wall quantities used in the model: $[A_{sites}] = 800$ mole m^{-3}, pK = 3.0, $\xi^* = 0.71$, h = 1.0 μm and $\lambda = 0.5$. The diffusion coefficients of cations in the DFS is 1/5 of those in the WFS. The external medium is BSM. It was assumed that there are 10 cells in the thickness of a tissue.

Figure 8.13

Proton (a) and calcium (b) net fluxes (efflux negative) during 10^{-3} mole m^{-3} fusicoccin (FC) action on 6- to 7-day-old peeled pea 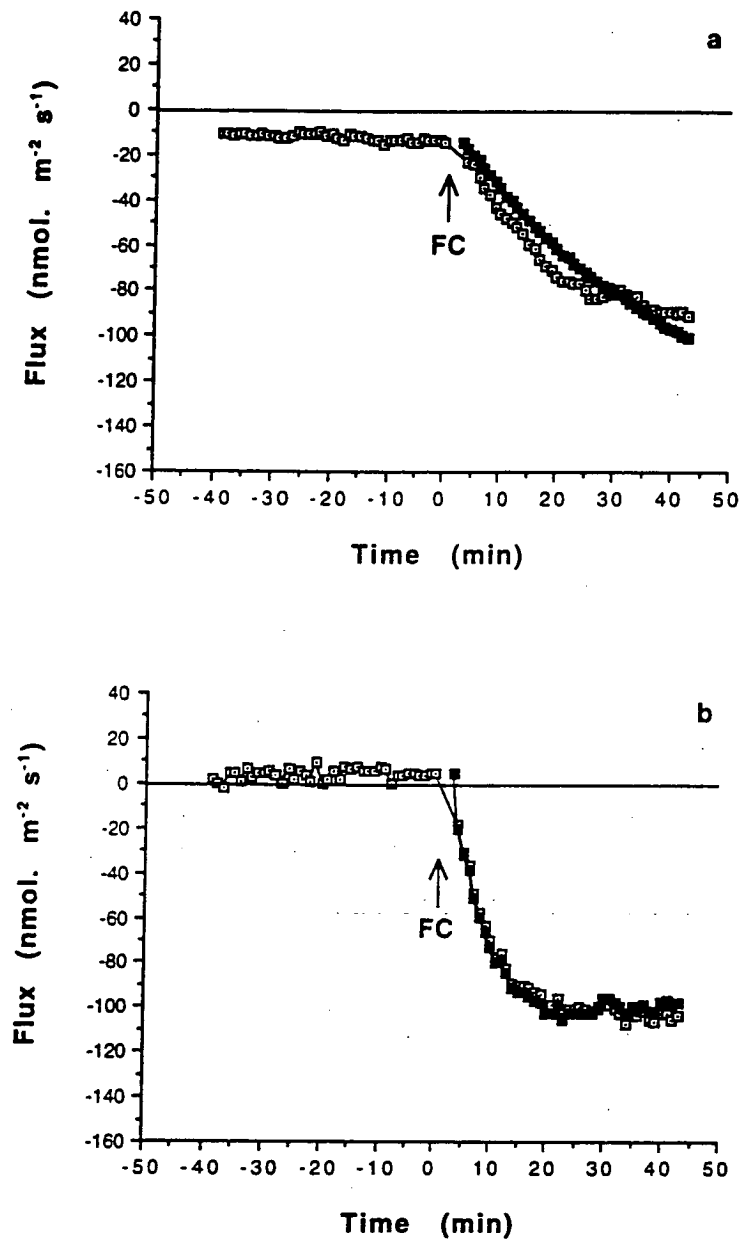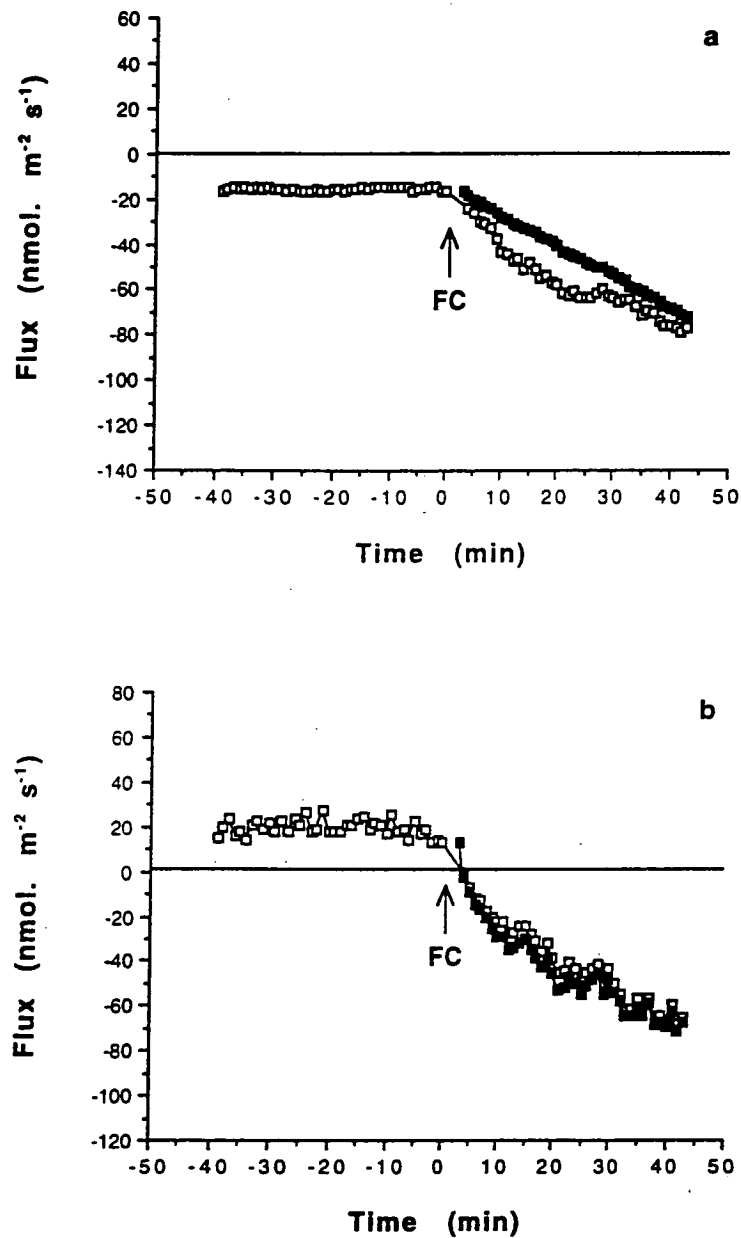epicotyl segments preincubated in BSM for 4.5 hours. Solid symbols (■) represent the outputs of the "weak acid Donnan Manning" (WADM) model for fluxes. Other details are as in Figure 8.12.

8.2 Results

The results of the measurements of proton, calcium and potassium net fluxes and pH adjacent to the cut tissue surface during fusicoccin and IAA action are presented in Figures 8.1, 8.2 and 8.3. For membrane potential, the results of the measurements are presented in Figures 8.4, 8.5 and 8.6. For comparison between Figures 8.1 and 8.2 and between Figures 8.4 and 8.5, the results of proton flux, calcium flux, potassium flux, pH and membrane potential are combined in Figures 8.7, 8.8, 8.9, 8.10 and 8.11.

In BSM, segments of pea epicotyls preincubated for 4.5 hours show a net proton efflux in the range 5-15 nmol. m^{-2} s^{-1} (Figures 8.1a, 8.2a, 8.3a). The application of 10^{-2} mole m^{-3} fusicoccin increases the proton efflux so that within 40 minutes the proton efflux is 80 nmol. m^{-2} s^{-1} larger than the initial value. For 10^{-3} mole m^{-3} fusicoccin, the increase of the proton efflux is slower (see Figure 8.7). In this case the proton efflux is 60 nmol. m^{-2} s^{-1} larger than the initial value after 40 minutes. After the application of 10^{-2} mole m^{-3} IAA, the proton efflux increases transiently about 5 nmol. m^{-2} s^{-1} and the transient lasts about 15 minutes.

In BSM, the pH of the solution close to the tissue surface decreases with time due to proton extrusion. Before the treatments of fusicoccin or IAA, the pH is between 5.28-5.38 (Figures 8.1d, 8.2d, 8.3d). When 10^{-2} mole m^{-3} fusicoccin is applied, the pH increases transiently and then decreases again. After 40 minutes, the pH is about 0.2 below the pH before the application of fusicoccin. The application of 10^{-3} mole m^{-3} fusicoccin also increases transiently the pH. In this case, the pH decrease after the transient is initially slower (see Figure 8.10). After 40 minutes, the pH is 0.25 below the pH before the application. The transient increase of the pH is not observed after the application of 10^{-2} mole m^{-3} IAA. The pH starts to decrease almost immediately so that after 40 minutes the pH is 0.2 below the pH before the application of IAA.

In BSM, the initial net flux of calcium varies between experiments from 20 nmol. m^{-2} s^{-1} influx to zero (Figures 8.1b, 8.2b, 8.3b). After the application of 10^{-2} mole m^{-3} fusicoccin, the calcium influx decreases to become an efflux which levels off at about 25 minutes. At this time, the efflux is about 100 nmol. m^{-2} s^{-1}. After 10^{-3} mole m^{-3} fusicoccin is applied, the fusicoccin-induced calcium efflux decreases slower. The efflux is about 80 nmol. m^{-2} s^{-1} after 40 minutes.

The application of 10^{-2} mole m^{-3} IAA causes a transient calcium efflux up to about 25 nmol. m^{-2} s^{-1} that lasts about 15 minutes.

In BSM, the net potassium flux is an efflux that ranges between 20-70 nmol. m^{-2} s^{-1} (Figures 8.1c, 8.2c, 8.3c). After the application of 10^{-2} mole m^{-3} fusicoccin, the potassium efflux increases about 120 nmol. m^{-2} s^{-1}. For 10^{-3} mole m^{-3} fusicoccin, the increase is about 30 nmol. m^{-2} s^{-1}. They both level off at about 20 minutes. The big error bars indicate that the fusicoccin-induced potassium flux varies much between plants. The effect of 10^{-2} mole m^{-3} IAA on potassium flux is not clear because the response is noisy. The effect may be a small reduction (10 nmol. m^{-2} s^{-1}) in net efflux, maintained for over 40 minutes.

In BSM, the initial membrane potential is between -125 to -130 mV (Figures 8.4, 8.5, 8.6). After the application of 10^{-2} mole m^{-3} fusicoccin, the membrane potential hyperpolarizes so that within 5 minutes it has a new level of about 35 mV more negative. For 10^{-3} mole m^{-3} fusicoccin, a new level of about 22 mV more negative than the initial membrane potential is reached within about 15 minutes. After 10^{-2} mole m^{-3} IAA is applied, there is a transient membrane hyperpolarization of about 5 mV. The membrane potential then depolarizes again to approach a new level within 15 minutes. The new level is 5 mV more positive than the membrane potential before the application of IAA.

8.3 Discussion

8.3.1 Fusicoccin Effects

As on oat coleoptile segments, flux observation using the MIFE technique shows that on pea epicotyl segments, fusicoccin also induces proton efflux and the proton efflux is accompanied by the efflux of calcium. The observed fusicoccin-induced proton efflux is consistent with the reported fusicoccin-induced medium acidification (Marrè et al. 1974, Talbott et al. 1988, Marrè 1979). Fusicoccin also hyperpolarizes the membrane potential. Unlike the transient potassium efflux observed in oats, the fusicoccin-induced potassium efflux on peas levels off.

For reasons similar to those described in Chapter 5, the likely source of the emerging calcium during fusicoccin-induced calcium efflux is the cell walls where calcium is released from the condensed phase of the walls. The process

of the calcium release happens by exchanging the condensed calcium with protons extruded from the cells during fusicoccin action. The mechanism of the proton-calcium exchange in the walls and the resultant proton and calcium effluxes outside the walls are explained and analysed using the WADM model for fluxes as described in Chapter 4.

During fusicoccin action, protons are extruded from the cells to the cell walls. Some of the extruded protons decrease the pH of the walls so that some of the wall's weak acids are protonated by releasing calcium from the condensed phase in the walls. The rest of the extruded protons and the released calcium diffuse to the external medium and they are observed as proton and calcium effluxes.

Since the amount of extruded protons for decreasing the pH of the DFS in the walls is relatively small, the efflux of protons through the plasmalemma necessary for the analysis of the WADM model for fluxes can be obtained from the rate of the total charge transported out by the observed effluxes of both protons and calcium. Again, the involvement of the fluxes of other monovalent cations is ignored because the transported monovalent cations do not interact with the condensed calcium in the walls. In fact the fluxes alter their concentration in the walls but the effect is small and negligible. During this time, since calcium is still available in the walls, monovalent cations do not condense in the walls. Therefore there is not other exchange with extruded protons. In the absence of reliable knowledge for peas, the same values of wall parameters necessary for the analysis of the WADM model for fluxes applied on oats are used: A_{sites}=800 mole m^{-3} for *Chara* (Dainty et al. 1960), pK=3, ξ^*=0.71 for *Sphagnum russowii* (Richter and Dainty 1990a), 1 μm wall thickness (Nobel 1974, M.J. Canny personal communication), 50% DFS:50% WFS (Dainty and Hope 1959). It was also assumed that the diffusion coefficients of cations in the DFS are about 1/5 of those in the WFS. For anions, the diffusion coefficient in the WFS is used because most of the anions are excluded from the DFS.

Now, with pH 6 BSM as the external solution, the WADM model for fluxes was then applied to estimate proton and calcium effluxes outside the walls as the result of the proton-calcium exchange in the walls during proton efflux from the cells to the cell walls. Figures 8.12 and 8.13 show both the observed effluxes and the calculated effluxes for 10^{-2} and 10^{-3} mole m^{-3} fusicoccin. The calculated proton and calcium effluxes almost match the

observed effluxes. This indicates that not only the proportion of the effluxes (since the sum of the effluxes is constrained) but also the form of the effluxes are tested successfully by the model. Therefore this strongly supports that the proton-calcium exchange takes place in the walls during fusicoccin-induced proton extrusion on peas and that the WADM model for fluxes is adequate to describe the mechanism of the exchange. The small difference between the calculated and the measured effluxes is probably due to the variation of the response in each plant. Besides, the process of proton-calcium exchange is not the only process that happens during fusicoccin-induced proton extrusion.

The same wall parameters are applied in the model for both peas and oats. Although they have different walls, it is shown that the outputs of the model match well with the observed effluxes. This suggests that values of wall parameters matter little (see Chapter 4 for the effects of wall parameter uncertainties).

As described for oats (see Chapter 5), the proton-calcium exchange acts on the calcium bound by condensation on the wall's weak acids. Based on the evidence obtained from calcium chelator studies (Virk and Cleland 1990, Cleland et al. 1990), the calcium binding should have a direct association with wall stiffening. Furthermore, the wall's polymers and proteins, where the wall's weak acids reside, are also broken down by low-pH activated wall enzymes during proton extrusion (Hoson et al. 1991, Inouhe and Nevins 1991). Therefore, the proton-calcium exchange and the activation of wall enzymes during wall acidification happen together to cause wall loosening and growth.

The proton and calcium effluxes observed during fusicoccin action on peas (Figures 8.1a&b, 8.2a&b) are smaller than on oats (Figures 5.1a&b, 5.2a&b). This indicates that fusicoccin induces smaller proton efflux at the plasmalemma on peas than on oats. The fusicoccin-induced membrane hyperpolarization on peas (Figure 8.5) is also smaller than on oats (Figure 5.5).

The measured membrane potential is about -125 mV in BSM. This is above the Nernst potential of potassium (about -150 mV). Therefore the electrochemical potential of potassium inside the cell is higher than outside. This is consistent with the observed potassium efflux in BSM being passive.

As with oats, fusicoccin induces potassium efflux from peas. However, fusicoccin-induced potassium efflux on peas is not transient for as long as measured. On peas, it was reported that fusicoccin induces potassium uptake (Marrè et al. 1974) and it was suggested that the uptake is due to the fusicoccin-induced membrane hyperpolarization (see also Marrè 1979). In this present work, fusicoccin also hyperpolarizes the membrane potential. But the observed fusicoccin-induced potassium efflux certainly contrasts with the reported fusicoccin-induced potassium uptake. The hyperpolarized membrane potential is below the Nernst potential of potassium (Figure 8.4, 8.5). This indicates that the potassium efflux is active during this time. There is no clear explanation for this active potassium efflux.

The proton, calcium and potassium effluxes and membrane hyperpolarization induced by 10^{-2} mole m^{-3} fusicoccin are all bigger than those induced by 10^{-3} mole m^{-3} fusicoccin. Therefore, unlike the results on oats, 10^{-3} mole m^{-3} fusicoccin is not the maximum concentration that can be applied to obtain the maximum responses on peas.

8.3.2 IAA Effects

The responses of peas to IAA following 4.5 hour preincubation are different from oats. The IAA-induced proton efflux, calcium efflux, and membrane hyperpolarization start immediately, without 7-13 minute lags. They are smaller, transient and last about 15 minutes.

Are the transient responses due to the solution mixing when IAA is applied? It seems that this is unlikely. In the experiments to observe the IAA effects on peas, the method of the IAA application was not the same as in the experiments on oats. In this case, as with the application of fusicoccin, the IAA was applied by adding very concentrated IAA solution to the solution in the measurement chamber and mixing to give the final IAA concentration of about 10^{-2} mole m^{-3}. The responses obtained using this method indicated that this method caused less disturbance to the tissue (see Chapter 5). Therefore, it was also applied in the experiments to observe the IAA effects on peas. If the solution mixing caused any effects, there should be responses similar to the responses of the solution change (a spike of proton efflux , a spike of calcium influx, a depolarization, see Chapter 6). The responses after IAA application do

not contain these responses (see Figures 8.3 and 8.6). Therefore the responses should be due to IAA.

The question now is "why do the IAA-induced proton efflux and membrane hyperpolarization on peas happen without lag?". Do intracellular processes that stimulate the activation of proton pumps in the plasmalemma happen much faster? If this is the case, the IAA-induced proton extrusion and membrane hyperpolarization will happen immediately. This is notable because the lag of IAA-induced growth, proton extrusion, and membrane hyperpolarization is about 10 minutes for oats. There has been a tendency to assume that this 10 minute lag occurs for all plants.

When IAA induces proton efflux across the plasmalemma, according to the WADM model, the extruded protons acidify the walls so that proton-calcium exchange happens in the walls. Therefore, not only protons, but also the released calcium, diffuse from the walls to the external medium. The relative timing of the observed IAA-induced proton and calcium effluxes supports the hypothesis of proton-calcium exchange in the wall during proton extrusion.

The IAA-induced proton and calcium effluxes and membrane hyperpolarization on peas are relatively smaller and shorter than on oats. Smaller responses are also observed on peas during fusicoccin action.

Unlike the case for fusicoccin, a transient increase in pH close to the tissue surfaces due to the solution mixing is not observed after the IAA application on peas (Figure 8.3d). IAA is a weak acid so that the addition of IAA will decrease the pH of the solution. In this case, at pH higher than the pH of the added IAA solution, the magnitude of the pH decrease depends on the amount of protons produced as the result of the dissociation of IAA during the addition. At pH about 5.3, it is calculated that the amount is reasonable for the eliminated transient pH increase after the addition. The IAA itself begins to decrease the pH close to the tissue surface with little delay.

It is interesting that in Figure 8.3d, the pH of the solution adjacent to the tissue decreases continuously while the observed proton efflux has come back to its initial value (Figure 8.3a). Do extruded protons diffuse as protonated organic compounds which release them in the solution? This needs some explanation. This pH response is similar to that reported by Jacobs and Ray (1976).

After the observed IAA-induced transient membrane hyperpolarization (Figure 8.6), the membrane potential has a new level of about 5 mV more positive than the initial value. This IAA response is in stark contrast to oats. Does this depolarization relate to the observed small potassium influx after the application of IAA? Again, there is no clear explanation for this response.

8.4 Conclusion

Again, using the MIFE technique, it has been confirmed that on peas, fusicoccin and IAA also induce proton extrusion. During the fusicoccin- and IAA-induced proton extrusion on peas, calcium is also emerging from the tissue to the external medium. The analysis of the WADM model for fluxes on the observed proton and calcium effluxes during fusicoccin action confirms that proton-calcium exchange happens in the walls during fusicoccin-induced proton extrusion. The responses of the IAA action also indicate the presence of the exchange.

Furthermore, fusicoccin and IAA also hyperpolarize the membrane potential on peas. For IAA, the membrane hyperpolarization is followed by membrane depolarization.

There is a large contrast between pea and oat responses to IAA.

Chapter 9

CONCLUSION

The distinction between calcium in the DFS and calcium condensed on the weak acids of cell walls, as proposed in the WADM model (Richter and Dainty 1990b, Ryan, Newman, Arif 1992) leads to the study of proton-calcium exchange in the walls when protons are extruded during the growth of plant cells. It has been suggested before that calcium in the walls of plant cells performs the role of stiffening the walls and that, during the growth of plant cells, this calcium is released from the walls so that the walls become loosened (Calcium bridge hypothesis, see Chapter 1 for detailed discussion). However, this hypothesis has been put into question because significant loss of calcium during the growth has not been observed and removal of wall calcium using calcium chelators does not cause an immediate increase of wall extensibility. Proton extrusion is widely observed during the growth of plant cells. Based on this evidence, it was proposed that the pH of the walls decreases during proton extrusion and the lowered pH activates some wall enzymes to break bonds between growth-restrictive polysaccharides so that the walls become loosened (Acid growth hypothesis, see also Chapter 1 for detailed discussion). The activation of wall enzymes by low pH to cause wall loosening may be the case. However, according to the WADM model of the walls, the lowered pH also causes proton-calcium exchange in the condensed phase of the walls where some weak acids of wall polymers are protonated releasing the condensed calcium. As a consequence, not only extruded protons, but also released calcium come out of the cell walls to the external medium. The exchange may also have a role in the wall loosening process because the removed calcium could include calcium that cross links between the wall macromolecules.

In the present work, proton-calcium exchange in the walls during the growth of oat coleoptile and pea epicotyl segments induced by fusicoccin and IAA has been studied by measuring simultaneously the fluxes of protons and calcium outside the tissues. The measurements of the fluxes were carried out using the Microelectrode Ion Flux Estimation (MIFE) technique (Newman et al 1987). This technique is capable of determining simultaneously fluxes of several ions in low salt unbuffered solutions by measuring their electrochemical potential gradients adjacent to the tissue surfaces. For charge balancing, fluxes of potassium and chloride and membrane potential were also measured.

The determination of proton flux in buffered solution by measuring the proton electrochemical potential gradient is in error because some of the protons diffuse as protonated buffer. The ratio between the protonated buffer flux and the proton flux has been calculated and the result shows that the ratio depends on the pH of the solution. Unbuffered solutions still have the buffering effect of water itself and carbonates due to carbon dioxide dissolved from the atmosphere. However, at pH 6, the flux ratio is still much smaller than 1. For this reason, the measurements of proton flux, and also other measurements, in this present work were carried out in pH 6 unbuffered solutions.

Based on the steady state WADM model (Richter and Dainty 1990b, Ryan Newman, Arif 1992), the WADM model for fluxes has been developed to provide a quantitative analysis to estimate the wall quantities and the ion fluxes from the walls to the bathing medium during proton extrusion from the cells to the cell walls. It is shown that when there is calcium condensation in the walls, proton extrusion from the cells to the cell walls causes effluxes of both protons and calcium outside the walls. However when calcium condensation in the walls is not allowed (for example when the walls are considered as a classical Donnan system only, which is a special case of the WADM model for fluxes), proton extrusion from the cells to the cell walls does not cause any calcium release from the walls. This indicates that Manning condensation must be included in the model of cell walls to allow calcium release from the walls by extruded protons. It is also shown that during proton extrusion, the estimated pH of both the DFS and the WFS decreases, the estimated Donnan partition coefficient decreases and the estimated Donnan potential depolarizes.

Using the MIFE technique, it was observed that fusicoccin induces both proton and calcium effluxes on oats. Similar responses to fusicoccin were also observed on peas. These results have been analysed using the WADM model

for fluxes. The calculated proton and calcium effluxes match well with the observed effluxes. This indicates that proton-calcium exchange takes place in the walls of oats and peas during fusicoccin-induced proton extrusion. IAA also induces proton and calcium effluxes in both oats and peas although the responses are not as large and simple as the responses to fusicoccin. The responses are also consistent with the proton-calcium exchange in the walls during IAA-induced proton extrusion. All of this evidence confirms the hypothesis that the WADM model is suitable to describe the walls of plant cells and that proton-calcium exchange takes place in the walls during proton extrusion.

The WADM model does not specify the function of condensed calcium in the walls. However as a result of the discussion presented in this present work, it seems likely that condensed calcium acts to stiffen the walls, perhaps by making cross-links between wall polymers as suggested by the calcium bridge hypothesis. The wall loosening itself may be the result of both proton-calcium exchange in the condensed phase of the walls (which acts to break calcium bindings) and activation of wall enzymes as suggested by the acid growth hypothesis (which acts to breakdown wall polymers). The activation of wall enzymes may also interact with the proton-calcium exchange since both processes take place in the same locations, wall proteins and polymers. Therefore it seems likely that both processes happen together, without the absence of each other, to cause wall loosening as the pH of the walls drops during proton extrusion.

The WADM model for fluxes also provides an estimate of the wall pH (DFS and WFS). This is helpful since the pH of the walls is difficult to determine. The process of proton-calcium exchange also provides some explanation of why the lag of the IAA-induced proton extrusion could be shorter than the lag of the observed IAA-induced proton efflux outside the walls, and thereby the lag of the IAA-induced medium acidification. This removes the question regarding the acid growth hypothesis that the timing of the IAA responses (growth, proton extrusion and membrane hyperpolarization) do not match.

In both oats and peas, fusicoccin induces potassium efflux and membrane hyperpolarization. There is still no clear explanation about this potassium efflux. In both plants, IAA does not cause any significant change in potassium flux. In oats, IAA hyperpolarizes transiently the membrane potential

with several minute lag. In peas, the transient membrane hyperpolarization is immediate and followed by membrane depolarization. This is new information with respect to peas.

Using solid-state chloride microelectrodes on oats, it is shown that, like potassium flux, chloride flux also does not change significantly during IAA action. Therefore the involvement of potassium and chloride fluxes in charge balancing during IAA action on oats is still unclear. This needs to be studied further. The observed continuous pH decrease without further proton efflux during IAA action on peas also need some explanation. Perhaps, organic acid anions produced during the IAA-induced growth are involved in carrying the IAA-induced extruded protons.

Appendix A

DETERMINATION OF ION FLUXES
AND MEMBRANE POTENTIAL

A.1 Ion Fluxes

Microelectrodes with ion selective liquid membranes are widely used to measure the activities of ions in solution (see Ammann 1986 and its references). Because of their small size, microelectrodes are even used to determine intracellular ion activities in living cells. Activities of many ions now can be measured with this method and it seems likely that it will replace the previous methods used for measuring ion activities, such as glass membrane microelectrodes.

In the Department of Physics, University of Tasmania, the use of ion selective microelectrodes, following Lucas and Kochian (1986), has been expanded by Dr. I.A. Newman for measuring fluxes of particular ions and the description of what is now known as the Microelectrode Ion Flux Estimation (MIFE) technique has been given before (Newman et al. 1987, Ryan et al. 1990, Henriksen et al. 1990, Henriksen et al. 1992). In this appendix, the technique is summarized in relation to its application for the study of ion fluxes during the growth of plant cells carried out in the present work.

A.1.1 Preparation

Microelectrode Fabrication

Ion selective microelectrodes can be fabricated from micropipettes in many different ways. The micropipettes themselves can be made from various

glass tubing with different characteristics and different shapes. In general, the glass tubing for micropipettes should have high specific resistivity, a relevant melting point, and high water resistivity (Ammann 1986). The high specific resistivity of the glass tubing prevents leakage of electric current through the glass tubing and their melting point determines what kind of microelectrode pullers can be used. The water resistivity of the glass tubing determines how thick is the hydrated layer on the glass surface in which the ion transport may be influenced.

In this laboratory, the micropipettes are made from borosilicate glass tubing from Clark Electromedical Instruments Company, Pangbourne, Berks, UK. Borosilicate glass tubing is commonly used for microelectrodes with ion sensitive liquid membranes. For ion selective microelectrodes, the diameter of the glass tubing used in the present work is 1.5 mm. In this case, glass tubing without filling fibres (GC150-10) is used. We found that ion selective microelectrodes made from glass tubing with filling fibres cannot hold ion selective liquid membranes long enough.

To make micropipettes, a glass tube was mounted on a microelectrode puller and heat was applied on the middle of the glass so that the glass tubing was pulled apart into two micropipettes. The tips of the micropipettes were less than 1 μm in diameter.

The surfaces of the micropipettes, including the tips, are quite hydrophilic because the surfaces are mostly occupied by hydroxyl groups. Therefore, ion selective liquid membranes made from organic liquids in the tips of the micropipettes can be displaced easily from the tips by aqueous solution used in experiments. This can be avoided when the surfaces, especially the inner surfaces, of the micropipette tips are lipophilic. This is usually obtained by allowing reaction between reactive silicon compounds with the surfaces of the micropipettes. This technique is commonly called silanization.

In the present work, silanization was carried out in the following way. About 35 micropipettes were placed on an aluminium plate with the tips face up. The micropipettes were then predried in an oven with a temperature of about 200 °C for at least 5 hours. Sometimes, they were predried over night. After this long predrying, water was expected to have been removed from the surfaces of the micropipettes. The presence of water in the tip surfaces of the micropipettes may result in blocking the tips because of its reaction with the

reactive silicon compound to form polymeric silicon compounds (see Patnode and Wilcock in Ammann 1986). While still in the oven, the dried micropipettes were covered with an upturned steel beaker in which the tips of the micropipettes were just below the bottom of the beaker. A small amount (~ 25×10^{-9} m^{-3}) of tributylchlorosilane (90796, Fluka Chemie AG, Buchs, Switzerland) was then injected into the beaker. The tributylchlorosilane immediately evaporated; however the vapour was trapped in the beaker, and it was expected to react with the surfaces of the micropipette tips. To allow this reaction to be optimal, the oven was kept at 200 °C for 15-30 minutes. After that, the beaker was removed and the micropipettes were left in the oven for another 30 minutes. After the micropipettes were cold, they were ready to be used to make microelectrodes. Silanized micropipettes were still good for making microelectrodes several days even weeks after silanization.

In order to make an ion selective microelectrode, a silanized micropipette was held on a stand and cut about 4 cm from the tip. The uniformity of the microelectrode length facilitated the positioning of the microelectrode tips during the measurement. A small part of the tip of the silanized micropipette was then broken by advancing a glass tube tip with a precision micromanipulator to the micropipette tip. The broken tip was about 3-5 μm in diameter. The micropipette with the broken tip was back filled with an appropriate filling solution using a filling micropipette. It was necessary to make sure that there were no air bubbles in the tip, i.e the tip was perfectly filled with the filling solution. Using the same micromanipulator, a glass tube filled with the ion selective liquid was then advanced to the tip of the filled micropipette so that the tip slightly touched the liquid. As a result, the ion selective liquid filled the micropipette tip, by pushing the filling solution from the tip. After the length of the liquid membrane in the tip reached about 50 μm, the glass tube with the ion selective liquid was removed. To complete the process, the filled micropipette with ion selective liquid membrane in its tip was mounted in a microelectrode holder. The ion selective microelectrode was then ready for calibration.

In Chapter 2, it has been mentioned that there are three ion selective liquids used in this present work. These are 60031 K$^+$-cocktail for potassium selective microelectrodes, 82500 H$^+$-cocktail for proton selective microelectrodes, and 21048 Ca^{2+}-cocktail for calcium selective microelectrodes. These cocktails were obtained from Fluka Chemie AG, Buchs, Switzerland.

As a note, filling micropipettes were made in a similar way as micropipettes for ion selective microelectrodes. However, in the making process, the heated area on the glass tubing was wider so that they had longer tips. Glass tubing with a bigger diameter (2mm) and without filling fibres was usually used in this laboratory.

For different ions, the filling solution was also different. Because the microelectrodes would be connected to the measurement devices with Ag/AgCl half cell electrodes, the filling solution had to contain Cl⁻ ions and the ion of interest. Their concentration had also to be constant and high enough to avoid a big variability of the junction potential that appears between the filling solution and the half cell electrodes. In this present work, for potassium, calcium, and proton ion selective microelectrodes, the filling solutions were respectively 5×10^2 mole m⁻³ KCl, 5×10^2 mole m⁻³ $CaCl_2$, and 0.15×10^2 mole m⁻³ NaCl + 0.4×10^2 mole m⁻³ KH_2PO_4 adjusted to pH 6 using NaOH.

Reference electrodes used in these experiments were Ag/AgCl half cell electrodes inserted into agar plastic tubes. Agar plastic tubes were made by filling a long plastic tube (2mm in diameter) with a boiled mixture of 10^3 mole m⁻³ KCl and 1% agar. After the long agar plastic tube was cold, the tube was stored by bathing the tube with 10^3 mole m⁻³ KCl solution. In the making of a reference electrode, an agar tube segment with a desired length was cut and an Ag/AgCl half cell electrode made with standard technique was inserted into the agar tube segment. In order to avoid the movement of the half cell electrode inside the tube, the connection was secured with parafilm.

Microelectrode Calibration

Before calibration of the ion selective microelectrodes was carried out, standard solutions of the ion of interest with different ionic strength were made. It is desirable to make standard solutions close to the range of the ionic strength of the observation solution.

In this laboratory, the system developed by Dr. I.A. Newman has 4 channels so that we can use up to 4 ion selective microelectrodes simultaneously. For the present work, three channels were used simultaneously. In the case of calibration of microelectrodes, however, since a

group of standard solutions was made just for a particular ion, the calibration must still be carried out for each electrode separately.

The ion selective microelectrodes were connected to the system with standard Ag/AgCl half cells and the reference electrode was connected to the ground (earth) of the system. The resistivities of the microelectrodes were measured by injecting a constant current through them. Generally the resistivities of the microelectrodes were about 5 GΩ. However, when the resistivities were high, breaking the tips of the microelectrodes a bit more may have decreased the resistivities. For a particular microelectrode, the calibration was done by measuring the potential difference between the tip of the microelectrode and the reference electrode in every standard solution appropriate for the microelectrode. When both the microelectrode and the reference electrode are in a standard solution, the measured potential difference E can be represented by the following equation (see Newman et al. 1987).

$$E = E_e + E_s + (V-V_o).$$
<div style="text-align:right">a.1</div>

E_e is total junction potentials, constant potentials which appear across Ag/AgCl/Cl$^-$ half cells of both electrodes. V and V_o are electric potentials in solution just outside the tips of the microelectrode and the reference electrode respectively. E_s is the potential across the ion sensitive liquid membrane in the tip of the microelectrode, which is

$$E_s = \left(\frac{2.303\ gRT}{zF}\right) \log\left(\frac{C}{C_e}\right) = \alpha \log\left(\frac{C}{C_e}\right)$$
<div style="text-align:right">a.2</div>

where R, T, z, F, C, and C_e are respectively gas constant, temperature, valency of the ion, the Faraday number, concentration of the ion in solution just outside the tip, and concentration of the ion in the filling solution which is constant. g is a factor introduced for the degree of the selectivity of the membrane to the ion and is usually near unity. α is defined as (2.303 gRT/zF). Therefore, equation a.1 becomes

$$E = E_o + \alpha \log\left(\frac{C}{C_o}\right) + (V-V_o)$$
<div style="text-align:right">a.3</div>

where

$$E_o = E_e + \alpha \log \left(\frac{C_o}{C_e}\right).$$ a.4

In these equations, C_o represents the reference concentration of the ion in solution just outside the tip of the reference electrode. In a standard solution where the distribution of the ion is homogeneous, $V=V_o$ and $C=C_o$. Therefore from equation a.3, E will equal E_o. Hence,

$$E = E_o = E_e + \alpha \log \left(\frac{C_o}{C_e}\right).$$ a.5

Because E_e and C_e are constant, when the observed potential differences are plotted against the log of the ion concentration in the standard solutions, α is represented by the slope of the curve. For an ideal ion selective liquid membrane, α would be the theoretical Nernst slope, that is 58.2 for univalent ions and 29.1 for divalent ions at 20° C. In this case, factor g is unity. However, the selectivity of the microelectrodes may not be perfect so that the observed slope α may be shifted from the theoretical value. Therefore, calibration of the microelectrodes is necessary before the experiments are carried out. In the ion flux measurements, the observed Nernst slope (α), the potential in a standard solution where the ionic strength is close to the ionic strength in the measurement medium ($E_o'=E=E_o$), and the ion concentration in the standard solution ($C_o'=C=C_o$) are used to convert potential difference observed using the microelectrode during the measurements to its concentration. This is discussed below.

A.1.2 Ion Flux Measurements

Newman et al. (1987) have given the details of the theory for the ion flux calculation when cylindrical symmetry is used. For fluxes of ions through a planar surface, which happens on the cut surface of tissues, the calculation of the flux is different. However, since the calculation is determined just for the flux density, the calculation in the above paper can be used with a slight change. In this section, the calculation is rewritten in relation to the present conditions.

During the measurements of the activities and the fluxes of particular ions from a tissue segment, the tips of the microelectrodes were placed close to the cut tissue surface while the reference electrode was placed far from the

tissue (Figure 2.1). In this condition, the concentration of the ions at the tips of the microelectrodes are represented by the potential E_i measured by the associated microelectrodes with respect to the reference electrode. Using equation a.3, the concentration of the ions can be calculated when α, E_o and C_o, for the ions are provided. In this case, α, E_o' and C_o' obtained from the calibration are used to provide the quantities. Therefore,

$$C = C_o' \, 10^{\left(\frac{E_i - E_o'}{\alpha}\right)}$$
a.6

In this case, the effect of the electric potential difference on the calculation of the concentration, that is $10^{[(V_i - V_o)/\alpha]}$, is assumed to be unity because $(V_i - V_o)$ is very small compared to α.

For observation of the fluxes of the ions, the microelectrode tips were moved a desired distance further back from their initial position (i), perpendicular to the cut surface of the tissue. In this present work, the tips were moved 40 μm from the initial position. The microelectrodes then detected the potentials E_f at the new position (f) with respect to the reference electrode. In a similar way, these potentials were used for determining the concentration of the ions at the new position.

When the flux of an ion J is present across the cut surface of the coleoptile tissue, the electrochemical potential of the ion μ must change as a function of the position across the surface. In this case, the flux is assumed to be steady and the direction of the flux is just perpendicular to the surface (x direction). The relation of the flux to the electrochemical potential can be written as

$$J = -u \, C \frac{d\mu}{dx}.$$
a.7

Here, u and C are respectively the mobility and the concentration of the ion. In this measurement, pressure and gravitational effects on the electrochemical potential are neglected, thus the electrochemical potential can be written as

$$\mu = \mu_o + 2.303 \, RT \log\left(\frac{C}{C_o}\right) + zF(V - V_o)$$
a.8

Here, μ_o is the electrochemical potential where the concentration and the electrical potential of the ion are C_o and V_o. When equation a.3 is substituted into this equation, the equation becomes

$$\mu = \mu_o + \frac{zF}{g}[(E-E_o) - (1-g)(V-V_o)]$$

a.9

In this equation, μ_o, E_o, and V_o are constant, thus when equation a.9 is substituted into equation a.7, the equation becomes

$$J = -u\, C\, \frac{zF}{g}\left[\frac{dE}{dx} - (1-g)\frac{dV}{dx}\right]$$

a.10

In this present work, the flux observation was carried out by measuring potentials at two different positions in a direction perpendicular to the cut surface. Between those positions, the electric potential difference was relatively very small. Beside that, g was nearly unity. Therefore, the contribution of the electrical potential difference dV to the flux in equation a.10 can be neglected. Hence,

$$J = -u\, C\, \frac{zF}{g}\frac{\Delta E}{\Delta x}$$

a.11

In the application of this equation for the present experiments, ΔE was the difference of potentials measured by the electrometer in position i and position f in which the distance Δx was 40 μm. The mean concentration of the ion at position i and f calculated using equation a.6 was used to represent C in equation a.11 because the concentration of the ion between the two positions was not very different. The factor g is determined from α.

A.2 Membrane Potential

For membrane potential measurements, glass tubing with filling fibres were used (GC150F-10, Clark Electromedical Instruments Company, Pangbourne, Berks., UK). Firstly, a glass tube 1.5 mm in diameter was mounted on the microelectrode puller and heat applied in the middle of the glass tube caused drawing the tube into two micropipettes. The tips of the micropipettes were less than 1 μm. For membrane potential measurements, the micropipettes were not silanized and the tips were not broken. A micropipette

was held on a stand and cut about 4 cm from the tip. The micropipette was then back filled with 5×10^2 mole m^{-3} KCl. In the filling process, a small amount of the solution was firstly dropped using a filling pipette in the back end of the pipette. Capillary force along the filling fibre of the pipette allowed the solution to move to the tip and filled the tip. The presence of air bubbles in the tips during this process did not occur. After this, the filling process was completed by adding more solution into the micropipette using the filling pipette. The micropipette was then held with a microelectrode holder.

During the measurements, the membrane potential microelectrode was connected to the measurement system using an Ag/AgCl half cell. The same reference electrode which was an Ag/AgCl half cell in an agar tube was also used. The potential difference between the tip of the microelectrode and the reference electrode was measured before and after insertion of the microelectrode tip into a cell. Impalement was done using a high precision hydraulic manipulator to allow fine movement of the tip. When the tip of the microelectrode was in the cell, the potential difference represented the membrane potential. The resistance of the electrode can be detected by injecting a constant electric current through it.

Appendix B

PLANAR DIFFUSION

When the concentration of species j, C_j (in mole m^{-3}), in some regions is less than in a neighbouring region, the planar flux of the species j, J_j (in mol. m^{-2} s^{-1}) is given by Fick's first law of diffusion (Nobel 1974):

$$J_j = - D_j \frac{\partial C_j}{\partial x},$$

b.1

where D_j is the diffusion coefficient of species j (in m^2 s^{-1}) and x is the position (in m). For charged species, this flux is also affected by the presence of electric potential. In this case, it is assumed that the effect is already included in the diffusion coefficients of the species. Now at position x, it is supposed that there is a volume element of thickness dx in the direction of the flow and it has a cross sectional area A (Figure b.1). For this condition, the following relation is obtained :

$$J_j A - \left(J_j + \frac{\partial J_j}{\partial x} dx \right) A = \frac{\partial C_j}{\partial t} A \, dx.$$

b.2

When equation b.1 is substituted into this equation, the equation becomes

$$\frac{\partial C_j}{\partial t} = - \frac{\partial}{\partial x} \left(- D_j \frac{\partial C_j}{\partial x} \right).$$

b.3

The equation is recognised as Fick's second law of diffusion. When D_j is constant, the equation becomes :

$$\frac{\partial C_j}{\partial t} = D_j \frac{\partial^2 C_j}{\partial x^2}.$$
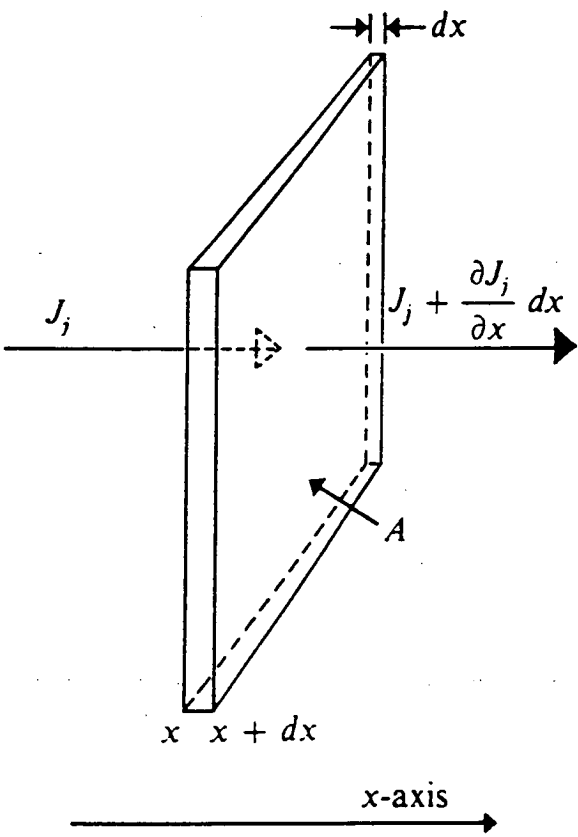
b.4

Figure b.1

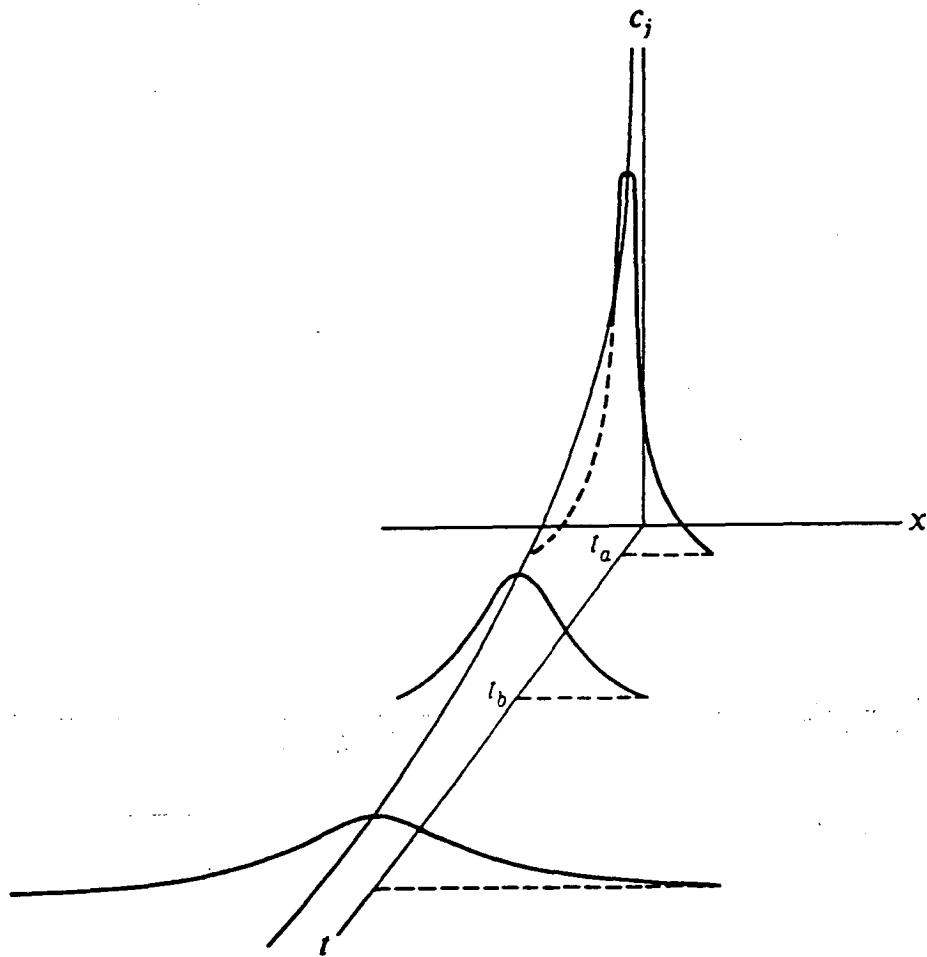Diagram of fluxes. (From Nobel 1974 p.12)

Figure b.2

Distribution of concentration as function of position and time.
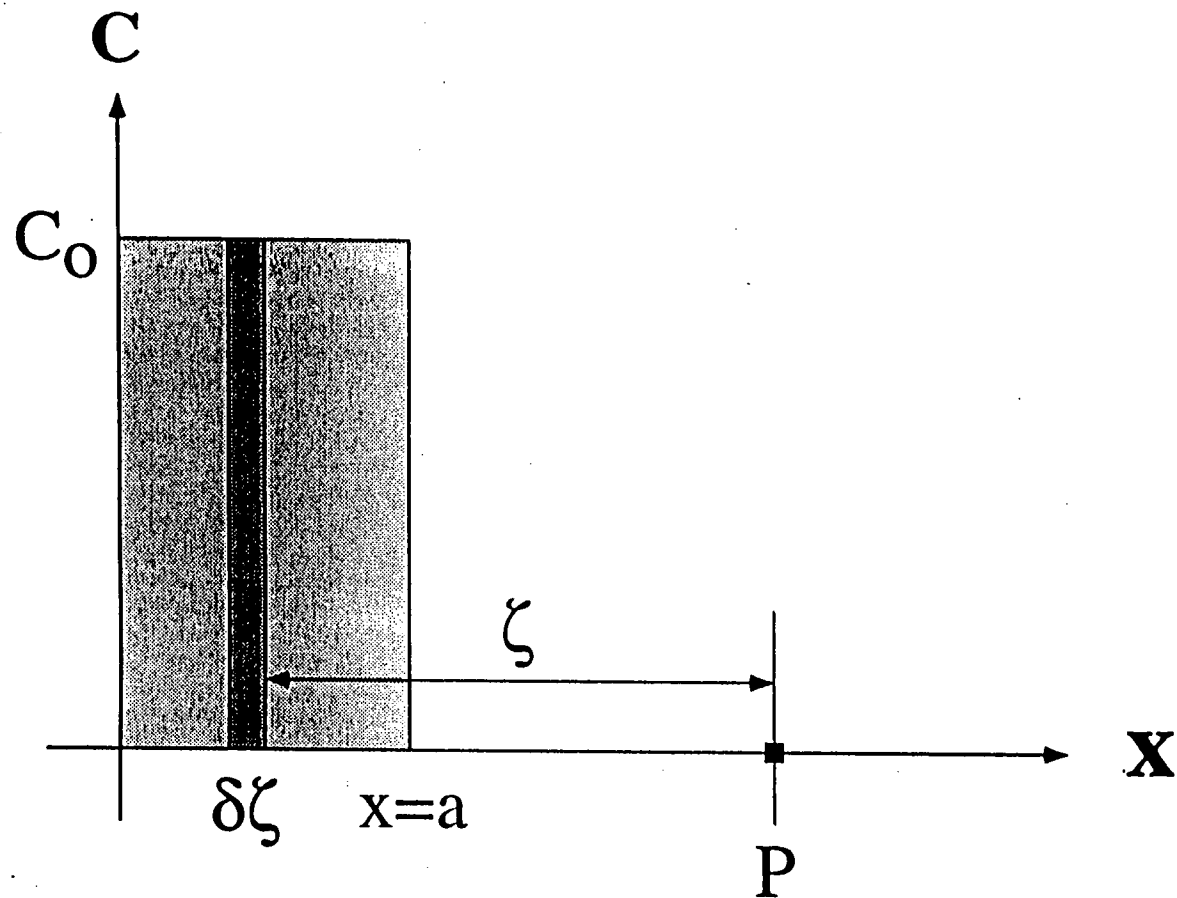
(From Nobel 1974 p.16)

Figure b.3

Extended initial distribution of concentration.

The solution of this equation is (Nobel 1974, Crank 1975):

$$C_j(x,t) = \frac{M_j}{2\sqrt{\pi D_j t}} e^{-\left(\frac{x^2}{4 D_j t}\right)}, \qquad\qquad b.5$$

where M_j is the total amount of solute j per unit area initially placed in a plane located at the origin of the x-direction. At t=0, C_j is infinity because all of the total amount of the solute is placed at the origin. For t>0, the solute starts to diffuse away from the origin. The concentration of the solute at the origin decreases and the average distance of the diffusing solute from the origin increases with time (Figure b.2). In estimating how far molecules diffuse in time t, a useful parameter is the distance at which the concentration has dropped to 1/e of its value in the plane at the origin. From the last equation, this is satisfied when the exponent of e in the equation is -1. So that, the distance of diffusion as function of time is given by

$$x^2 = 4 D_j t. \qquad\qquad b.6$$

It is supposed that there is an efflux of protons from a tissue sample to the bathing medium. The diffusion coefficient of protons is approximately 10^{-9} m^2 s^{-1}. When the bathing medium is replaced with the fresh one, the concentration gradient of protons that has been established is replaced. After the replacement, the protons start to diffuse away from the tissue surface to establish a new concentration gradient. Now to establish a new concentration gradient of 1 mm thickness, based on the time-distance relation for diffusion, the required time is about 4 minutes. In conclusion, after solution change, time is required to establish a new concentration gradient.

Now we consider a semi-infinite system in the x-direction that has an initial distribution of solute j defined by

$$C_j(x, 0) = C_o \text{ for } 0 \leq x \leq a; \quad C_j(x, 0) = 0 \text{ for } x > a. \qquad\qquad b.7$$

Figure b.3 shows this distribution. For the diffusing solute j in an element of width $\delta\zeta$ to be a line source of strength $C_o\delta\zeta$, based on equation b.5, the concentration at point P, distance ζ from the element, at time t is (Crank 1975):

$$\frac{C_0\,\delta\zeta}{2\,\sqrt{\pi\,D_j\,t}}\,e^{-\left(\frac{\zeta^2}{4\,D_j\,t}\right)},$$

and the complete solution due to the initial distribution is obtained by summing over successive elements $\delta\zeta$,

$$C_j(x,t) = \frac{C_0}{2\,\sqrt{\pi\,D_j\,t}} \int_{\zeta=x-a}^{x} e^{-\left(\frac{\zeta^2}{4\,D_j\,t}\right)}\,\delta\zeta. \qquad \text{b.8}$$

When it is defined that

$$\eta^2 = \frac{\zeta^2}{4\,D_j\,t}, \qquad \text{b.9}$$

equation b.8 becomes

$$C_j(x,t) = \frac{C_0}{\sqrt{\pi}} \int_{\eta=\frac{(x-a)}{2\,\sqrt{(D_j t)}}}^{\frac{x}{2\,\sqrt{(D_j t)}}} e^{-(\eta^2)}\,\delta\eta. \qquad \text{b.10}$$

Based on the definition of the error function,

$$\text{erf } z = \frac{2}{\sqrt{\pi}} \int_{0}^{z} e^{-(\eta^2)}\,\delta\eta. \qquad \text{b.11}$$

where

$$\text{erf}(0) = 0;\ \text{erf}(\infty) = 1;\ \text{erf}(-z) = -\text{erf } z;\ \text{erfc } z = 1 - \text{erf } z. \qquad \text{b.12}$$

we obtain,

$$C_j(x,t) = \frac{C_0}{2}\left(\text{erf}\left(\frac{a-x}{2\,\sqrt{D_j\,t}}\right) + \text{erf}\left(\frac{x}{2\,\sqrt{D_j\,t}}\right)\right). \qquad \text{b.13}$$

In the origin, there is no flow of the diffusing solute. Therefore we can consider that the concentration curve is reflected at this boundary and the reflected curve is superposed on the original curve (Crank 1975). The complete solution for the concentration of the solute through time and space becomes

$$C_j(x,t) = \frac{C_o}{2} \left\{ \left(erf\left(\frac{a-x}{2\sqrt{D_j\,t}}\right) + erf\left(\frac{x}{2\sqrt{D_j\,t}}\right) \right) + \left(erf\left(\frac{a+x}{2\sqrt{D_j\,t}}\right) + erf\left(\frac{-x}{2\sqrt{D_j\,t}}\right) \right) \right\}$$

$$= \frac{C_o}{2} \left(erf\left(\frac{a-x}{2\sqrt{D_j\,t}}\right) + erf\left(\frac{a+x}{2\sqrt{D_j\,t}}\right) \right). \qquad \text{b.14}$$

In equation b.12, erfc is the complement of the error function. When the definition is applied on equation b.14, we obtain the expression of the concentration in terms of the error function complement.

$$C_j(x,t) = \frac{C_o}{2} \left(erfc\left(\frac{x-a}{2\sqrt{D_j\,t}}\right) - erfc\left(\frac{x+a}{2\sqrt{D_j\,t}}\right) \right). \qquad \text{b.15}$$

At x=a, the flux of solute j is defined by,

$$J_j(a,t) = -D_j \left(\frac{dC_j(x,t)}{dx}\right)_{x=a}. \qquad \text{b.16}$$

In this equation, the concentration gradient in the x direction is calculated from equation b.14. In this case, the Laplace transform is used so that the calculation can be carried out easily. After that, the result is substituted into equation b.16 and x is set to equal a. As a result, the following equation is obtained.

$$J_j(a,t) = \frac{C_o}{2} \sqrt{\frac{D_j}{\pi\,t}} \left(1 - e^{-\left(\frac{a^2}{D_j\,t}\right)}\right). \qquad \text{b.17}$$

The total amount of the solute that is transported out across the boundary x=a at time $t=t_i$ is

$$T_j^{x>a} = \int_{t=0}^{t_i} J_j(a,t)\,dt. \qquad \text{b.18}$$

When equation b.17 is substituted into this equation, we obtain

$$T_j^{x>a} = C_o \left\{ a\,erfc\left(\frac{a}{\sqrt{D_j\,t_i}}\right) - \sqrt{\frac{D_j\,t_i}{\pi}} \left(1 - e^{-\left(\frac{a^2}{D_j\,t_i}\right)}\right) \right\}. \qquad \text{b.19}$$

Appendix C

THE WADM MODEL

Following Richter and Dainty (1989a&b, 1990a&b), Ryan, Newman, Arif (1992) have used the WADM (Weak Acid Donnan-Manning) model to estimate the concentrations of ions in cell walls when the external pH or the external potassium concentration are altered. In this appendix, the WADM model is used again with different solutions applied in the present work.

Referring to those papers (Richter and Dainty 1989a&b, 1990a&b, Ryan, Newman, Arif 1992), the WADM model can be summarised in the following description. Cell walls of plant cells contain ionogenic species such as uronic acid in the pectin and hemicellulose polymers, the acidic and basic amino acids of the wall proteins, and the phenolics of lignin and other polyphenols. They are weak acids. Therefore, the degree of their ionization depends on the pH of the cell walls and the pK of the polymers according to the Henderson-Hasselbalch equation,

$$\frac{[A_{diss}]}{[A_{sites}]} = \frac{10^{(pH_w-pK)}}{1 + 10^{(pH_w-pK)}},$$
\qquad c.1

where $[A_{sites}]$ is the concentration of the ionisable sites in the walls and $[A_{diss}]$ is the concentration of the dissociated ionizable sites. These species provide indiffusible anions in the cell walls. They should be regarded as being in the DFS in contrast to the WFS.

According to Manning's condensation theory (Manning 1969), when the linear charge density parameter, defined by

$$\xi = \frac{[A_{diss}]}{[A_{sites}]} \xi^* \qquad \qquad \text{c.2}$$

where ξ^* is its intrinsic value, is higher than the reciprocal of the highest valency of cations in the walls ($1/z$), the condensation of the highest valency cations on some of the dissociated ionizable sites takes place. As a result, the linear charge density parameter of the walls decreases. The condensation process continues until the linear charge density parameter is equal to $1/z$, or until all of the cations are depleted from the DFS. When the latter case happens, cations with lesser valency will condense if the linear charge density parameter is still bigger than the reciprocal of the valency of those cations. In the walls, calcium is a major cation with the highest valency. Therefore when $\xi > 0.5$, calcium condensation takes place until ξ reduces to 0.5. In this case, as long as calcium is still present in the DFS, monovalent cations will not condense. After the calcium condensation is completed, the remaining fixed negative charges act as the fixed anions for the classic Donnan system,

$$[A_{Donn}] = \xi^{eff} \frac{[A_{sites}]}{\xi^*} \qquad \qquad \text{c.3}$$

Here, ξ^{eff} is the effective linear charge density parameter, which is 0.5. In the case where ξ is already less than 0.5 and thereby there is not calcium condensation, all of the dissociated ionizable sites are available for the Donnan equilibrium,

$$[A_{Donn}] = [A_{diss}] \qquad \qquad \text{c.4}$$

In this case, $\xi^{eff} = \xi$.

For the Donnan equilibrium, electric neutrality in the Donnan free space (DFS) of the walls must be satisfied by all the involved ions,

$$[A_{Donn}] = \sum_{all\ N} z_N [N_w] \qquad \qquad \text{c.5}$$

Here, N is the symbol for ions. The ratio of the ion activity in the DFS and in the WFS, which is the same as in the external medium, is represented by the Donnan partition coefficient σ.

$$\frac{\gamma_{zw} [N_w]}{\gamma_{zo} [N_o]} = \sigma^z.$$

c.6

In this equation, the activity coefficient of ions of valency z in the DFS, which has a high concentration of fixed charges, is provided by Richter and Dainty (1990b) with the following equation.

$$\ln \gamma_{zw} = - (z_N)^2 \frac{\xi^{eff} [A_{Donn}]}{4 I_w},$$

c.7

where the ionic strength in the DFS is

$$I_w = 0.5 \sum_{all\ N} (z_N)^2 [N_w].$$

c.8

The activity coefficient in the WFS and in the external medium is given by the Debye-Hückel equation,

$$\log \gamma_{zo} = - 0.509 (z_N)^2 \left(\frac{\sqrt{I_o}}{1 + \sqrt{I_o}} \right),$$

c.9

where the related ionic strength is

$$I_o = 0.5 \sum_{all\ N} (z_N)^2 [N_o].$$

c.10

In this treatment, the small concentration of fixed positive charges in the walls is ignored.

The description above shows that the determination of the concentration of the dissociated ionizable sites, and thereby the concentration of fixed negative charges for Donnan equilibrium depends on the pH of the walls. However, the determination of the wall pH, together with the concentration of other wall ions, depends on the concentration of fixed negative charges for the Donnan equilibrium and the composition of ions in the external solution. Therefore, to determine the complete ionic condition in the DFS of the walls, all of the equations must be solved simultaneously by iteration. The Donnan potential of the DFS in respect to the external medium is obtained from

$$E_{wo} = - \frac{RT}{F} \ln x.$$

c.11

In this model, parameters that must be provided are $[A_{sites}]$, pK and ξ^* of the walls. These parameters are not available for many plants. For *Chara*, Ryan, Newman, Arif (1992) used 800 mole m^{-3} for $[A_{sites}]$ and 2.2 for the pK based on the report of Dainty et al. (1960). Because ξ^* is not available for *Chara*, they used $\xi^*=0.71$ obtained by Richter and Dainty (1990a) from *Sphagnum russowii*. In this appendix, the WADM model is used to estimate the ionic conditions in walls of plant cells bathed with the solutions used in the present work. In this case, it is supposed that the DFS of the walls has $[A_{sites}]=800$ mole m^{-3} and $\xi^*=0.71$. For the pK of the wall's weak acids, pK=3.0 is used. This is based on the report that one of two classes of weak acids found in *Sphagnum russowii* has pK between 2 and 4 (Richter and Dainty 1989a).

In this present work, the basic solution is BSM that contains 0.1 mole m^{-3} KCl and 0.1 mole m^{-3} $CaCl_2$ adjusted to pH 6 using NaOH which gives a final sodium concentration of 0.02 mole m^{-3}. When BSM is the external medium, based on equation c.5 and c.6, the equation that must be solved to calculate the Donnan partition coefficient σ is :

$$\sigma^3 + \frac{\gamma_{1o}\,\gamma_{2w}\,([H_o]+[K_o]+[Na_o])}{2\,\gamma_{2o}\,\gamma_{1w}\,[Ca_o]}\,\sigma^2 - \frac{\gamma_{2w}\,[A_{Donn}]}{2\,\gamma_{2o}\,[Ca_o]}\,\sigma - \frac{\gamma_{1o}\,\gamma_{2w}\,[Cl_o]}{2\,\gamma_{2o}\,\gamma_{1w}\,[Ca_o]} = 0.$$

c.12

Here, H_o, K_o, Na_o, Ca_o and Cl_o are the concentrations of hydrogen, potassium, sodium, calcium, and chloride ions in the external medium respectively,

When IAA was applied on the tissues during the experiments, the application was carried out by adding solution containing IAA (BEI) to the measurement chamber. BEI contains BSM plus 0.01 mole m^{-3} IAA adjusted to pH 6 using NaOH which gives a final sodium concentration of about 0.03 mole m^{-3}. IAA (pK=4.75) as a weak acid must be included in the calculation. The related equation to solve for the Donnan partition coefficient is :

$$\sigma^3 + \frac{\gamma_{1o}\,\gamma_{2w}\,([H_o]+[K_o]+[Na_o])}{2\,\gamma_{2o}\,\gamma_{1w}\,[Ca_o]}\,\sigma^2 - \frac{\gamma_{2w}\,([A_{Donn}]+0.5\,[IAA_o]\,10^{(pH_w-pK)})}{2\,\gamma_{2o}\,[Ca_o]}\,\sigma$$

$$- \frac{\gamma_{1o}\,\gamma_{2w}\,([Cl_o]+0.5\,[IAA_o])}{2\,\gamma_{2o}\,\gamma_{1w}\,[Ca_o]} = 0.$$

c.13

IAA$_o$ is the concentration of IAA anions in the external medium.

The estimation of the concentration of ions, including IAA, in the DFS of the cell walls described above is carried out with the assumption that there is no transport of the ions across the plasma membrane. IAA itself is assumed not to have hormonal effects on the wall. Table c.1 is the results of the calculation when the external medium is BSM or BEI.

	BSM	BEI	Units
External Medium:			
pH_o	6.0	6.0	
$[K_o]$	0.1	0.1	mole m^{-3}
$[Na_o]$	0.02	0.03	mole m^{-3}
$[Cl_o]$	0.3	0.3	mole m^{-3}
$[Ca_o]$	0.1	0.1	mole m^{-3}
$[IAA_o]$		0.0095	mole m^{-3}
I_o	0.411	0.420	mole m^{-3}
γ_{1o}	0.977	0.977	
γ_{2o}	0.911	0.910	
Cell Walls:			
$[A_{sites}]$	765.1	765.1	mole m^{-3}
ξ	0.679	0.679	
$[A_{Donn}]$	563.4	563.4	mole m^{-3}
$[Cat_{cond}]$	201.8	201.8	mole m^{-3}
γ_{1w}	0.843	0.843	
γ_{2w}	0.506	0.506	
σ	39.39	39.39	
E_{wo}	-92.75	-92.75	mV
pH_w	4.341	4.341	
$[K_w]$	4.563	4.562	mole m^{-3}
$[Na_w]$	0.913	1.369	mole m^{-3}
$[Cl_w]$	0.009	0.009	mole m^{-3}
$[Ca_w]$	279.4	279.2	mole m^{-3}
Total $[Ca_w]$	380.3	380.1	mole m^{-3}
$[IAA_w]$		0.0002	mole m^{-3}
I_w	561.6	561.4	mole m^{-3}

Table c.1

The results of the estimation of ion concentration in cell walls using the WADM model when the external medium is BSM or BEI.

Appendix D

ABBREVIATIONS AND SYMBOLS

Abbreviation	Full word or expression
$[A_{diss}]$	concentration of dissociated ionisable sites in the DFS
$[A_{Donn}]$	concentration of the fixed negative charges available for the Donnan equilibrium
$[A_{sites}]$	concentration of ionisable sites in the DFS of the wall
β	buffering capacity
BSM	0.1 mole m^{-3} KCl + 0.1 mole m^{-3} CaCl$_2$ pH6 with NaOH
BET	BSM + 0.5% ethanol
BEI	BSM + 0.5% ethanol 0.01 mole m^{-3} IAA
C	concentration
Ca	calcium
$[Ca_{cond}]$	concentration of condensed calcium in the wall's weak acids
Cl	chloride
D	diffusion coefficient
DFS	Donnan free space
E	electric potential
E_{wo}	Donnan potential of the DFS in respect to the WFS
EDTA	ethylenediamine tetraacetic acid
EGTA	ethyleneglycol-bis-(β-aminoethylether)-N,N,N',N'-tetraacetic acid
ER	endoplasmic reticulum
F	Faraday number
γ	activity coefficient
FC	fusicoccin
J	flux

Quin 2	2-[(2-bis-[carboxymethyl]amino-5-methylphenoxy)methyl]-6-methoxy-8-bis[carboxymethyl]aminoquinoline
h	thickness of the walls
H	protons
I	ionic strength
IAA	indole-3-acetic acid
K	potassium
λ	portion of the DFS in the walls
$(1-\lambda)$	portion of the WFS in the walls
MIFE	microelectrode ion flux estimation
N	ion
Na	sodium
pH	minus the log of the proton activity
pK	minus the log of the dissociation constant
PD	membrane potential
r	flux ratio
R	gas constant
σ	Donnan partition coefficient
SE	standard error
t	time
T	temperature
T_N	amount of ion N
TEA	tetraethylammonium
u	mobility
μ	electrochemical potential
WADM	weak acid Donnan Manning
WFS	water free space
x	position
ξ	linear charge density parameter
ξ^*	intrinsic linear charge density parameter of the walls
z	valency

REFERENCES

Ammann, D. (1986) Ion-selective microelectrodes. Springer-Verlag, Berlin Heidelberg New York Tokyo

Amstrong, W.M., Wojtkowski, W., Bixenman, W.R. (1977) A new solid-state microelectrode for measuring intra-cellular chloride activities. Biochimica et Biophysica Acta **465**, 165-170

Arif, I., Newman, I.A. (1993) Proton efflux from oat coleoptile cells and exchange with wall calcium after IAA or fusicoccin treatment. Planta **189**, in press

Ballio, A. (1977) Fusicoccin: Structure-activity relationships. In: Regulation of cell membrane activities in plants, p. 217-223, Marrè, E., Ciferri, O., ed. Elsevier/North-Holland Biomedical Press, Amsterdam

Bates, G.W., Goldsmith, M.H.M. (1983) Rapid response of the plasma-membrane potential in oat coleoptiles to auxin and other weak acids. Planta **159**, 231-237

Bates, G.W., Ray, P.M. (1981) pH dependent interactions between pea cell wall polymers possibly involved in wall deposition and growth. Plant Physiol. **68**,158-164

Baumgarten, C.M. (1981a) Chloride ion-selective microelectrodes: An improved ion-exchange resin (Abstarct). Biophys. J. **33**, 187a

Baumgarten, C.M. (1981b) An improved liquid ion exchanger for chloride ion-selective microelectrodes. Am. J. Physiol. **241**, c258-c263

Baumgarten, C.M., Fozzard, H.A. (1981) Intracellular chloride activity in mammalian ventricular muscle. Am. J. Physiol. **241**, c121-c129

Bennet-Clark, T.A. (1956) Salt accumulation and mode of action of auxin. A preliminary hypothesis. In: The chemistry and mode of action of plant growth substances, p. 283-291, Wain, R.L., Wightman, F., ed. Butterworth, London

Bert, A., Felle, H. (1985) Cytoplasmic pH of root hair cells of synapis alba recorded by a pH-sensitive micro-electrode. Does fusicoccin stimulate the proton pump by cytoplasmic acidification? J. Exp. Bot. **36**, 1142-1149

Blatt, M.R. (1988) Mechanisms of fusicoccin action: A dominant role for secondary transport in a higher-plant cell. Planta **174**, 187-200

Blatt, M.R., Clint, G.M. (1989) Mechanisms of fusicoccin action: Kinetic modification and inactivation of K^+ channels in guard cells. Planta **178**, 509-523

Boyer, J.S. (1985) Water transport. Annu. Rev. Plant Physiol. **36**, 473-516

Brummell, D.A., Hall, J.L. (1987) Rapid cellular responses to auxin and the regulation of growth. Plant Cell Environ. **10**, 523-543

Brummer, B., Bertl, A., Potrykus, I., Felle, H., Parish, R.W. (1985) Evidence that fusicoccin and indole-3-acetic acid induced cytosolic acidification of *Zea mays* cells. FEBS Lett. **189**, 109-114

Brummer, B., Felle, H., Parish, R.W. (1984) Evidence that acid solutions induce plant cell elongation by acidifying the cytosol and stimulating the proton pump. FEBS Lett. **174**, 223-227

Brummer, B., Parish, R.W. (1983) Hypothesis: Mechanisms of auxin-induced plant cell elongation. FEBS Lett. **161**, 9-13

Carlier, A., Buffel, K. (1955) Polisacharide changes in the cell walls of water absorbing potato tuber tissue in relation to auxin action. Acta Bot. Nèerl. **4**, 551-564

Chang, R. (1977) Physical chemistry with applications to biological systems. p. 338-365, Macmillan Publishing Co. Inc., London

Chastain, C.J. Hanson, J.B. (1982) Control of proton efflux from corn root tissue by an injury-sensing mechanism. Plant Sci. Lett. **24**, 97-104

Cleland, R.E. (1960) Effect of auxin upon loss of calcium from cell walls. Plant Physiol. **35**, 581-584

Cleland, R.E. (1971) Cell wall extension. Annu. Rev. Plant Physiol. **22**, 197-222

Cleland, R.E. (1975) Auxin induced hydrogen ion excretion: Correlation with growth, and control by external pH and water stress. Planta **127**, 233-242

Cleland, R.E. (1976) Kinetics of hormone-induced H^+ excretion. Plant Physiol. **58**, 210-213

Cleland, R.E. (1980) Auxin and H^+-excretion: The sate of our knowledge. In: Plant growth substances 1979, p. 71-78, Skoog, F., ed. Springer, Berlin Heidelberg New York

Cleland, R.E. (1983) The capacity of acid-induced wall loosening as a factor in the control of *Avena* coleoptile cell elongation. J. Exp. Bot., **34**, 676-680

Cleland, R.E. (1991) The outer epidermis of *Avena* and maize coleoptiles is not a unique target for auxin in elongation growth. Planta **186**, 75-80

Cleland, R.E., Buckley, G., Nowbar, S., Lew, N.M., Stinemeztz, C., Evans, M.L. (1991) The pH profile for acid-induced elongation of coleoptile and epicotyl sections is consistent with the acid-growth theory. Planta **186**, 70-74

Cleland, R.E., Prins, H.B.A., Harper, J.R., Higinbotham, N. (1977) Rapid hormone-induced hyperpolarization of the oat coleoptile transmembrane potential. Plant Physiol. **59**, 395-397

Cleland, R.E., Rayle, D.L. (1977) Reevaluation of the effect of calcium ions on auxin-induced elongation. Plant Physiol. **60**, 709-712

Cleland, R.E., Virk, S.S., Taylor, D., Björkman, T. (1990) Calcium, cell walls and growth. In: Calcium in plant growth and development, p. 9-16,

Leonard, R.T., Hepler, P.K., ed. American Society of Plant Physiologists, Rockville

Clint, G.M., Blatt, M.R. (1989) Mechanisms of fusicoccin action: Evidence for concerted modulations of secondary K^+ transport in a higher plant cell. Planta **178**, 495-508

Cohen, J.D., Nadler, K.D. (1976) Calcium requirement for indoleacetic acid-induced acidification by *Avena* coleoptiles. Plant Physiol. **57**, 347-350

Coleman, H.A. (1986) Chloride currents in *Chara*. A patch-clamp study. J. Memb. Biol. **93**, 55-61

Cosgrove, D. (1986) Biophysical control of plant cell growth. Annu. Rev. Plant Physiol. **37**, 377-405

Crank, J. (1975) The mathematics of diffusion. p. 11-27, Clarendon Press, Oxford

Dainty, J., Hope, A.B. (1959) Ionic relations of cells of *Chara Australis*. I. Ion exchange in the cell wall. Aus. J. Biol. Sci. **12**, 395-411

Dainty, J., Hope, A.B., Denby, C. (1960) Ionic relations of cells of *Chara Australis*. II. The indifussible anions of the cell wall. Aus. J. Biol. Sci. **13**, 267-276

Durran, H., Rayle, D.L. (1973) Physiological evidence for auxin induced hydrogen ion secretion and the epidermal paradox. Planta **114**, 185-193

Evans, M.L., Ray, P.M. (1969) Timing of the auxin response in coleoptiles and its implications regarding auxin action. J. Gen. Physiol. **53**, 1-9

Evans, M.L. and Vesper, M.J. (1980) An improved method for detecting auxin induced hydrogen ion efflux from corn coleoptile segments. Plant Physiol. **66**, 561-565

Felle, H. (1988) Auxin causes oscillations of cytosolic free calcium and pH in *Zea mays* coleoptiles. Planta **174**, 495-499

Felle, H., Brummer, B., Bertl, A., Parish, R.W. (1986) Indole-3-acetic acid and fusicoccin cause cytosolic acidification of corn coleoptile cells. Proc. Natl. Acad. Sci. USA **83**, 8992-8995

Goldsmith, M.H.M. (1977) The polar transport of auxin. Annu. Rev. Plant Physiol. **28**, 439-478

Grant, G.T., Morris, E.R., Rees, D.A., Smith, P.J.C., Thom, D. (1973) Biological interactions between polysaccharides and divalent cations: The egg-box model. FEBS Lett. **32**, 195-198

Gronewald, J.W., Hanson, J.B. (1980) Sensitivity of the proton and ion transport mechanisms of corn roots to injury. Plant Sci. Lett. **18**, 143-150

Hager, A., Menzel, H., Krauss, A. (1971) Experiments and hypothesis concerning the primary action of auxin in elongation growth. Planta **100**, 47-75

Haschke, H.P., Lüttge, U. (1977) Action of auxin on CO_2 dark fixation in *Avena* coleoptile segments as related to elongation growth. Plant Sci. Lett. **8**, 53-58

Haschke, H.P., Lüttge, U. (1977) Auxin action on K^+-H^+ exchange and growth, $^{14}CO_2$ fixation and malate accumulation in *Avena* coleoptile segments. In: Regulation of cell membrane activation in plants, p. 243-248, Marrè, E., Ciferri, O., ed. Elsevier/North-Holland Biomedical press, Amsterdam

Hasenstein, K., Evan, M.L. (1986) Calcium dependence of rapid auxin action in maize roots. Plant Physiol. **81**, 439-443

Henriksen, G.H., Bloom, A.J., Spanswick, R.M. (1990) Measurement of net fluxes of ammonium and nitrate at the surface of barley roots using ion-selective microelectrodes. Plant Physiol. **93**, 271-280

Henriksen, G.H., Raman, D.R., Walker, L.P., Spanswick, R.M. (1992) Measurement of net fluxes of ammonium and nitrate at the surface of barley roots using ion-selective microelectrodes. II. Patterns of uptake along the root axis and evaluation of the microelectrode flux estimation technique. Plant Physiol. **99**, 734-747

Hepler, P.K., Wayne, R.O. (1985) Calcium and plant development. Annu. Rev. Plant Physiol. **36**, 397-439

Hoson, T., Masuda, Y., Sone, Y., Misaki, A. (1991) Xyloglucan antibodies inhibit auxin-induced elongation and cell wall loosening of azuki bean epicotyls but not of oat coleoptiles. Plant Physiol. **96**, 551-557

Hush, J.M., Overall, R.L. (1989) Steady ionic currents around pea (*Pisum sativum* L.) root tips: The effects of tissue wounding. Biol. Bull. **176(S)**, 56-64

Hush, J.M., Newman, I.A., Overall, R.L. (1992) Utilizition of the vibrating probe and ion-selective microelectrode techniques to investigate electrophysiological responses to wounding in pea roots. J. Exp. Bot. **43**, 1251-1257

Inouhe, M., Nevins, D.J. (1991) Inhibition of auxin-induced cell elongation of maize coleoptiles by antibodies specific for cell wall glucanases. Plant Physiol. **96**, 426-431

Jacobs, M., Ray, P.M. (1976) Rapid auxin-induced decrease in free space pH and its relationship to auxin-induced growth in maize and pea. Plant Physiol. **58**, 203-209

Key, J.L. (1969) Hormones and nucleic acid metabolism. Annu. Rev. Plant Physiol. **20**, 449-474

Klämbt, D. (1990) A view about the function of auxin-binding proteins at plasma membranes. Plant Mol. Biol. **14**, 1045-1050

Kutschera, U., Bergfeld, R., Schopfer, P. (1987) Cooperation of epidermis and inner tissues in auxin-mediated growth of maize coleoptiles. Planta **170**, 168-180

Kutschera, U., Briggs, W.R. (1987a) Rapid auxin-induced stimulation of cell wall sinthesis in pea internodes. Proc. Natl. Acad. Sci. USA **84**, 2747-2751

Kutschera, U., Briggs, W.R. (1987b) Differential effect of auxin on in vivo extensibility of cortical cylinder and epidermis in pea internodes. Plant Physiol. **84**, 1361-1366

Kutschera, U., Schopfer, P. (1985a) Evidence against the acid growth theory of auxin action. Planta **163**, 483-493

Kutschera, U., Schopfer, P. (1985b) Evidence for the acid growth theory of fusicoccin action. Planta **163**, 483-493

Lockhart, J.A. (1965a) Cell extension. In: Plant biochemistry, p. 827-849, Bornner, J., Varner, J.E., ed. Academic, New York

Lockhart, J.A. (1965b) An analysis of irreversible plant cell elongation. J. Theor. Biol. **8**, 264-275

Lucas, W.J., Kochian, L.V. (1986) Ion transport processes in corn roots: An approach utilising microelectrode techniques. In: Advanced agricultural instrumentation. design and use, p. 402-425, Gensler, W.G., ed. M. Nijhoff, Dordrecht

Lüthen, H., Bigdon, M., Böttger, M. (1990) Reexamination of the acid growth theory of auxin action. Plant Physiol. **93**, 931-939

Lüthen, H., Böttger, M. (1989) Significant participation of protons in the control of IAA-induced growth. In: Plant membrane transport. The current position, p. 423-424, Dainty, J., Demichelis, M.I., Marrè, E., Caldogno, F.R., ed. Elsevier, Amsterdam New York Oxford

Manning, G.S. (1969) Limiting laws and counterion condensation in polyelectrolyte solution. I. Colligative properties. J. Chem. Phys. **51**, 924-933

Marrè, E. (1979) Fusicoccin: A tool in plant physiology. Annu. Rev. Plant Physiol. **30**, 273-288

Marrè, E., Lado, P., Rasi Caldogno, F., Colombo, R., DeMichelis, M.I. (1974) Evidence for the coupling of proton extrusion to K^+ uptake in pea internode segments treated with fusicoccin or auxin. Plant Sci. Lett. **3**, 365-379

Masuda, Y. (1980) Auxin-induced changes in noncellulosic polysaccharides of cell walls of monocot coleoptiles and dicot stems. In: Plant growth substances 1979, p. 79-89, Skoog, F., ed. Springer, Berlin Heidelberg New York

Masuda, Y., Yamamoto, R., Tanimoto, E. (1972) Auxin-induced changes in cell wall properties and growth of *Avena* coleoptiles and green pea epicotyls. In: Plant growth substances 1970, p. 17-22, Carr, D.J., ed. Springer-Verlag, Berlin Heidelberg New York

McQueen-Mason, S., Durachko, D.M., Cosgrove, D.J. (1992) Two cell wall associated proteins that induce extension of cell walls. (Abstr.) Plant Physiol. **99**, Suppl., 33

Morgan, J.M. (1984) Osmoregulation and water stress in higher plants. Annu. Rev. Plant Physiol. **62**, 423-429

Neild, T.O., Thomas, R.C. (1973) New design for a chloride-sensitive micro-electrode. J. Physiol. London **231**, 7p-8p

Newman, I.A. (1963) Electric potentials and auxin translocation in *Avena*. Aust. J. Biol. Sci. **16**, 629-646

Newman, I.A., Kochian, L.V., Grusak, M.A., Lucas, W.J. (1987) Fluxes of H^+ and K^+ in corn roots: Characterization and stoichiometries using ion selective microelectrodes. Plant Physiol. **84**, 1177-1184

Nobels, P.S. (1974) Introduction to biophysical plant physiology. W.H. Freeman and Co., San francisco

Peters, W.S., Richter, U., Felle, H.H. (1992) Auxin-induced H^+-pump stimulation does not depend on the presence of epidermal cells in corn coleoptiles. Planta **168**, 313-316

Raven, P.H., Evert, R.F., Eichhorn, S.E. (1986) Biology of plants. Worth Publishers, Inc., New York

Rayle, D.L. (1973) Auxin induced hydrogen ion secretion in *Avena* coleoptiles and its implications. Planta **114**, 63-73

Rayle, D.L. (1989) Calcium bridges are not load-bearing cell-wall bonds in *Avena* coleoptiles. Planta **178**, 92-95

Rayle, D.L., Cleland, R.E. (1970) Enhancement of wall loosening and elongation by acid solutions. Plant Physiol. **46**, 250-253

Rayle, D.L., Cleland, R.E. (1992) The acid growth theory of auxin-induced cell elongation is alive and well. Plant Physiol. **99**, 1271-1274

Rayle, D.L., Nowbar, S., Cleland, R.E. (1991) The epidermis of the pea epicotyl is not a unique target tissue for auxin-induced growth. Plant Physiol. **97**, 449-451

Rees, D.A. (1977) Polysaccharide shape. Outline studies in botany series. Chapman and Hall, London

Reddy, A.S.N., Koshiba, T., Theologis, A., Pooviah, B.W. (1988) The effect of calcium antagonists on auxin-induced elongation and on the expression of two auxin-regulated genes in pea epicotyls. Plant Cell Physiol. **29**, 1165-1170

Reid, R.J., Walker, N.A. (1984) The energetics of Cl⁻ active transport in *Chara*. J. Memb. Biol. **78**, 35-41

Richmond, P.S., Metraux, J.P., Taiz, L. (1980) Cell expansion patterns and directionality of wall mechanical properties in *Nitella*. Plant Physiol. **65**, 211-217

Richter, C., Dainty, J. (1989a) Ion behavior in plant cell walls. I. Characterization of the *Sphagnum russowii* cell wall ion exchanger. Can. J. Bot. **67**, 451-459

Richter, C., Dainty, J. (1989b) Ion behavior in plant cell walls. II. Measurement of Donnan free space, anion-exclusion space, anion-exchange capacity, and cation-exchange capacity in delignified *Sphagnum russowii* cell walls. Can. J. Bot. **67**, 460-465

Richter, C., Dainty, J. (1990a) Ion behavior in plant cell walls. III. Measurement of the mean charge separation distance and the linear charge

density parameter in delignified *Sphagnum russowii* cell walls. Can. J. Bot. **68**, 768-772

Richter, C., Dainty, J. (1990b) Ion behavior in plant cell walls. IV. Selective cation binding by *Sphagnum russowii* cell walls. Can. J. Bot. **68**, 773-781

Rincon, M., Hanson, J.B. (1986) Controls on calcium ion fluxes in injured or shocked corn root cells: Importance of proton pumping and cell membrane potential. Physiol. Plant **67**, 576-583

Ryan, P.R., Newman, I.A., Arif, I. (1992) Rapid calcium exchange for protons and potassium in cell walls of *Chara*. Plant Cell Environ. **15**, 675-683

Ryan, P.R., Newman, I.A., Shields, B. (1990) Ion fluxes in corn roots measured by microelectrodes with ion-specific liquid membranes. J. Memb. Sci. **53**, 59-69

Salisbury, F.B., Ross, W.D. (1985) Plant physiology. p.459-470, Wadsworth Publishing Company, California

Sanders, D. (1980) The mechanism of Cl transport at the plasma membrane of *Chara corallina*. I. Cotransport with H^+. J. Memb. Biol. **53**, 129-141

Saunders, J.H., Brown, M. (1977) Liquid and solid-state Cl^--Sensitive microelectrodes. J. Gen. Physiol. **70**, 507-530

Schopfer, P. (1989) pH-dependence of extension growth in *Avena* coleoptiles and its implications for mechanism of auxin action. Plant Physiol. **90**, 202-207

Schulz, S., Oelgemöller, E., Weiler, E.W. (1990) Fusicoccin action in cell-suspension cultures of *Corydalis sempervirens* pers. Planta **183**, 83-91

Senn, A.P., Goldsmith, M.H.M. (1988) Regulation of electrogenic proton pumping by auxin and fusicoccin as related the growth of *Avena* coleoptiles. Plant Physiol. **88**, 131-138

Sentenac, H., Grignon, C. (1981) A Model for predicting ionic equilibrium concentrations in cell walls. Plant Physiol. **68**, 415-419

Silk, W.K. (1984) Quantitative descriptions of development. Annu. Rev. Plant Physiol. **35**, 479-518

Smith, F.A. (1980) Comparison of the effects of ammonia and methylamine on chloride transport and intracellular pH in *Chara corallina*. J. Exp. Bot. **31**, 597-606

Smith, F.A., MacRobbie, E.A.C. (1981) Comparison on cytoplasmic pH and Cl⁻ influx in cells of *Chara corallina* following "Cl⁻ starvation". J. Exp. Bot. **32**, 827-835

Smith, F.A., Walker, N.A. (1976) Chloride transport in *Chara corallina* and the electrochemical potential difference for hydrogen ions. J. Exp. Bot. **27**, 451-459

Smith, F.A. and Whittington, J. (1988) Uptake of imidazole and its effects on the intracellular pH and ionic relations of *Chara corallina*. J. Exp. Bot. **39**, 1549-1560

Stout, R., Cleland, R.E. (1980) Partial characterization of fusicoccin binding to receptor sites on oat root membranes. Plant Physiol. **66**, 353-359

Talbott, L.D., Ray, P.M., Roberts, J.K.M. (1988) Effects of indoleacetic acid- and fusicoccin-stimulated proton extrusion on internal pH of pea internode cells. Plant Physiol. **87**, 211-216

Tagawa, T. Bonner, J. (1957) Mechanical properties of the *Avena* coleoptile as related to auxin and to ionic interactions. Plant Physiol. **32**, 207-212

Taiz, L. (1984) Plant cell expansion: Regulation of cell wall mechanical properties. Annu. Rev. Plant Physiol. **35**, 585-657

Tepfer, M., Taylor, I.E.P. (1981) The Interaction of divalent cation with pectic substances and their influence on acid-induced cell wall loosening. Can. J. Bot. **59**, 1522-1525

Terry, M.E., Jones, R.L. (1981) Effect of salt on auxin-induced acidification and growth by pea internode sections. Plant Physiol. **68**, 59-64

Tominaga, Y., Tazawa, M. (1981) Reversible inhibitions of cytoplasmic streaming by intracellular Ca^{2+} in tonoplast-free cells of *Chara australis*. Protoplasma **109**, 103-111

Tyerman, S.D., Findlay, G.P., Paterson, G.J. (1986) Inward membrane current in *Chara inflata*: II. Effects of pH, Cl^--channel blokers and NH_4^+, and significance for the hyperpolarized state. J. Memb. Biol. **89**, 153-161

Vanderhoef, L.N. (1980) Auxin-regulated elongation: A summary hypothesis. In: Plant growth substances 1979, p. 90-96, Skoog, F., ed. Springer, Berlin Heidelberg New York

Vesper, M.J., Evans, M.L. (1978) Time-dependent changes in the auxin sensitivity of coleoptile segments. Plant Physiol. **61**, 204-208

Virk, S.S., Cleland, R.E. (1988) Calcium and the mechanical properties of soybean hypocotyl cell walls: Possible role of calcium and protons in cell-wall loosening. Planta **176**, 60-67

Virk, S.S., Cleland, R.E. (1990) The role of wall calcium in the extension of cell walls of soybean hypocotyls. Planta **182**, 559-564

White, A., Handler, P., Smith, E.L. (1968) Principles of biochemistry. p. 95-101, McGraw Hill Inc., New York

Yamaoka, T., Chiba, N. (1983) Changes in the coagulating ability of pectin during the growth of soybean hypocotyls. Plant Cell Physiol. **24**, 1281-1290